UNIVERSITY OF SOUTHAMPTON

An Investigation into an Empirically Designed Passive Sound Absorber for use in Recording Studio Control Rooms

Stuart Colam

Doctor of Philosophy

Fluid Dynamics and Acoustics Group
Institute of Sound and Vibration Research
Faculty of Engineering and Applied Science

April 2002

UNIVERSITY OF SOUTHAMPTON

ABSTRACT

FACULTY OF ENGINEERING AND APPLIED SCIENCE
INSTITUTE OF SOUND AND VIBRATION RESEARCH

Doctor of Philosophy

An Investigation into an Empirically Designed Passive Sound Absorber for use in Recording Studio Control Rooms

by Stuart Colam

The purpose of the research is to investigate how an empirically designed sound absorber works. Particular attention is given to its performance below 400 Hz.

Anecdotal evidence regarding its performance is ratified through in situ measurements of a recently built studio, with the results showing that the room exhibits little spatial variation in low frequency reverberant energy.

Measurements made at different stages of room construction show that the short reverberation time in a room in which the absorber is used is not directly related to the surface area of porous absorbent present. A Sabine diffuse field absorption coefficient model alone is unable to account for the behaviour of the absorber. The multi-layer absorbent wall used in the design is shown to be effective below 100 Hz by virtue of damped resonances within its structure.

Through experimental and numerical investigations, the attenuation of sound as it propagates past the absorber when implemented on the side wall of a duct is shown to be highly dependent on the wall construction. Large transmission losses are evident when the absorber presents a particular surface normal acoustic impedance. The results from a theoretical model suggest that the attenuation is caused by an acoustic surface wave. Diffraction is noted, though significant effects are not evident at the low frequencies of interest. Filtering effects are also restricted to high frequencies. All results indicate that there is no 'trapping' of sound at low frequencies.

A hypothesis relating to the normal incidence absorption coefficient of the absorber is ratified by using absorbent Finite Elements in a numerical model. Though secondary to the absorption noted at odd integer multiples of ¼ wavelength, further research could lead to a new design of modular low frequency absorber.

CONTENTS

FIGURES

ACKNOWLEDGEMENTS

The author wishes to thank the following people for their contributions to this work:

Dr Keith Holland, for supervising the project and providing general guidance.
Professor Chris Morfey and Dr Phil Joseph, for their valuable input at the review meetings.
Tom Hidley, Philip Newell and Sergio Castro, for essential practical support and advice.
Professor Frank Fahy, for his ideas relating to *Chapter 7*.
Dr Alan McAlpine, for his assistance with some of the maths.
Dr Chris Jones, for help with the Finite Element Analysis software.
Nick Merricks, for proof reading the final draft.

NOTATION

A	Cross sectional area
c	Sound speed
c_0	Sound speed in air
dB	Decibel
f	Frequency
FEA	Finite Element Analysis
FFT	Fast Fourier Transform
ITF	Impedance transformation formula
j	$\sqrt{-1}$
k	Wavenumber
k_0	Freefield wavenumber
M	Mass per unit area
p	Pressure
q	Volume velocity
Q	Quality factor
R	Reflection coefficient; acoustic resistance
RT_{30}	Reverberation time, decay by 30 dB
RT_{60}	Reverberation time, decay by 60 dB
S	Surface area; stiffness
SDoF	Single degree of freedom
T	Transfer function
TL	Transmission loss
u	Particle velocity
V	Volume
X	Acoustic reactance
z	Acoustic impedance
α	Absorption coefficient; attenuation constant
β	Phase constant
λ	Wavelength of sound

ρ	Density
ρ_0	Density of air
σ	Resistivity
ω	Angular frequency

CHAPTER 1

The Development, Context and Construction of an Empirically Designed Sound Absorber

Introduction

The subject of this research project is a passive sound absorber used primarily in recording studio control rooms. These rooms are where the recording engineer and/or producer assesses the quality of the recorded material reproduced over loudspeakers. Whilst the application of the absorber is not limited to such an environment, it is the control room that will provide the context for this research. The absorber is an integral part of the room design and not of the stand alone type which might be introduced retrospectively to correct for an unacceptable reverberation characteristic.

The objective of this research is to provide a scientifically based investigation in which the absorber, or elements of it, are modelled and measured, in order that the primary mechanisms by which it works can be found. Through the use of experimental, theoretical and numerical investigations, the results obtained may be ratified by comparison, one with another. Insight into the way in which the absorber works will enable it to be improved beyond its present acoustic performance.

Due to its construction and particular efficiency in absorbing low frequency sound, it has earned the unofficial title of *Bass Trap*, by which it will be referred to hereafter. Before the design is introduced, the history of its evolution and development is summarised.

1.1 History and Development of the *Bass Trap*

As mentioned, the *Bass Trap* is empirically designed, the starting point for which was purely accidental.

1.1.1 The Discovery of the *Bass Trap*

According to Tom Hidley [1.1], an advocate of the *Bass Trap* design, the conception of the absorber occurred in the early 1960's. A new design of JBL loudspeaker was being demonstrated to recording engineers and producers in one of the conference rooms of one of the company's offices. The room had been used earlier in the week for a series of lectures and in preparation for the demonstration, the moveable blackboards were positioned at the back of the room. In order to occupy less of the room and look tidy, the blackboards were placed parallel with each other, but at an angle to the wall. The loudspeakers were played to those invited and all present remarked on their sound quality. Such was the enthusiasm for the loudspeakers, that record company executives were invited to hear them later that week – by which time the blackboards had been removed. Unfortunately for JBL, the second round of demonstrations did not yield the same response as the first, with the executives being largely unimpressed by the loudspeakers. In trying to explain the discrepancy in opinion between the two groups of music industry professionals, listening to the same pair of loudspeakers, it was realised that the blackboards were the only variable that had changed. Once reinstated in the back of the room, the listening environment was dramatically improved, from which it was concluded that the positive comments from the first demonstration were more to do with the change to the acoustical behaviour of the room, than the loudspeakers themselves.

On commenting about the blackboard arrangement and hypothesising on the possible acoustic mechanism involved, one member of JBL staff remarked to Tom Hidley, that the ". . . bass was trapped." [1.1] – from which point the name *Bass Trap* was coined.

1.1.2 Panel Construction

Hidley moved into studio design soon after this discovery and in 1969 introduced the fledgling *Bass Traps* to three large installations in north Hollywood. The key element of the design was the parallel panels placed on the walls and ceiling, though by now they were freely suspended to isolate them from any structural

vibration. The construction of the side wall panels was ½ inch thick lightweight plasterboard, the height of the room and covered on either side with 3 inches of fibreglass. In 1975, a studio in Nashville attempted to incorporate the *Bass Trap* in one of their control rooms, but the anticipated performance was not achieved. Hidley was contacted and found that the traps consisted only of 3 inch thick fibreglass – the plasterboard core had been omitted. Hidley experimented with different types of panel construction over the following months and concluded that ¾ inch chipboard yielded an improvement on account of its higher density.

1.1.3 Panel Orientation

Five years before the importance of the panel core was noted, Hidley had arranged for listening tests to take place in a newly constructed studio in Sausalito, USA. Two identical rooms were constructed side by side and A-B comparisons were made for panels different distances apart and at various angles to the side walls. Ten recording engineers and producers spent several days evaluating the different designs of *Bass Trap* and unanimously concluded that when the traps were spaced 30 cm apart and at an angle of 45^0 the room was ". . the most musical and natural." [1.1]. These and other positive responses led Hidley to develop a control room design philosophy, in which the *Bass Trap* would play an integral part – the *non-environment* room.

1.1.4 The *Non-environment* Room Design Philosophy

After a number of years of designing very many control rooms with the *Bass Trap*, Hidley concluded that the overwhelming agreement and enthusiasm for something as subjective as studio design pointed to an acoustic environment that was much better than what had gone before. (Control rooms were generally designed on an intuitive basis, or would simply try to copy another successful studio). From discussion with those involved in the recording industry and after much trial and error in studio construction, he decided that the best listening conditions for the critical appraisal of recorded material, reproduced by loudspeakers, would be one in which the room was acoustically transparent – hence the *non-environment* room. In such a room the floor and monitor wall are the only reflective boundaries, with all others being as absorptive as possible, to as low a frequency as possible. In addition to the

basic philosophy was Hidley's conviction that the extreme low frequency information in recorded material was important to the subjective assessment of the remainder of the audible spectrum. The need to monitor such low frequencies meant the *Bass Traps* represented an all important part in the room design, as they were found to be extremely effective in absorbing sound right down the lowest frequency limit of human hearing.

Over three decades since their introduction, *Bass Trap* control rooms are still designed and built all over the world, primarily by Hidley and English studio designer Philip Newell. Two of Newell's control rooms will figure in some of the investigations described later in this thesis. Given the popularity and effectiveness of the *Bass Trap* it was important that the empirical design was unravelled and the mechanisms by which it works identified. These questions will be partially addressed later in this chapter, after the design itself is illustrated and explained in more detail.

1.2 Description of the *Bass Trap* Absorber

The *Bass Trap* consists of two main elements, the aforementioned freely suspended angled panels and a multi-layer absorbent wall. The latter is built flush against the structural shell (assumed rigid in all subsequent analysis and discussion), with the panels in front, further into the room. *Figure 1.1* illustrates a *Bass Trap* control room, typical of those designed by Newell, in plan and elevation.

1.2.1 Construction of the Multi-layer Absorbent Wall

The multi-layer wall is constructed from a number of different materials, that can be grouped as either panels or porous absorbents. Only a qualitative description is given here, as the wall is dealt with in more detail in *Chapter 3* where its acoustic properties are modelled. The panel materials are chipboard, plasterboard and mineralised rubber matting (also known as deadsheet); the porous absorbents used are mineral wool and cotton waste felt. Two air spaces are also included in the design. It is useful to mention at this point that the outer-most layer of the wall is a 4 cm thickness of cotton waste felt. As with all other aspects of the *Bass Trap*, the multi-layer wall has also been designed on an empirical basis.

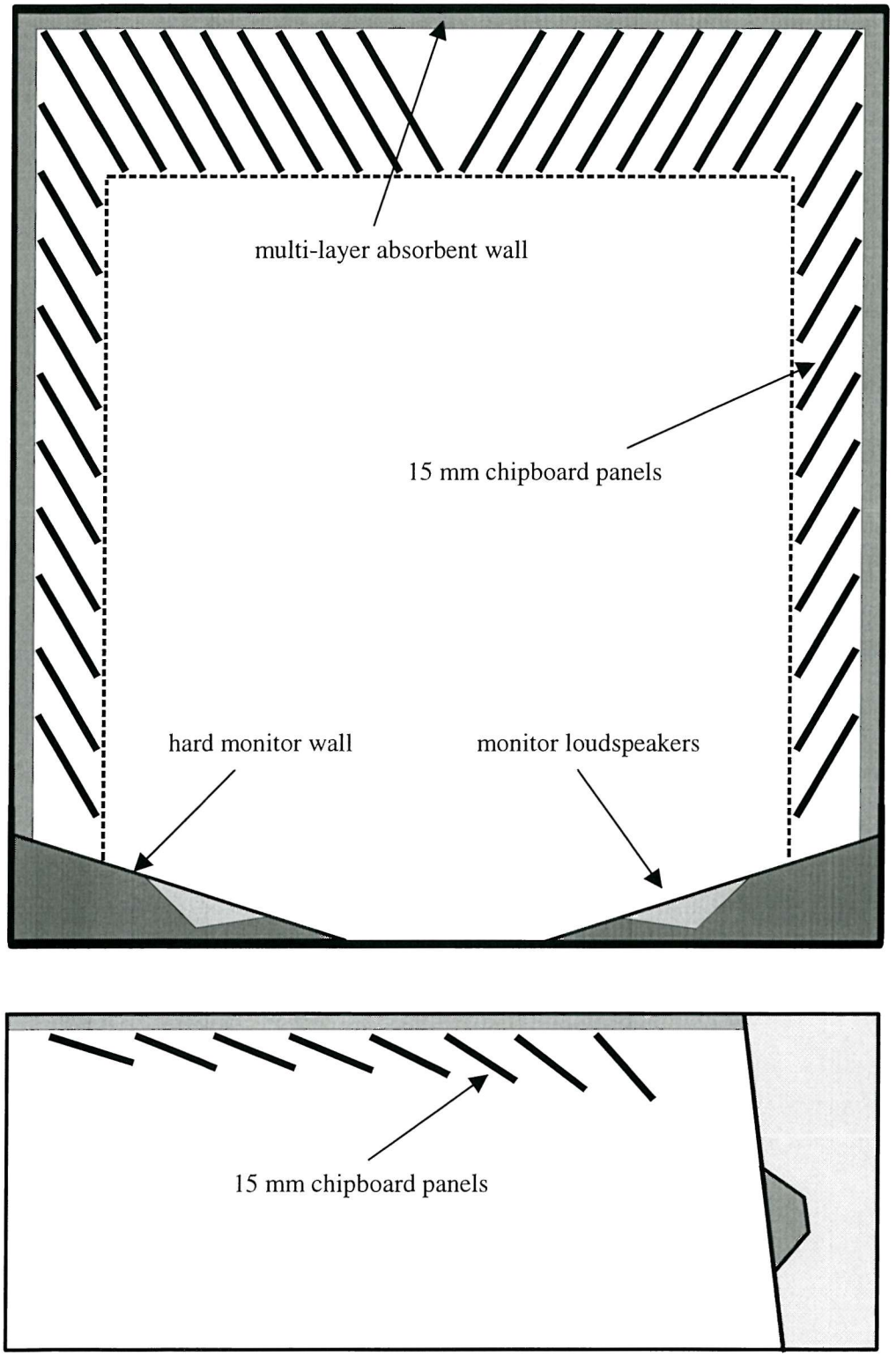

Figure 1.1 – Typical geometry of a Bass Trap control room

1.2.2 Construction of the Hanging Panels

The design of the hanging panels has evolved over the years and the present construction is illustrated in *Figure 1.2*. The core is 15 mm thick chipboard (composite particle board) and the typical height and depth is 3 m (or the height of the room) and 1.2 m respectively. Given a density of 650 kg m^{-3}, such a panel weighs around 35 kg. Stapled to the panel is an equal area of deadsheet, which for a typical 5 mm thickness has a mass per unit area of 7 kg m^{-2}. Finally, both sides of the panels are covered in 3 - 4 cm thick cotton waste felt, fibreglass, or similar porous material. The density of these layers is around 40 kg m^{-3}, giving a total panel weight of 70 kg. Short metal chains are used to suspend the panels from the ceiling framework.

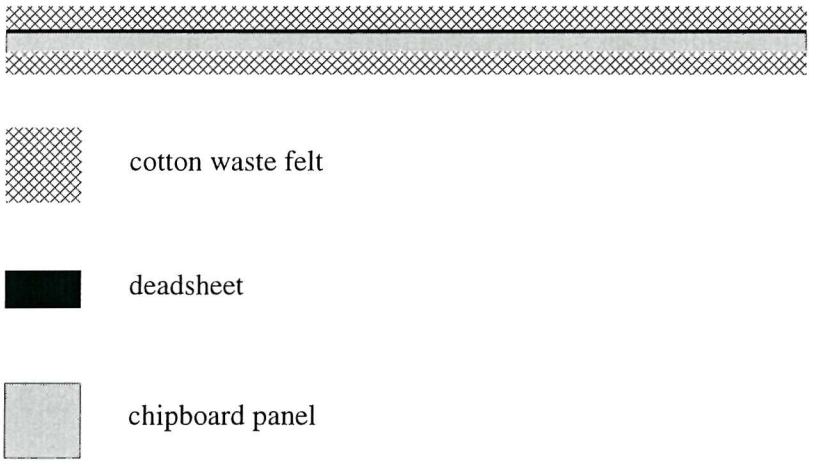

Figure 1.2 – Typical cross section of a hanging panel used in the Bass Trap design

1.2.3 Positioning of the Hanging Panels

Figure 1.1 shows how the side and rear wall panels are placed parallel with each other but at an angle of between 30^0 and 45^0 to the room boundary; the spacing is between 30 and 60 cm. The ceiling panels are slightly different in orientation. While the same depth of 1.2 m is used, they extend the full width of the room. The angle between them is not constant and are suspended so they face the monitors (elevation view of *Figure 1.1*). The reason for this, given by the designers,

is to present the sound easy access to the *Bass Trap*, but a tortuous exit, in the hope that more energy will be dissipated.

Whilst the panels are placed as close to the wall as possible, in practise there is a small air gap between the two; this is especially true of the ceiling traps because of the way they are suspended.

The design described is only the general form of the *Bass Trap* and constraints in space, time and money often require that the side wall panels are not employed. Failure to use ceiling traps however is regarded as detrimental to the performance of the room [1.2]. Rear wall traps are the minimum requirement for the design.

From the discussion in this and previous sections, some initial hypotheses can be drawn up regarding the mechanisms involved in the performance of the *Bass Trap.* In doing so, relevant literature will be cited to give context and justification for the discussion. A more general literature review on the subject of passive sound absorption, particularly at low frequencies, is given in *Appendix 1.*

1.3 Hypotheses on the Mechanisms of Absorption of the *Bass Trap*

The geometry and construction of the *Bass Trap* mean that it can be considered in many different ways. The ones considered in this section are:

a) Absorption solely due to the large amount of porous absorbent placed within a proportionally small volume.

b) Filtering of sound as it propagates down the length of the room due to the periodic array of panels.

c) Absorption due to ¼ wavelength resonances in the channels between panels.

d) Attenuation of sound as it travels down the traps, which effectively act as lined ducts.

e) Panels acting as waveguides, forcing the sound to be incident on the multi-layer wall at a particular angle.

Before each of the above is discussed, previous research on the *Bass Trap* will be summarised as a foundation for this and the following chapters.

1.3.1 Previous Research into the *Bass Trap* Absorber

Three authors have investigated the way in which the *Bass Trap* works, all as part of research projects at the ISVR, University of Southampton.

In 1991, Soares [1.3] constructed a $^1/_{10}$ scale model of a *Bass Trap* control room to investigate the decay characteristics of the room as a whole, for different arrangements of panels. The room was modelled using a concrete box and the chipboard panels scaled down to 0.9 mm thick aluminium plates – no acoustically resistive elements were included. The only conclusive result obtained was the observation of a peculiar reverberation time decay curve. Rather than a straight line decay of amplitude in dB against time, the RT_{60} decayed more quickly immediately after the source was silenced, than later on in the reverberant tail. The result of this being that the RT_{60} was not simply twice the RT_{30}[1]. It was concluded that, in the absence of any absorptive material, the geometrical arrangement of the panels removed the sound energy from the room before allowing it back. This added weight to the idea that the design *trapped* the sound.

Several years later, Walters [1.4] carried out experiments in the ISVR's anechoic chamber to determine the waveguide effect of a panel array. Several large chipboard panels, with and without a covering of cotton waste felt, were freely suspended from a supporting structure and band limited pink noise was directed at it using a large loudspeaker. The pressure amplitude was measured in front, within and behind the panel array and the results showed that the direction of incident plane wave was changed such that it emerged at the other side at an angle equal to the panels. This proved again that the panels were effective in acting as waveguides, even at very low frequencies. It also explained why the initial design of the studio in Nashville in 1975 failed to yield the absorption expected.

Finally in 1998, research was undertaken by the author [1.5] to find out whether or not the low frequency absorption afforded by the *Bass Traps* was due to flexural vibration in the panels themselves. This phenomenon was investigated by placing accelerometers at 72 different positions on a panel freely suspended in the ISVR anechoic chamber. The vibration response of the panel was measured for low

---

[1] The RT_{60} is defined as the time taken for a continuous source stopped at $t = 0$ to decay in pressure amplitude by 60 dB. Similarly RT_{30} is the time taken to decay by 30 dB. For a straight line decay (constant gradient), the RT_{60} is twice the RT_{30}.

frequency pink noise incident at three different angles (20^0, 40^0 and 60^0). The results showed that the power dissipated by the panel was five orders of magnitude less than the incident sound power, apart from a number of narrow frequency bands, shown to be the natural frequencies of the panel. This significant result would allow for the chipboard panels to be considered as **limp masses** in any subsequent research. As part of the same research project, the effect of the covered panels was investigated [1.6]. It was hypothesised that in covering the panels with absorbent material, more effective porous absorption might occur as the absorbent was supported in a region of high particle velocity, a requirement for the dissipation of sound energy into heat through the oscillatory motion of air through the material's porous skeleton. The experiments showed that the same absorption was achieved with a covered panel normal to a rigid wall, as the same amount of absorptive material placed directly on the wall. The conclusion of this research was that mechanisms other than those investigated were responsible for the performance of the *Bass Trap*.

1.3.2 The *Bass Trap* as a Large Porous Absorber

Second to the dissipation of low frequency sound energy through panel absorption, the next most obvious mechanism responsible for the performance of the *Bass Trap* is the huge amount of mineral wool and cotton waste felt used as a covering for the panels and as part of the multi-layer wall. By lining both sides of the 3.6 m^2 panel with felt, a large surface area of porous absorbent is introduced into a proportionally small volume of room. In addition, the outer layer of the multi-layer wall is also a 4 cm thickness of felt. The way in which sound is dissipated by porous materials has already been briefly touched on, though Cremer and Muller's standard text [1.7] is recommended for a more in depth discussion of the subject.

Sabine [1.8] was the first to investigate the effect on the RT_{60} of a room as a function of the surface area of absorbent material therein and his work is sufficiently well represented in acoustics texts [1.9] to make a detailed discussion here unnecessary. Sabine arrived at a formula connecting the volume of the room (V) and surface area (S) of a material with diffuse field absorption coefficient (α), with the RT_{60}. Only the result is quoted here as: $RT_{60} = \frac{0.161\,\mathrm{V}}{S\alpha}$. From this equation it can be seen that as the surface area and/or absorption coefficient increase, the reverberation time will become shorter. One should expect therefore the *Bass Trap* control room to exhibit a

low RT_{60} on account of the amount of cotton waste felt alone – this is investigated in *Chapter 3*.

1.3.3 The *Bass Trap* as an Acoustic Filter

The way in which the sound propagates in a *Bass Trap* control room is important in the consideration of possible absorptive mechanisms. Given the hard monitor wall and reflective floor and assuming near unity absorption of the back wall, the similarity between the room and a semi-infinite duct can be seen. Viewing the room in this way allows the performance of the *Bass Trap* to be evaluated in terms of the **attenuation** of the direct sound as it travels the length of the room. *Section 1.4* will include more on the choice of suitable descriptors for the *Bass Trap's* performance. Thin protrusions into an otherwise uniform duct, are widely used in air conditioning and exhaust silencers to reduce the transmission of sound from the source (air conditioning compressor) to the receiver (microphone in a recording studio) [1.10]. In the absence of absorbent material, this is achieved through frequency dependant reflection at the impedance discontinuity in the duct. Numerous references cite the way in which different arrangements of sidebranches, splitters (analogous to the panels in the *Bass Trap* room) and resonators yield varying degrees of sound attenuation [1.11]. This possible mechanism by which the *Bass Trap* works will be dealt with in *Chapter 4*.

An extension to a purely reactive filter system (such as periodic splitters in a duct) is to line the duct with an acoustically resistive material **and** employ splitters or resonators. Research by Lapin [1.12] describes how resonators (a Helmholtz[2] type is cited) can be used to transform the lightly damped low order modes into higher order modes which are more readily absorbed by the duct lining. The intense scattering of sound required to generate these higher order modes takes place at frequencies close to the natural frequency of the resonator. This situation is close to that of the side wall and ceiling *Bass Trap* and the investigation of *Chapter 6* will consider this mechanism further.

---

[2] A Helmholtz resonator is a rigid cavity with a small opening (known as the neck), the fundamental natural frequency of which is a function of the volume of enclosed air and the area and effective length of the neck.

1.3.4 Resonant Absorption Due to the *Bass Trap* Channels

This possible mechanism follows closely on from the previous section. The closed end channels formed by adjacent panels and the multi-layer wall will exhibit resonances on account of their 'effective' depth. As will be shown in *Chapter 5*, this 'effective' depth is not easily related to the depth of the angled panels or the distance they protrude from the wall. At odd integer multiples of a ¼ wavelength, the reflected sound from the wall will be in anti-phase with the incident sound at the opening (or mouth) of the channel. The acoustic impedance at this point and at these frequencies, will be purely real, i.e. governed entirely by the acoustic resistance of the channel and a maximum in absorption will occur. Whilst the relevance of this to the rear wall *Bass Trap* can be readily seen (as the sound is close to normally incident), the channel resonance also has an impact on the transmission of sound down the room.

An undesirable phenomenon was noted in theatres and concert halls in the early 1960s that is appropriate to the discussion in this section. It was widely reported that a listening position on the balcony of a concert hall was far superior to one in the stalls. The complaint was that in the latter position, the sound appeared to be lacking in low frequencies. Schultz and Watters [1.13] and Sessler and West [1.14] were those responsible for the first extensive research into the matter. The only physical difference that could be identified was that when seated in the balcony, the direct sound is the predominant source, whereas the sound would have to travel at close to grazing incidence over a number of rows to arrive at a seat in the stalls. Measurements in concert halls and using $^{1}/_{10}$ scale models confirmed that low frequencies were attenuated by up to 20 dB over a two octave bandwidth. The conclusion of both investigations were that the primary effect responsible for the attenuation was a ¼ wavelength resonance operating between the floor and the top of the seat. A secondary effect was noted at higher frequencies, that was attributable to diffraction from the top of the seats. The existence of an acoustic surface wave was proposed by Schultz as another possible mechanism, though a lack of suitable in situ concert hall measurements prevented any firm conclusions on the subject. One of the conclusions of Bradley's research [1.15] was that at larger angles of incidence the ¼ wavelength resonance was prevalent, whilst nearer grazing incidence a ½ wavelength resonance between seat rows is more efficiently excited.

From this brief discussion one can see how research into so called 'seat dip' has a direct bearing on the side wall *Bass Traps*, indeed the mechanisms identified may contribute to the attenuation of sound in the control room. *Chapters 5 – 7* will explore the possibility of a seat dip related attenuation further.

1.3.5 Absorption Due to a Lined Duct Attenuation

This mechanism by which the *Bass Trap* may absorb sound will only be mentioned in passing, as the subject was dealt with to a certain extent in [1.6]. As sound travels between the *Bass Trap* panels, it will be attenuated in the same way that ducts lined with absorbent material attenuate sound as it propagates along an air conditioning conduit. More detailed discussion and presentation of experimental results is given in Ingard's work [1.16] and only selected examples are given here as to the degree of absorption that can be expected from a *Bass Trap* channel. Below the cut-on frequency of the duct, where only plane waves can propagate[3] the attenuation of sound is poor, as the particle velocity normal to the duct boundary is not significant. This is especially true at low frequencies where the wavelength of sound is many times greater than the thickness of the lining. Of the four main variables associated with porous materials [1.7], it is the resistivity that is most important in choosing the most effective duct lining. Ingard shows that if the resistivity σ of a lining of thickness d is too low such that $\sigma < \frac{2\rho_0 c_0}{d}$, the low frequency attenuation will be minimal. Thus for the *Bass Trap* panel covering 4 cm thick, the resistivity needs to be in excess of 2×10^4 Pa s m^{-2} if it is to introduce any useful attenuation of the primary wave at low frequencies.

1.3.6 Oblique Incidence Absorption of the Multi-Layer Wall

Until now, little mention has been made of the role of the multi-layer wall, which itself is the result of decades of empirical design. Measured values of RT_{60} of a control room with only the multi-layer wall clearly show that it is a very significant element of the *Bass Trap* [1.2]. The total depth of the wall is around 35

---

[3] Strictly speaking, a plane wave cannot propagate along a duct with non-rigid boundaries because of the requirement of non-zero particle velocity normal to the wall, instead it is referred to as primary wave.

cm, a considerable loss of space that must be justified by a high absorption coefficient particularly at low frequencies. The construction of the wall, illustrated in *Figure 3.3* suggests that the combination of panels acting as limp masses and air spaces providing a compliance may result in a low frequency absorption dominated by a single degree of freedom resonance. In addition, some coupling between the pressure field in the *Bass Trap* channel at the wall and the wave bearing panels may introduce a degree of panel absorption. In the light of [1.5] however, a significant force (i.e. a large pressure acting on a small area) would be required to yield such an effect. Results pertaining to this are presented in *Chapter 7.* In order to ascertain the influence the multi-layer wall has on the total performance of the *Bass Trap* it needs to be modelled. In his paper, Guy [1.17] uses earlier work [1.18] on modelling porous materials to show how the absorption coefficient of complicated structures can be predicted. It is this work that is used in *Chapter 3* to investigate the effectiveness of the multi-layer wall. Guy's model is not limited to the normal incident acoustic characteristics of a multi-layer wall, as it can be extended to account for, among other things, coincidence effects in panels, a phenomenon associated with sound incident at oblique angles – a situation that may be encountered given the waveguide effect of the panels.

1.3.7 Summary

The mechanisms identified in the previous sections outline some of the possible ways in which the *Bass Trap* absorber is working, though they do not represent an exhaustive list. From the research described in the following chapters it will be seen how different avenues of investigation become apparent as the work progresses and results are obtained.

The concluding section of this introductory chapter will consider, in the light of the mechanisms discussed, the most appropriate means of quantifying the performance of the *Bass Trap.*

1.4 Suitable Descriptors for the Effectiveness of the *Bass Trap*

When Sabine introduced the RT_{60}, he provided a subjectively relevant way of quantifying an aspect of the acoustic behaviour of a room. A measure of frequency dependent reverberation time gave an immediate idea of how music would

be perceived in a concert hall, or how intelligible a lecturer might be if a listener is sat at the back of a lecture room. The purpose of this section is to explain and justify the quantities that will be used in the following chapters to describe different elements of the *Bass Trap*. In *Chapter 3* measured values of RT_{60} of a control room are presented and compared with theoretical values based on the size of the room and the specific design of the *Bass Trap*. However, such a global measure is unable to quantify the acoustic properties of different parts of the *Bass Trap*, parts which are effective in different ways. *Chapters 4 & 6* investigate the use of the *Bass Trap* on the side walls, while *Chapters 5 & 7* consider the effect of using it on the rear wall. The distinction between the two is made also in the way their performance is evaluated.

1.4.1 Rear Wall *Bass Trap* Descriptor

Referring back to the philosophy of the *non-environment* room, one will recall how the aim is to have the direct sound pass the listening position once, after which point it is absorbed by the boundary it is incident upon. In such a room, the sound field at any one point is dominated by the direct sound, as reflections are negligible and thus a reverberant sound field never strictly exists. In view of this, the sound will propagate down the room from the loudspeakers to the rear wall, with some (as yet unquantified) absorption due to the side walls.

At the rear wall, the wavefront will be largely plane (i.e. little variation in pressure amplitude across the width of the room) as the two spherically radiating sources at the front of the room would have sufficiently superposed at this position. The wavefront can definitely be considered plane across the *Bass Trap* channels, which are about 40 cm in width. A suitable description of the effectiveness of the rear wall *Bass Trap*, given the design criteria, is the ratio of reflected to incident sound. A term introduced by Sabine and used many times in this chapter already, is the sound absorption coefficient – the fraction of the incident sound power that is not reflected at the boundary [1.19]. Thus it is this measure, together with the surface normal acoustic impedance[4] that is used in connection with the rear wall *Bass Trap*.

[4] The surface normal acoustic impedance is the complex ratio of pressure to normal particle velocity at the face of a boundary, normally expressed in units of $\rho_0 c_0$, the characteristic impedance of air.

1.4.2 Side Wall *Bass Trap* Descriptor

The purpose of any measure used to describe the performance of the side wall *Bass Trap* is to quantify the attenuation of sound as it propagates from the front to the rear of the room. The direction of propagation is important. In this context it is the difference between the positive going wave (defined here as front to rear) at the loudspeakers and the positive going wave at the rear wall that is of interest. Munjal [1.11] describes this quantity as the Transmission Loss (TL). The results presented for the side wall *Bass Trap*, therefore, will be in terms of transmission. This will quantify in dB the difference in pressure amplitude between the positive going wave propagated by the source and the positive going wave after it has passed the side wall *Bass Trap*. This will allow easy analysis of the effectiveness of the side walls in attenuating the sound along the room.

CHAPTER 2

Evaluation of a *Bass Trap* Control Room

Introduction

In the chapters to follow, possible mechanisms by which the *Bass Trap* absorbs sound will be investigated. As part of this research, the performance of a *Bass Trap* control room recently built by Mr Newell near Porto, Portugal, was evaluated objectively and subjectively. The objective evaluation is based on in situ transfer function measurements made by the author in August 2001. Given that the control room was visited in person, comments on the perceived acoustic quality will also be made once the measurements have been presented.

2.1 Description of the Control Room

The design of the room is typical of one where space is limited, with angled panels only suspended from the ceiling and in front of the rear wall. The side walls are constructed from a number of different layers of mineral wool, plasterboard and mineralised rubber matting. The performance of this multi-layer wall is included in the investigation of *Chapter 3*. As a near anechoic environment is uncomfortable to work in, the floor and monitor wall are reflective. The placement of these reflective surfaces, however, does not compromise the performance of the room at the listening position, as long as the walls (particularly the rear wall) and ceiling are sufficiently absorptive. The right-front of the room is illustrated at the top of *Figure 2.1*. Access to the machine room is via a sliding glass door and a window has also been incorporated to allow the equipment to be viewed from within the main room. Above the ceiling cloth are the hanging panels, orientated in the manner described in *Figure 1.1* of the previous chapter. The bottom part of *Figure 2.1* shows a photograph of the left-rear part of the room. The side wall includes the door and window into the corridor that runs alongside the control room. Behind the rear wall cloth covering are the 1.2 metre deep hanging panels at an angle of 40^{0}.

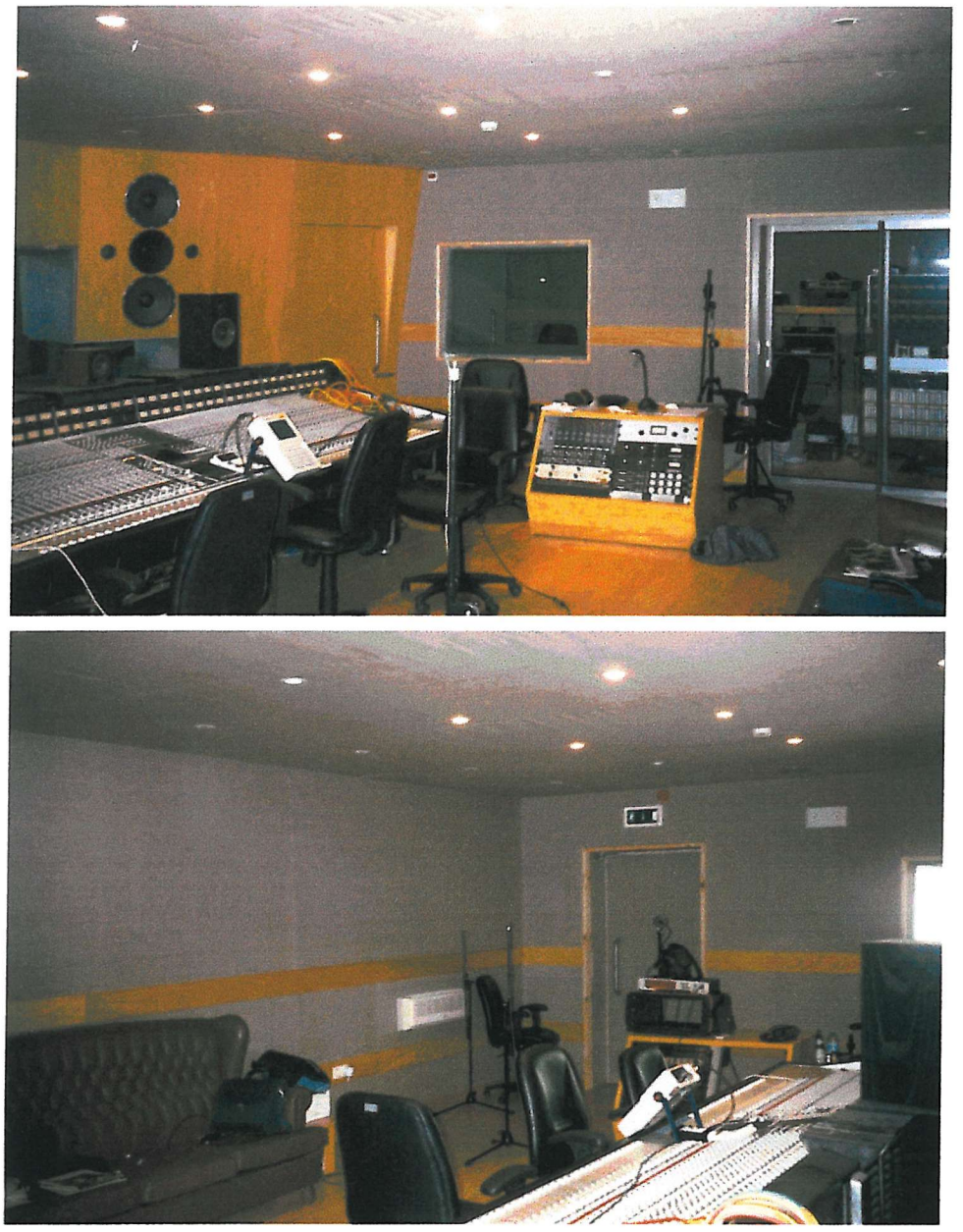

Figure 2.1 – Photographs showing the Porto control room from two positions

2.2 Experimental Evaluation

In this section an explanation of the measurement procedure and data manipulation will be given, after which the results are presented.

2.2.1 Description of the Measurement Procedure

The purpose of the measurements was to provide an objective measure of the performance of the room at a number of different positions. A broad band

noise source was used as the test signal, via the mixing console, power amplifiers and loudspeakers. Only the left hand loudspeaker was used in the measurements.

The quantity measured was the transfer function between the input to mixing console (channel 1 of the FFT analyser) and a microphone 1.5 metres above the floor, in one of nine points in the room (channel 2) – this will be referred to as the room transfer function. As the loudspeakers themselves were not of interest, an additional measurement was made between the input to the mixing console (channel 1) and a microphone a couple of centimetres from the low frequency drive unit (channel 2) – the loudspeaker transfer function. *Figure 2.2* shows a photograph of how this measurement was made.

Division of the room transfer function by the loudspeaker transfer function, allows the contribution from the measurement equipment (microphone, amplifiers etc.) and loudspeaker to be accounted for, resulting in a transfer function which characterises

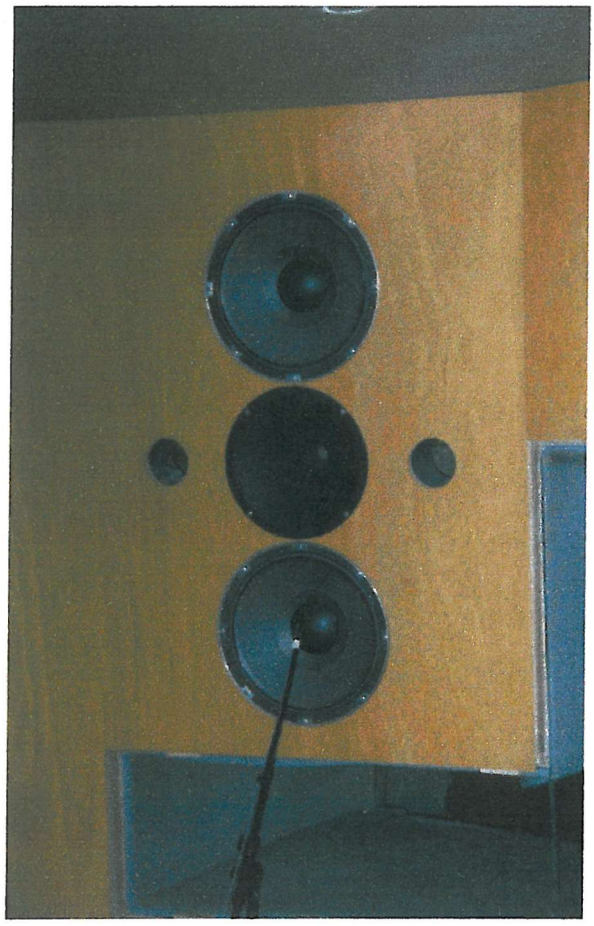

Figure 2.2 – Photograph describing the loudspeaker transfer function measurement

the room alone. *Figure 2.3* describes the control room in plan view, with the nine microphone positions labelled *a, b, c, . . . i*; position *b* will be referred to as the engineer's listening position, as this is typically where the recording engineer sits. In the following section, explanation will be given of how the measured data was used to provide a meaningful assessment of the performance of the room.

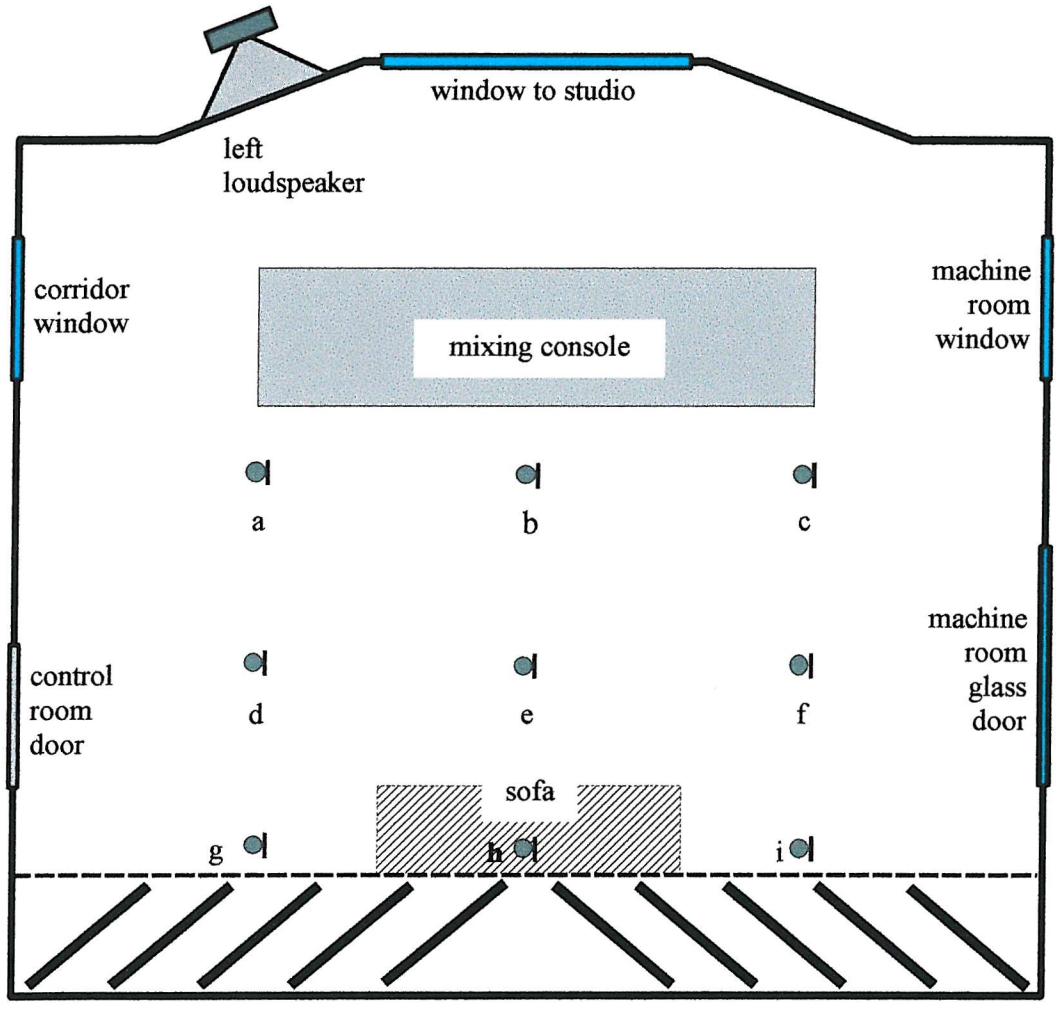

Figure 2.3 – Plan view of Porto control room and microphone positions

2.2.2 Filtered Schroeder Plots as a Measure of Room Response

As mentioned in *Section 1.4*, the time taken for a continuous noise source, stopped abruptly at $t = 0$, to decay by 60 dB is a very useful objective measure of the acoustic performance of a room. Given the description of the RT_{60} it is not

surprising that the traditional means of measuring it is by the *interrupted noise method*, where the sound pressure at a point in the room is recorded, from the moment the noise source is switched off and subsequently converted to dB. The disadvantage of this method, is that the average of many such measurements is necessary to give a suitably smooth decay curve. Schroeder [2.1], however, showed that the ensemble average of an infinite number of decay curves obtained by the interrupted noise method could be found by the backward integration of the squared impulse response at the position of interest. The resultant curve, or Schroeder plot, provides a far clearer measure of the rate of decay of the squared sound pressure and is therefore employed in this chapter as a means of evaluating the reverberation time at the different positions in the control room.

In order to calculate the Schroeder plots from the measured transfer function, described in *Section 2.2.1*, the data was manipulated in *MatLab*. Firstly, the impulse response for each transfer function was calculated by performing an inverse Fourier transform. This was then filtered using a 4^{th} order elliptical *MatLab* filter, with 0.5 dB of ripple in the passband and a –40 dB stopband. The frequency limits of the filter were chosen as 40 and 400 Hz for the wideband Schroeder plots and $f \times 2^{\pm\frac{1}{6}}$ for the $^1/_3$ octave bands centred on frequency f. Once filtered, the impulse response was squared and integrated backwards. To present the decay curve in dB, the logarithm (base 10) of the squared impulse response was multiplied by 10.

2.2.3 Schroeder Plots at Various Room Positions

Five of the nine measurements will be shown in this section to demonstrate the variation in reverberant decay, across the width and length of the room. A Schroeder plot of the elliptical filter alone is also shown to demonstrate its influence on the measured result. Generally the product of filter bandwidth and room reverberation time must exceed 10 to ensure the filter itself is not included in the result [2.2]. While this is the case in the wideband Schroeder plot, it is not for all of the $^1/_3$ octave bands result shown in the following section.

Figure 2.4 shows the reverberant decay at three positions in the centre of the room, starting at the listening position and moving backward to the rear wall (*b, e and h* in *Figure 2.3*). The traces are very similar to one another, suggesting that there is little spatial variation in reverberant decay, front to back. Given that the room is largely

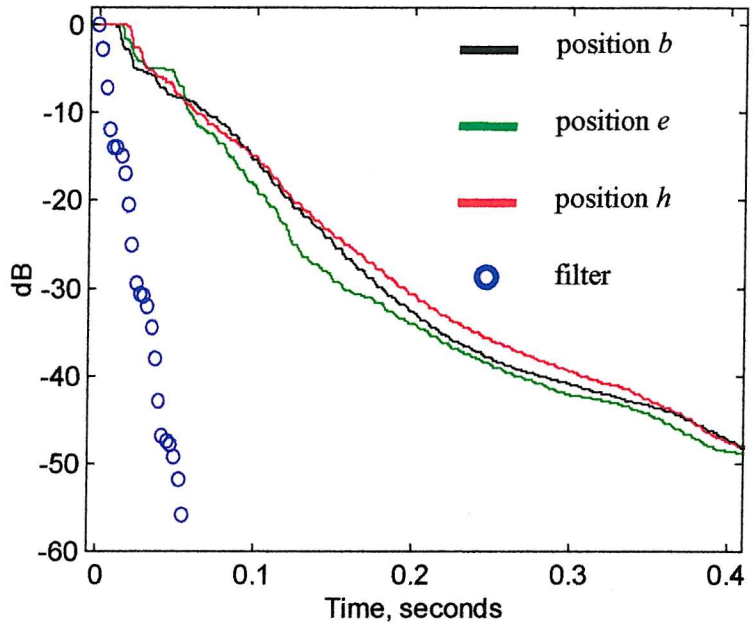

Figure 2.4 – Schroeder plot at three positions for 40 < f < 400 Hz

symmetrical about its centre line (front to back), this result is not altogether surprising. The time taken for the sound to decay by 30 dB, a useful indicator of the subjective performance, is only 0.18 seconds at the listening position. Such a short reverberation time, in this low frequency range, should allow the recording engineer to monitor the reproduced material with little adverse contribution from the room. The similarity in reverberant decay at different positions suggests that the modal activity in the room is well damped by the *Bass Trap* design.

Figure 2.5 shows the Schroeder plots at the middle and the extremities of the mixing console (positions *b, a and c* in *Figure 2.3*). The difference between the traces is greater than the previous result, with the sound at the left hand end of the mixing console taking 80 ms less time to decay to –40 dB, than at the primary listening position. However, with the presence of large items of furniture (the mixing console being the most significant), specular reflections are unavoidable and thus some spatial variation in reverberation is to be expected.

In the following section, the Schroeder plot at the listening position is filtered in narrower frequency bands to give $^1/_3$ octave values for RT_{30} and RT_{60}.

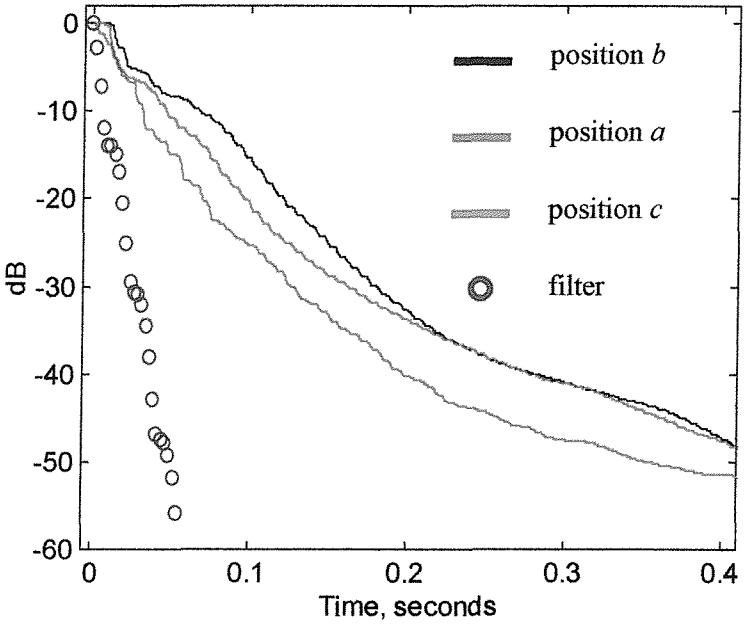

Figure 2.5 – Schroeder plot at three positions for 40 < f < 400 Hz

2.2.4 Filtered Reverberation Times at the Listening Position

The reverberation times presented in this section were calculated from the Schroeder plot by finding the time taken for each $^1/_3$ octave band to decay by 30 and 60 dB. The RT_{30} is included primarily because of its subjective importance. The centre frequencies of the bands are logarithmically spaced from 20 Hz to 1 kHz. At the low end of the spectrum, the $^1/_3$ octaves span only a narrow band of frequencies, which together with the short decay time of the room, compromises the aforementioned bandwidth-time product criteria. As a comparison therefore, the RT_{30} and RT_{60} is given for the filter alone.

Figure 2.6 shows the reverberation times at the listening position and *Figure 2.7* the same quantities for the filters. An exponential decay of squared pressure results in a straight line reverberation time characteristic, when plotted on a dB scale. In such a situation, the value for the RT_{60} is twice that of the RT_{30}. *Figure 2.6* however shows that this clearly isn't the case with the Porto control room, with the RT_{30} being around a factor of 5 shorter than the RT_{60}. Further comment will be made on this in the next section. The time taken for the sound to decay by 30 and 60 dB is fairly constant across the frequency range shown, with average values of around 0.1 and 0.5 seconds

respectively. An earlier reverberation time measurement of a different *Bass Trap* control room, showed far lower values above 100 Hz [2.3], though the room in question contained no equipment or furniture.

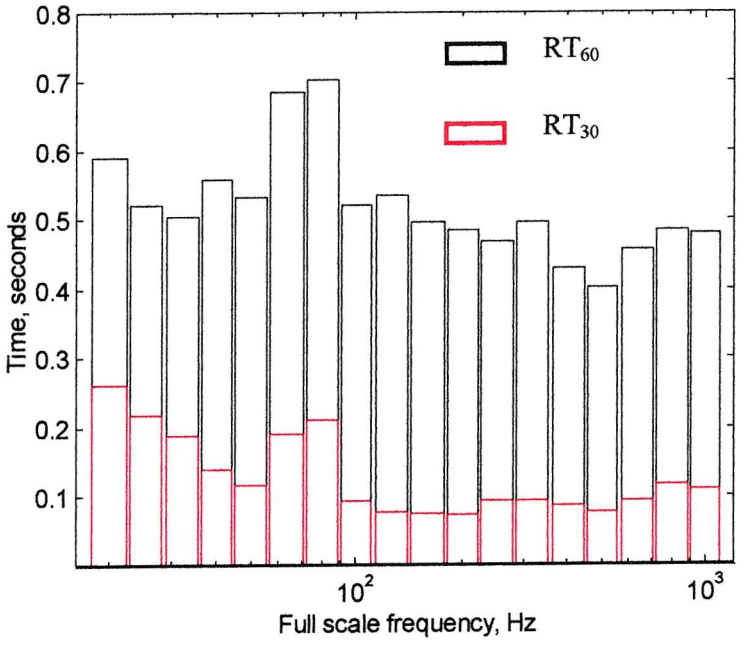

Figure 2.6 – Comparison of reverberation times at the listening position

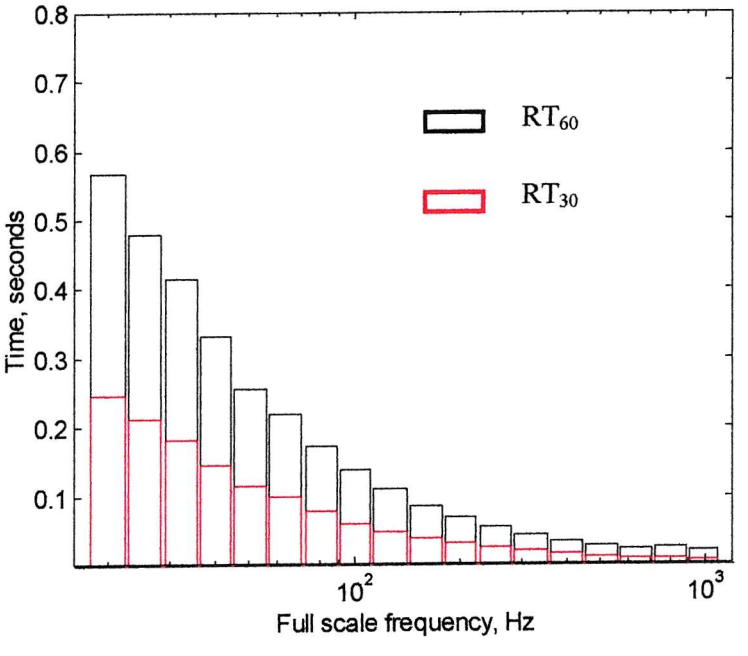

Figure 2.7 – Comparison of reverberation times for the $^1/_3$ octave band filters

The presence of large reflective surfaces, in an otherwise very absorptive room, will undoubtedly have a large influence on the reverberation time. Judging by the values for RT_{30}, any reflections present only affect the end of the reverberant tail, with the all important early part of the curve decaying very quickly. Given the aforementioned criteria, the effect of the filters suggest that for the RT_{30}, only the $^1/_3$ octave bands above 200 Hz are reliable. As the values for RT_{60} are that much longer, the results above 100 Hz can be considered as unaffected by the filters.

2.2.5 Reverberant Decay Characteristic

The reverberation time results of the previous section identified a decay that is not a constant gradient when plotted on a dB scale. Further discussion will be given in this section as to the possible reason why this might be. Referring to *Figure 2.6*, it can be seen that in the 125 Hz $^1/_3$ octave band, the ratio between the RT_{60} and RT_{30} is the greatest (535 and 78 ms respectively). The Schroeder plot of this frequency band is shown in *Figure 2.8* as the most extreme example of a non-straight line decay. As hypothesised in the previous section, the decay curve exhibits a significant 'knee' at –45 dB and 0.15 seconds, resulting in two distinct decay rates. Such deviation from a straight line decay is known as 'sagging' and various reasons

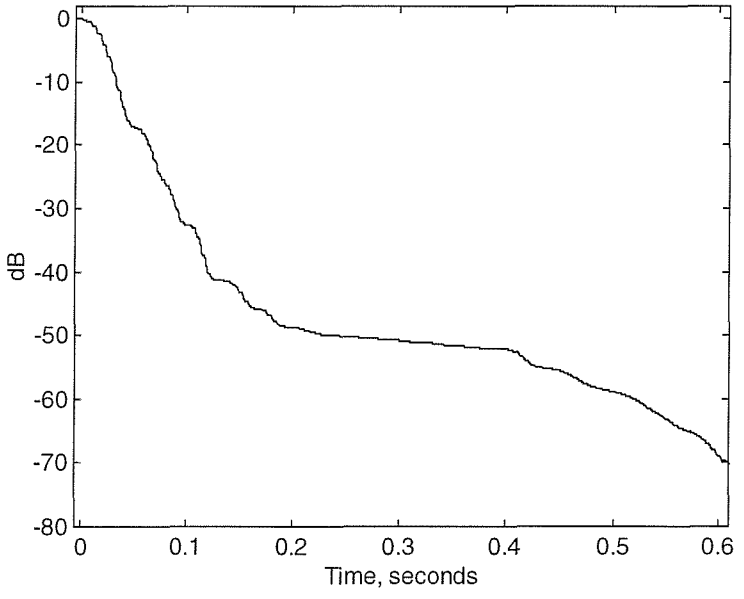

Figure 2.8 – Schroeder plot at the listening position for the 125 Hz $^1/_3$ octave band

can be given by way of explanation [2.4]. In the absence of any measurement error, sagging of the reverberant decay can be the result of more than one damping constant in the room. This non-isotropic sound field has been shown to be related to the distribution of absorption within the room, a feature that is very contrasting in the *Bass Trap* control room. In addition, the large mixing console will most probably contribute to the lower damping constant responsible for the reverberant decay after 0.15 seconds.

Another possible reason for the 'sagging' was identified in an earlier investigation into *Bass Trap* control rooms. As mentioned in *Section 1.3.1*, Soares [2.5] noted that the reverberant decay, in the scale model of a *Bass Trap* room used in his experiments was also not a straight line of dB vs. time. The conclusion was that sound was 'trapped' within the array of panels on the side and rear walls. He hypothesised that the sound was delayed within the traps and emerged a short time later, resulting in the longer reverberant tail. It was as if some of the reverberant energy was 'scooped out' of the early decay and added to the end. The major difference between his experiments and the measurements presented here is that the former employed no absorbent material, as porous material is not easily scaled down by a factor of 10. In the absence of any absorbent, the *Bass Trap* design is purely reactive and energy storage can be the only means of obtaining any kind of reverberant decay. By contrast, however, the sound trapped in the Porto control room is unlikely to re-emerge into the room with any significant energy content, because of the large amounts of absorbent material covering the panels and the multi-layer wall. Nevertheless, the knee of *Figure 2.8* is at –45 dB and this could be attributed to the small amount of sound that is not absorbed within the *Bass Trap* system.

The most likely explanation, however, for the sagging reverberant decay is an insufficient signal to noise ratio. As no ear defenders were available, the white noise source was limited to around 80 dB(A). In order, therefore, for a 60 dB dynamic range to be measured reliably, the noise floor of the studio would need to be less than 20 dB(A). Given the level of activity in the studio complex the day the measurements were made, it is unlikely that this figure was achieved. The result of this is seen in *Figure 2.8* as a levelling off of the decay curve, due to the addition of the noise floor with the desired signal from the loudspeakers. Due to a noise floor of around 30 dB(A) it is difficult to gauge the RT_{60} of the control room, without repeating the measurements. Whilst it is tempting to simply double the value of the RT_{30}, the

research cited in [2.5] suggests that this may not be valid. What is clear from the results presented in this chapter, is that the early part of the reverberation decays very quickly and as such, a listener should be aware of very little contribution from the room itself.

2.3 Conclusions and Subjective Impression

As well as making the measurements described in the previous sections, the author was also able to assess the acoustic quality of the control room by listening to familiar recordings. Recent popular music with prominent low frequency instruments (bass drum, bass guitar etc.) was used for this purpose and particular attention was given to how the room responded to the lower end of the frequency spectrum. The overwhelming impression was that all transients were clearly audible, with clear definition of the start and end of impulsive sounds (the bass drum is a good example of this). No build up of low level, low frequency, reverberation was noticeable and aspects of the recording, masked in other monitoring environments were now audible. Moving around the room did not unduly effect the subjective impression, with no apparent modal activity which would be heard as peaks and troughs at low frequencies. It would appear, therefore, that the perceived performance of the room correlates well with the measured results.

Concluding these results, a number of comments can be made. Firstly, the Schroeder plots at different positions show that little spatial variation exists in the decade above 40 Hz, suggesting that modal activity is well damped. Secondly, the reverberation time is relatively constant from 20 Hz to 1 kHz, despite the presence of large items of furniture. Thirdly, the early part of the reverberation decays very rapidly, resulting in low values for RT_{30}. As previously mentioned, the measurements made do not allow clear evaluation of the reverberant decay beyond –50 dB. Even from a subjective viewpoint, it is unclear as to the extent to which this low level reverberant tail will be audible, as only a small sample of music was used in forming the opinion described above.

CHAPTER 3

Diffuse Field Model of a *Bass Trap* Control Room

Introduction

The investigation described in this chapter will consider a possible mechanism by which the *Bass Trap* absorber works. The results and conclusions presented will provide a foundation on which the following chapters will build. The investigation will be primarily concerned with modelling two distinct aspects of the absorber in order to obtain a measure of its effect on the reverberation time of a room. These theoretical results will be compared with physical measurements made in the room on which the theoretical model is based.

3.1 Room Measurements

The recording studio control room that is the subject of this investigation utilises the *Bass Trap* absorber on its rear wall and ceiling only, as space constraints don't allow it to be employed on the side walls. It was designed and built by Mr Philip Newell in the town of Tio Pete, Portugal. A scale diagram of the control room is shown in *Figure 3.1.* In a continuing effort to understand how the *Bass Trap* works, Mr Newell made a series of transfer function measurements between the output of the loudspeaker and the intended recording engineer listening position, at ten different stages of the room's construction. It was hoped that such a set of measurements would shed light on the effect different parts of the *Bass Trap* design have on the acoustic behaviour of the room [3.1]. From the measured transfer functions $^1/_3$ octave band reverberation times (RT_{60}) were calculated. Given that the previous chapter identified that an insufficient signal to noise ratio can compromise the results, the RT_{60} quoted in this chapter is derived from the values of RT_{30}, assuming a straight line decay of dB with time. The RT_{60} is the key descriptor of the room used in this chapter. For the purposes of this investigation, it is only the final four measurements that are presented and used as a comparison with the theoretical model.

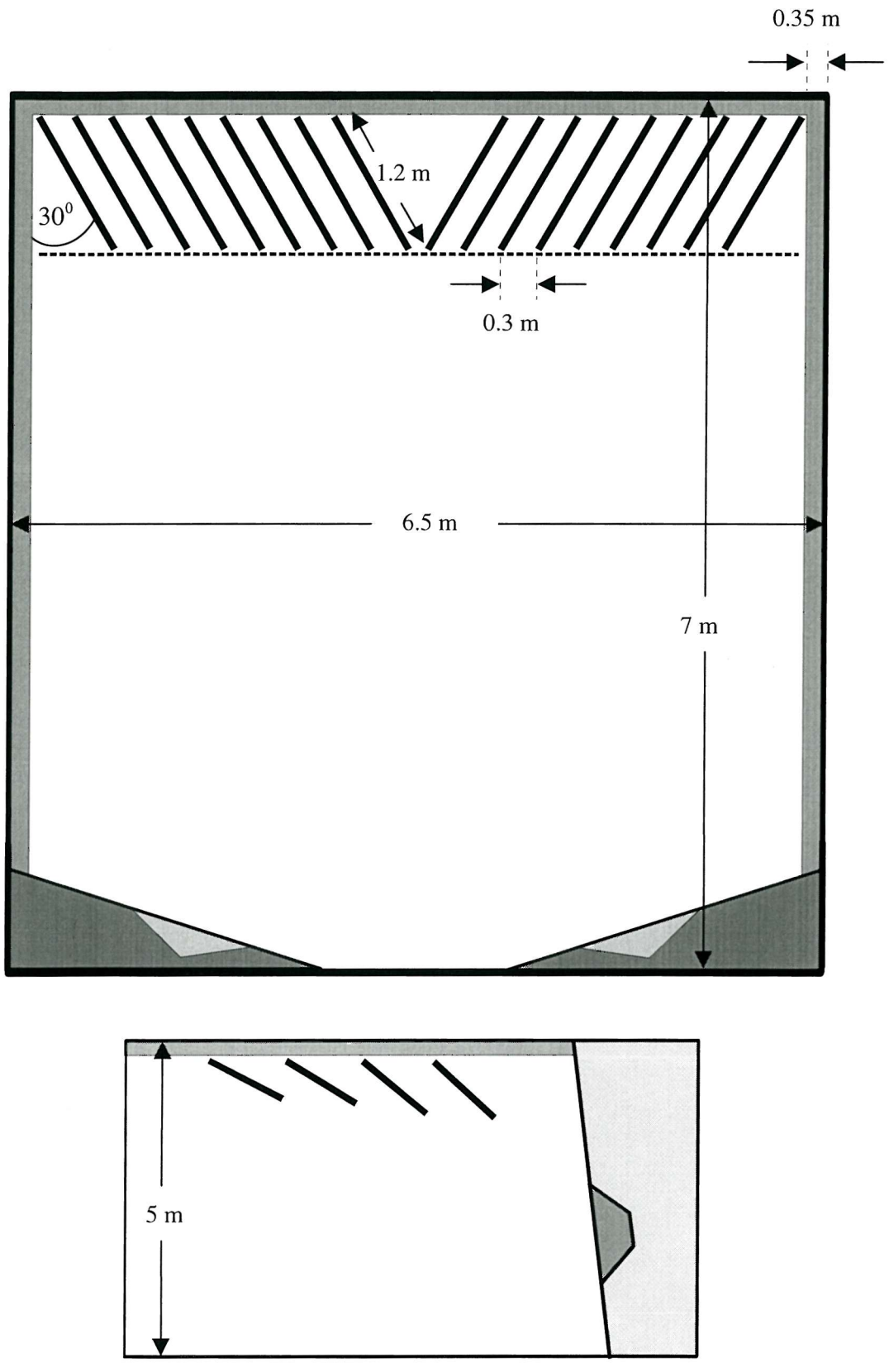

Figure 3.1 – Scale diagram (plan and section) of the Tio Pete control room

3.2 Introduction to the Theoretical Model

The systematic measurement of the control room during construction not only provides insight into the performance of the *Bass Trap*, it can also be used as a powerful tool in testing a theoretical model. In choosing the way in which to model the *Bass Trap* in the aforementioned room, two considerations were made. Firstly, the model must allow direct comparison with the measured results, i.e. be able to calculate a frequency dependent reverberation time. Secondly, it should provide a suitably basic starting point which the rest of the research can expand upon.

The model used is based on a diffuse field model of sound in the control room. Considering the sound field in this way allows the Sabine formula for reverberation time [3.2] to be used – thus the first requirement is met.

In addition to this, the Sabine formula is suitably simple, as it requires a knowledge of only the surface area of a given diffuse field absorption coefficient and the volume of the room. As will have been evident from the generic description of the *Bass Trap* in *Chapter 1*, the absorber uses large amounts of cotton waste felt as a covering for the panels and as part of the construction of the multi-layer wall. As such, the theoretical model begins with the calculation of the diffuse field absorption coefficient of both the cotton waste felt and the multi-layer wall. As the complex geometry of the *Bass Trap* (angle, spacing and depth of panels) is ignored, the theoretical model provides a basic start point for the remainder of the research and satisfies the second requirement.

The model will be constructed in three parts: first the diffuse field absorption coefficient of the cotton waste felt will be found, secondly (using this quantity) the diffuse field absorption coefficient of the multi-layer wall will be calculated. Finally, the RT_{60} of the room will be calculated.

3.3 Model of the Cotton Waste Felt

The cotton waste felt represents an integral part of the *Bass Trap*. It is a porous material belonging to the same group of materials as mineral wool. As described in *Chapter 1*, such porous materials are widely used in noise control situations to absorb sound by means of viscous losses caused by oscillatory particle velocity in the pores. The purpose of this section is to measure and quantify in more general terms the acoustic properties of the cotton waste felt.

3.3.1 Calculation of the Random Incidence Absorption Coefficient

Acoustically, porous absorbers are typically quantified by their surface normal acoustic impedance. This measure is the complex ratio of the pressure and normal particle velocity at the surface of the material. As many porous materials can be assumed to be locally reacting [3.3], the random incidence absorption coefficient may be found from a knowledge of the surface normal acoustic impedance, assuming this quantity to be independent of angle of incidence. For details of the following analysis, the reader is referred to [3.4] and [3.5].

The oblique incidence complex reflection coefficient takes the form $R(\theta)=\frac{z\cos\theta-\rho_0 c_0}{z\cos\theta+\rho_0 c_0}$ from which we may write $\alpha(\theta)=\frac{4\rho_0 c_0 r\cos\theta}{(r\cos\theta+\rho_0 c_0)^2+(x\cos\theta)^2}$, where r and x are the real and imaginary parts of the surface normal acoustic impedance, respectively.

In order to arrive at a value for diffuse field absorption coefficient, consideration must be given to both the increased probability of sound being incident at near grazing and the associated reduction in projected surface area of the boundary in question. This leads to a weighted average given by the integral $\alpha_d = 2\int_0^{\frac{\pi}{2}}\alpha(\theta)\cos\theta\sin\theta\,\mathrm{d}\theta$ which if more usefully expressed as $\alpha_d = 2\int_0^1\alpha(\cos\theta)\cos\theta\,\mathrm{d}(\cos\theta)$ allows the diffuse field absorption coefficient to be expressed in terms of surface normal acoustic impedance

$$\alpha_d = 8\int_0^1 \frac{\left(r/\rho_0 c_0\right)\cos^2\theta}{\left(\left(r/\rho_0 c_0\right)\cos\theta+1\right)^2+\left(\left(x/\rho_0 c_0\right)\cos\theta\right)^2}\,\mathrm{d}(\cos\theta)$$

which may be solved explicitly.

From this brief discussion it is clear that one of the required quantities for Sabine's reverberation formula can be calculated from the surface normal acoustic impedance. The way in which this is found for the felt is the subject of the next section.

3.3.2 Measurement of Surface Normal Acoustic Impedance

The first step in modelling the control room was to measure the surface normal acoustic impedance of the cotton waste felt. A standard experimental procedure [3.6], qualitatively explained below, was employed to do this.

A 17 mm thick sample of the felt was placed flush against the rigid termination of a 100 mm diameter tube. A loudspeaker was placed at the opposite end to the termination, the input signal to which was white noise. A moveable microphone within the tube was used to measure the pressure at two points a known distance from the face of the sample. By measuring the transfer function between the input to the loudspeaker and the output of the microphone at these two points, the surface normal acoustic impedance of the sample can be found. *Appendix 2* gives a full explanation of the analysis involved. The result for the measured normal absorption coefficient of the felt will be shown later together with the theoretical value derived in the following section.

3.3.3 Theoretical Surface Normal Acoustic Impedance

In this section a theory will be presented from which the surface normal acoustic impedance of a porous material can be calculated from a knowledge of its resistivity. Research by Delany and Bazley [3.7] and later work by Qunli [3.8] showed that there is a direct relationship between the resistivity of a porous material and its propagation constant and surface normal impedance. In this situation, however, it is the resistivity that is unknown and the surface impedance that is known (having been measured experimentally), so the equations are used in reverse. A program was written in *MatLab* which outputs a frequency dependent normal absorption coefficient for two input variables: resistivity and thickness of porous material. While the thickness variable was kept constant at 17 mm, the resistivity was changed until the theoretically predicted absorption coefficient approximated to the measured value. When this match was achieved the value for the resistivity of the felt had been found. This then would allow the absorption coefficient for different thicknesses of the felt to be found. The power relations, derived by Qunli and used in the program are given in the table overleaf.

Acoustical properties	Power relations
$\frac{R}{\rho_0 c_0}$	$1+0.209\,\mathrm{B}^{-0.548}$
$\frac{X}{\rho_0 c_0}$	$-0.105\,\mathrm{B}^{-0.607}$
$\frac{\alpha}{k_0}$	$0.163\,\mathrm{B}^{-0.592}$
$\frac{\beta}{k_0}$	$1+0.188\,\mathrm{B}^{-0.554}$

Here R is the characteristic acoustic resistance, X is the characteristic acoustic reactance, α is the attenuation constant, β is the phase constant and k_0 is the free field wavenumber. B is the non-dimensional variable given by $\frac{f\rho_0}{\sigma}$, where f is the frequency (Hz) and σ is the resistivity (MKS units). The characteristic impedance of air is given by the product of its density and sound speed (ρ_0 and c_0 respectively) and is used to normalise the acoustic impedance of the felt. Thus for a given value of resistivity, the surface normal acoustic impedance of a rigidly backed absorbent of thickness d is given by : $z_L = z_a \coth(kd)$, where $z_a = R_a + jX_a$ and $k = \alpha + j\beta$. From this impedance, the normal incidence absorption coefficient is given by : $\alpha_n = 1 - \left| \frac{z_L - \rho_0 c_0}{z_L + \rho_0 c_0} \right|^2$.

3.3.4 Results of Measured and Predicted Felt Absorption Coefficients

In this section the frequency dependent normal and random incidence absorption coefficients for a 17 mm sample of the cotton waste felt are presented. *Figure 3.2* shows the three traces plotted on the same graph for ease of comparison. The figure shows the fit between the Qunli model and the measured result (red and black lines respectively). The absorption coefficient is typical of a medium resistivity porous material of this thickness [3.9], with a steady rise of absorption with frequency. The resistivity that was used in the *MatLab* program was 3.8×10^4 Pa s m^{-2} and this value is used in a later section to predict the absorption coefficient of a thicker sample of the felt used as a covering for the panels.

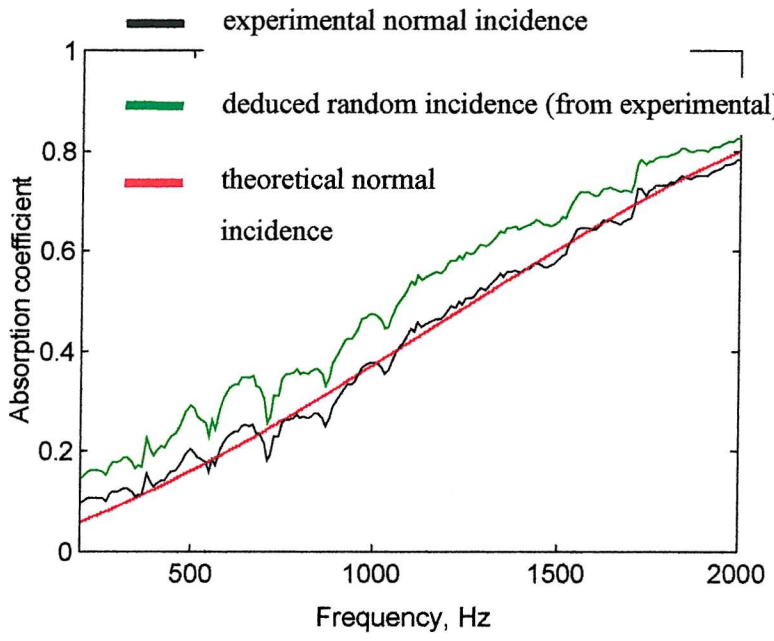

Figure 3.2 – Measured and predicted absorption coefficient of 17mm thick felt

It will also be used in the following section to help model the propagation of sound through the felt as part of the multi-layer wall.

3.4 Model of the Multi-Layer Wall

3.4.1 Physical Description of the Multi-Layer Wall

In *Chapter 1* it was shown that one of the key elements of the *Bass Trap* is a multi-layer wall that occupies the space between the structural shell and the hanging felt covered panels. The multi-layer wall is constructed from a number of different elements and is loosely based on the *Camden Partition* developed by the BBC in the 1950's [3.10]. The precise design of the multi-layer wall used in the Tio Pete control room is the result of many years of trial and error and the studio designers who advocate its use claim the acoustic performance is optimised [3.11]. *Figure 3.3* describes the cross section of the design used for the side walls. The design used on the ceiling is slightly different and extends only as far as the left hand air space, labelled *a* in *Figure 3.3*. The materials used can be split into three categories: panels, porous absorbent and vibration damping sheets. One layer is attached to the other by large staples and the large amount of mineral wool in the middle of the wall is held in place with a wooden stud frame. In addition to the

dimensions of the different materials, the table below gives the other properties required in the theoretical model.

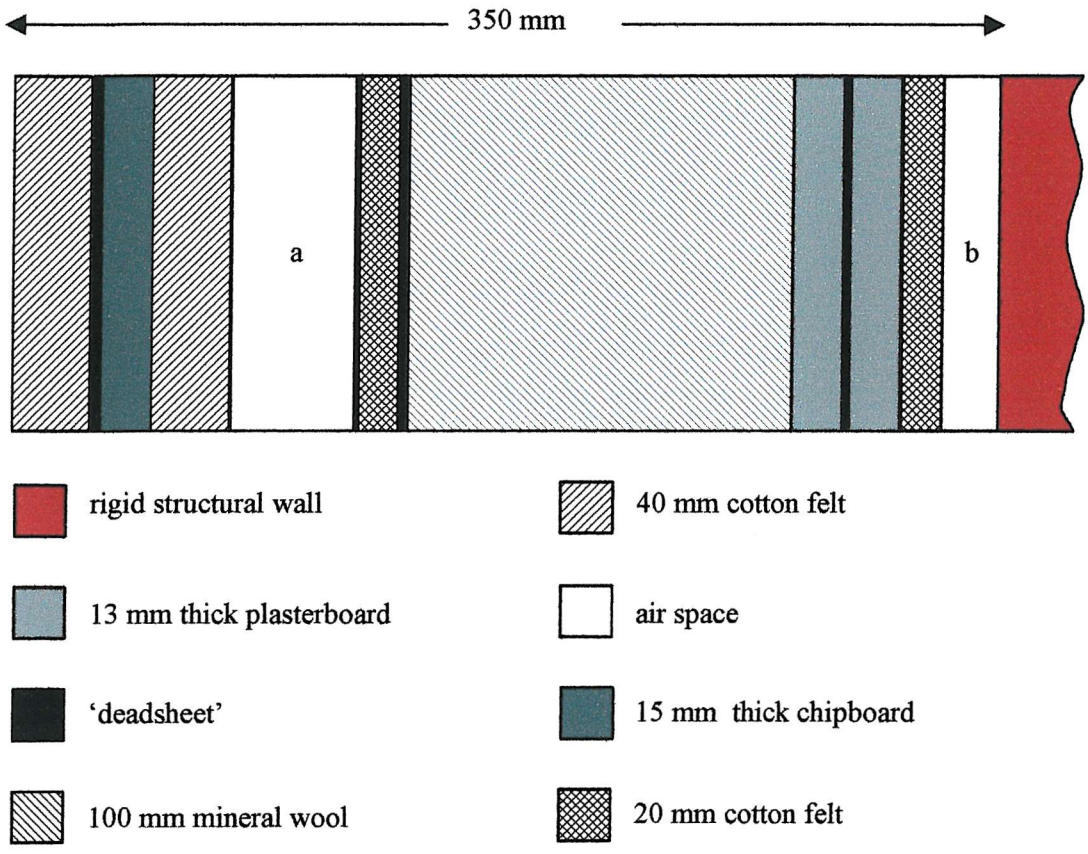

Figure 3.3 – Cross section of the Tio Pete multi-layer wall model

Material	**Thickness** (mm)	**Density** ($kg\,m^{-3}$)	**Mass/unit area** ($kg\,m^{-2}$)	**Resistivity** ($Pa\,s\,m^{-2}$)
Cotton waste felt	40 or 20	35	n/a	3.8×10^{4}
Mineral wool	100	40	n/a	4.5×10^{4}
Deadsheet	5	n/a	3.5 (two outer layers) 5 (innermost layer)	n/a
Plasterboard	13	1000	13	n/a
Chipboard	15	650	9.75	n/a
Air	50 (a) or 20 (b)	1.205	n/a	n/a

3.4.2 Theoretical Description of the Multi-Layer Wall

As with the cotton waste felt, the surface normal acoustic impedance of the multi-layer wall needs to be estimated in order to find the diffuse field absorption coefficient required in the Sabine formula for reverberation time. The way in which this is achieved, given the complicated structure of the wall shown in the previous section, is to use a model that builds on the work of Qunli.

In his paper, Guy [3.12] describes how the surface normal acoustic impedance of a multi-layer structure can be found through equations of impedance continuity at each layer junction and the characteristic impedance and wavenumber (if applicable) of the individual material layers. Considering *Figure 3.3* for example, one starts at the known surface normal impedance of the structural wall (assumed infinite) and works left through each layer. Two sets of equations are used in the model, one to characterise the different categories of layer, the other to describe the impedance continuity at each layer junction. The former are shown in the table below, where z_p is the characteristic impedance of the panels, z_a the impedance of the air or absorbent, k is the wavenumber (a complex value in the case of the absorbent) and M is the panel's mass per unit area. The complex variables required in modelling the absorbent materials are identical to those described in *Section 3.3.3*, where the acoustical properties are estimated from a knowledge of the material's resistivity.

Material layer	Impedance	Wavenumber
Panels and 'deadsheet'	$z_p = j\omega M$	n/a
Air	$z_a = \rho_0 c_0$	$k = \frac{j\omega}{c_0}$
Absorbent	$z_a = R_a + jX_a$	$k = \alpha + j\beta$

For the purposes of this investigation the chipboard, plasterboard and mineralised rubber matting (or 'deadsheet') are only considered as limp masses, thus unable to support flexural vibration. Justification for this will be given in *Section 3.5.2.1.*

The table below gives the equations from which a known impedance, z_R, together with the relevant material property, z_a, z_p, k, can give the surface impedance one layer to the left, z_L. In the case of the air and absorbent, d is the thickness of the layer.

Material layer	Layer surface impedance relationship
Panels and 'deadsheet'	$z_L = z_p + z_R$
Air and absorbent	$z_L = z_a \dfrac{\coth(kd) + z_a/z_R}{1 + (z_a/z_R)\coth(kd)}$

3.4.3 Absorption Coefficients for Multi-Layer Wall

The diffuse field absorption coefficients for the multi-layer side wall, ceiling and 4 cm sample of the cotton waste felt are shown in *Figure 3.4*, plotted with a logarithmic (base 10) frequency axis in order to make the extreme low frequency performance more clear. As explained before, the diffuse field absorption coefficient is calculated from the surface normal acoustic impedance, predicted by the model presented in the previous section.

Considering the multi-layer side wall first, a significant low frequency peak is noted, which itself comprises two resonances. The low frequency resonances at 25 and 55 Hz are caused by two mass-spring-damper systems within the wall. The panels comprise the mass elements while the two air spaces act as springs; the absorbent materials provide the damping which broadens the Q of the resonant peaks such that they blur into one. A normal incidence absorption coefficient of 0.3 at 25 Hz is very impressive given that the wall is only 0.35 metres thick. If only the 4 cm thick outer layer of felt were placed 0.35 metres from the wall, a peak in absorption would be expected at 243 Hz, due to a maximum in particle velocity occurring $\frac{\lambda}{4}$ from the wall[1]. The fact that this is not observed, is due to the six rigid layers within the wall impeding the motion of particle velocity. By comparing the result for the side wall with that of the felt, it can be seen that this outer layer is responsible for the rise in

[1] For a sound speed of 340 ms^{-1} a ¼ of the wavelength at 243 Hz equals 0.35 metres

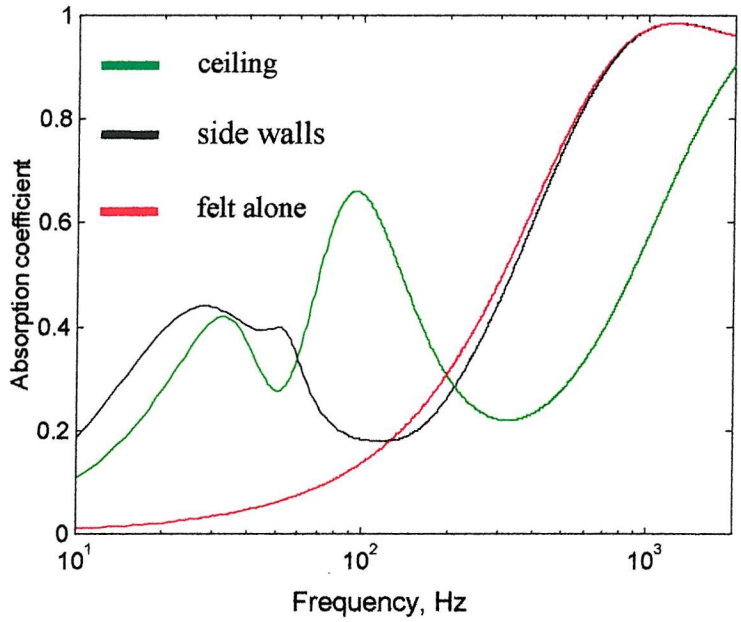

Figure 3.4 – Theoretical diffuse field absorption coefficient of felt, multi-layer wall and ceiling

high frequency absorption above 200 Hz and well into the frequency range where, due to the ever shortening wavelengths, the reverberation time of a room can be controlled by porous absorption alone. The large absorption coefficient at frequencies close to the lower limit of human hearing, where the wavelengths are up to 13 metres long, is proof that the many years of empirical changes to the wall have resulted in a successful design. It is very interesting to note that in the frequency range where the side walls exhibit the lowest absorption, the multi-layer ceiling reaches a peak of close to 0.7. The double resonance in the ceiling is caused by the springiness of the rockwool and the air space adjacent to the structural wall. As such, the absorption coefficients of the side wall and ceiling complement each other and it is likely that the reverberation time of the room with only the multi-layer wall/ceiling in place, will be short and reasonably frequency independent.

3.5 Comparison of Room Reverberation Times

3.5.1 Description of the Four Room Construction Stages

In the previous two sections, the surface normal acoustic impedance and the associated diffuse field absorption coefficient have been measured and/or calculated for the cotton waste felt and the multi-layer wall. In order to use these quantities to calculate the RT_{60} from the Sabine formula, the area of the surfaces with the aforementioned absorption coefficients and the volume of the room must be known. As mentioned in *Section 3.1*, ten measurements were made during the construction of the room and the four used in this investigation are:

a) multi-layer wall

b) multi-layer wall and ten rear panels

c) multi-layer wall and twenty rear panels

d) multi-layer wall, twenty rear panels and four ceiling panels (i.e. complete room)

For each of the four stages the room will have a different volume and different surface area of the cotton waste felt (and to a lesser extent the multi-layer wall). These differences are summarised in the table below.

Construction stage	**Volume of room**, m^3	**Wall surface area**, m^2	**Felt surface area**, m^2
Multi-layer wall	179.4	127.5	/
Multi-layer wall and 10 rear wall panels	175.3	123.0	96
Multi-layer wall and 20 rear wall panels	171.2	118.5	192
Complete room	168.9	118.5	244.8

The Sabine formula that is used to calculated the reverberation time is $RT_{60} = \frac{0.161V}{\alpha_w S_w + \alpha_p S_p}$, where V is the volume of the room, α_w and S_w are the diffuse field absorption coefficient and area of the wall respectively and similarly α_p and S_p for the panels [3.13]. Together with the results presented in previous sections, the above formula may be used to calculate the reverberation time for each of the four stages of construction and allow direct comparison with the measured results.

3.5.2 Multi-Layer Wall

The construction stage considered in this section does not include any freely suspended angled panels, with the only absorption provided by the multi-layer wall. Unlike the actual room, the geometry of the room model used here is simple, in that each of the six room boundaries are flat surfaces. The floor and monitor wall are considered as perfectly reflective, while the other surfaces are characterised by the relevant diffuse field absorption coefficient. Whilst introduction of the panels will contribute additional absorption, the sound field between them will not be diffuse within the frequency range considered. As a consequence, modelling their absorptive behaviour solely on the surface area of felt with which they are covered, is likely to lead to an artificially short reverberation time for the room as a whole. Therefore, if the theoretical model is a valid way of describing the room, one would expect the closest agreement between the measured results and the predicted Sabine reverberation time, when only the multi-layer wall is present. As such, the comparison made in this section, will impact the way in which the theoretical reverberation time results for the other stages are viewed. Poor agreement without panels present, suggests an unreliable prediction of RT_{60} when they are.

Figure 3.5 shows the two plots of reverberation time. In the measured result, an average value of between 0.3 and 0.4 seconds is noted, with higher values at the low frequencies and near anechoic performance at 2 kHz. In the mid frequencies, the reverberation time shows more variation, with particularly noticeable peaks in the 63, 100 and 500 Hz $^1/_3$ octave bands.

The measured RT_{60} only approximates to the design criteria of BBC control rooms, which aim to have a frequency independent reverberation time of about 0.4 seconds up to 1 kHz, dropping to 0.3 seconds at 8 kHz [3.14]. The justification for such a RT_{60} characteristic is to minimise the spectral colouration of reproduced male speech caused by the room. Even without the hanging panels on the rear wall and ceiling, the Tio Pete control room would be considered to have too much absorption, over much of frequency range. In addition, the aforementioned peaks in the reverberation time suggest that the room has an element of spectral colouration unacceptable to the BBC criteria. That said, the low RT_{60} across the frequency range is evidence of the effectiveness of the multi-layer wall.

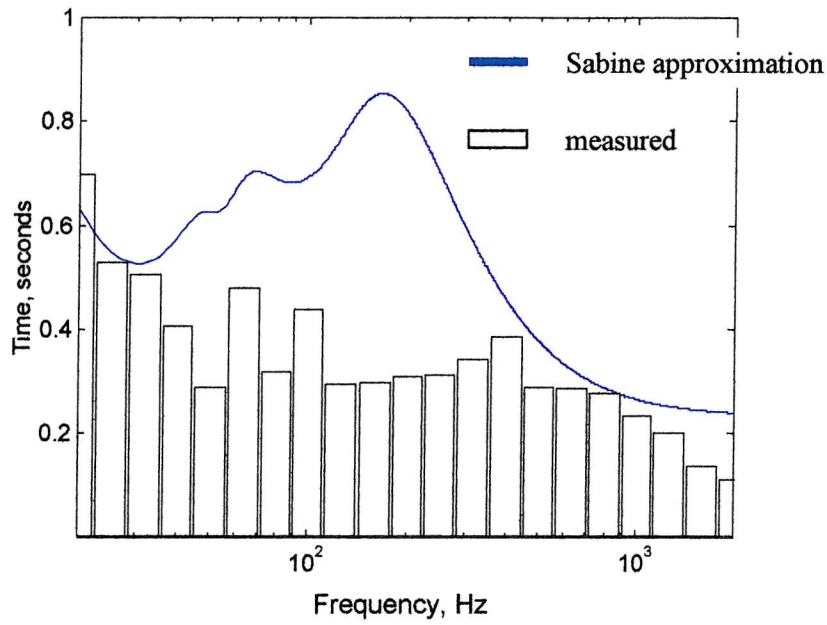

Figure 3.5 – RT_{60} of Tio Pete control room with only the multi-layer wall and ceiling

Unlike the measurement, the theoretical reverberation time has no obvious average value, as an otherwise smooth trend from 0.6 seconds at 20 Hz to about 0.2 at 2 kHz is marred by a large peak centred on 170 Hz. The primarily reason for this high value is the low absorption coefficient of the side walls. A reverberation characteristic like this would result in an unsuitable environment in which to critically appraise reproduced audio. Indeed, a frequency independent value of 0.8 seconds (the highest value of the theoretical trace) would be preferable, despite the longer decay time, as the spectral colouration would be less. As a result of the poor combined performance of walls and ceiling, the agreement between the measured and theoretical RT_{60} is poor between 32 and 500 Hz.

Before the results for the other stages of construction are presented, explanations will be given for the difference between theory and measurement, for the situation where the best agreement was expected. Three possible reasons for the poor agreement are considered, two which relate to the theory and one which is associated with the measurement procedure.

3.5.2.1 Reasons for Poor Agreement Between Theory and Measurement

A possible source of error in the theoretical model, is the way in which the multi-layer wall is characterised. The analysis used to model it did not allow for any wave bearing elements (such as the chipboard panel), with panel resonance and coincidence effects ignored. The reason for this simplification in the model, however, was based on the way in which the panels are used within the wall and was not made arbitrarily. The outermost chipboard panel is freely suspended and heavily damped by the attached layer of deadsheet. Investigations into the radiation efficiency of panels have shown that the edge conditions are critical [3.15], which implies (by the principle of reciprocity) that it is also an important factor in their use as absorbers. A recent investigation concluded that a panel with free edge conditions demonstrates almost no vibration velocity in response to high incident sound power [3.16]. Such research indicates that the coupling of the incident sound field to a freely suspended panel is very poor, allowing it to be characterised simply as a limp mass. One may conclude, therefore, that the model of the wall is not the primary reason for the lack of agreement evident in *Figure 3.5*.

The other aspect of the theory that may have compromised the result is the assumption of a diffuse field that underpins the Sabine formula for reverberation time. At low frequencies, a room is dominated by distinct modes, which are related to its dimensions. At higher frequencies, the modal density increases, until such a point that the phase of the individual modes can be considered as statistically random. This diffuse field allows the sound field at any point in the room to be quantified by the mean square pressure amplitude. Schroeder [3.17] showed that the onset of the diffuse field is a function of the volume of the room V (cubic metres) and the Sabine reverberation time RT_{60} (seconds). The frequency at which this occurs (the so called *Schroeder frequency*) is given by $f_s = 2000\sqrt{\frac{RT_{60}}{V}}$. Using the measured results for the reverberation time, the approximate frequency above which a diffuse field will dominate is $2000\sqrt{\frac{0.3}{179.4}} = 82\,\text{Hz}$. If this were the only condition for a diffuse field, the above result would suggest that only in the lowest two octaves is the theoretical model invalid.

However, from a more physical standpoint, it can be seen that a diffuse field is unlikely to be present even above 82 Hz. In order for a random sound field to develop, the room boundaries must be non-absorbent enough to allow multiple reflections. Thus in a room with very absorptive surfaces, a steady state reverberant field will not be present and the behaviour of the sound within the room will be dominated by the direct sound at high frequencies and well damped modes at low frequencies. In addition, the Sabine formula assumes a regular distribution of absorption throughout the room. If this condition is not satisfied (as in the Tio Pete control room, which has a reflective floor and monitor wall), any measure of reverberation time will be highly dependent on the positioning of the source and receiver. The theory cannot account for this and assumes that the sum of absorption (the denominator in Sabine's equation) is representative of all the room boundaries. It seems therefore, that the huge difference in absorption between the floor and monitor wall (very reflective) and the remaining walls and ceiling (highly absorptive), compromises the diffuse field assumption and this is, in part, to blame for the discrepancy between measurement and theory seen in *Figure 3.5.*

As previously mentioned, the measured results are not truly representative of the room as a whole. The results were obtained by measuring the transfer function between a loudspeaker in the monitor wall and a microphone placed at the main listening position. From the transfer function, $^1/_3$ octave band Schroeder integration plots were calculated (as in *Chapter 2*), to give the time taken for the sound to decay by 60 dB and thus the RT_{60}. The use of Schroeder plots (which assume a diffuse sound field) is questionable in the light of the previous discussion, where it was argued the direct sound dominates. In addition to this, a vastly different result would have been obtained if the source had been placed near the rear wall of the room and the microphone positioned in the vicinity of the monitor wall. It is likely that such a measurement would have resulted in a higher value of reverberation, on account of the reflective monitor wall. It should be said, however, that the point of the measurement was to provide an objective measure of what a recording engineer sat at the mixing console would hear. The purpose was not to find a spatially averaged reverberation time to compare with theory. In that sense, the two results in *Figure 3.5* describe different quantities, though if the sound field were more diffuse, the discrepancy would decrease.

In the discussion above, an explanation has been given for the lack of agreement between theory and measurement. The measured RT_{60}, although not strictly valid, provides an objective quantity with which to describe the sound field at the listening position. It is not representative of the whole room, but rather is particular to a source placed in the monitor wall. The theoretical model, on the other hand, cannot account for the vastly different absorption coefficients of the room boundaries and assumes the mean squared pressure is independent of position. This assumption of a diffuse field is not valid because of the highly absorptive walls and ceiling.

Based on these conclusions, it is the measured results that are used hereafter to identify the effects different elements of the *Bass Trap* have. The theoretical RT_{60} predictions will also be included, though little significance will be afforded them. The only difference anticipated in the theoretical results to follow, is a steady reduction in the reverberation time above about 100 Hz, as increasing amounts of felt are added.

3.5.3 Multi-Layer Wall and Ten Rear Panels

Figure 3.6 shows the measured and theoretically predicted RT_{60} for this construction stage. Considering the measured result first, the trend for shorter reverberation time with higher frequency, noted in the previous section, is continued when ten additional panels are introduced. At frequencies greater than 400 Hz, the RT_{60} is shorter by up to 0.1 seconds, however, it is longer in the 50, 63, 125 and 160 Hz $^1/_3$ octave bands. The lower reverberation time at the high frequencies is evidence that the absorption of the felt has an additive effect to the performance of the multi-layer wall. Even though the panels are placed directly in front of the wall, the total absorption is not less than the sum of the parts. It is not obvious why the absorption of the multi-layer wall is worsened by the panels at the aforementioned frequencies. One possible reason might be resonances within the channels formed by the adjacent panels, though one would expect these to be well damped given the large amount of felt present. On the whole, it would appear that the ten panels cause the RT_{60} to be more frequency dependent, thus from a subjective viewpoint, the room is likely to be more suitable for critical listening without them.

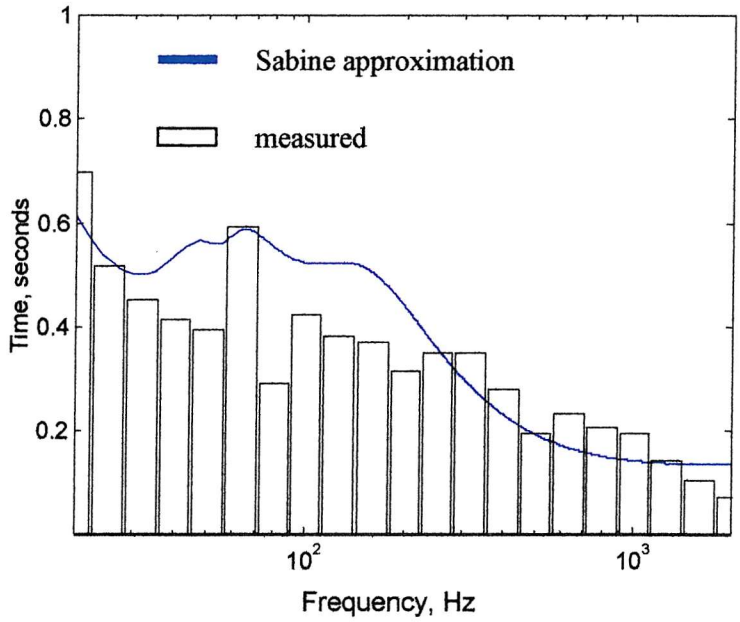

Figure 3.6 – RT_{60} of Tio Pete control room with 10 rear wall panels

As predicted, the theoretical reverberation time has decreased in line with the absorption coefficient of the felt, reducing the peak at 170 Hz by 0.3 seconds. Interestingly, the agreement between the two is fairly good, though as explained in the previous section, this is not an indication that the theory is an accurate descriptor of the room.

3.5.4 Multi-Layer Wall and Twenty Rear Panels

In *Figure 3.7* the reverberation time of the control room with twice as many rear panels as *section 3.5.3* is presented. If the angled panels affect the reverberation only by virtue of the large amounts of absorbent which are introduced into the room, then the RT_{60} would be expected to be shorter than the previous plot above a frequency of 200 Hz. Instead, the measured result exhibits even greater variation than before, making the effect of ten **more** panels unclear. They make no difference to the lowest and four highest $^1/_3$ octave band measurements, though the reverberation time in between has changed by a maximum of 0.15 seconds.

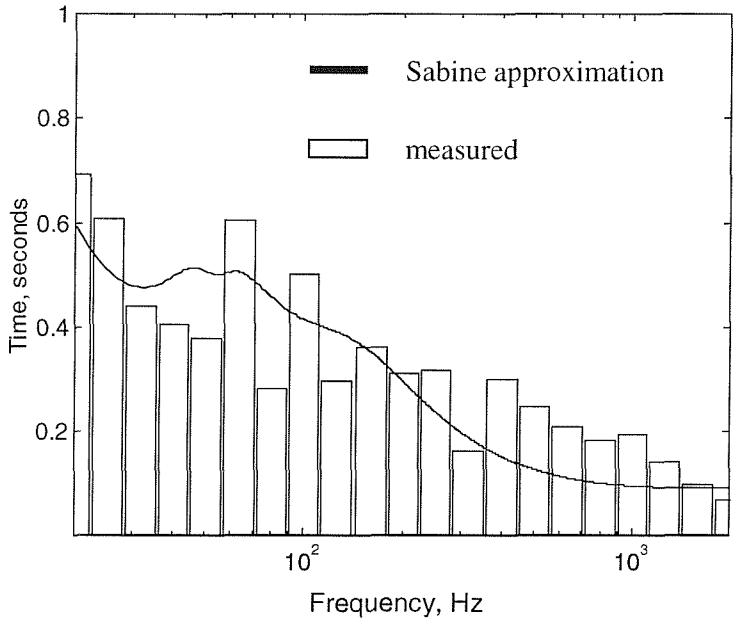

Figure 3.7 – RT_{60} of Tio Pete control room with 20 rear wall panels

While the additional felt would not be expected to make a difference at 20 Hz, it is surprising that the top octave is unaffected. This would imply that the placement of the extra felt in the room does not lend itself to further reduction of the energy in the reverberant field. Unlike the previous result, where the panels were about 0.6 metres apart, it appears in this case that the benefit of more felt is cancelled by a shadowing of the wall and its contribution to high frequency absorption. From this result we can conclude that the influence of the felt covered panels on the room's RT_{60} does not increase proportionally with greater surface area – a law of diminishing returns perhaps.

3.5.5 Complete Room

The completed room differs from the previous construction stage because of four 6.6 m^2 freely suspended angled panels covered on each side with 4 cm of cotton waste felt. Unlike the rear wall panels, those hung from the ceiling are not parallel with one another, instead their leading edge faces the loudspeakers (see the lower part of *Figure 3.1*). The reason given by the designer is to present the propagating wavefront easy access to the *Bass Trap* but a more tortuous exit, in the hope that more of the sound is absorbed. This intuitive design feature will be

investigated in *Chapter 6*. Subjectively the addition of the ceiling traps resulted in improved monitoring conditions for the low frequencies and also served to remove a standing wave (albeit highly damped) between the reflective floor and ceiling [3.1]. The measured and predicted reverberation time for the completed room is shown in *Figure 3.8*. Apart from a couple of exceptions, each $^1/_3$ octave band RT_{60} is shorter than, or the same as without the ceiling panels. The shape of the reverberation time with frequency is far smoother than the previous plot, though a 0.2 second difference

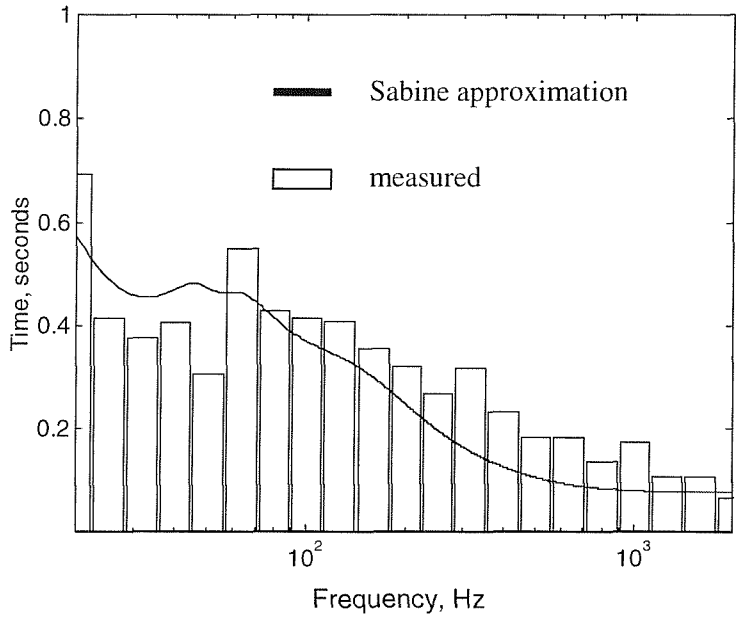

Figure 3.8 – RT_{60} of Tio Pete control room with all panels

between the 50 and 63 Hz bands still remains. The ceiling panels actually introduce less felt than ten of the rear panels (52.8 m^2 and 96 m^2 respectively) and yet the ceiling traps produce a more significant reduction in reverberation time. This observation suggests, as before, that the positioning and orientation of the panels is important. It also adds weight to the argument that the hanging panels do not merely provide a space efficient means of introducing large amounts of absorbent material into a small room. Whilst porous absorption is clearly an important factor in the performance of the *Bass Trap*, the measured results here suggest that other mechanisms are at work also.

As in the previous two plots, the theoretical RT_{60} is reduced further, while maintaining the general shape.

3.6 Conclusions

The comparison between measured and theoretical RT_{60} for the multi-layer wall alone led to the conclusion that a diffuse field porous absorption model is not a valid means of predicting the performance of a *Bass Trap* control room. As a consequence, it has been the measured results that have given the insight into whether or not the reverberation time of the room decreases proportionally with an increase in surface area of felt present. The fact that the theoretical results illustrate such a trend is to be expected given the diffuse field assumptions that underpin it.

Figure 3.5 illustrated that the vast majority of the absorption in the room is due to the multi-layer wall. Though the panels (particularly those on the ceiling) serve to lower the RT_{60}, the results presented here do not suggest that their inclusion in the room design is particularly beneficial.

The measurements show that the reverberation time does not shorten solely because of more felt present. The addition of 96 m^2 of felt due to ten more panels actually made the RT_{60} more frequency dependent and slightly longer on the whole. In contrast, a smaller amount of felt introduced by the ceiling panels had a far more significant effect. This observation makes a strong case for further investigation into the *Bass Trap* as any change in reverberation time appears to be dependent on the positioning and orientation of the panels. A diffuse field, porous absorption argument alone is not able to account for such construction variables.

CHAPTER 4

Transmission of Sound Along a Hard-Walled Duct Lined with Splitters

Introduction

One of the conclusions of the previous chapter was that the placement and orientation of the panels influences the performance of the *Bass Trap* of which they are part. The change in measured reverberation time at different stages of construction showed no correlation with increasing amounts of porous absorbent. In this chapter it is this placement and orientation of panels that is explicitly investigated. As was discussed and illustrated in *Chapter 1*, the hanging angled panels are placed on the side walls, ceiling and rear wall (though space constraints often only allow for their use on the back wall [4.1]). The other key features are the positioning of the loudspeakers in a hard wall and the reflective floor (normally wood panelling). The aim of the *non-environment* room design is to prevent any sound (in the form of reflections or reverberation) returning to the listening position once the direct sound from the loudspeakers has passed. As a result of these features the *Bass Trap* panels can be split into two categories: *side wall* panels and *rear wall* panels.

The *side wall* panels are those for which the sound passes at a grazing angle as it propagates from the loudspeakers to the other end of the room – the panels on the side walls and ceiling fall in this category. The *rear wall* panels, by contrast, hang next to the room boundary for which the propagating sound is normally incident, i.e. the panels are placed in front of the rear wall.

Throughout this research the investigations will be concerned with either the influence of the ***side wall*** panels on the **transmission** of the sound down the room, or the effect the ***rear wall*** panels placed in front of an absorbent wall have on the rear wall **normal absorption coefficient**.

The aim of this chapter is to prove whether or not the periodic array of rigid panels placed along the side walls and ceiling of a *Bass Trap* control room influence the transmission of sound down the room – the back wall is ignored. Specifically, the hypothesis that the panels act in a similar manner to splitters in a duct (e.g. as used in

exhaust silencers [4.2]) is investigated. Two methods of investigation will be employed in this chapter: experimental and theoretical, the detail of each will be given in the following sections.

As mentioned in *Chapter 1*, cross-sectional area changes and protrusions into a duct cause acoustic impedance discontinuities. In the absence of any resistive elements (i.e. porous materials that dissipate sound energy into heat) the sound is reflected and transmitted at these junctions. However, this behaviour is normally frequency dependent, with some frequencies reflected and others transmitted. The exact nature of the area change or protrusion governs this selective filtering. In order to consider this purely reactive mechanism as a possible means by which the *Bass Trap* works, some of its design features will be ignored. The panels themselves will be considered as consisting only of their chipboard core and the multi-layer wall will not figure in any of the modelling. Removing these variables will allow any significant filtering to be easily identified.

Both the experiment and theory are based on the same assumptions of how the sound will propagate in a *Bass Trap* control room.

a) As no acoustically resistive elements figure in the investigation, the experiment and theory will model the room on a $^1/_{10}$ scale. Geometrical scaling is valid in acoustics given the reciprocal relationship between frequency and distance (e.g. wavelength), though care has to be taken when scaling materials like chipboard panels – this will be mentioned later. The $^1/_{10}$ scale will make the experimental set-up a practicable size, the results obtained from which will be similarly scaled, i.e. a factor of ten higher.

b) Both models will consider only the transmission of the plane wave. This mode is less easy to attenuate than higher order modes, so transmission **loss** (TL) in the plane wave suggests more significant attenuation in the other modes. Ignoring the other modes also simplifies the experimental procedure and theoretical model.

c) The *Bass Trap* control room will be considered symmetrical about a vertical plane running from the centre of the monitor wall to the centre of the rear wall. The experiment and theory therefore model a room **half** the width, one wall of which is hard and reflective and represents the plane of symmetry. The opposite side wall will be a $^1/_{10}$ scale model of different arrays of uncovered *Bass Trap* panels.

d) Finally, the models will assume that the rear wall *Bass Trap* is so effective that the room can be considered as an anechoically terminated duct, where the duct's width is a $^1/_{10}$ scale model of half the room's width.

4.1 Experimental Investigation into Transmission

In this section the objectives of the experimental investigation are described and explanation given as to how these objectives were achieved. It will conclude with a presentation of the results obtained.

4.1.1 Description of Experimental Objectives and Set-up

As mentioned in the introduction to this chapter, the *non-environment* philosophy and design of the *Bass Trap* control room lead to the quantification of the performance of the side wall implementation of the absorber in terms of sound transmission. By transmission we mean the ratio of the forward going component of the pressure field either side of the absorber, expressed in dB. Thus if any filtering has occurred the value of transmission will be negative, as the magnitude of the forward going component of the pressure is less after propagating past the side wall absorber. The set-up used to achieve this experimentally, in the light of the assumptions outlined in the previous section, is shown schematically in *Figure 4.1*. For a clearer idea of how the duct looks in reality, the reader is referred to *Figure 6.1* where photos of the duct with panels and an absorbent foam liner are shown.

The duct represents a scale model of half of a control room's width and is constructed from twelve 600 mm x 300 mm x 42 mm (length, width, depth) smooth concrete paving slabs. Three were laid length-ways end to end, a further six were placed on the edge of the base to form the side walls, leaving the final three to form a lid. The base and side walls were fixed in position using a hard drying adhesive grout, the other three slabs were not, as the lid needed to be removable in order to allow access to the inside of the duct. After construction the internal dimensions of the duct measured 1.8 m x 0.215 m x 0.3 m (L, W, H).

The wide-band noise source used as the test signal was produced by six 75 mm direct radiating loudspeakers placed in a common baffle at one end of the duct. This arrangement was chosen because the superposition of the individual sources would provide a better approximation to a plane wave than one larger source (e.g. 200 mm

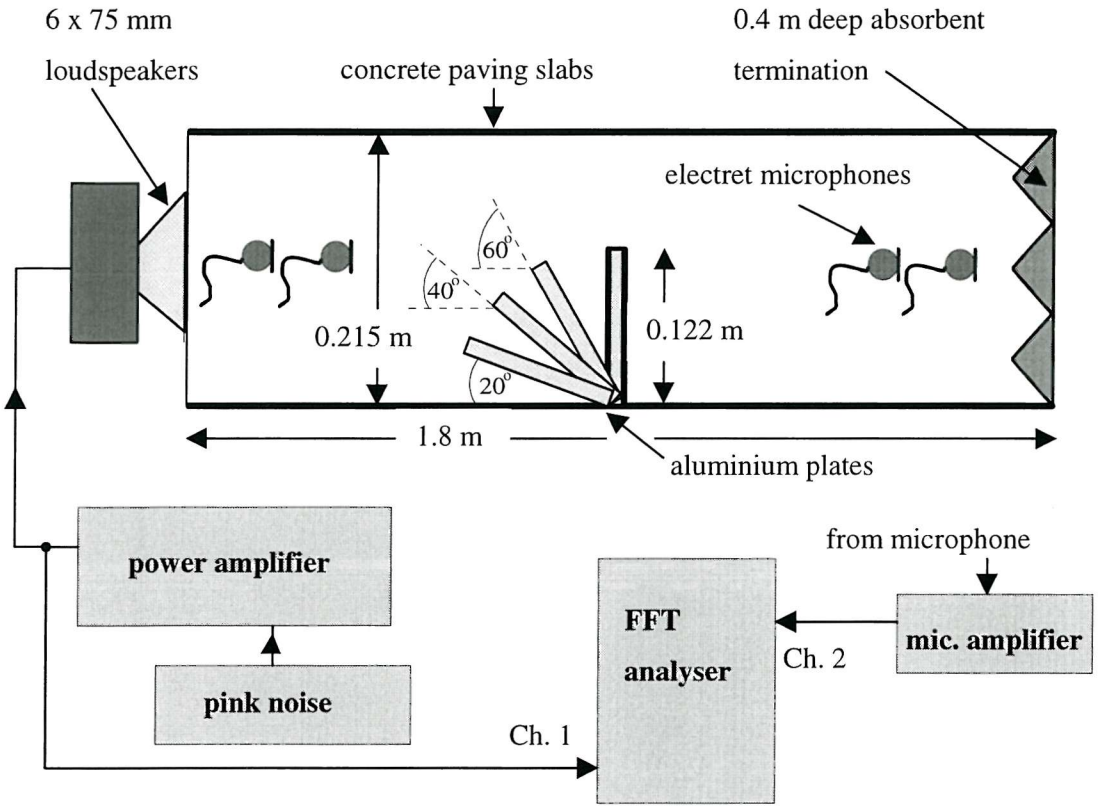

Figure 4.1 – Schematic description of the hard-walled duct experimental set-up

loudspeaker). A 40 cm deep triangular wedge was placed at the opposite end to the loudspeakers, ensuring an anechoic termination above about 250 Hz.

In between the loudspeakers and the termination were placed the different arrangements of panels. The $^1/_{10}$ scale equivalent of the chipboard panels used in the *Bass Trap* are 0.9 mm thick aluminium plates [4.3], though previous research has shown that the chipboard panels can be considered as acoustically rigid [4.4]. In the light of this the aluminium plates were fixed in position with sticky tape, rather than being freely suspended as in the full scale design. The height and width of the aluminium plates (herein referred to as *the panels*) were $^1/_{10}$ of the full scale chipboard panels, 300 mm and 122 mm respectively. For the sake of clarity, each different array of panels will be referred to from now on as the *absorber* and the length of the duct it occupies will be called the *absorber length*. Three variables were changed in the experiment: number of panels, spacing between adjacent panels and the angle the panels made with the side wall.

In order to calculate the transmission from one side of the absorber to the other, four measurements were made, two on either side. One of the key design features of the duct are the two regions either side of the absorber where the walls are bare. In these parts of the duct there is no scattering from the panels and thus only the plane wave will propagate (below the duct cut-on frequency). It was in these positions, therefore, that the measurements were made. The two microphones used were held 165 mm apart by a thin wire frame. For each microphone position the transfer function was calculated between the input signal to the loudspeaker and the output signal from the microphone amplifier. This measured transfer function was multiplied by the microphone cross-calibration transfer function, to correct for any differences in the magnitude and phase responses of the two microphones. The measurements described allow for a decomposition of the sound field – detail of this analysis is given in *Appendix 3.*

The transmission results are presented in the following section.

4.1.2 Presentation Style of Transmission Results

As mentioned, three variables were investigated experimentally: the angle, spacing and number of panels. The table below summarises the variable changes.

Spacing between panels, cm	**Angle of panels**	**Number of panels**
6	20^0, 60^0 & 90^0	2, 4, 6, ... 14, 16
9	20^0, 40^0, 60^0 & 90^0	2, 4, 6, ... 10, 12
15	20^0, 40^0, 60^0 & 90^0	2 - 7
21	20^0, 40^0, 60^0 & 90^0	1 - 5

As the spacing between the panels increases so the number of them has to decrease, as the length of the duct is fixed. From the table it can be seen that the transmission for 92 different absorber arrangements were measured, i.e. 368 transfer functions.

When the results were analysed it became clear that obvious deviation from 0 dB transmission (i.e. un-attenuated) only occurred when the absorber length was a significant proportion of the duct length. The results presented in this section

therefore are grouped according to angle for the absorber arrangements described in the table below.

Spacing between panels, cm	**Number of panels**	**Total absorber length,** cm
6	16	90
9	12	99
15	7	90
21	5	84

As it is the plane wave transmission that is of interest, the frequency range of the results is constrained to below the first cut-on mode across the width of the duct. As the height of the duct is greater than the width, the first cut-on mode will operate in this direction. However as the microphones were held in a position half the height of the duct, the first vertical mode is ignored, as there will be a pressure anti-node at that point.

4.1.3 Transmission for Panels at 20^0

Figure 4.2 shows the experimental transmission results when the panels are at an angle of 20^0 to the side wall. The y-axis scale is kept constant for all of the results to ease comparison and extends to –50 dB because of the results to follow later in the chapter.

Two main features are evident in *Figure 4.2*, small dips at the lower frequencies and a noticeable deviation from 0 dB transmission above 700 Hz. The former effect, occurring at 180, 260, 360 and 490 Hz is due to the small inconsistencies in the cross-sectional area of the duct. Although every effort was made to ensure that opposite duct boundaries were parallel with each other, there were slight differences between different sections, with the duct being marginally wider at the top than the bottom in some cases. As mentioned previously, such discontinuities effect the propagation of the sound along the duct and in this case the small dips are caused by the reflected sound constructively interfering at frequencies where the length of the slabs equals integer multiples of ½ wavelength. More mention about this will be made in *Section 4.2.6.*

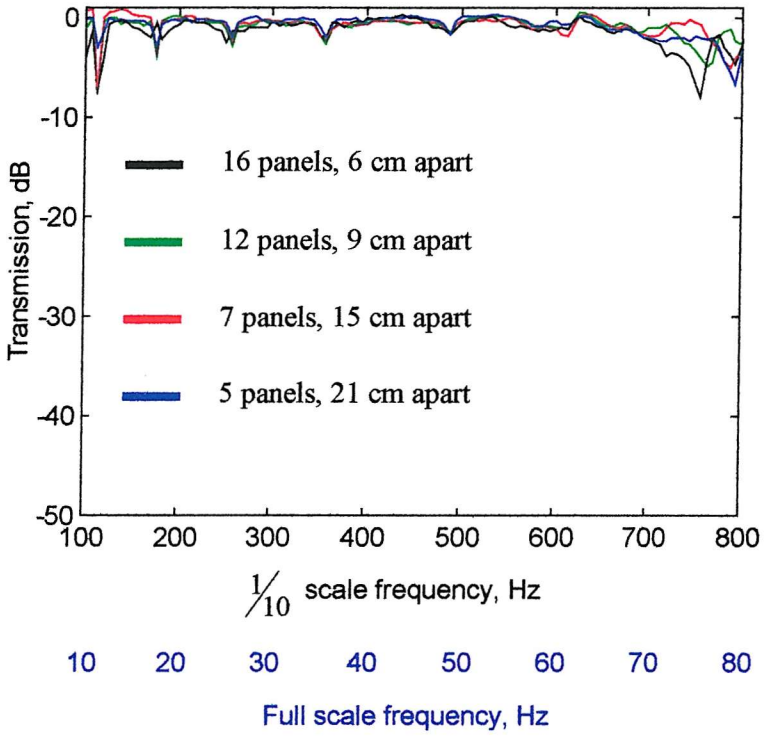

Figure 4.2 – Comparison of transmission for panels at 20°

The increasingly uneven transmission above 700 Hz does not suggest any clear trend and it is difficult to draw any plane wave conclusions given that the first cut-on mode across the duct's width occurs near this frequency range. At this shallow angle the absorber does not have much influence within the plane wave limit. At this point it is difficult to ascertain whether or not this observation is purely because the panels only protrude 42 mm into the duct (20% of the total width).

4.1.4 Transmission for Panels at 40°

In this section the same four arrangements of absorber are considered but with the panels making a 40° angle to the side wall, the result is shown in *Figure 4.3*. The same small dips caused by the grouting discontinuities are present, but are far less significant than the high pass filtering that occurs above 600 Hz. With the panels 9 and 15 cm apart the transmission tends to –10 dB at 800 Hz, though both traces are far from smooth. More dramatic is the transmission when 5 panels are spaced 21 cm apart. In this trace the filtering effect is far clearer apart from a sharp dip at a frequency close to the predicted frequency of the first horizontal cut-on mode.

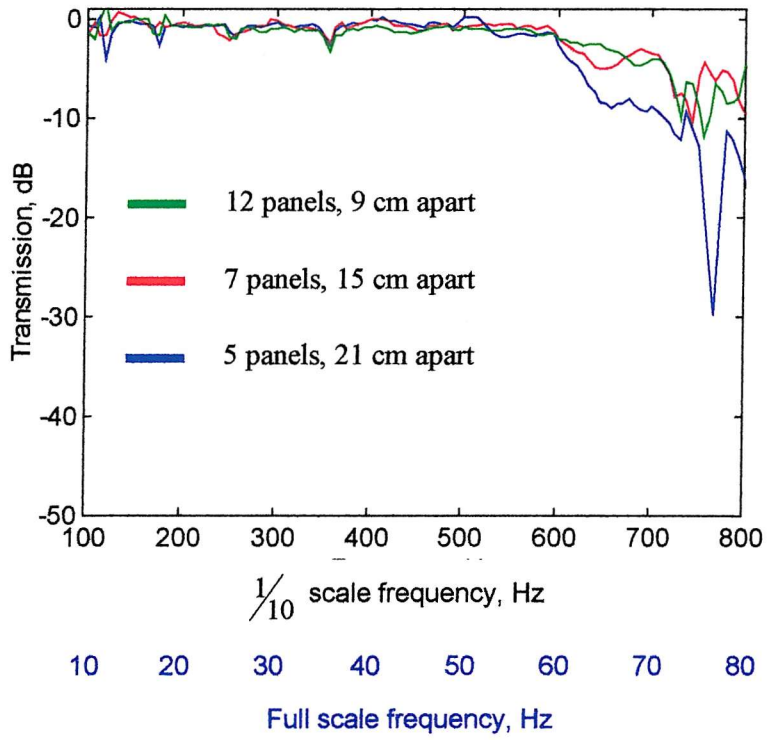

Figure 4.3 – Comparison of transmission for panels at 40°

A comparison with *Figure 4.2* suggests that two of the variables effect the transmission.

Firstly, a greater filtering effect is seen when the panels make a more obtuse angle with the duct wall. It is interesting to speculate whether or not it is the angle of panel or merely the distance they protrude into the duct that is the significant variable. At 40^0 for example the panels protrude 86% further into the duct than at 20^0 (78 mm for 40^0 and 42 mm for 20^0). This mini-investigation will be considered in the light of a theory presented in the following section.

Secondly, the TL increases with increasing spacing between the panels. Both of these observations point to a wavelength dependence. At lower frequencies, the proportion of the duct width occupied by the panels makes no difference and yet this variable is significant at frequencies where higher order modes propagate. In the same way, it is the distance between the panels, not the number that differentiates between the transmission results for the same angle, indicating that as the spacing approaches the wavelength of sound so the filtering at that frequency increases (at 600 Hz, 21 cm is over $1/3$ wavelength).

4.1.5 Transmission for Panels at 60^0

The plot presented in this section (*Figure 4.4*) will conclude the first set of experimental results and is for panels positioned at an even more obtuse angle than before. At the end of the chapter the final experimental result will be presented (panels at 90^0 to the wall) and will be directly compared to a theoretical model – the subject of the following section.

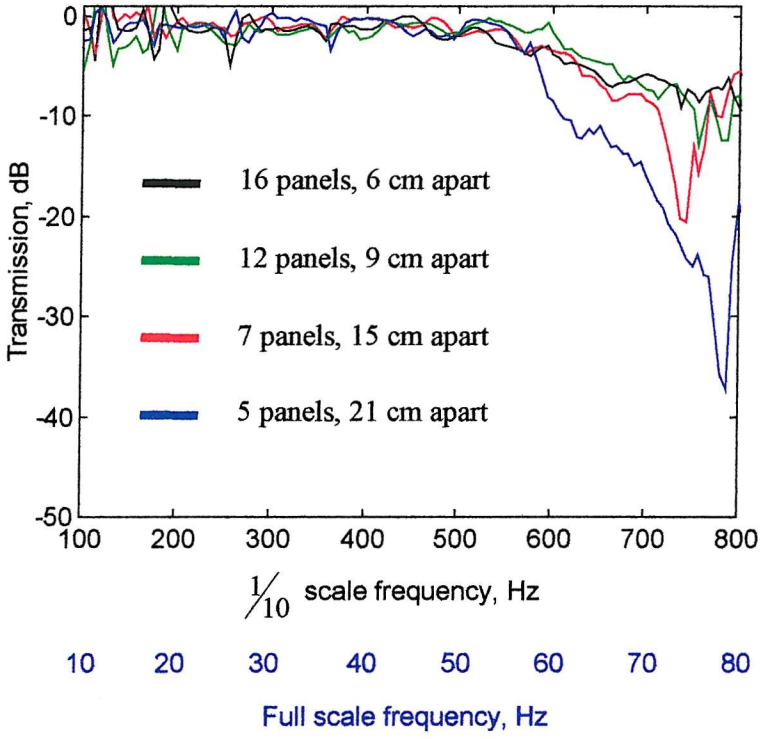

Figure 4.4 – Comparison of transmission for panels at 60^o

The comparisons made between *Figure 4.2 & 4.3* led to the conclusion that the spacing and angle of the panels, were both significant variables in effecting the TL at the higher frequencies. With the panels at 60^0 to the side wall, the same is true. The 6 cm absorber arrangement yields a gradual drop in transmission to about –10 dB at 800 Hz, additionally it appears that the frequency at which the TL deviates from 0 dB is lower than before, occurring at around 520 Hz. With the panels 9 cm apart, the TL is greater at this angle than the previous angles and also slightly greater than for the 6 cm absorber. The increase in TL between 40^0 and 60^0 is considerable at a panel spacing of 15 cm and there is a clearly defined trough centred on 740 Hz, though it is

difficult to explain the behaviour above this frequency, as it is very close to the plane wave limit of the duct. The most notable of the four traces relates to the 21 cm absorber. For this arrangement, a steady increase in TL is seen from around 520 Hz until it reaches a maximum of –38 dB at the plane wave limit of the duct. Together with the previous two plots, this trace is conclusive evidence that the TL increases when the panels make a more obtuse angle with the wall and are separated by a distance that is a significant proportion of the wavelength.

In order to shed light on these experimental results, a plane wave theoretical model will be described in the following section. It will allow some of the key variables identified in the previous section to be further investigated. In particular, it will be used to show the effect of changing the distance the panels protrude into the duct, without changing their angle. In fact, the model will not be able to consider angled panels as it is only one-dimensional model.

4.2 Theoretical Investigation into Transmission

Having established that the presence of rigid panels placed against a hard side wall does effect the transmission of sound along the duct, the next stage in the investigation was to construct a theoretical model.

4.2.1 Introduction to the Theoretical Model

The model presented in this section does not offer a complete description of the duct described in *Section 4.1* primarily because it is one dimensional. Only plane wave propagation is considered, meaning that any variation in the sound field across the width and height of the duct is ignored. This limitation means that the angle of the panels cannot be included, so all the results presented are for panels at 90^0 to the wall. Unlike the experiment however, the effect of varying the width of the panel can be investigated, enabling a comparison to be made with the panel angle. As with the experiment, no acoustically resistive elements are included in the theoretical model, as it is only the effect the geometry of the panels (spacing, width and number) that is of interest.

The theoretical model is constructed in two parts. Firstly, the analysis forms equations of pressure and volume velocity continuity for one period of the absorber. One period is defined as a section of duct that extends halfway between panel $n-1$

and panel n, to halfway between panel n and panel $n+1$, where n is an individual panel within the absorber and panels $n-1$ and $n+1$ are the adjacent panels to the left and right respectively. From the equations of continuity expressions for acoustic impedance can be found.

The second stage is to theoretically propagate a unit amplitude plane wave down the duct by using forward and backward going waves as a description of a plane wave pressure field. The amplitude of the forward going wave after passing the absorber is dependent on the impedances formed in the first part of the analysis, which in turn are a function of the geometry of the absorber. The theoretical model is therefore able to calculate the transmission for any variation (panel spacing, width and number) of absorber array.

4.2.2 The Empirical *Edge Effect*

As mentioned in *Section 4.1*, area changes and protrusions (splitters in an exhaust silencer for example) in an otherwise constant cross-section duct give rise to frequency dependent plane wave transmission and/or reflection. A full description of the change in sound field however, requires a knowledge of the activity of higher order modes and their propagation or otherwise. When a plane wave propagating along the duct in *Figure 4.1* meets the sharp edge of the first panel, it is scattered into an infinite number of higher order modes. The modes subsequently interfere constructively and destructively and decay or propagate depending on the dimensions of the duct and their wavenumber. This complicated interaction of modes results in a sound field at any given point that cannot be accurately described by considering the plane wave only. In order to keep the model relatively simple while not compromising it by ignoring the effect of the higher order mode activity, an empirical approximation was used. The *edge effect* described is used in the commercial design of exhaust and air conditioning silencers [4.5] and approximates to the complicated diffraction and refraction effects that occur in the near field of the panel. The *edge effect* model is illustrated in *Figure 4.5*. The duct is shown as having a width *dw* while the panel is *pw* wide and *pt* thick. As mentioned, no account is made for variation of the sound field over the duct's width, so only the horizontal direction of *Figure 4.5* is considered. It has been shown [4.5] that the higher order mode activity caused by the panel is well approximated by a sidebranch of depth *d* and width *pw* (i.e. the same width as the panel). Given the presence of both forward and backward

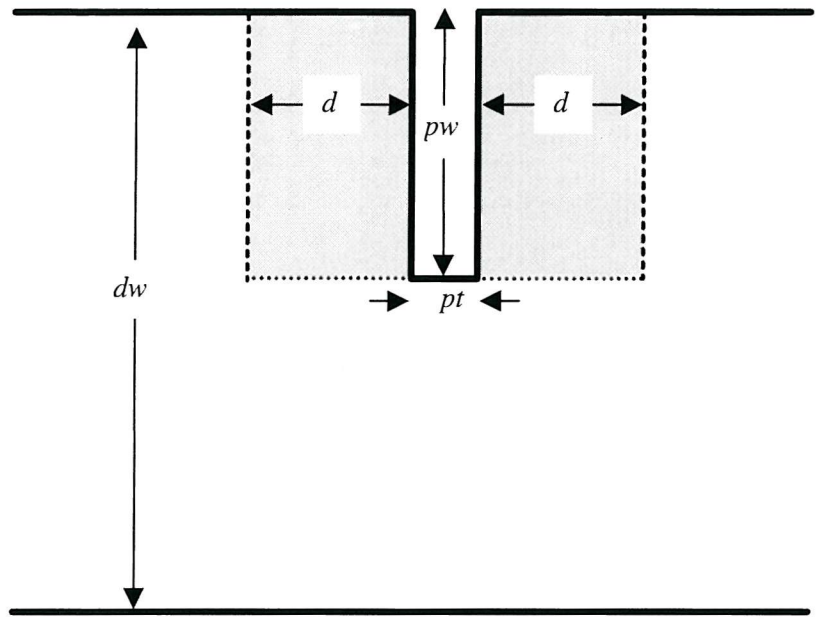

Figure 4.5 – Model of empirical edge effect

going waves the *edge effect* sidebranch is required on both sides of the panel. These mini-sidebranches, whose depth is a function of the dimensions of the duct and panel, can be considered as rigidly terminated pipes of length d. This allows the impedance at the mouth of the sidebranch to be found, which is a key quantity in forming the equations of pressure and velocity continuity. The equation relating the panel and duct dimensions to the *edge effect* depth d is:

$d = 0.63 \times S_o \times \left(1 - e^{(1-S_d/S_o)/1.5}\right)$, where S_o and S_d are the equivalent circular radii of the open area A_o and total area of the duct A_d respectively, calculated from the dimensions of the physical duct by: $S_o = \sqrt{\frac{A_o}{\pi}}$ and $S_d = \sqrt{\frac{A_d}{\pi}}$.

Before introducing the full theoretical model, a final principle is explained, that of the impedance transformation formula or ITF.

4.2.3 Description of the Impedance Transformation Formula

The analysis explained in this subsection has already been applied in *Section 3.4.2*, used in the model of the multi-layer wall in its more general form, though it was not explicitly explained. Here, the analysis is concerned with

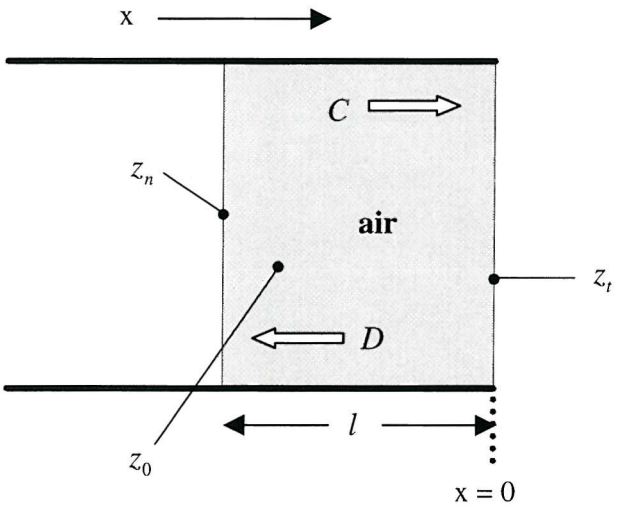

Figure 4.6 – Impedance transformation formula (ITF) model

transforming a known impedance a distance l through the characteristic impedance of air: $\rho_0 c_0$. The model is illustrated in *Figure 4.6*.

At $x=0$ is the known terminating impedance z_t and the desired impedance z_n is at $x=-l$. A plane standing wave field is formed by the forward and backward going waves C and D respectively. By considering C, D and the characteristic impedance of the medium, the acoustic impedance at a position x can be expressed as

$$z(x)=\left(\frac{e^{-jkx}+R\left(e^{jkx}\right)}{e^{-jkx}-R\left(e^{jkx}\right)}\right)\rho_0 c_0 \tag{4.1}$$

where the complex reflection coefficient R is defined at $x=0$ as $\frac{D}{C}$.

Evaluating *equation 4.1* at $x=0$ and rearranging to make R the subject yields

$$R=\frac{z_t-\rho_0 c_0}{z_t+\rho_0 c_0} \tag{4.2}$$

Which when substituted back into *equation 4.1* gives an equation for the impedance at any point x in terms of the terminating impedance of the duct and characteristic impedance of the medium, air.

$$z(x)=\rho_0 c_0\frac{\left(z_t+\rho_0 c_0\right)e^{-jkx}+\left(z_t-\rho_0 c_0\right)e^{jkx}}{\left(z_t+\rho_0 c_0\right)e^{-jkx}-\left(z_t-\rho_0 c_0\right)e^{jkx}} \tag{4.3}$$

From Euler's equation, *equation 4.3* can be expressed in terms of trigonometric quantities, thus the impedance a distance $-l$ from a known terminating impedance is

$$z_n = \rho_0 c_0 \frac{z_t \cos kl + j\rho_0 c_0 \sin kl}{\rho_0 c_0 \cos kl + j z_t \sin kl} = \rho_0 c_0 \frac{z_t + j\rho_0 c_0 \tan kl}{\rho_0 c_0 + j z_t \tan kl} \qquad (4.4)$$

Equation 4.4 will be referred to herein as the impedance transformation formula, or ITF. With reference to the previous chapter, one will note that the ITF is used by Guy as one of the two layer surface impedance relationship equations. The model described in the next section will build on the theory described in this and the previous section, in characterising the hard walled splitter duct at specific points with equations of pressure and velocity continuity.

4.2.4 Derivation of Continuity and Impedance Equations

The single period of the absorber, on which the model is based, that was mentioned in *Section 4.2.1* is illustrated in *Figure 4.7*. The panel and its associated *edge effect* sidebranches are shown in the middle of the figure, with the adjacent panels at the extreme left and right. The only additional model dimension is

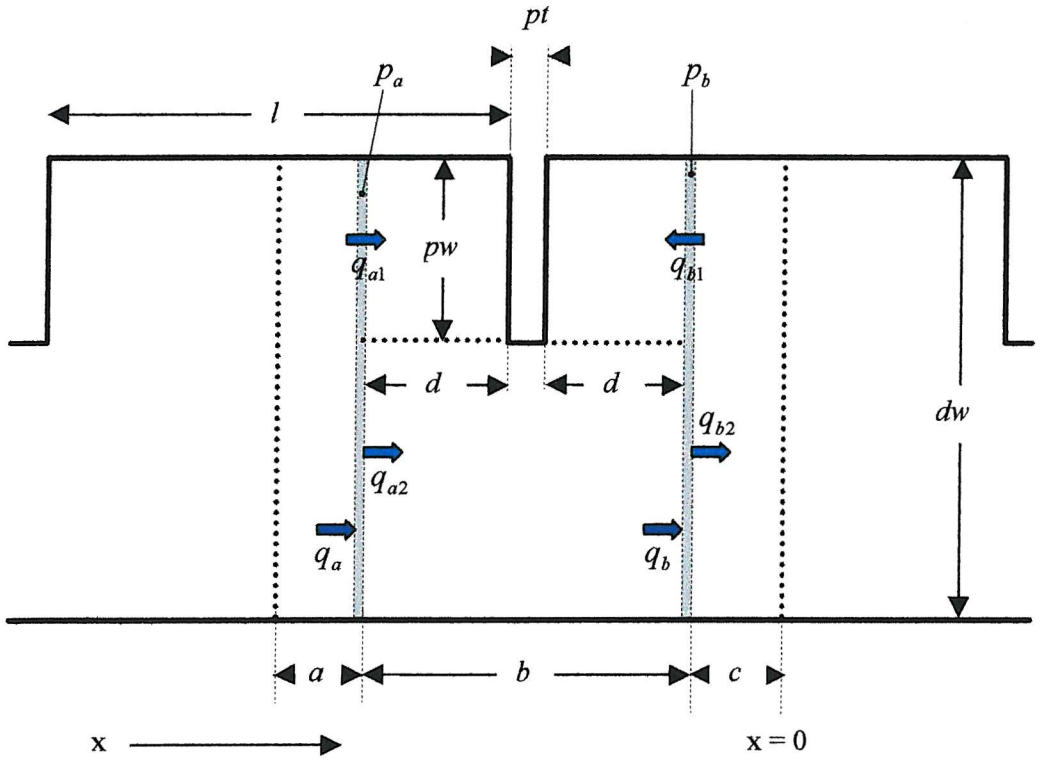

Figure 4.7 – Dimensions, pressures and velocities within the theoretical reactive model

l, the distance between panels. Starting from $x=0$, half way between the middle and right panel and moving left, three distances are specified. Distance c is from halfway between adjacent panels and the opening of the right *edge effect* sidebranch, b is the sum of the two sidebranch depths and panel width and a is the distance from the left sidebranch opening to the left panel mid point, thus $a=c$. In this section the impedances at four points, $x=0,-c,-(c+b)$ and $-(c+b+a)$, are found via equations of pressure and volume velocity continuity. At $x=-c$ and $-(c+b)$ control volumes are specified. The pressure within these volumes (p_b and p_a respectively) are assumed as being uniform.

The velocity continuity equations are formed by considering the net flow in and out of these volumes. For the two volumes shown there are different velocities, numbered q_a, q_{a1}, q_{a2} and q_b, q_{b1}, q_{b2}, each of which has an associated impedance (z_{a1} etc).

These equations of continuity are defined in terms of **volume** velocity q, while impedances are defined as the quotient of pressure and **particle** velocity u; the two of which are connected by the area a at that point in the duct, $q(x)=a(x)u(x)$.

Starting from a known terminating impedance z_t at $x=0$ the impedance at $x=-c$ is found by using the impedance transformation formula:

$$z_{b2}=\rho_0 c_0\left(\frac{z_t+j\rho_0 c_0\tan kc}{\rho_0 c_0+jz_t\tan kc}\right) \tag{4.5}$$

At this point a control volume is specified and mass conservation dictates that the net volume velocity remains constant, therefore the equation of continuity at $x=-c$ is:

$$q_b=q_{b2}-q_{b1} \tag{4.6}$$

At the same point, two volume velocities can be written in terms of duct dimensions and known impedances. z_{b2} is known from *equation 4.5* and z_{b1} is the impedance of a rigidly terminated pipe of length *d*, the standard result is:

$$z_{b1}=-j\rho_0 c_0\cot kd \tag{4.7}$$

Therefore we can state:

$$q_{b2}=\frac{p_b a_2}{z_{b2}} \text{ and } q_{b1}=\frac{p_b(a_2-a_1)}{z_{b1}} \tag{4.8a, b}$$

Where the cross sectional areas a_1 and a_2 are defined in terms of the duct height y (an arbitrary constant that cancels out) as:

$$a_1 = (dw - pw)y \quad \text{and} \quad a_2 = dw \cdot y \tag{4.9a, b}$$

Substituting *equation 4.8* into *equation 4.6* yields:

$$q_b = p_b\left(\frac{a_2}{z_{b2}} - \frac{(a_2 - a_1)}{z_{b1}}\right) \tag{4.10}$$

Which given the relationship between impedance, area and cross sectional area allows us to evaluate z_b as:

$$z_b = \frac{p_b a_1}{q_b} = \frac{a_1}{\frac{a_2}{z_{b2}} - \frac{(a_2 - a_1)}{z_{b1}}} \tag{4.11}$$

The procedure described in *equations 4.5 – 4.11* is the general way in which the necessary impedances are evaluated. For the sake of clarity and completeness the analysis for the remaining part of the period is given below in a less explicit manner.

As before, the ITF is used to find z_{a1} in terms of z_b:

$$z_{a1} = \rho_0 c_0\left(\frac{z_b + j\rho_0 c_0 \tan kb}{\rho_0 c_0 + j z_b \tan kb}\right) \tag{4.12}$$

At $x = -(c+b)$ the equation of mass conservation is:

$$q_a = q_{a1} + q_{a2} \tag{4.13}$$

Where the known volume velocities are given by:

$$q_{a1} = \frac{p_a(a_2 - a_1)}{z_{a1}} \quad \text{and} \quad q_{a2} = \frac{p_a a_1}{z_{a2}} \tag{4.14a, b}$$

From which the unknown impedance can be found according to:

$$z_a = \frac{p_a a_2}{q_a} = \frac{a_2}{\frac{a_1}{z_{a2}} + \frac{(a_2 - a_1)}{z_{a1}}} \tag{4.15}$$

Finally, the ITF is used for the last time to give the impedance z_0 a distance a to the left of z_a:

$$z_0 = \rho_0 c_0\left(\frac{z_a + j\rho_0 c_0 \tan ka}{\rho_0 c_0 + j z_a \tan ka}\right) \tag{4.16}$$

Thus *equation 4.16* gives the impedance a period distance $l+pt$ from a known terminating impedance z_t in terms of the geometry of the absorber and the dimensions of the duct.

From the impedances z_0, z_{a2} and z_{b2} forward and backward going waves are used to describe the propagation of sound in a duct with any given array of protruding panels.

4.2.5 Derivation of Transmission from Plane Wave Analysis

In the absence of acoustic resistance, a plane wave will be transmitted and reflected when it meets an impedance discontinuity, such as those evaluated in the previous section. The purpose of this section is to ascertain the frequency dependent transmission over one period of the absorber. The model used in the following analysis is illustrated in *Figure 4.8*. In addition to the relevant impedances from the previous section, the three pairs of forward and backward going waves are also

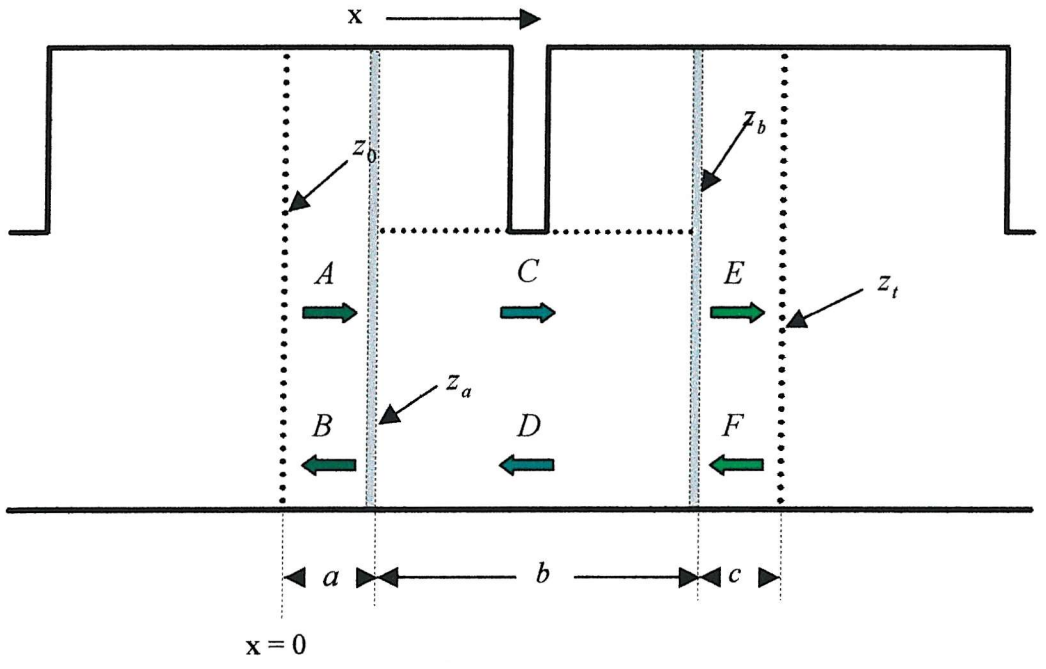

Figure 4.8 – Details of impedances and wave motion in the model

identified. The analysis will start at $x=0$ and conclude at $x=a+\mathrm{b}+\mathrm{c}$. The *MatLab* program based on this section repeats as many times as is necessary to calculate the transmission for the number of panels of interest. For each iteration, the starting impedance z_0 is the terminating impedance z_t from the previous period.

The general form of a plane wave pressure field takes the form:

$$p(x) = Ae^{-jkx} + Be^{jkx} \tag{4.17}$$

At $x = 0$ the relationship between A, B and z_0 is given by:

$$z_0 = \rho_0 c_0 \left(\frac{A+B}{A-B} \right) \tag{4.18}$$

A frequency independent unit amplitude forward going plane wave is assumed as the starting point for the analysis, given which allows B to be expressed as:

$$B = \frac{z_0 - \rho_0 c_0}{z_0 + \rho_0 c_0} \tag{4.19}$$

which when substituted into *equation 4.17* and evaluated at $x = a$ yields:

$$p_a = e^{-jka} + \left(\frac{z_0 - \rho_0 c_0}{z_0 + \rho_0 c_0} \right) e^{jka} \tag{4.20}$$

As both the pressure and impedance are known at this point, the unknowns C and D can be found. Rearranging $z_{a2} = \rho_0 c_0 \left(\frac{C+D}{C-D} \right)$ to make D the subject gives:

$$D = C \left(\frac{z_{a2} - \rho_0 c_0}{z_{a2} + \rho_0 c_0} \right) \tag{4.21}$$

From here we can rearrange $p_a = C + D$ and substitute in to *equation 4.21* yielding:

$$D = p_a \left(\frac{z_{a2} - \rho_0 c_0}{z_{a2} + \rho_0 c_0} \right) - D \left(\frac{z_{a2} - \rho_0 c_0}{z_{a2} + \rho_0 c_0} \right) \tag{4.22}$$

Which when rearranged gives C and D in terms of the pressure and impedance at $x = a$:

$$D = \frac{p_a \left(\frac{z_{a2} - \rho_0 c_0}{z_{a2} + \rho_0 c_0} \right)}{1 + \left(\frac{z_{a2} - \rho_0 c_0}{z_{a2} + \rho_0 c_0} \right)} \quad \text{and} \quad C = p_a - D \tag{4.23a, b}$$

In the same manner as before (*equation 4.11*) the pressure at $x = a + b$, p_{b2}, is evaluated using the values for C and D calculated in *equation 4.23*:

$$p_{b2} = Ce^{-jkb} + De^{jkb} \tag{4.24}$$

And using the same analysis as *equations 4.20 – 4.23* the forward and backward going waves in the final section are given by:

$$F = \frac{p_b\left(\frac{z_{b2}-\rho_0 c_0}{z_{b2}+\rho_0 c_0}\right)}{1+\left(\frac{z_{b2}-\rho_0 c_0}{z_{b2}+\rho_0 c_0}\right)}, \text{ and } E = p_b - F \qquad (4.25a, b)$$

The transmission loss as defined in *Section 4.1.1* is, for one period, proportional to the ratio of wave *A* to wave *E*. Which when expressed in dB is:

$$TL = 20\log_{10}\left|\frac{A}{E}\right| \qquad (4.26)$$

From the analysis of the previous sections it can be seen that the desired quantity expressed in *equation 4.26* requires the knowledge of only five variables, given the assumptions outlined in *Sections 4.2.1 & 4.2.2*: panel width and depth, duct width, the number of panels and the distance between them. The following section presents the results from this analysis.

4.2.6 Presentation of Theoretical Transmission Results

The purpose of presenting the theoretical results is two-fold: it will provide insight into the plane wave transmission behaviour beyond the plane wave limit of the experimental duct and will enable the preliminary conclusions of *Sections 4.1.4 & 4.1.5* to be validated. Two theoretical transmission results will be included in this section, grouped according to panel depth/angle, after which a final result is directly compared with experiment. It was hypothesised in *Section 4.1.5* that the angle of the panels were not of themselves important, rather it was the distance of panel protrusion into the duct that was responsible for the increase in TL at the more obtuse angles. While the theory is unable to separate the two variables it is able to test this hypothesis by investigating the change in TL between different depths of panel, all at 90^0 to the side wall. To simulate the panels at an angle of 40^0 the panel depth is $122\text{ mm}\times\sin 40^0 = 78\text{ mm}$ and similarly at 60^0 the panels are 106 mm deep.

4.2.6.1 Theoretical Transmission for 78 mm Deep Panels

The plot shown in *Figure 4.9* gives the same comparison between absorber arrangements as in the experimental results. The key difference in the presentation of the theoretical and experimental results is the frequency range that

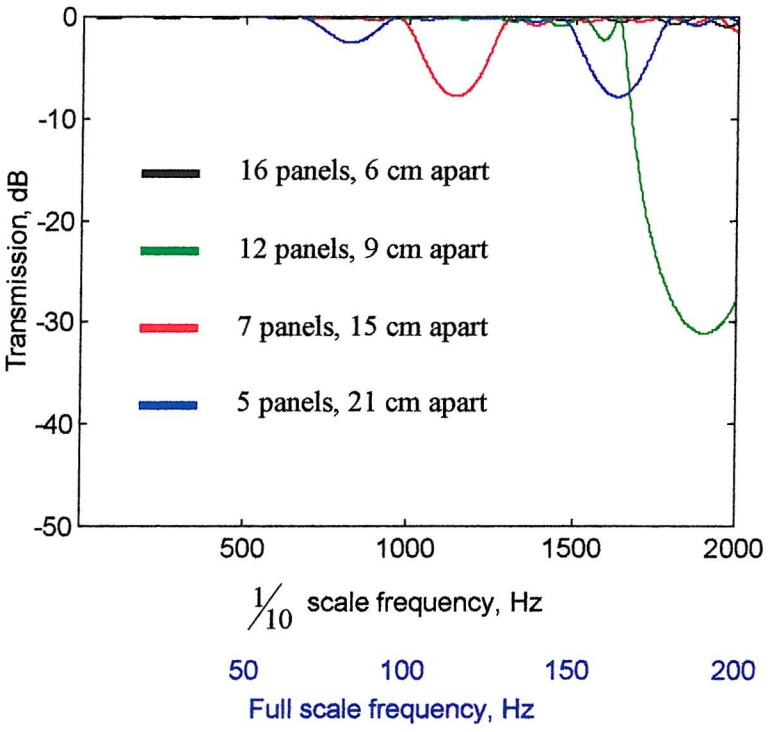

Figure 4.9 – Theoretical transmission for 78 mm deep panels

extends to 2 kHz instead of 800 Hz. The two features that will be commented on are the value of maximum transmission loss and the frequency at which it occurs.

With the panels spaced only 6 cm apart, no discernible deviation from 0 dB transmission is evident, though small oscillations can be seen near 2 kHz. When the panels occupy only about $^1/_3$ of the duct width, this spacing offers almost no filtering of the plane wave down the duct.

By contrast a spacing of 9 cm yields a significant (-31 dB) stop band centred on 1.9 kHz. The wavelength at this frequency is 0.18 m, thus the panel spacing represents a ½ wavelength. The mechanism involved is the same as the small dips noted in the experimental results caused by the small changes in duct cross section. An analogous situation is encountered if one shouts at a flight of uncarpeted stairs. At frequencies where the depth of each stair is an integer multiple of ½ wavelength, the reflected sound constructively interferes, resulting in a reflection that is far stronger. The stair case thus filters the reflective sound on account of its dimensions. In the same way, the sound is reflected by the panels at all frequencies, but only where the reflected sound sums, does the transmission loss become significant.

The 15 cm absorber arrangement also gives rise to a stop band, extending to –8 dB at 1140 Hz. As before, the wavelength of this frequency of maximum TL is twice the separation distance of the panels.

Due to the proportionally wide separation, the absorber with panels 21 cm apart causes two stop bands within the frequency range. At 820 Hz the transmission only reaches –3 dB, though at 1630 Hz the maximum is –8 dB. This trace gives more insight into the mechanism responsible for the plane wave filtering, as the TL is larger when the panel separation distance is equal to a wavelength, than when equal to ½ wavelength.

Comparison between the four traces indicates that, for a ½ wavelength stop band, the maximum TL is larger for absorbers with more panels. This means however, that to achieve significant TL at low frequencies, the room will need to be large in order to accommodate many panels a large distance apart.

4.2.6.2 Theoretical Transmission for 106 mm Deep Panels

Figure 4.10 shows the predicted transmission for different arrangements of absorber whose panels occupy about half of the duct width. The trends observed in the previous figure continue here, with fewer panels yielding less TL and wider separations lowering the frequency of maximum TL. The same relationship between this latter dependency exists with the deeper panels, with stop bands centred on integer multiples of ½ wavelengths. The difference between this figure and the last is the greater TL achieved, in fact close to a three fold decibel increase in TL is seen for only a 36% increase in depth. This observation agrees with the experimental results.

In the final section of this chapter, the theoretical results for 122 mm panels at 90^0 to the side wall are compared directly with the experimental results for the same set-up. The frequency range will be constrained to the limit dictated by the experiment, i.e. a scale frequency of 100 to 800 Hz.

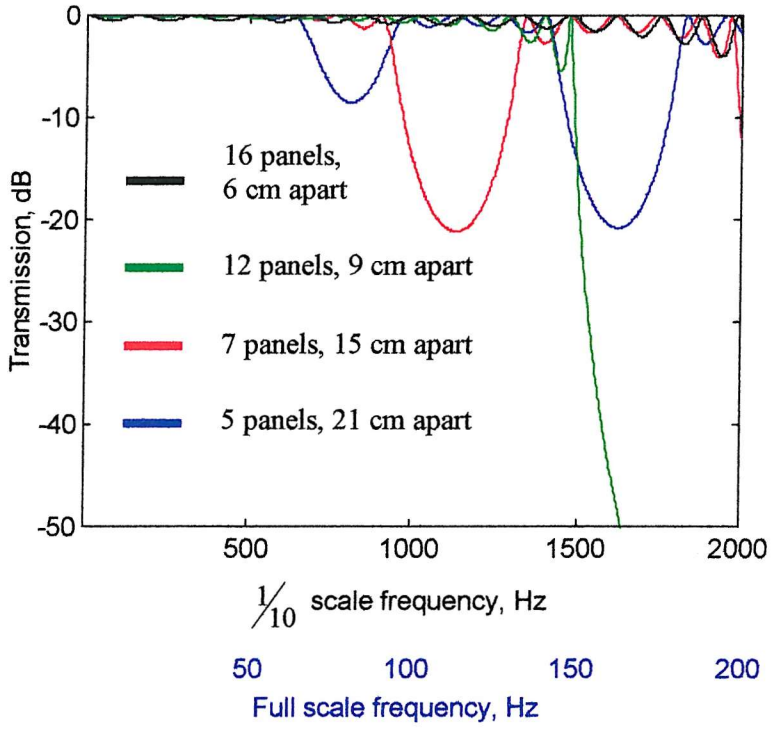

Figure 4.10 – Theoretical transmission for 106 mm deep panels

4.3 Comparison between Experimental and Theoretical Transmission for Panels at 90^0

Up to this point, the experimental and theoretical have been presented in isolation, to aid observation and analysis and also because only one comparison is valid, that of absorber arrangements with panels at 90^0 to the side wall of the duct. As the significant theoretical TL for the 6 and 9 cm absorbers occurs above 1 kHz, these two traces are not presented with the experimental results. The experimental transmission will be discussed first, before the theoretical and then the comparison between the two.

Figure 4.11 shows the transmission results for both experimental and theoretical. As would be expected from the trend set in the earlier experimental results and the dependency identified in the previous section, the 6 cm absorber exhibits a greater TL than when the panels are at more acute angles. The frequency at which the transmission deviates from 0 dB is similar to the result at 60^0, around 520 Hz. The same trends are evident in the other experimental traces with greater TL than for the

previous arrangements and occurring at lower frequencies as the panels are spaced further apart. In the same way, the theoretical TL for the 21 cm absorber is around 3 dB greater at 800 Hz than with panels 106 mm in depth. In the frequency range shown, it is difficult to make many conclusions regarding the 15 cm theoretical trace.

4.4 Conclusions

The investigation described in this chapter is intended to be the first stage in understanding the way in which the side wall *Bass Trap* effects the sound as it propagates down the duct, or in the real life situation, the recording studio control room. Purposefully removing any acoustically resistive elements from both the experimental work and the theoretical analysis allowed the reactive filtering to be more clearly identified.

The experimental investigation did not produce results from which any obvious conclusion could be drawn, primarily because of the plane wave limitation of the frequency range. However, a couple of trends were observed which gave a better idea of what to expect from the theoretical investigation. The spacing of the panels was shown to be in some way connected to the frequency range in which the filtering took place, a filtering that increased in magnitude as the panels protruded further into the duct.

The theoretical results confirmed these two observations and was able to show that a stop band will occur at frequencies where the panel spacing is equal to an integer multiple of ½ a wavelength. This fact explains why in the experimental frequency range, the clearest result was for panels spaced 21 cm apart.

Additionally, as the number of panels increase, for a given ½ wavelength stop band, it has been shown that the maximum value of TL also increases.

The comparison between the two sets of results in *Figure 4.11* illustrated the discrepancy between experiment and theory, though the lack of similarity can be explained.

Although the experimental set-up was designed to be purely reactive, through the use of aluminium plates and concrete paving slabs for example, it is inevitable that some sound energy will have been dissipated in one way or another. It is possible that the draft excluder strip lining the top of the side wall, used to ensure an air tight seal, may have contributed a small amount of acoustic resistance. The effect of such resistance

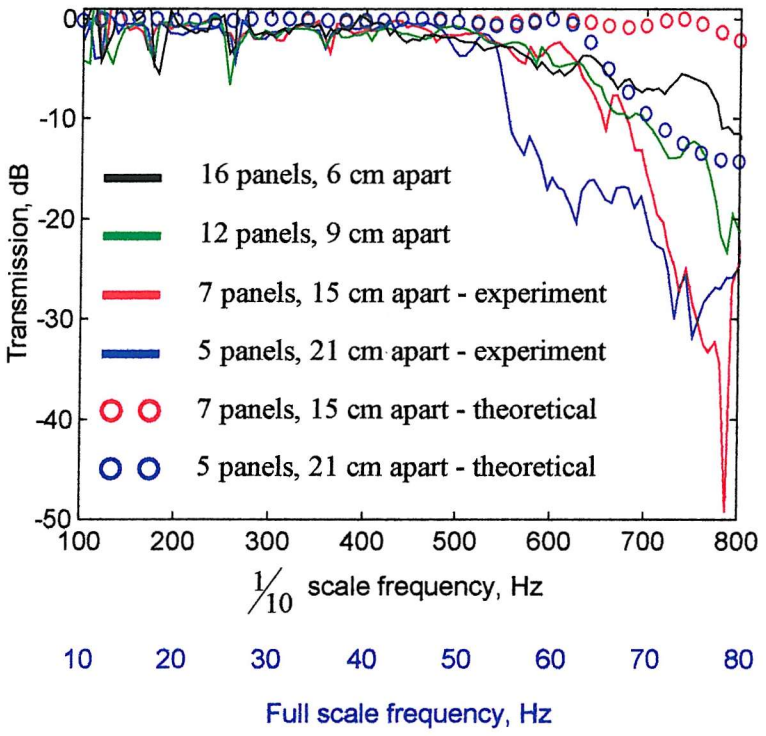

Figure 4.11 – Theoretical and experimental comparison for panels at 90°

may be to reduce the Q factor of the stop bands, spreading a less pronounced filtering effect over a wider range of frequencies.

The presence of the cut-on mode operating in the vertical direction of the duct may also have influenced the experimental results, yielding apparent TL far in excess of those predicted by the theory.

It is worth making the point, however, that the real life design uses panels even closer together (scaled up) than the smallest separation distance in this investigation. It is unlikely therefore that even in the larger control rooms, a transmission of –10 dB would be achieved from the front to the back of the room below 100 Hz (see black trace of *Figure 4.4*). That said, at the lower mid frequencies (150 – 300 Hz), the significant stop bands predicted in the theory, broadened by the addition of resistive material on the panels, would be expected to yield a large amount of attenuation.

CHAPTER 5

Absorption Coefficient of the Open End of a Rhomboidal Channel Terminated by a Soft Boundary

Introduction

Having investigated the effect that the large amount of porous absorbent, used in the design of the *Bass Trap*, has on the reverberation time of a real life control room (*Chapter 3*), the research then turned to consider the influence the periodic array of uncovered panels placed on a rigid side wall has on the propagation of sound down the room (*Chapter 4*). In this chapter, the primary focus is the absorption coefficient of the *Bass Trap* when placed on the **rear** wall. As mentioned in *Chapters 1 & 4*, given that the wavefront of sound propagating from the front monitor wall is approximately normally incident on the rear wall, the quantity chosen to best describe its effectiveness is the normal incidence absorption coefficient.

Note, this quantity would not have been appropriate in investigating the performance of the absorber arrangements in the previous chapter. Indeed, the normal absorption coefficient of the side wall described would have been zero and yet it was clearly shown – through the use of TL – that even with no resistive elements, the arrangement of panels has a considerable effect on the sound field.

The way in which the rear wall *Bass Trap* is investigated is by splitting the array of panels into individual *channels*, that is, the volumes formed by the multi-layer wall and adjacent angled panels. The cross section of such a channel is rectangular, though in the horizontal plane it is rhomboidal. For the purposes of this investigation the region of interest in this rhomboidal channel is the open end, i.e. the point at which the panels protrude most into the room. It is here that the absorption coefficient will be evaluated.

In addition to the normal incidence absorption coefficient, the associated real and imaginary part of the surface normal acoustic impedance (resistance and reactance respectively) will also be presented. These results will help in explaining the absorption and point to other more subtle quantities that will be used in this and later chapters.

Three means of investigation will be used: analytical theory, numerical and experimental. By approaching the problem from different directions, it will be possible to ratify results, allowing confidence to placed in the conclusions reached. The theoretical and numerical analysis will be explained first, followed by the results obtained. The experimental investigation will then be described, after which conclusions will be drawn.

5.1 Description and Explanation of the Theoretical Model

The geometry of the rhomboidal *Bass Trap* channel described in the previous section is not straight forward to model analytically. Although the open end of the channel is parallel with the soft termination, the angled panels which connect the two introduce the problem of which direction to formulate the analysis. The theoretical model presented in this section and illustrated in *Figure 5.1*, simplifies the problem by making a couple of key assumptions.

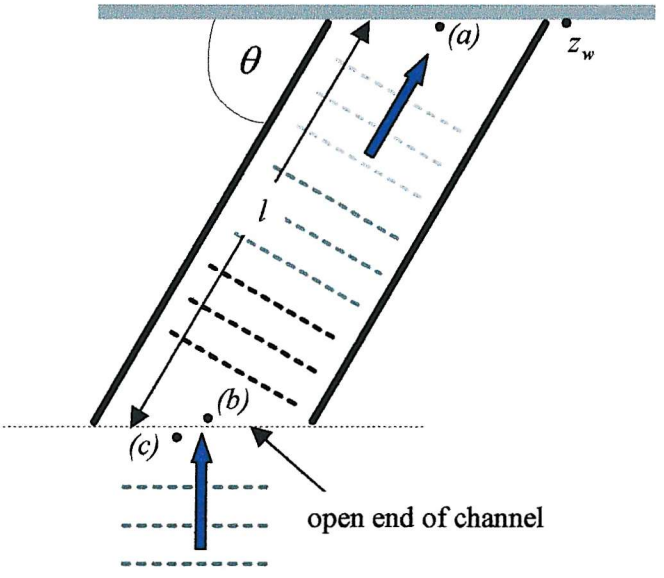

Figure 5.1 – An illustration of the model used for the simple theory

Only plane wave propagation is considered, thus the generation of higher order modes due to diffraction and refraction is ignored. The soft termination (an approximation to the multi-layer wall), of surface normal impedance z_w, is assumed to be locally reacting, from which the oblique angle surface impedance at position (a) in *Figure 5.1*

is $z_w \sin\theta$. Using the analysis described in *Section 4.2.3*, the impedance transformation formula (*equation 4.4*) is employed to give the acoustic impedance a distance l away, at position (b). In order to find the surface acoustic impedance at this position, but parallel with the wall, the same angular transform as before is used as before to give the impedance at position (c). The resultant surface normal impedance at the open end of the channel is thus a function of the depth and angle of the panels and the normal surface impedance of the termination.

As with the investigation of *Chapter 4* the theoretical model is on a $^1/_{10}$ scale so as to allow direct comparison with experiment. This part of the investigation will be described later in the chapter. The other requirement for comparison is that the channel is terminated by the same value of surface normal acoustic impedance. The experiment uses a 26 mm thick open cell low resistivity foam partially covered in sticky tape to represent the soft rear wall. The acoustic impedance of this sample was measured experimentally using the white noise, two microphone technique described in *Section 2.3.2*. This measured value will prove key in the results that are to follow, as it is used as an approximation to the multi-layer wall in both models of the rhomboidal channel.

Whilst the theoretical model is by no means an accurate descriptor of the physical system, it may provide a reasonable approximation. A qualitative explanation of a far more rigorous analytical method is given in *Chapter 8*.

Recent research [5.1] has shown that, in a free field environment, a low frequency wavefront normally incident on an array of angled panels is redirected such that after passing through, the angle of the wavefront is the same as the angle of the panel array. This suggests that the panels act as waveguides, forcing the sound to propagate in a different direction, as shown in *Figure 5.1*.

In order to provide a more accurate model of the rhomboidal channel, a numerical investigation was also employed using Finite Element Analysis.

5.2 Description and Explanation of the Finite Element Model

A description will be given in this section as to how the rear wall *Bass Trap* rhomboidal channel is modelled using numerical techniques. However, before this, a brief synopsis will be given of the way in which Finite Element Analysis (FEA) works and the more general applications for its use.

5.2.1 Overview of Finite Element Analysis

Only a summary is given here and the interested reader is referred to Petyt's book on the subject [5.2]. Numerical methods of analysing acoustical problems are based on the description of sound by the three-dimensional wave equation - in the frequency domain the Helmholtz form is used. The name *Finite Element Analysis* comes from the fact that it is limited to a finite domain, such as an interior or a room, where boundaries do not extend to infinity. The geometry to be modelled is described by constructing a mesh which also contains the dimensions of all the boundaries. Within the volume of interest, elements are described which are used to discretise any given geometry. Each two-dimensional element (to which this discussion is limited) may have from three to eight sides, joining at the element's *nodes*. These nodes are also the points which connect one element to another and where the wave equation is solved. The acoustic properties of the elements can be specified, from as simple a description as sound speed and density, to porosity, structure factor and resistivity used to characterise absorbent materials. In addition to the element specifications, the boundaries which constrain the model can be assigned with material properties – the most useful for this discussion being a surface normal impedance. It is also possible to import external values (experimental results for example) and assign these to particular boundaries through the use of frequency dependent tables. Once the set of equations for the model have been solved to give pressure, velocity and intensity at **every** node (often many thousand), the results can be presented in a number of different formats. For the purposes of this investigation the velocities at certain nodes were exported into a file which was then read by *MatLab* and subsequently manipulated. The FEA software used for this and later investigations was *Sysnoise v 5.3a* developed by *LMS Numerical Technologies*.

5.2.2 Description of the Finite Element Model

Three Finite Element (FE) meshes were constructed for three angles of *Bass Trap* channel, 20^0, 40^0 and 60^0; the 40^0 mesh is shown in *Figure 5.2*. Each model uses the same depth of panel (122 mm) and width of channel (60 mm), as comparison with the other methods of investigation required the FE model to be on a $^1/_{10}$ scale also.

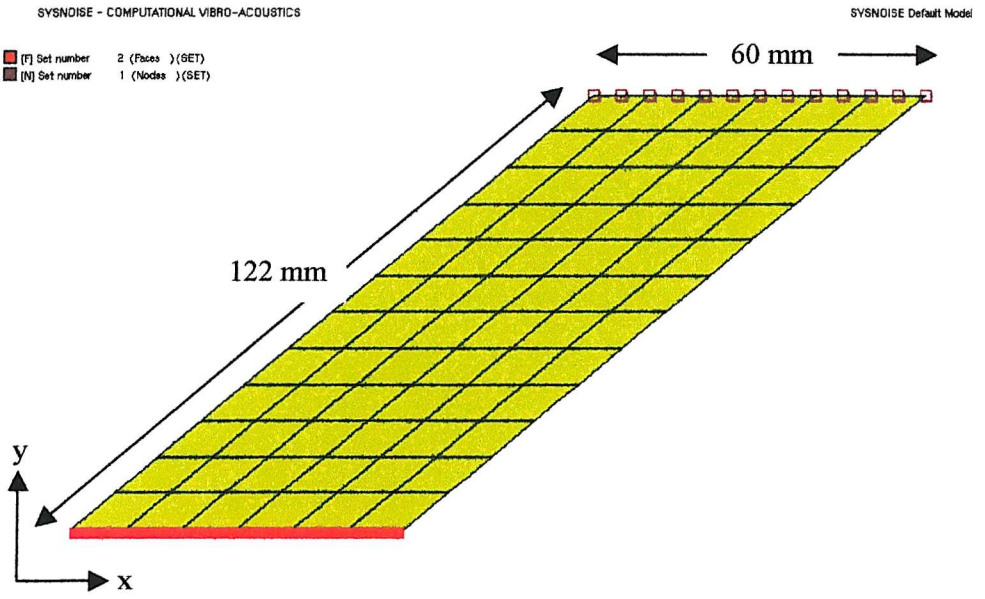

Figure 5.2 – Finite Element mesh of a 40^0 channel showing the two boundary conditions

In *Figure 5.2* two regions are highlighted: the soft wall boundary condition at $y = 0$ shown as a red line and the brown squares at the open end of the channel identifying 13 nodes. As in the theoretical model, the soft termination in the FE model required the same surface normal acoustic impedance as the experiment. This was achieved by reading into *Sysnoise* the measured impedance of the 26 mm thick foam and assigning it to the $y = 0$ boundary. The excitation used in the FE analysis was a unit amplitude plane wave source positioned at the channel mouth. This pressure boundary condition was imposed by assigning a pressure of magnitude 1 and phase 0 to the element faces at $122 \sin\theta$ (in mm), where θ is the angle of the panels. The surface impedance in this plane was calculated by exporting the $-y$ direction velocity at the nodes (brown squares) from *Sysnoise* and into *MatLab*. The arithmetic mean of the 13 complex values of normal particle velocity was calculated to give an average over the width of the channel. Together with a knowledge of the pressure p, the desired surface normal acoustic impedance of the channel opening is calculated as $z_n = \frac{p}{u_n}$, where u_n is the average normal particle velocity at the open end of the channel.

5.3 Comparison of *Bass Trap* Channel Absorption Coefficient

In *Sections 5.1 & 5.2* the two models of a single channel of the *Bass Trap* rear wall have been described. In this section, the results obtained will be presented. The measured value of absorption coefficient for the soft termination alone is. As mentioned in *Section 5.1*, **the measured surface normal acoustic impedance of the tape covered foam is used in both the Finite Element and theoretical model**. The associated absorption coefficient of the foam is plotted together with the channel absorption coefficients calculated by the theory and the FEA, to allow easy comparison. The results are grouped according to angle of channel, starting with 60^0 and moving to more acute angles.

5.3.1 Comparison of Channel Absorption Coefficient at 60^0

The absorption coefficient for the termination alone and the theoretical and numerical prediction for a 60^0 channel is shown in *Figure 5.3*.

The 26 mm sample of foam by itself exhibits a similar absorption coefficient characteristic to the cotton waste felt of *Chapter 3* – as is typical of porous materials,

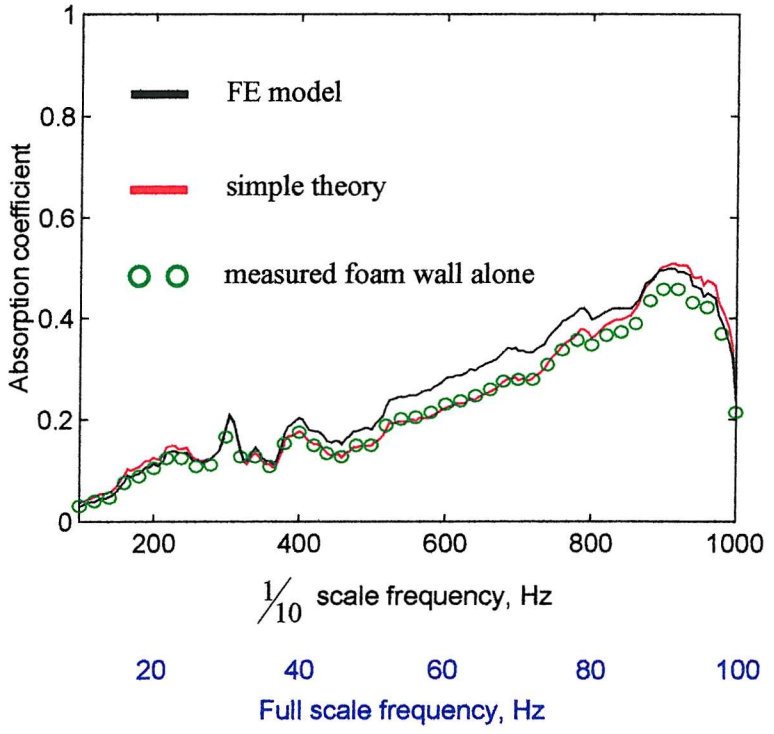

Figure 5.3 - Comparison of absorption coefficients for panels at 60^o

the absorption rises with increasing frequency. The slight difference however, is the drop in absorption above 900 Hz, which is caused by the reflective qualities of the tape at these higher frequencies. At 60^0, the channel would be expected to make the least difference to the absorptive qualities of the foam by itself, as at 90^0 normally incident sound would not be affected by the channel at all and if such a result was presented the three traces would be identical.

The red trace, describing the theoretical absorption coefficient, is indeed very similar to the foam, the only slight differences occurring above 800 Hz. The FEA trace differs more, particularly in the mid frequencies, where slightly higher absorption is predicted.

Comparing the two models, good agreement is noted especially at the two extremes of the frequency range. The similarity between the three traces below 400 Hz suggests that at this angle, the panels make little difference when the wavelength of sound is more than 4 times greater than the largest channel dimension. Established theory on the diffraction of low frequency sound around objects [5.3] supports this conclusion. Relating this result to the real world situation of the rear wall *Bass Trap*, it is clear that little benefit over the soft wall alone is had by placing panels at 60^0 in front of it, especially because at this angle the full scale panels would protrude over a metre into the room. Further insight into the absorption coefficient shown in *Figure 5.3* is given in *Figure 5.4* where the associated normalised surface normal acoustic resistance and reactance is shown. In the same way as for absorption, the two models show very good agreement, so for the purposes of this discussion will be considered as one. Both models exhibit extremely low normalised acoustic resistance over the majority of the frequency range, only above 800 Hz does this change. The foam by contrast starts at a higher value and drops with increasing frequency. The reason why this difference is not evident in the absorption coefficient is given in the plot of normalised acoustic reactance. Due to the distance between the position at which the impedance is calculated and the termination, the reactance becomes large and negative at a lower frequency for the *Bass Trap* channel. At these low frequencies, the reactance of the channel is dominated by the stiffness S of the air, which is proportional to $-\frac{S}{f}$. This is considerably less for the channel **and** foam than the foam alone, thus the reactance is, for a given frequency below the zero crossing, more

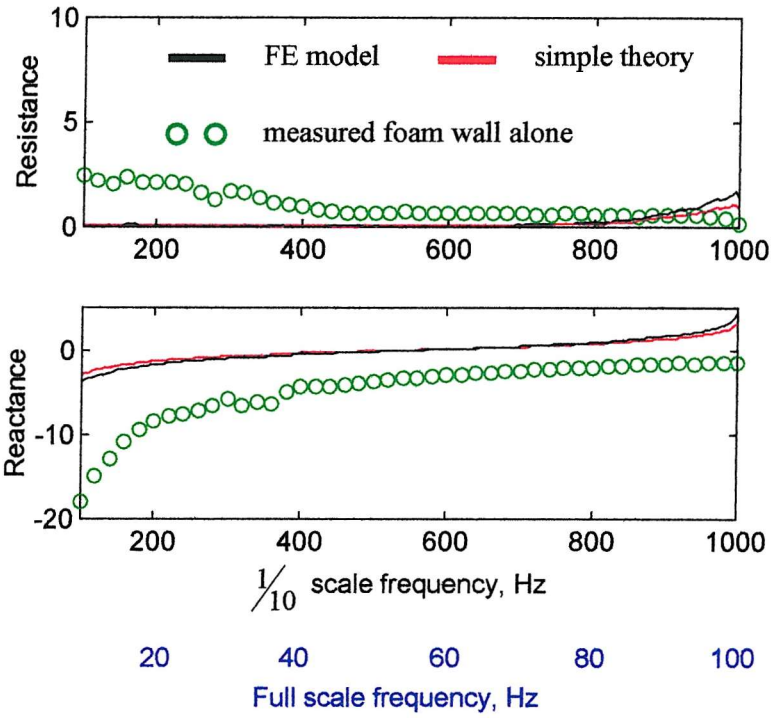

Figure 5.4 – Comparison of normalised surface normal impedance for panels at 60°

negative without the channel. The result of this is that the channel reactance is closer to zero in the frequency range of interest, meaning that the absorption coefficient is dominated by the resistive part of the impedance. If the resistance was larger (ideally close to a normalised value of 1) then the associated absorption coefficient would be much closer to unity.

5.3.2 Comparison of Channel Absorption Coefficient at 40°

This section considers the absorption coefficient of the *Bass Trap* channel at 40°, the results for which are shown in *Figure 5.5*.

The subtle difference between the theory and the wall alone noted in the previous channel is more significant here, with greater absorption below 300 Hz and an even more above 700 Hz. Given the aforementioned diffraction effects the difference at the low frequencies is surprising, especially as little difference is noted in the mid frequencies.

The FE predicted absorption coefficient by contrast shows an additional increased absorption between 400 and 700 Hz by up to 0.2, whereas at the extreme high and low frequencies the trace is largely similar to the wall alone. In the same way that the

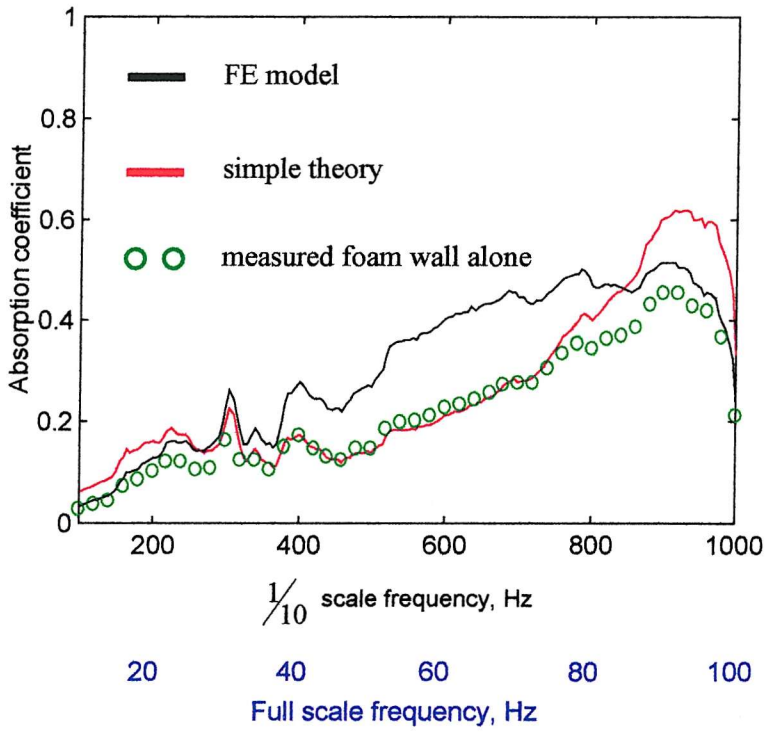

Figure 5.5 - Comparison of absorption coefficients for panels at 40°

panels do not affect the absorption at the low frequencies, where the wavelengths are long in comparison with the dimensions, a reduction in high frequency absorption would be expected as the sound exhibits a more ray-like behaviour. In this case the analogy with light is more valid, where a 'line of sight' argument could be used to explain why the sound is reflected more as the wavelength becomes shorter.

At this angle, the FE model suggests the presence of the panels makes a significant improvement over the wall alone for the majority of the frequency range considered.

The associated normalised acoustic impedance is shown in *Figure 5.6*. The difference between the two models is seen in both plots of resistance and reactance. In the resistance plot, the FE model indicates a higher value from 600 Hz upwards, being four times that of the theory at 1 kHz. The reason for this rise is that the resistive part of the impedance increases as the frequency approaches a ½ wavelength resonance of the channel depth [5.4]. The reactance is also affected in this region and does not become infinite, as would be the case with a perfectly reflective pipe. An additional effect of absorption in a terminated pipe is a low resistance at frequencies between the ½ wavelength resonance – a feature evident in *Figure 5.4* also. In the FE model, the

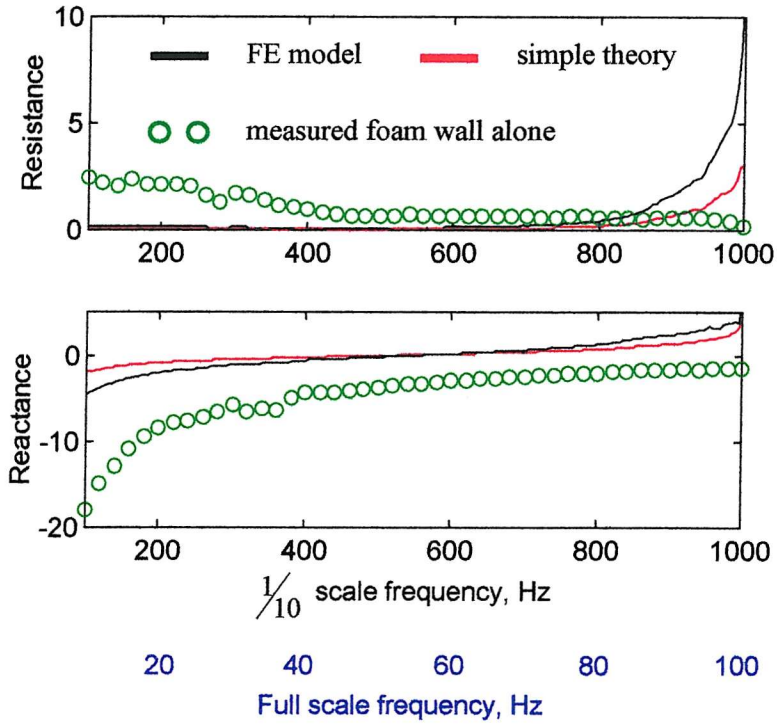

Figure 5.6 – Comparison of normalised surface normal impedance for panels at 40°

reactance indicates an effective shortening of the channel's depth as the low frequency values are more negative (greater air stiffness). The theory on the other hand shows little difference to that at 60^0, except at around 1 kHz.

An interesting feature to note, is the frequency at which the reactance is zero, as this indicates the 'effective depth' of the channel. Zero reactance occurs in a closed end pipe, at odd integer multiples of ¼ wavelength, as the reflected sound is in anti-phase with the incident sound at the channel opening. For a rigidly terminated 90^0 channel the depth would be equal to the panel depth, however when the panels are angled this is not the case, in fact the 'effective depth' of the channel **increases**. The impedance of the termination also has a large bearing on this effective channel depth, as the reactive part (which is dependent on the angle of incidence) indicates the depth of the foam alone. For both FEA and the theory the ¼ wavelength occurs at 558 Hz, which implies a depth of 152 mm (at a sound speed of 340 ms^{-1}), which is 25% more than for a 90^0 channel.

5.3.3 Comparison of Channel Absorption Coefficient at 20^0

This section is concluded with the results for channel absorption coefficient at 20^0, as shown in *Figure 5.7.*

The trends noted in the previous plots are continued here in a very clear manner. The theoretical absorption is again higher than the wall alone at the extreme high and low frequencies. The difference at high frequencies is particularly striking, as it peaks 0.4 higher than the wall at 900 Hz. As previously mentioned, neither result would be expected given the size of the physical system considered and the behaviour of sound at these frequencies. The FE model on the other hand exhibits the anticipated absorption characteristic, with a performance similar to the wall alone at low frequencies and slightly reduced at high frequencies. The most noticeable aspect of the FEA absorption is the peak between 200 and 800 Hz – the slightly erratic nature of the trace is a function of the measured result of the wall alone, subsequently amplified in the analysis. If the FEA is a reliable result, then placing panels at this angle in front of a soft wall would yield a significant improvement in absorption at low full scale frequencies (40 – 60 Hz in particular) for only a 0.42 m panel protrusion.

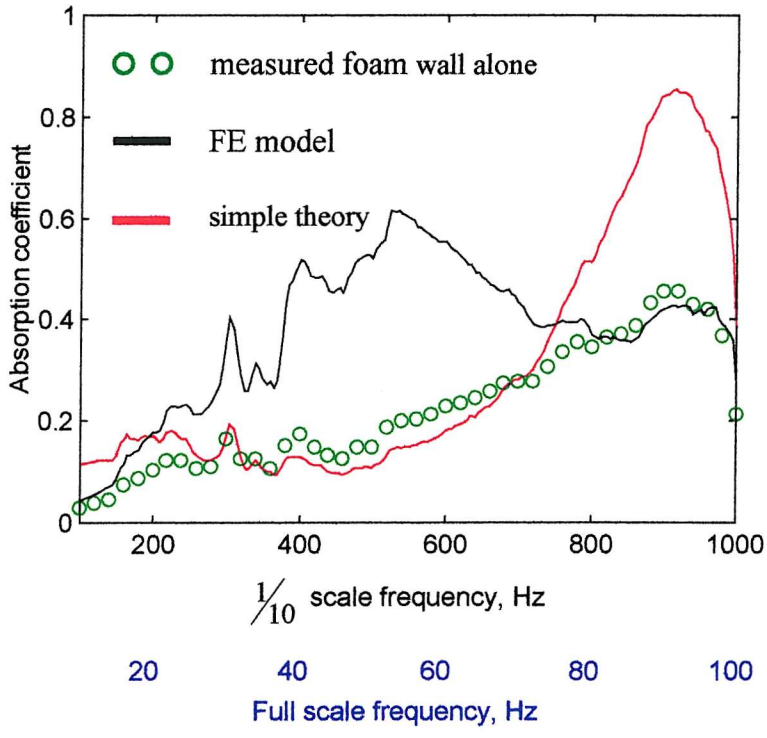

Figure 5.7 - Comparison of absorption coefficients for panels at 20^o

The explanation for the absorption coefficient results is given in the impedance plot for the 20^0 channel shown in *Figure 5.8*. The most significant change is the increased resistance across the frequency range predicted by the FE model, which together with the near zero reactance at the mid frequencies (because of the acoustic depth of the channel) gives rise to the high absorption noted in the previous figure. The expected rise in resistance as the frequencies approach the ½ wavelength resonance is clearly noted in the FEA and to a lesser extent the theory, though at a slightly lower frequency than anticipated (~ 980 Hz, given the ¼ wavelength resonance at 490 Hz). The more complicated geometry of the angled panels is the reason for the small deviation from the straight pipe result.

From the comparisons made in this section, it is possible to draw conclusions regarding the accuracy, particularly of the theory. The Finite Element model should, if used correctly, give an exact answer, as the Helmholtz equation is solved at hundreds of discrete positions in the channel and effects such as diffraction and higher order modes are accounted for. The theory, however, makes a number of assumptions which it was hoped would not compromise the results, though the discrepancy with FE model suggests otherwise. It appears that the simple way in which a change in

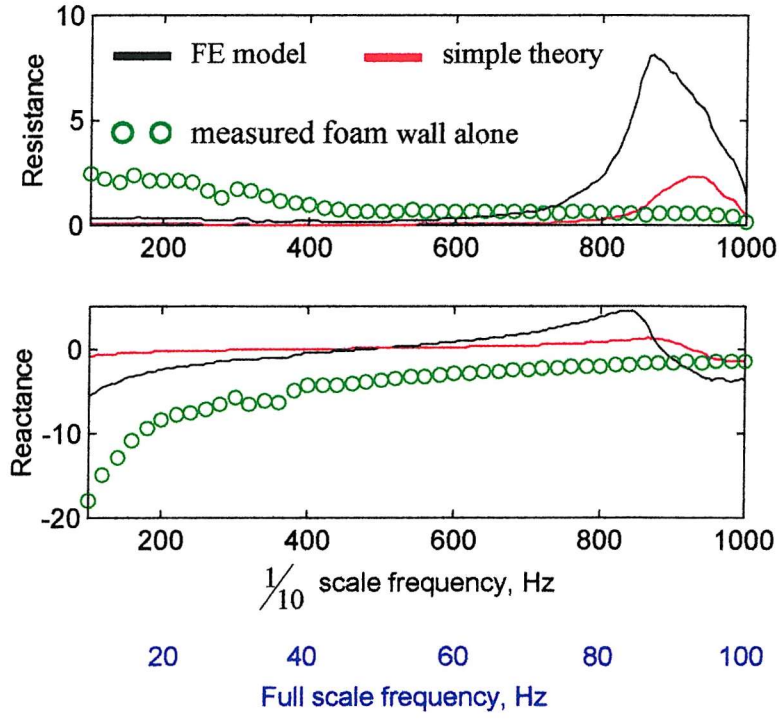

Figure 5.8 – Comparison of normalised surface normal impedance for panels at 20^o

angle of propagating sound was modelled, gave rise to results that did not adhere to physical principles (diffraction etc., see *Figure 5.7*) or tally with the exact numerical results predicted by the *Sysnoise* mesh of *Figure 5.2*.

In the hope that a third method of investigation can confirm the inaccuracy of the theory and reliability of the FEA, an experiment was designed to measure the surface normal acoustic impedance of the open end of the *Bass Trap* rear wall channel.

5.4 Experimental Measurement of Channel Absorption

In describing the experimental procedure to find the absorption coefficient of the rear wall *Bass Trap* channel, the duct of *Chapter 4* and impedance tube measurements of *Chapter 3* are re-introduced.

5.4.1 Description and Explanation of Experiment

In *Section 3.3.2*, brief explanation was given of the method by which the surface normal acoustic impedance of the felt was measured using two microphones in a standing wave tube. The minimum equipment required for such an experiment is a duct or tube with a noise source at one end and a rigid termination at the other, against which the sample of interest is placed. It was decided therefore to adapt the concrete duct, used to measure the side wall transmission in *Chapter 4*, to enable its use as a standing wave (or impedance) tube. Unlike earlier measurements, the surface at which the impedance would be measured was not the face of a piece of felt, but the open end of a rear wall *Bass Trap* channel. A photo of the adapted duct is shown in *Figure 5.9*, looking from the loudspeaker end. As can be seen, the width of the duct had to be reduced in order to create an angled channel at the termination end and this was achieved by using a spare concrete slab as a new side wall. The unused part of the duct (the trapezoidal region on the right of *Figure 5.9*) was sealed by placing a specially cut piece of wood at the loudspeaker end. A diagram illustrating the detail at the termination end of the duct is shown in *Figure 5.10*. The two microphones are positioned in the narrow part of the duct, with the channel formed by triangular pieces of wood and terminated by the aforementioned 26 mm thick tape covered foam. The figure shows how, in order to maintain the same 122 mm panel depth, the new side wall had to be able to move as the angle of channel was changed.

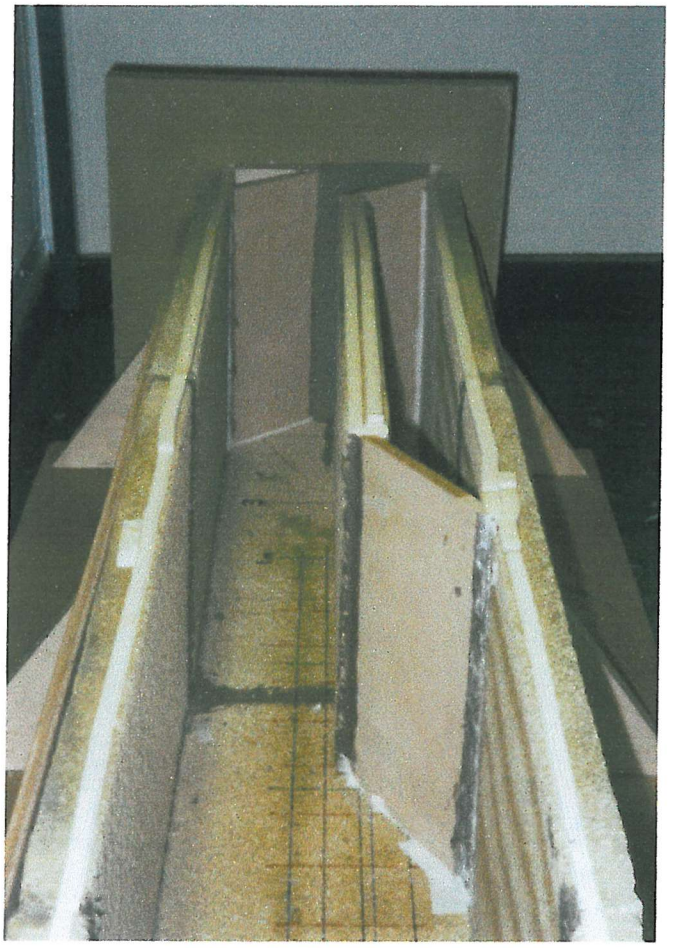

Figure 5.9 – Photograph of the angled channel experimental set-up

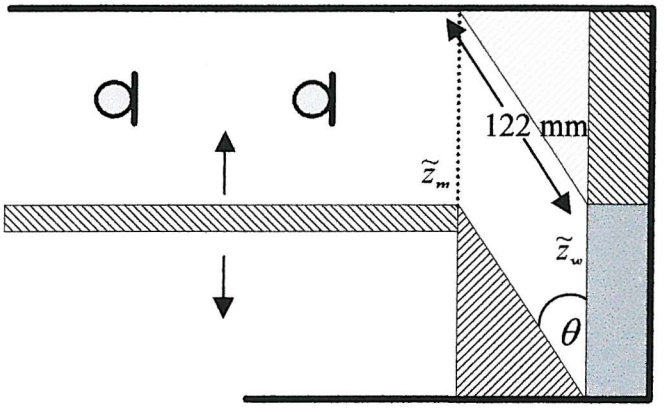

Figure 5.10 – Schematic diagram of the channel impedance experiment set-up

As the permanent duct width was fixed, the experimental set-up described resulted in the channel being different widths for different angles (100 mm at 20^0, 154 mm at 60^0). The measurements were only made once the construction of the duct had been rigorously checked, in particular, ensuring every join of wood and concrete was air tight. Even though five angles of channel were constructed and measured, only one of the results is presented here, the reason for which will become clear.

5.4.2 Comparison Between Experiment and FEM for 40^0 Channel

In *Figure 5.11* the absorption coefficient measured in the duct is compared directly with that predicted by the Finite Element model. Due to the plane wave limit of the concrete duct, described in the previous chapter, the frequency range only extends to 800 Hz.

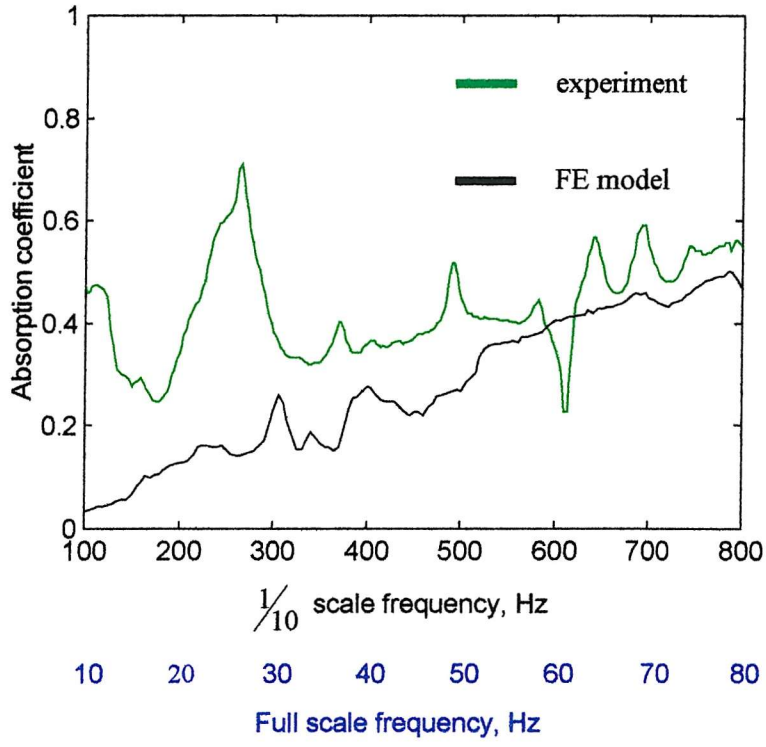

Figure 5.11 – Comparison between FE and measured channel absorption for a 40^o channel

The measured value of absorption coefficient at the open end of the 40^0 channel exhibits a general trend that rises with increasing frequency, though some large peaks and troughs in the trace detract from this. At the high frequencies, the agreement

between experiment and FEA is relatively good, though this is clearly not the case at the lower frequencies. Particularly noticeable are the two peaks at 120 and 270 Hz and even at the higher frequencies the trace is erratic. Although the measurement does show an improved absorption of the channel over the wall alone, further investigation into the cause of the peaks and troughs needs to be made before conclusions can be drawn.

5.4.3 Experimental Channel Absorption With and Without Foam

In order to explain the peculiar nature of the measured channel absorption coefficient, the experiment was modified slightly by removing the 26 mm foam termination, leaving only the rigid concrete. The reason for this was to see if the duct, rather than the angled channel, was contributing to the apparent absorption[1] of

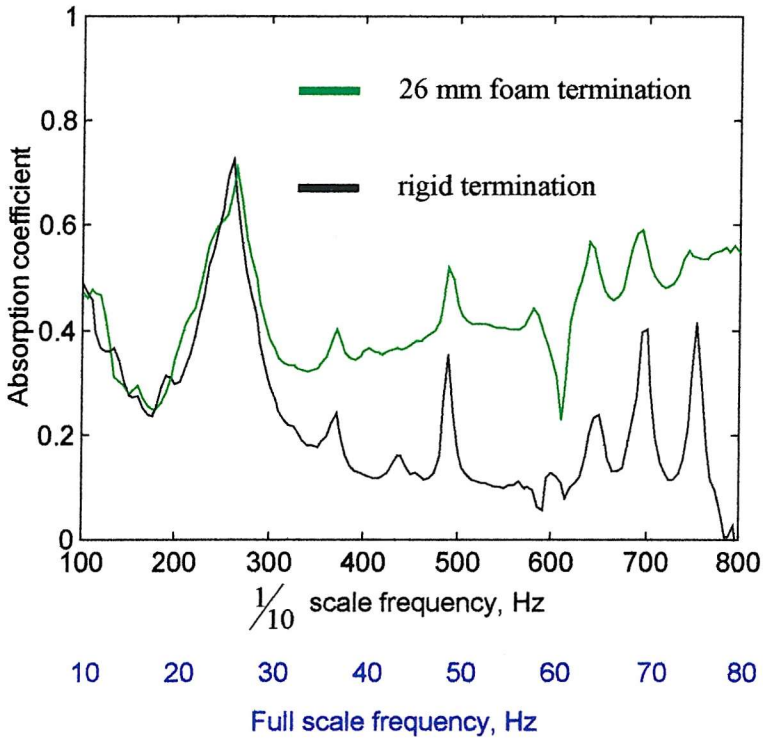

Figure 5.12 – Experimental absorption coefficient for a 40° angled channel

[1] The surface normal acoustic impedance was calculated from the transfer function between two pressure microphones, thus the absorption coefficient is only a derived quantity. As it cannot be directly measured, strictly speaking it can only be referred to as 'apparent' absorption.

Figure 5.11. Without the foam, no acoustic resistance is present, thus assuming the experiment is sufficiently well designed, no absorption should be evident. The comparison of channel absorption is shown in *Figure 5.12* from which it is clear the experimental set-up is far from satisfactory. Below 300 Hz the two traces are almost identical, which is not surprising given the absorptive qualities of the foam. Across the frequency range however, sharp peaks are noted in the rigid channel, which correlate to the peaks when the foam is present. The black trace clearly shows that the experiment and/or measurement procedure is flawed, with huge absorption coefficients apparent in a system that should exhibit almost none. Despite very careful design and construction it appear that the measured results are wholly unreliable. One of the explanations for the absorption at these frequencies is that the sound is efficiently transmitted out of the duct through the back wall and even into the trapezoidal void space necessary in forming the angled channel. Some of the absorption may actually be leakage of sound.

Secondly, some of the responsibility for the result may lie with the way in which the impedance was measured. The two microphone, white noise, standing wave method is very sensitive to errors. The distance of the microphones from each other and the sample is critical, as is the temperature, as these variables heavily influence the transfer function estimated between the microphone and noise source. Another important feature of a successful impedance tube measurement is confidence in a plane standing wave field, as the analysis rests on this assumption. Considering the way in which the duct width is constricted, it is likely that the subsequent higher order modes may not have decayed sufficiently for a strong plane standing wave field to exist in the region where the microphones were positioned. Given the results of *Figure 5.10 & 5.11* and the above discussion, the experimental part of this investigation cannot be used to explain the absorption coefficient of a rear wall *Bass Trap* channel.

5.5 Multi-Layer Wall Channel Absorption Coefficient

In this final section of the chapter the FE model introduced in *Section 5.2.2* is adapted to investigate the absorption coefficient of the full scale rear wall *Bass Trap* with the modelled multi-layer wall (*Chapter 3*) as the termination for the

rhomboidal channel. As in *Section 5.3* the angle of channel will be the variable that is changed, with the results presented on the same plot for ease of comparison.

Two results will be presented, the first for four different channel angles without any absorbent panel lining and the second for a 20^0 channel with the theoretical value of surface normal impedance of the felt (*Section 3.3*) assigned to the surface of the panels. This latter result will provide the most complete description of the normal incidence absorption coefficient of the rear wall *Bass Trap* in the research so far.

The rear wall *Bass Trap* will be investigated further in *Chapter 7* where the FE analysis is extended to consider a more subtle possible mechanism of absorption.

5.5.1 FE Calculated Absorption Coefficient Without Panel Lining

In order to investigate the real life absorption, the FE mesh shown in *Figure 5.2* is changed so that the panel depth and separation are now a factor of ten greater, 1.22 and 0.6 metres respectively. In the same way as the measured values of surface normal acoustic impedance of the 26 mm foam was read into *Sysnoise* in *Section 5.3*, so the predicted value for the multi-layer wall, estimated in *Section 3.4*, is used as the terminating boundary of the channel. The frequency range of the analysis is extended to 400 Hz (four times the full scale frequency of *Section 5.3*), meaning the ¼ wavelength resonance will be evident a number of times. The result is shown in *Figure 5.13*. The pink trace at the bottom of the figure is the absorption coefficient of the wall alone (the black trace in *Figure 3.4* shows the diffuse field value), the main characteristics of which are the low frequency resonances and high frequency porous absorption.

At 60^0, where the channel is only slightly angled, the low frequency performance has improved by a small amount, though the biggest change is seen at frequencies above 200 Hz. The absorption for the 60^0 channel increases up to a maximum of near unity at about 320 Hz. The reason for this is the presence of a cut on mode between the walls of the channel, the complicated behaviour of which is also the reason for the sharp trough at 350 Hz. At 60^0 the channel walls are $0.6 \times \sin 60 = 0.52$ m apart, the first higher order mode for which will occur at 327 Hz. As with the previous results at this angle, no clear ¼ wavelength resonance is evident.

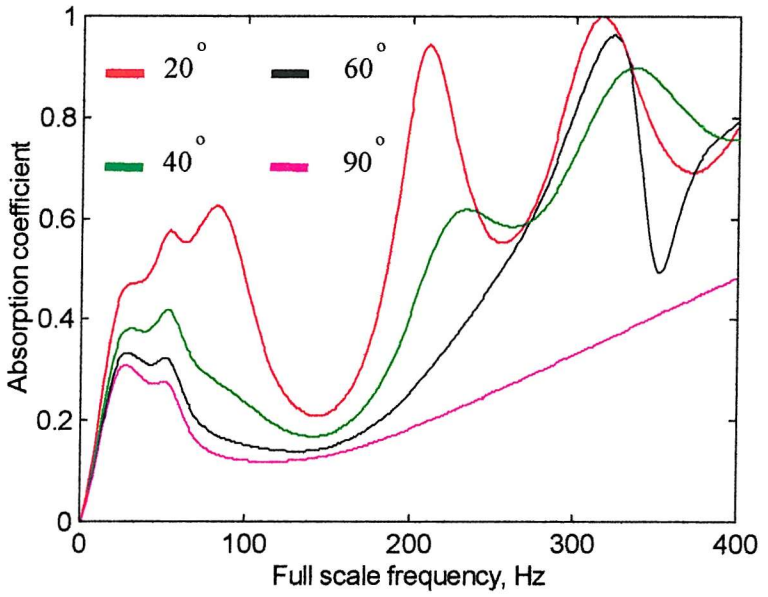

Figure 5.13 – Comparison of FE calculated absorption coefficients for various angles of panel terminated by the theoretically modelled multi-layer wall

At 40^0 however, the 2nd and 3rd resonances can be seen at 230 and 300 Hz. As mentioned, the reason for the frequencies not tying in exactly with the expected values is the complicated geometry of the channel. The low frequency absorption is improved even more than for 60^0, though again, to a lesser extent than the higher frequencies. No explicit higher order mode activity can be seen as the first cut-on mode at this angle doesn't occur until 441 Hz.

The 20^0 channel exhibits the most clear closed pipe effect with resonances at about 80, 210 and 315 Hz, with unity absorption achieved at ¼ wavelength. The lowest of these resonances usefully extends the existing performance of the multi-layer wall, resulting in an extremely good absorption ($0.4 < \alpha < 0.6$) between 30 and 100 Hz. The considerable absorption at these particular frequencies does however highlight the parts of the spectrum where the *Bass Trap* is less effective. The model and results presented in the next section will show whether or not the addition of absorbent lining on the panels serves to reduce such troughs in absorption coefficient.

5.5.2 FE Calculated Absorption Coefficient With 4 cm Thick Felt Lining on Panels

As mentioned in *Chapters 1 & 3*, the angled panels in the *Bass Trap* design are not bare, but covered in 4 cm thick cotton waste felt. It is anticipated that the addition of such absorbent material will increase the absorption above 200 Hz, change the resonant peaks evident in *Figure 5.13* and yield an absorption coefficient that is far less frequency dependent.

In *Figure 5.14* the comparison between the lined and unlined 20^0 channel is shown and as expected, significant differences are noted. With the felt, the resonant peaks in absorption occur at lower frequencies, though this is mainly due to the FE model. As the acoustic reactance of a porous material indicates its 'effective' thickness, the channel width is actually widened on account of assigning the surfaces of the panels with the impedance of the felt. Such a result shows that the width of the channel, as well as its angle, has an influence on the frequencies at which normally incident sound is best absorbed.

Apart from the change in the frequency of the resonant peaks, the felt also increases the amount of absorption at these points. Even below 100 Hz, the felt has a significant effect. In addition, the absorption between the resonant peaks is increased

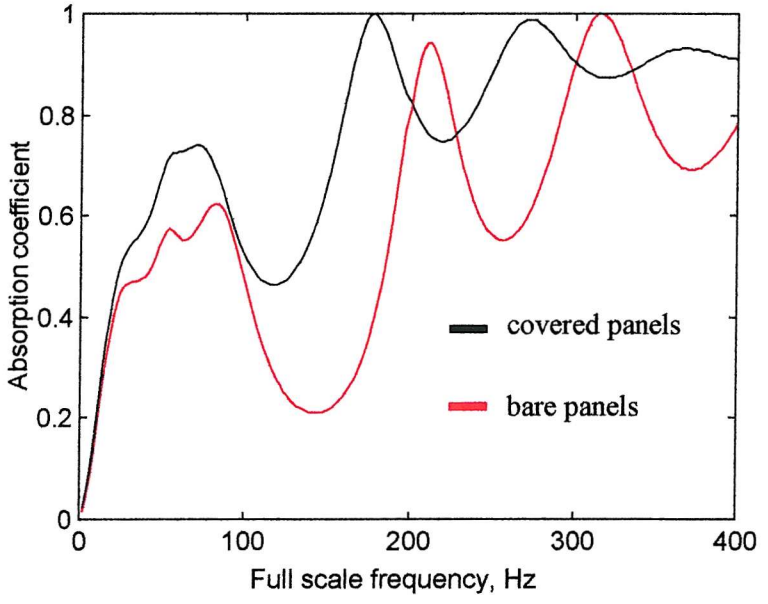

Figure 5.14 – FE calculated comparison of 20^0 channel absorption coefficients with and without felt covering on panels

by about 0.2, resulting in an absorption characteristic that shows less variation with frequency. Above 300 Hz, the normal incidence absorption coefficient of the full scale 20^0 channel terminated by the multi-layer wall and lined with 4 cm of felt, appears to tend to near unity.

5.5.3 Further Comments

Whilst the main features of the rear wall *Bass Trap* are accounted for in this last FE model, some more subtle effects are ignored. The multi-layer wall is modelled here simply as a surface normal impedance, thus no account is given for particle velocity motion through the outer felt layer. This feature may well alter the results presented in this section and will be investigated in *Chapter 7*.

Even without such effects, the presence of the channel in addition to the wall at no point degrades the absorption of the wall alone and, particularly at the most acute angles, improves the performance significantly.

In the following chapter, the research will continue with an investigation into the transmission achieved by an **absorbent** side wall and angled panels. It is interesting to hypothesise, at this stage, that any peaks in TL may correspond to the peaks in absorption of the individual *Bass Trap* channels – peaks chiefly governed by their 'effective depth' and the associated ¼ wavelength resonance. Given the plots of surface normal acoustic impedance presented in this chapter, any link between the two will be easily recognisable.

CHAPTER 6

Transmission of Sound Along a Soft-Walled Duct Lined with Splitters

Introduction

The research described in *Chapter 3* concluded that the position and orientation of the *Bass Trap* panels has a significant effect on the reverberation time of a room in which it is placed. This was confirmed in the simplified model of the side wall *Bass Trap* of *Chapter 4* where both the panel spacing and angle were shown to affect the transmission along a duct. In this chapter, the hard wall duct model of *Chapter 4* is modified by placing a 26 mm thickness of foam, partially covered in sticky tape, between the panels and the duct wall. In doing so, the model is more representative of the real life *Bass Trap* side wall, where the 35 cm thick multi-layer wall separates the hanging panels from the structural shell of the room.

The objective of this investigation is to ascertain whether or not the presence of a soft wall changes the results of *Chapter 4*. If it does, then the other objective is to explain how and why, in terms of the variables that are changed. This would enable the transmission to be predicted for the side wall *Bass Trap*, a design that employs both multi-layer wall and periodic array of angled panels.

This chapter will be structured according to the method of investigation. Firstly, the experimental part will be presented, including transmission results for different angle, spacing and number of panels. Secondly, a theory will be explained that uses some of the methods and results of *Chapter 5* to predict the transmission for two different *Bass Trap* orientations. Finally, two Finite Element models will be introduced to ratify both the theory and experiment. The conclusions from these three sets of results will lead to a discussion about the primary and secondary mechanisms at work in the side wall *Bass Trap*. As in the previous two chapters, the investigations will be based on $^1/_{10}$ scale models, so the frequency axis of the results will have a dual legend: $^1/_{10}$ scale and full scale frequency.

6.1 Experimental Investigation into *Bass Trap* Transmission

In this section, the changes to the experimental set-up are described and preliminary results presented, before the results for different arrangements of side wall *Bass Trap* are shown

6.1.1 Description of Experimental Set-up

Apart from the addition of the foam, the experimental procedure was exactly the same as in *Chapter 4*, with the same noise source, microphones, FFT analyser and method of decomposing the sound field into its forward and backward propagating components to yield the transmission down the duct length. The foam layer used in the experiments was arbitrarily chosen, its main purpose being to introduce some acoustic resistance behind the panels. The reason for its partial covering of sticky tape was to enable the different arrangements of panels to be firmly fixed in place. Together with double sided sticky tape on the duct floor, the panels could be positioned at the desired angle in any part of the duct, whilst allowing easy removal when the transmission of another absorber arrangement was measured. The normal absorption coefficient and surface acoustic impedance of the taped foam was presented in *Chapter 5*.

A photograph of the experimental rig is shown in *Figure 6.1*. The left hand part of the figure is looking from the loudspeakers to the termination, with the foam lining and angled panels clearly visible on the right of the duct. The right hand side of the figure shows the same duct but looking from the termination to the loudspeakers; the microphones and wire stand can also be seen. In addition, a schematic plan view diagram of the experimental duct is illustrated in *Figure 6.2*, though not to scale.

Due to the experience gained from the previous transmission experiments, fewer measurements were made in this investigation, as the importance of the different variables were more clearly known. The table below describes how the three variables were changed.

Angle of panel to side wall	**Spacing between panels**, cm	**Number of panels**
20^0, 40^0 & 60^0	3, 4.5, 6, 9 & 12	5, 9, 14 & 17

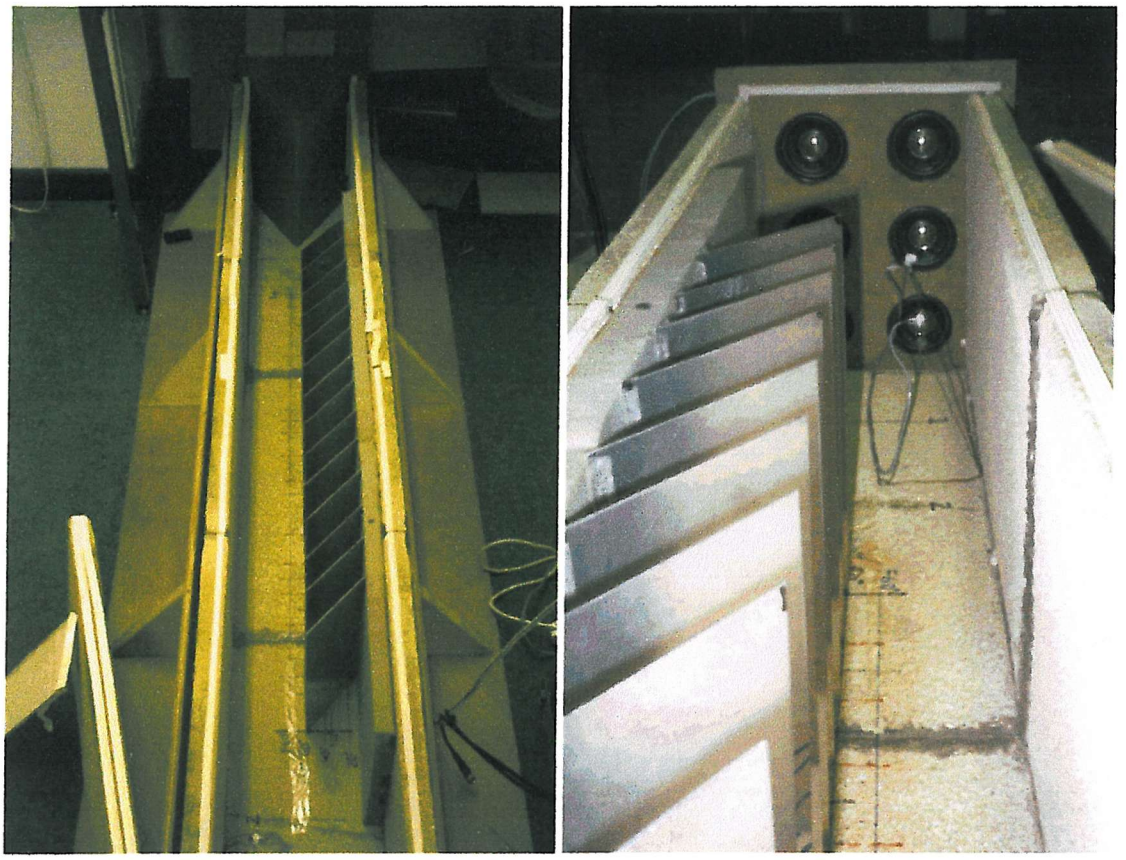

Figure 6.1 – Photographs showing the duct used for the soft wall transmission experiments

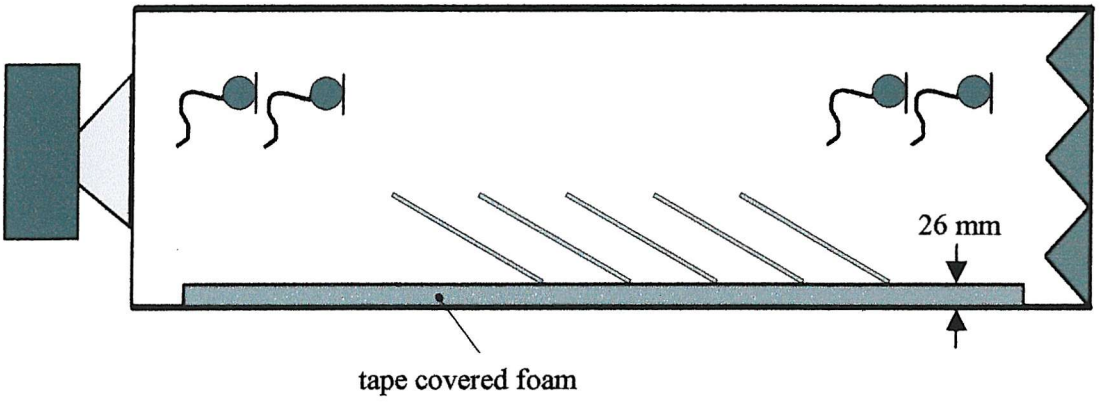

Figure 6.2 – Schematic plan view of duct used for soft wall transmission experiments

Not every variable was used with every other variable, as for example, at 20^0 it is not practical to space the panels 3 cm apart and 17 panels 12 cm apart would result in an absorber 1.94 m long, which is greater than the length of the duct.

6.1.2 Transmission for Duct Lined on One Wall with 26 mm Foam

Before the main set of experimental results are presented, the transmission down the length of the duct with one wall lined with only the 26 mm thick foam is shown. In *Figure 6.3* the transmission loss is seen to increase with frequency as a consequence of, among other things, the foam liner exhibiting a higher absorption coefficient (see *Figure 5.3*). The transmission monotonically decreases to a value of around –10 dB at 800 Hz. Thus by itself, the foam liner does not have a significance attenuating effect on the propagating sound and is in line with the results presented in [6.1]. It will be interesting to note whether the combination of soft wall and angled panels is greater than the sum of its parts, for example *Figures 4.4 & 6.3*.

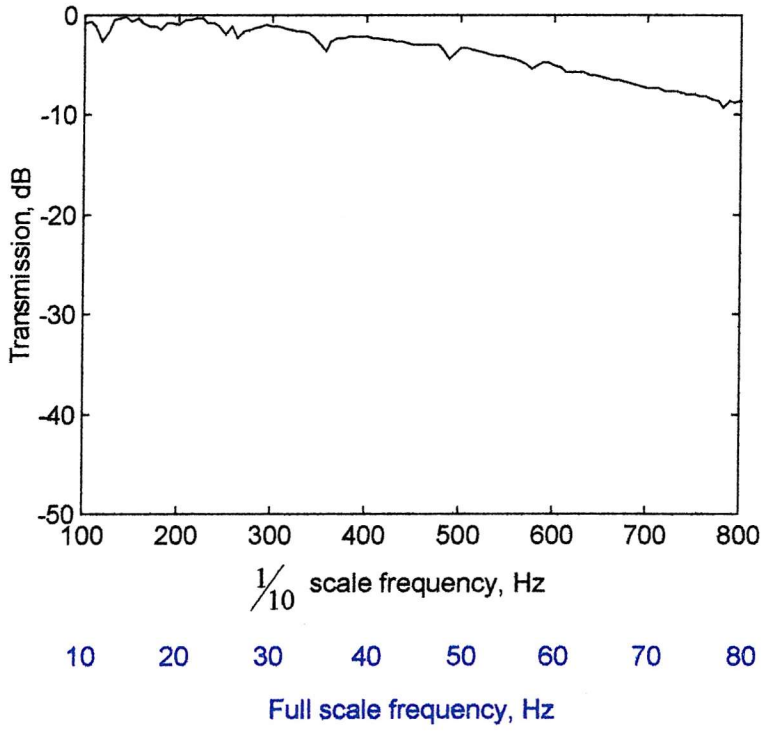

Figure 6.3 – Transmission for 26 mm thick tape covered foam liner alone

6.1.3 Transmission for Duct Lined with Foam and Angled Panels

The purpose of these experiments was not just to measure the amount of transmission yielded by a particular array of panels, but to identify the connection between the characteristics of the transmission (Quality factor, frequency of maximum TL) and the variables changed. To this end, the results in this section are grouped according to dependency, that is, the aspect of the absorber that is altered. Three of the transmission dependencies are: angle of panels, distance between panels and number of panels. The fourth is a normalised distance dependency, i.e. where the length of the absorber is kept constant while the separation distance between the number of panels is changed; for example 5 panels 12 cm apart compared with 9 panels 6 cm apart. By grouping the results in this way, the relationship between physical construction and duct attenuation should be easily identifiable.

Recalling the results of *Chapter 5*, it is interesting to hypothesise that the transmission noted in this section may be the inverse of the absorption coefficient of the channel calculated by the FE model, in the same way as the TL for the lined duct increases in line with the absorption coefficient of the foam.

6.1.3.1 Transmission as a Function of Panel Angle

Two results for the angular dependency of transmission along the duct are presented in this section, the first for a panel spacing of 3 cm and the second with them 6 cm apart. *Figure 6.4* shows the former of these results. As mentioned, at this spacing, it is very difficult to have the panels at an angle of 20^0, which is why there are only two traces.

The absorber arrangement associated with the green trace is a typical implementation of a side wall *Bass Trap*, as when scaled up it corresponds to the preferred panel orientation of Hidley (see *Section 1.1.3*). In contrast to the equivalent hard walled absorber, a considerable TL is observed across much of the frequency range. A gradual increase in TL is noted until 600 Hz, where it remains constant. In the absence of a liner, the experimental results of *Chapter 4* showed how, when the panels are close together, sound is completely unattenuated. The addition of the foam however, profoundly effects the transmission along the duct, even for an absorber with small panel spacing and an acute angle.

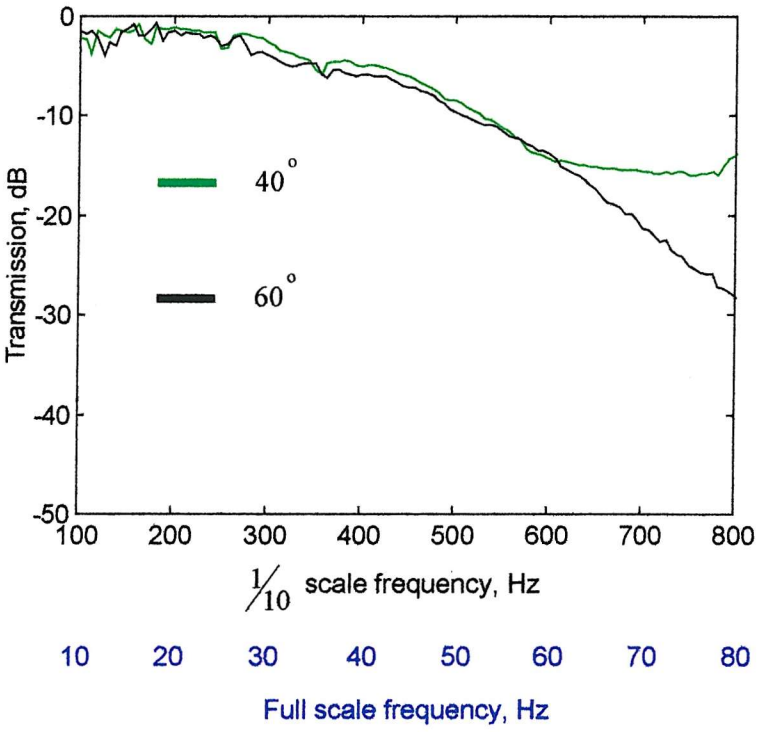

Figure 6.4 – Angle dependent transmission for 17 panels 3 cm apart

At 60^{0} the TL is even greater, as it continues to increase above 600 Hz, almost as far as –30 dB at 800 Hz. In the full scale design, this angle is too obtuse as it would result in the width of the structural shell being reduced by over 2.8 metres.

Comparing the two, one can see that the traces are almost identical up to 600 Hz, at which point the absorber with panels at 60^{0} yields a greater TL. This plot clearly shows that an intriguing effect (or effects) are at work in heavily attenuating sound as it propagates along the duct.

In *Figure 6.5* the transmission for three angles of panel is shown, while the spacing and number of panels is kept constant. The separation distance is greater in this plot and as a result, the absorber occupies more of the duct. It means however that the absorption coefficient results of *Chapter 5* can be directly compared, as the FE model was based on a *Bass Trap* channel 6 cm wide.

The 60^{0} trace again exhibits a steady increase in TL with frequency. Referring to *Figure 5.3* where the channel absorption coefficient is presented, one will recall how there was little difference between the foam and the foam and channel, at this angle. If therefore, the transmission is a function of the absorption coefficient of the duct

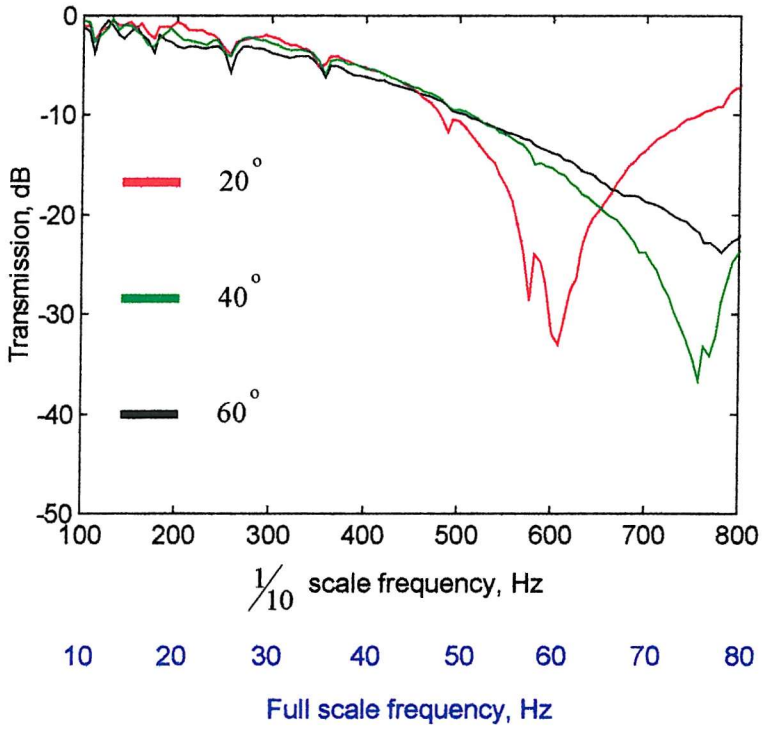

Figure 6.5 – Angle dependent transmission for 14 panels 6 cm apart

lining, then the black trace of *Figure 6.5* should be similar to the transmission of the foam alone. While the shape is similar, the presence of the 14 panels makes a 15 dB difference at 800 Hz – this may be evidence that the explanation for the transmission lies elsewhere. Recalling the hard wall experimental results for this arrangement (black trace of *Figure 4.4*) and the transmission for the soft wall alone, one can see how the combination of the liner and panels is slightly greater than the sum of the parts. At 800 Hz, for example the addition of –10 dB and –9 dB (hard wall absorber and foam respectively) is –16 dB, as opposed to –22 dB shown in *Figure 6.5*. The shape of the two traces would be very similar and accounting for possible experimental error, it could be argued that at this angle and spacing, the foam and panels are acting independently.

The 40^{0} trace is the first clear evidence of resonant behaviour, with a TL maximum of –37 dB occurring at 750 Hz. Considering the length of the absorber is only 78 cm (less than 2 wavelengths at this frequency), such attenuation in this frequency range is remarkable. Referring to *Figure 5.5* it is noted that, as before, the absorption coefficient of the channel does not tie in with the transmission.

When the panels make a 20^0 angle with the foam wall the resultant transmission is even more extreme than the 40^0 trace. Most importantly, the frequency of maximum TL is significantly lower than either of the other angles. It is also probable that in the absence of a higher order mode operating in the height of the duct, the magnitude of the TL would exceed that of the 40^0 absorber. The down side of the large magnitude, low frequency TL is that the attenuation is less at the higher frequencies. The Q of the trace does appear to be greater than the others, implying a stronger resonance, though this was one of the conclusions of the 20^0 channel in *Chapter 5*. Indeed, unlike the other traces, the transmission at 20^0 does bear some relation to the FE predicted absorption coefficient of the associated channel (see *Figure 5.7*), though comment on this will be saved for later in the chapter. The TL is all the more noteworthy given that, at this angle, the panels protrude only 42 mm into the duct.

Comparing the three arrangements, one can conclude that, at this spacing, more acute angles of panel yield a larger TL, at a lower frequency. When the panels are half as close together, as in the previous figure, the 60^0 absorber results in more attenuation than 40^0.

6.1.3.2 Transmission as a Function of Panel Separation

Figure 6.6 is the only plot in this section, in which a comparison of transmission is made for 9 panels at 20^0 spaced 6 and 9 cm apart. As with the only other results for panels at this angle, the TL increases to a definite maximum.

When spaced 6 cm apart, the absorber yields a minimum in transmission of almost –20 dB at around 600 Hz, after which it increases to –12 dB. By contrast, the wider separation produces almost –40 dB of attenuation at 680 Hz. The two traces are almost identical between 100 and 500 Hz and at the extreme high frequencies.

The larger TL for the 9 cm spacing is not surprising as the absorber length is almost 50% greater – even without the foam liner, the TL increases with the number of panels used. Less intuitive, is the fact that the closer spacing results in a lower frequency of maximum TL. This is the opposite to the hard walled absorbers, where stop band centre frequencies increased as the panels were moved closer together (see *Figure 4.10*). From this result, we can conclude that while the spacing of the panels influences the frequency at which the sound is most attenuated, it is not directly

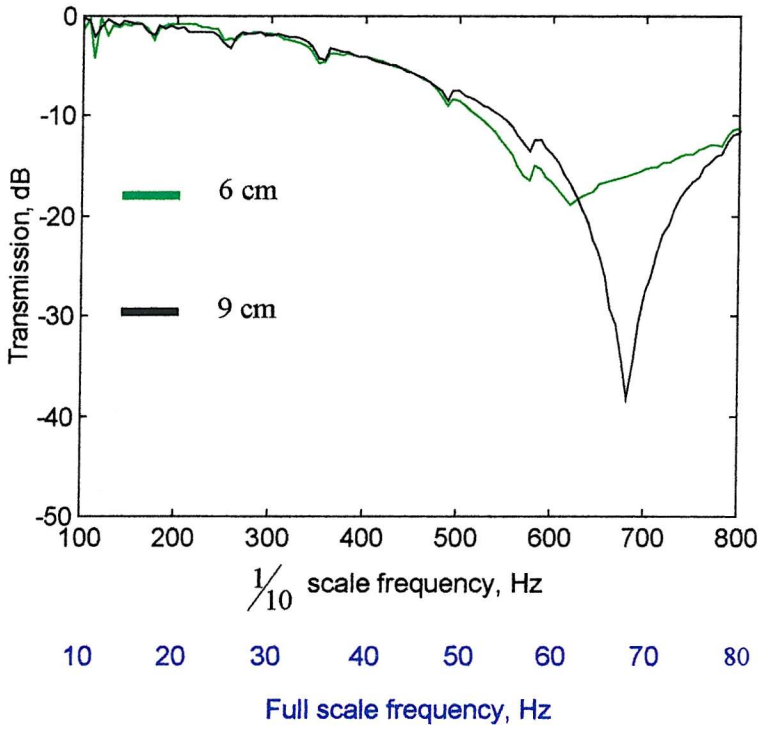

Figure 6.6 – Spatially dependent transmission for 9 panels at 20^{o}

responsible, as a ½ wavelength resonance between panels does not become apparent until 1.9 kHz for panels 9 cm apart (see *Figure 4.9*).

6.1.3.3 Transmission as a Function of the Number of Panels

Three plots are shown in this section, grouped according to panel angle, starting with the most obtuse. With the other two variables kept constant, the length of the absorber will vary in the same way as it did in the previous trace. In the following section this will be addressed as results for normalised distance are presented.

In *Figure 6.7* the transmission for 9 and 14 panels is shown, both at an angle of 60^{0} and spaced 6 cm apart. Surprisingly, both traces exhibit a very similar TL characteristic, monotonically increasing to a maximum of –24 dB at 775 Hz, only between 400 and 700 Hz is there any discernible difference (approximately 2 dB). Such as result is again very different to the hard walled duct, where more panels yielded greater TL. At this angle there seems little benefit of lengthening the absorber. This interesting result is analogous to the seat dip phenomenon mentioned

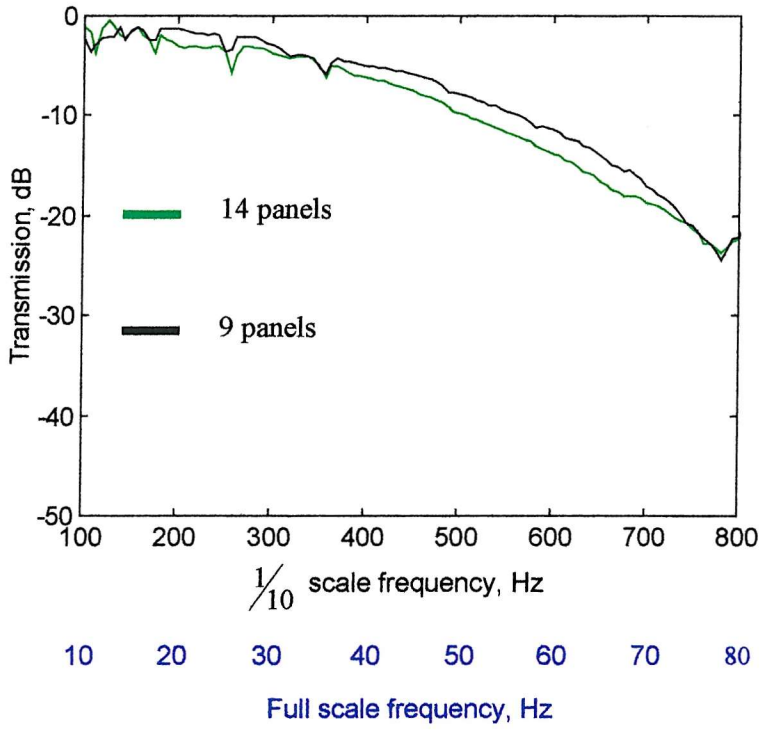

Figure 6.7 – Dependency on number of panels for 6cm and 60^{o}

in *Section 1.3.4.* Separate investigations into the low frequency absorption noted in concert halls all showed that the magnitude of the attenuation reaches a maximum a number of rows from the source, after which point it does not increase as the measurement position is moved further away (thereby including more rows of seats). Schultz and Watters [6.2] quantified this position of diminishing returns as 12 rows from the source, while Sessler and West [6.3] showed that the –15 dB of attenuation measured at the 15th row remained constant at both the 22nd and 27th row.

The similarity between these present results and those relating to seat dip may give some insight into the way in which the sound is attenuated. The primary mechanism cited in the seat dip research is a ¼ wavelength resonance operating in the seat height. The consequences for this investigation will be discussed in due course.

At 40^{0} the presence of more panels does effect the transmission, as can be seen in *Figure 6.8.* At every frequency, the absorber with 14 panels yields a greater TL than for only 9 panels. Both traces appear to exhibit a TL maximum at the same frequency. The difference between this plot and the last, suggests that a mechanism may be at work at 40^{0} that isn't at 60^{0}. The only clear physical reason for this is that

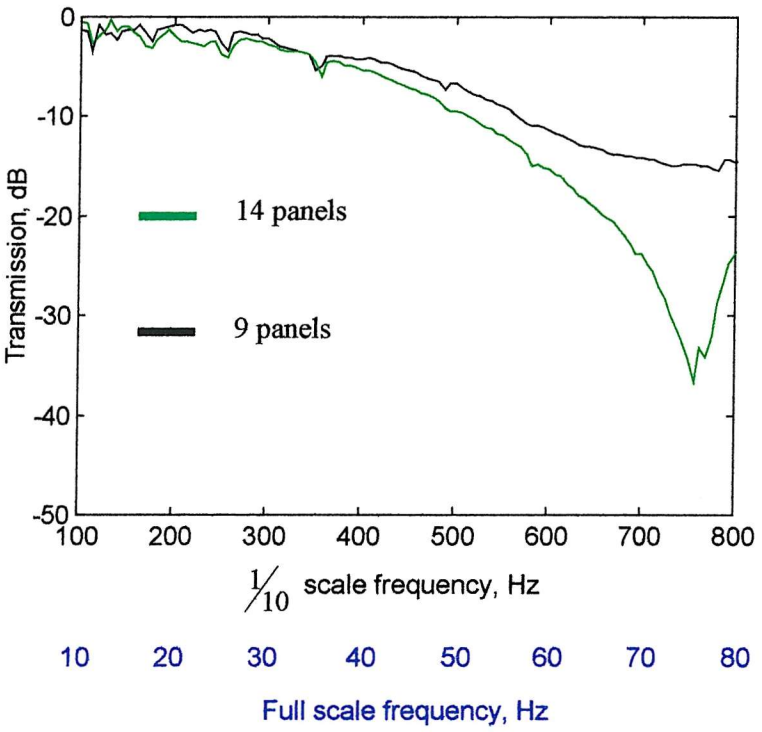

Figure 6.8 - Dependency on number of panels for 6cm and 40°

at the shallower angle the adjacent panels form a narrower channel. In fact, there is only 1 mm of overlap for panels at 60^0 and 6 cm apart, when looking normal to the side wall. If this is significant, then the results in the next section, of both larger and smaller separations, will prove it one way or the other.

The section is concluded with the number of panel dependency at 20^0 and 6 cm shown in *Figure 6.9*. The high Q shape, that has typified the 20^0 measurements, is here shown to be, in part, related to the number of panels. As with the previous plot, the resonant frequency is the same for the two traces, while the magnitude of the TL maximum increases with more panels. If the amount of foam in the duct was changed in line with the length occupied by the duct, it is likely that the shape of the 9 panel absorber would be far more similar to that of the 14 panel absorber. The reason being that, 9 panels cover 30 cm less of the foam than 14 panels do, thus whatever mechanism is at work in the region of the duct where there is panel and foam, is supplemented proportionally more with 9 panels than with 14. This is evident at high frequencies because that is the region where the foam yields the most attenuation.

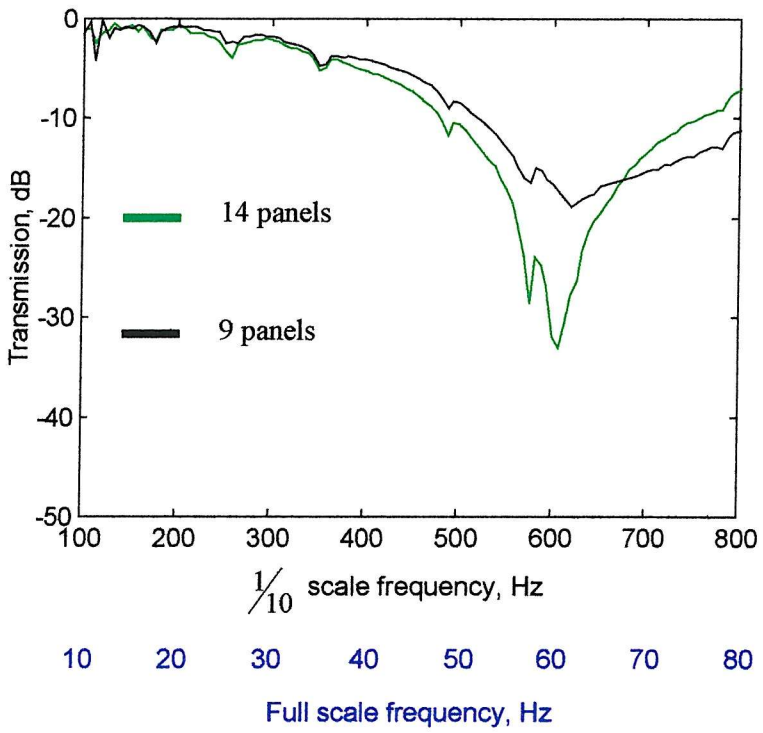

Figure 6.9 – Dependency on number of panels for 6cm and 20°

The same explanation can be given for the results in *Figure 6.6* where 9 panels 6 cm apart cover 24 cm less of the foam than when 9 cm apart.

Two conclusions can be made from this section. The first is that, for panels 6 cm apart, the angle determines the frequency of the maximum TL, or are at least highly correlated. The second, is that increasing the number of panels increases the attenuation, though the extent appears to be dependent on the panel angle.

6.1.3.4 Transmission as a Function of Normalised Distance

The results in this section combine the variables from the previous two. They also have important implications for the design and construction of a *Bass Trap* control room, as the length of the absorber is kept constant while the number and separation of the panels is varied. Once again, the plots are grouped according to panel angle.

Figure 6.10 shows the first of the comparisons, for the panels at their most obtuse. The three traces all relate to an absorber 48 cm in length. It is immediately obvious that the three absorbers yield very similar transmissions, though more panels closer

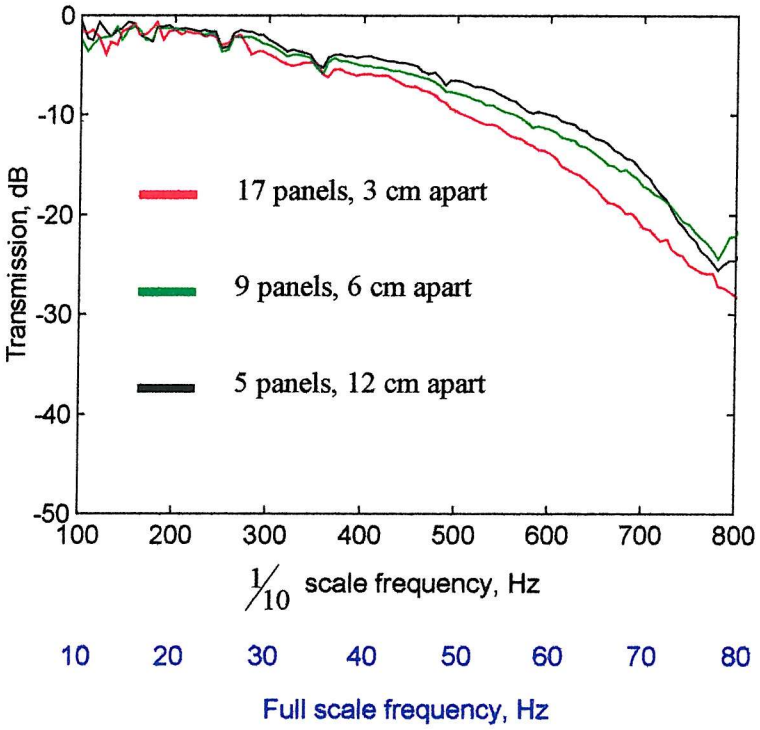

Figure 6.10 – Normalised distance dependency at 60°

together do perform slightly better. The difference is insignificant, however, when translated to the real life situation. The additional labour and material costs associated with using 12 more panels (on both side walls) is considerable and would undoubtedly be considered extravagant, given a maximum improvement of only 6 dB at a full scale frequency of 65 Hz. With panels at an angle of 60°, the law of diminishing returns is definitely applicable and it would seem sensible to use fewer panels further apart.

The absorbers which yield the transmission shown in *Figure 6.11* are again 48 cm long and as before the traces are almost identical. Interestingly, the comparison made here is directly relevant to the real life design, as the panels are at 40°. Indeed, the author has been asked by advocates of the *Bass Trap* design whether or not (at this angle) half as many panels, twice the distance apart, gives a comparable performance. *Figure 6.11* suggests that, like the previous plot, little gain is had by using a more dense side wall *Bass Trap*. At the frequencies considered, a more dense packing of panels would results in the panels and soft wall being seen as a lumped element, as the wavelengths are many times greater than the panel separation distance. As the

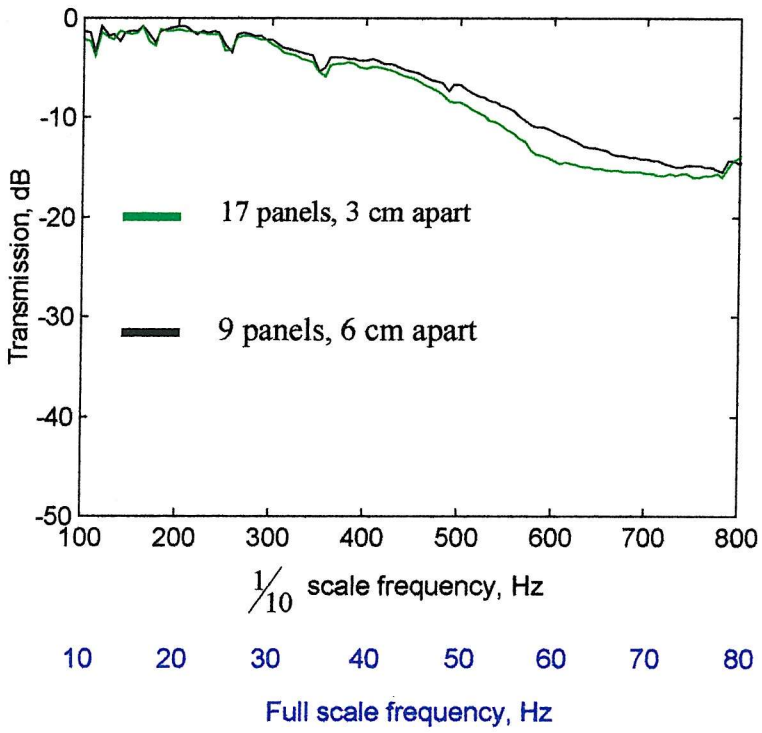

Figure 6.11 – Normalised distance dependency at 40°

distance between panels increases, the dominant effect may be a combination of the panels and the soft wall. Particularly at high frequencies, the propagating sound is able to distinguish between the two elements on account of the soft wall being more accessible and the panel spacing approaching the wavelength of sound. If this is the case, then the similarity between the black and red trace of *Figure 6.10* is purely coincidental. Further comment on this will be given at the end of this section.

Finally, the transmission for panels at 20^{0} is presented in *Figure 6.12.* The absorber here is 50% longer than the previous two in this section. Unlike the more obtuse angles, there is a distinct difference between the attenuation yielded by the two absorbers, differences that tally with earlier experimental results. With more panels closer together, the TL maximum is greater and occurs at a lower frequency; in addition, the Q of the attenuation is higher. At this angle and these spacings, the absorber presents a lumped element to the comparatively long wavelengths, thus it is feasible that the same mechanism is responsible for both transmission results. The larger TL maximum for more panels was identified in *Section 6.1.3.3* in all but the most obtuse panel angle and is an intuitive result. In the light of the results of

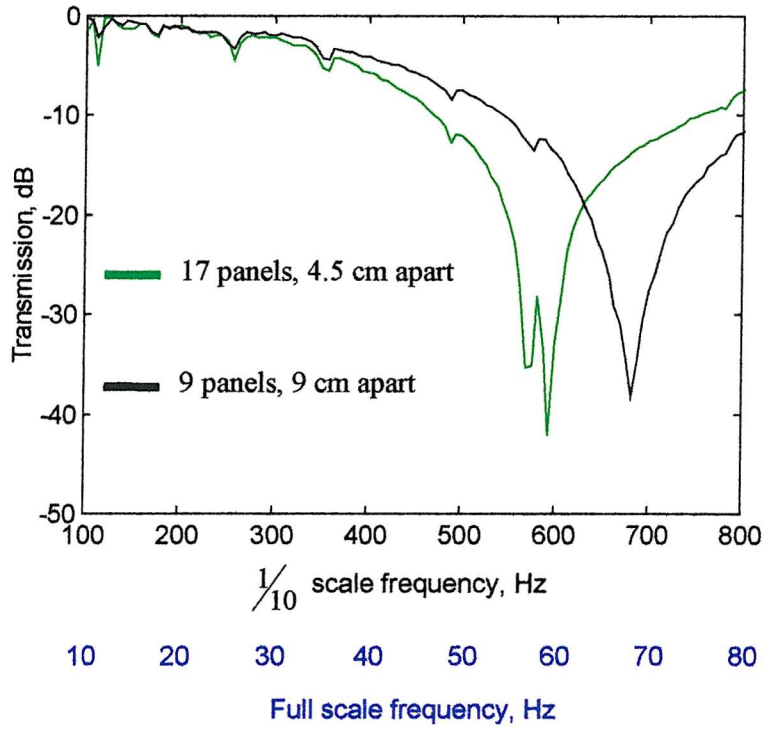

Figure 6.12 – Normalised distance dependency at 20°

Chapter 4, the lower frequency of this maximum for closer panel spacing is more surprising, though it is in agreement with the result for this dependency, shown in *Figure 6.6*. At such a shallow angle, the choice of number and spacing of panels is shown here to have a dramatic effect on the resultant transmission.

6.1.3.5 Further Discussion of the Experimental Transmission Results

Although some conclusions have been drawn already, some additional discussion is given here on more non-specific trends.

Comparing the cumulative effect of hard walled filtering and soft wall attenuation with one of the results of this section, has suggested that the mechanism by which sound is attenuated by a lined duct with angled panels may change depending on the orientation of the panels. The following discussion will be based on the results for which the number and spacing of panels was varied. It was noted that, at the shallower angles, the transmission was influenced when the length of the foam was not reduced in line with the length of the panel array. The explanation for this was that the foam caused additional attenuation, particularly noticeable at the high

frequencies, to that provided by the combination of foam and panels. Interestingly though, the same effect was not evident at 60^0, suggesting that the panels and foam may be acting independently. Given these observations, it is hypothesised that:

a) Given a sufficiently dense packing of panels (i.e. close spacing and shallow angle) the sound considers the two elements as one and in the region of absorber, one primary mechanism is operating.

b) When the panel spacing is a significant proportion of the wavelength of sound and there is a normal line of sight to the liner, the panels and foam do not act as a lump element. Instead, the panels scatter the plane wave into higher order modes which are absorbed by the foam. At higher frequencies, some ½ wavelength filtering also occurs.

These hypotheses will be tested in the following sections. If they are proved, then it suggests that the real life design of angled panels and multi-layer wall act as a lumped element at the lower end of the audible frequency spectrum.

6.2 Theoretical Investigation into *Bass Trap* Transmission

Having established, experimentally, that the combination of absorbent wall lining and angled panels significantly attenuates the sound propagating along a duct, this section will be concerned with formulating a theoretical model of the side wall *Bass Trap*. Firstly, the hypothesis that the panels and lining are acting independently, will be investigated, after which the lumped element mechanism will be considered.

6.2.1 Absorption Due to Panel Scattering into Higher Order Modes

Subtle inconsistencies in the experimental transmission results suggest that, depending on the orientation of the panels, the side wall *Bass Trap* may work in one of two ways. One of these mechanisms is where the panels scatter the plane propagating wave into higher order modes, which are more readily absorbed by the absorbent duct lining. This method of sound attenuation in ducts is exactly what Lapin [6.4] addresses in his paper and was briefly mentioned in *Section 1.3.3*. Before more detail is given, some basic theory on the subject of mode propagation in ducts is necessary and as a starting point, a hard walled duct will be considered. Only a

summary is given here, as many standard texts [6.5] deal with the subject in a rigorous and methodical manner.

In a duct with rigid walls, the propagation of sound is governed by the boundary conditions, that is, the behaviour of the pressure and particle velocity at the duct boundaries. On account of zero normal particle velocity at the rigid walls, the pressure distribution across the width and height of the duct (known as the mode shape) is cosinusoidal. The frequency above which a given mode can propagate is called the mode *cut-on frequency* and is determined by the dimensions of the duct. As a result it can be shown that, for a maximum transverse dimension l, only plane waves can propagate below a frequency given by $f_{clo} = \frac{c_0}{2l}$. For the experimental duct therefore, ignoring the height dimension, the first higher order mode is able to propagate above 791 Hz. As only plane wave attenuation is of interest in this investigation, this cut-on frequency explains why the frequency axis was truncated to 800 Hz. As briefly mentioned in *Section 1.3.3*, any impedance discontinuity in a duct will disturb a plane wave, scattering into higher order modes. Below the cut on frequency, these modes will decay evanescently and not propagate any significant distance. The panels in the duct used in this investigation will thus give rise to higher order modes, whose behaviour will **just** be evident in the frequency range shown, if the width of the duct is simply the distance between the side walls. With the addition of the foam liner, the first cut-on mode operating across the width of the duct will result in a pressure gradient in a direction given by the vector sum of the propagating wave and the transverse mode. The pressure gradient will in turn give rise to a particle velocity, a component of which will be normal to the liner, resulting in absorption and thus attenuation of the propagating wave. It is this behaviour that is thought to be responsible for the transmission noted in the black and green traces of *Figure 6.10* – the 60^0 absorber with panels 12 and 6 cm apart respectively. In these traces a TL maximum is evident at the predicted frequency of the first cut-on mode operating in the duct width (791 Hz). The reason why this behaviour is not evident in the other absorber arrangements is because the panels are too densely packed to allow effective absorption by the foam hidden behind. However, it is possible that for these arrangements a similar mechanism may be operating.

In *Chapter 5* it was observed that the rhomboidal *Bass Trap* channels exhibit a resonance at a ¼ wavelength associated with a depth greater than the panels

themselves. If, therefore, the channels have an 'effective depth' then it would imply that the duct has an effective width different to its physical dimensions. The result of this would be that the cut-on frequency may not occur at 791 Hz. From the results for *Bass Trap* channel surface normal acoustic reactance shown in *Figures 5.4, 5.6 & 5.8* the table below summarises the quantities relevant to the discussion.

It can be seen from the table that, based on the acoustic depth of the channels, the predicted cut-on frequency of the first higher order mode is considerably less than 791 Hz. It is also apparent that there is little agreement between the predicted frequencies and the frequencies of the TL maximum.

Angle of panel	FE resonant frequency of channel	Effective channel depth	Effective duct width	Predicted frequency of cut-on mode	Frequency of measured TL maximum
20^{o}	490 Hz	173 mm	320 mm	531 Hz	590 Hz
40^{o}	558 Hz	152 mm	263 mm	646 Hz	750 Hz

The panel scattering of the plane wave will occur and the subsequent absorption of higher order modes will result in attenuation at frequencies for which the higher order modes propagate. However, from the calculations shown in the table, it is unlikely that the hypothesis presented represents the primary mechanism responsible for the dramatic transmission plots of *Section 6.1.3*. Given this conclusion, another, more complicated theoretical model is presented.

6.2.2 Plane Wave Attenuation of a Duct with One Lined Wall

The theory presented in this section will use the results of *Chapter 5* to calculate the theoretical transmission of a plane wave as it propagates along the experimental duct. As the experiment was concerned with the plane wave attenuation, the theoretical model ignores all higher order modal activity. In addition, it is generally the primary mode that is the least attenuated. As well as the absorption coefficient of the *Bass Trap* channel opening, the associated surface normal acoustic impedance was also presented in the previous chapter. In the theoretical model, this impedance is assigned to one wall of a two-dimensional duct (height is ignored). From this starting point, the frequency dependent transverse wavenumber is

calculated for the experimental duct with one of two absorber arrangements placed on one side wall. Unlike a hard walled duct, the transverse wavenumber is complex and changes with frequency when one of the boundaries is non-rigid. As a result, the axial wavenumber is also complex and can be used to find the rate of decay of the plane wave. It is hoped that by characterising the angled panels and soft wall with only a surface impedance, a relatively simple theory can be used to predict the experimental transmission results. Given that the discussion of the measured results concluded that for closer separation and shallower angles the sound considers the panels and foam as one, it is reasonable to expect that the theory will provide an accurate model.

6.2.2.1 FE Calculation of *Bass Trap* Channel Side Wall Impedance

In this section, as in *Chapter 5*, the surface normal acoustic impedance of the open end of two *Bass Trap* channels is calculated using Finite Element Analysis. The two channels modelled are for panels at 20^{o}, 6 and 12 cm apart. **In the theoretical model, the impedance calculated by the FE model will be used as the boundary condition of one of the side walls**. In this way, a particular side wall *Bass Trap* can be described by a frequency dependent complex value and easily assimilated with mathematical analysis.

The FE models used are exactly the same as those described in *Chapter 5*, with the unit amplitude plane pressure boundary condition at the channel opening and the experimentally measured surface impedance of the taped foam used to characterise the termination. *Figure 6.13* shows the absorption coefficient of the two channels used in the theoretical model. As before, little difference is noted at the low frequencies, as the channel dimensions are small compared with wavelength. Above 500 Hz however, the wider channel exhibits a higher absorption coefficient. This result is in agreement with earlier FE results and identifies the more tortuous path the sound must take in the narrower channel. Thus when the panels move further apart, the absorption coefficient of the foam is more significant to the performance of the channel as a whole. Another, possibly more important, result from the FE model is the normal acoustic reactance of the channels (normalised to $\rho_0 c_0$), as shown in *Figure 6.14.*

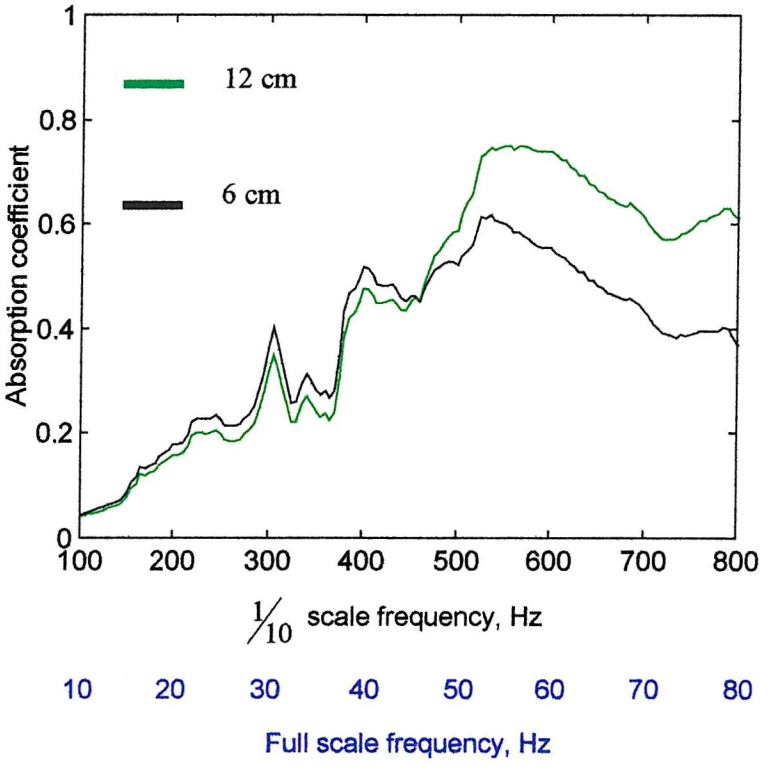

Figure 6.13 - FE calculated absorption for different widths of 20° channel

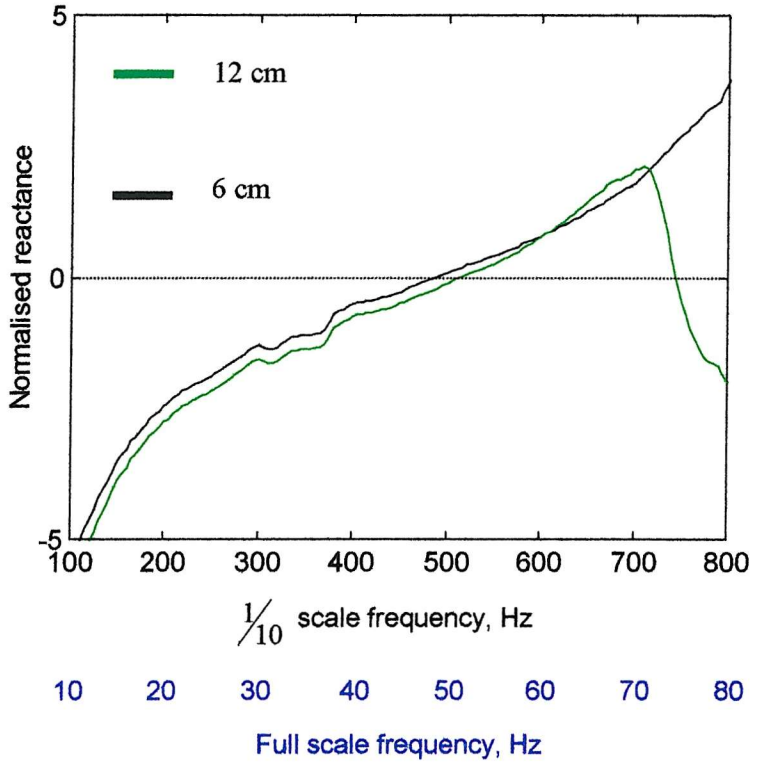

Figure 6.14 - FE calculated reactance for different widths of 20° channel

The key feature of this plot is the frequency at which the reactance is zero, as this gives the 'effective depth' of the channel. For the 6 cm wide channel, the frequency of zero reactance is 20 Hz lower then for the 12 cm panel separation.

The next step in the theoretical model is to calculate the transverse wavenumber when this FEA channel surface normal impedance is used as the side wall boundary condition of the experimental duct. The following section will describe this analysis for an arbitrary duct width b with wall impedance Z_1.

6.2.2.2 Analysis of Transverse Wavenumber in Soft Walled Rectangular Ducts

The mathematical derivation in this section is an adaptation of analysis presented by Munjal [6.6] in his book on duct acoustics. The model used is illustrated in *Figure 6.15*. The necessary decomposition of the plane wave pressure field in the x direction is achieved by using forward and backward going waves, A and B. The analysis will be based initially on a duct of width b, though later the solution for wavenumber with one soft wall and one hard wall will be given.

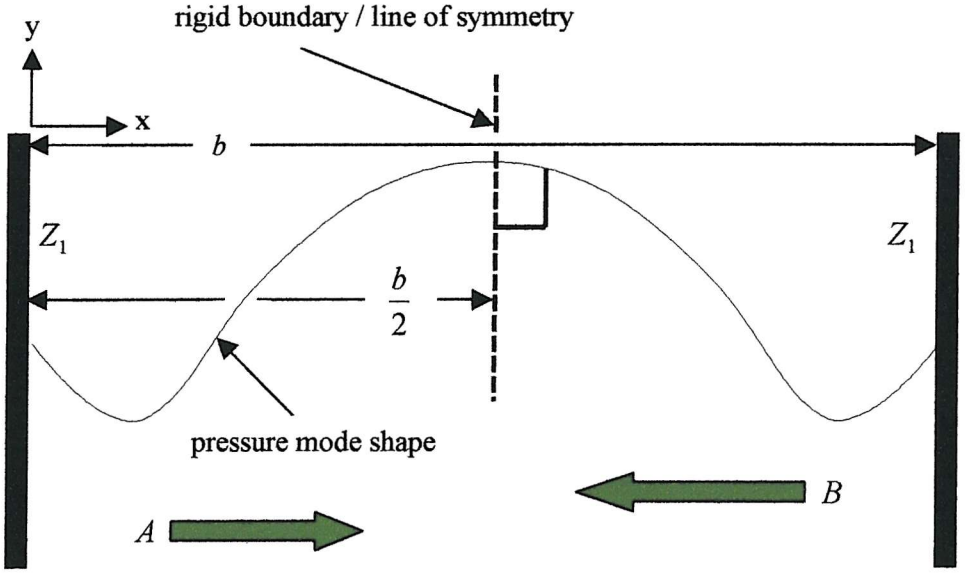

Figure 6.15 – Soft walled duct mode shape model

Considering *Figure 6.15*, the surface normal acoustic impedance of the walls Z_1 can be defined in terms of pressure p and normal particle velocity u as:

$$\frac{p_{x=0}}{-u_{x=0}} = \frac{p_{x=b}}{u_{x=b}} = Z_1 \tag{6.1}$$

When expressed in terms of forward and backward going waves the pressure field can be written as:

$$p(x) = Ae^{-jk_x x} + Be^{jk_x x} \tag{6.2}$$

and particle velocity:

$$u(x) = \frac{-1}{j\omega\rho_0}\frac{\partial p(x)}{\partial x} = \frac{k_x}{\rho_0 c_0 k_0}\left(Ae^{-jk_x x} - Be^{jk_x x}\right) \tag{6.3}$$

Substituting *equations 6.2 & 6.3* into *equation 6.1* results in the following boundary conditions:

$$\frac{p_{x=0}}{-u_{x=0}} = \frac{-\rho_0 c_0 k_0}{k_x}\left(\frac{A+B}{A-B}\right) = Z_1 \tag{6.4}$$

$$\frac{p_{x=b}}{u_{x=b}} = \frac{\rho_0 c_0 k_0}{k_x}\left(\frac{Ae^{-jk_x b} + Be^{jk_x b}}{Ae^{-jk_x b} - Be^{jk_x b}}\right) = Z_1 \tag{6.5}$$

By characterising the absorbent duct walls by the complex reflection coefficient $R = \frac{B}{A}$, substitution and rearranging of *equation 6.4* yields:

$$R = \frac{\frac{k_x Z_1}{\rho_0 c_0 k_0} + 1}{\frac{k_x Z_1}{\rho_0 c_0 k_0} - 1} \tag{6.6}$$

On substituting *equation 6.6* into *equation 6.5* and after considerable rearranging, a quadratic equation results with $\frac{k_x Z_1}{\rho_0 c_0 k_0}$ as its coefficient. Thus by using the standard quadratic equation formula, the solution is given as:

$$\frac{-\cos(k_x b) \pm 1}{j \sin k_x b} = \frac{k_x Z_1}{\rho_0 c_0 k_0} \tag{6.7}$$

Through the use of double angle formulas, the left hand side of *equation 6.7* can be written in terms of cot and tan, the former representing symmetric modes and the latter anti-symmetric modes :

$$\text{As } -\cos(k_x b)-1=-2\cos^2\left(\frac{k_x b}{2}\right) \tag{6.8}$$

$$\text{and } \sin(k_x b)=\sin\left(\frac{k_x b}{2}+\frac{k_x b}{2}\right)=2\sin\left(\frac{k_x b}{2}\right)\cos\left(\frac{k_x b}{2}\right) \tag{6.9}$$

$$\frac{-\cos(k_x b)-1}{j\sin(k_x b)}=j\cot\left(\frac{k_x b}{2}\right) \tag{6.10}$$

$$\text{and similarly } \frac{-\cos(k_x b)+1}{j\sin(k_x b)}=-j\tan\left(\frac{k_x b}{2}\right) \tag{6.11}$$

Thus far the analysis has considered **two** walls with surface normal impedance Z_1, when in fact the experimental duct has one hard wall and one wall against which the foam and panels are placed. By referring to *Figure 6.15* it can be seen how a nominal line of symmetry is drawn half way between the walls. The boundary condition to be satisfied at the rigid duct wall is zero normal particle velocity, which results in the pressure mode shape intersecting it at 90^{o}. This requirement is met by the **even** modes, as they exhibit a turning point in the middle of the duct. Therefore, from the analysis of a soft-soft duct of width b, the wavenumber for a soft-hard duct of width $\frac{b}{2}$ can be found by only considering the even modes.

Thus rearranging *equation 6.10* to express k_x in terms of known quantities gives:

$$\frac{\cot\left(k_x\frac{b}{2}\right)}{k_x\frac{b}{2}}=-j\frac{Z_1}{\rho_0 c_0 k_0\frac{b}{2}} \tag{6.12}$$

Equation 6.12 is known as a transcendental equation (as both Z_1 and k_x are complex) and has no analytic solution. In order to solve it numerically a Newton-Raphson iteration was used, the details of which will be given in a later section.

Once k_x has been found through the numerical iteration, it is used to solve for R (the complex reflection coefficient) by substitution into *equation 6.6*. This then allows both values to be substituted into *equation 6.2* to give the pressure distribution across a duct with one wall soft at $x=0$ and one rigid at $x=\frac{b}{2}$. Whilst the transverse mode shape is of interest and will be referred to as part of the investigation, it is the solution

for k_x that is the most important, as it allows the attenuation of the plane wave down the duct to be calculated.

6.2.2.3 Derivation of Axial Wavenumber in Soft Walled Rectangular Ducts

The purpose of the analysis of the previous section was to solve for the complex **transverse** wavenumber k_x, from which the **axial** wavenumber k_z can be found. The axial wavenumber for soft walled rectangular ducts is also complex and describes the rate of decay of a given mode. The relation between transverse and axial wavenumbers involves the free field wavenumber, $k_0 = \frac{\omega}{c_0}$, which for a two-dimensional duct is given by:

$$k_z = \sqrt{k_0^{\,2} - k_x^{\,2}} \tag{6.13}$$

Thus for a given frequency and transverse wavenumber, the axial wavenumber describing the attenuation of sound for a given mode can be found. The general form of the propagating sound in the axial direction is given by $e^{-jk_z z}$, where k_z can be expressed as its real and imaginary parts: $k_z = \alpha + j\beta$. From these equations it can be seen that it is the imaginary part of the axial wavenumber that describes the attenuation, while the real part is concerned with the change of phase. From a value of k_z therefore, the attenuation in dB over a distance z, is given by: $20\log\left(e^{\Im(\tilde{k}_z)z}\right)$. It is this value that will be compared with the measured and FEA results.

6.2.2.4 An Iterative Solution to the k_x Transcendental Equation

The analysis of the previous two sections explain how for a known side wall boundary condition, the attenuation of a particular mode can be found. As mentioned however, the equation derived for the transverse wavenumber has no analytic solution, so an iterative numerical method must be used. Many types of iterative methods exist and the one employed here is the Newton Raphson type [6.7]. For a function $f(x)$ and initial guess g_0, the first approximation g_1 is given by:

$$g_1 = g_0 - \frac{f(g_0)}{f'(g_0)} \tag{6.14}$$

where the prime denotes the differential of $f(x)$ with respect to x. The second approximation is found by substituting g_1 for g_0 and so on until the function converges. It is important, however that the initial guess is close to the solution, otherwise the iteration may converge to an incorrect answer. This problem is particularly relevant to wavenumbers in the complex plane.

As mentioned earlier, the transverse wavenumbers of hard walled ducts are not continuous but occur at frequencies equal to $\frac{n\pi}{b}$, where $n = 0, 1, 2\ldots$ and b is the width of the duct. It is known therefore, that for duct walls with very large impedances, the primary mode wavenumber is very close to zero. The impedance of the duct wall of the theoretical model is not close to infinity and as shown in *Chapter 5* exhibits values of resistance and reactance that are both close to zero. In order to ensure that the initial guess was sufficiently close to ensure convergence to the desired value, a second iteration was used. Firstly, a line was 'drawn' in the complex impedance plane, between a near infinite value $(14.7-14.7\text{j})\rho_0 c_0$ and the actual wall impedance and divided into 1000 equal size steps. Secondly, given the known properties of hard walled ducts, the Newton-Raphson routine solved for the near infinite impedance using an initial guess close to zero, $0.001+0.001j$. The value for k_x obtained was then used as the starting guess for the second most infinite wall impedance, to give a wavenumber for a slightly softer boundary. This process was repeated until the wavenumber for the 999$^{\text{th}}$ impedance was used as the starting guess for the actual wall impedance as calculated by the FE channel model. As a check, the routine was repeated with a different near infinite impedance of $(14.7+14.7\text{j})\rho_0 c_0$, to ensure that the same value of k_x was reached. A plot illustrating this tracing from near infinite to desired wall impedance is shown in *Figure 6.16* for the 6 cm channel at a frequency of 300 Hz. The transverse wavenumbers for the first four modes are shown. In the same way as the primary mode, the starting guesses for the higher order modes were given by the hard walled wavenumber as: $k_x = \frac{n\pi}{b}$ where $n = 1, 2\ \&\ 3$. As *Figure 6.16* shows, the same value of k_x is given regardless of the starting impedance and the closed loop confirms the correct answer.

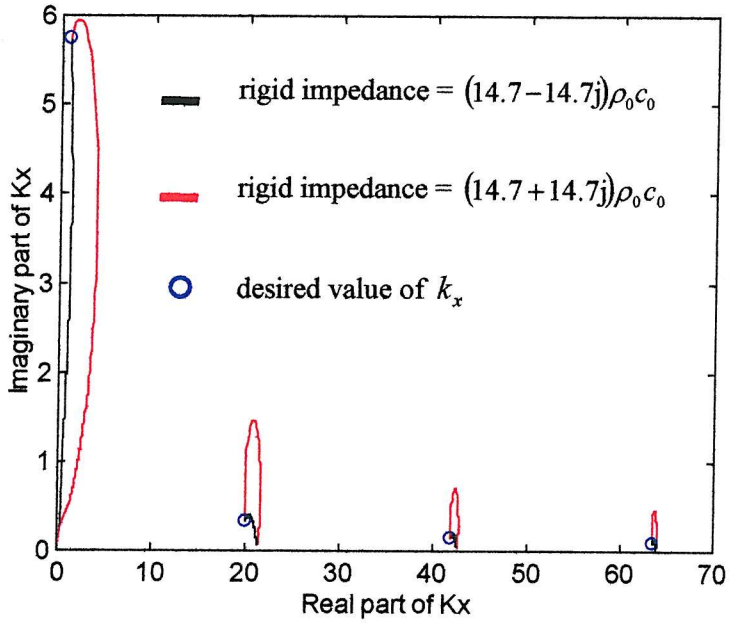

Figure 6.16 – Iterative solutions towards required wavenumber values at 300 Hz

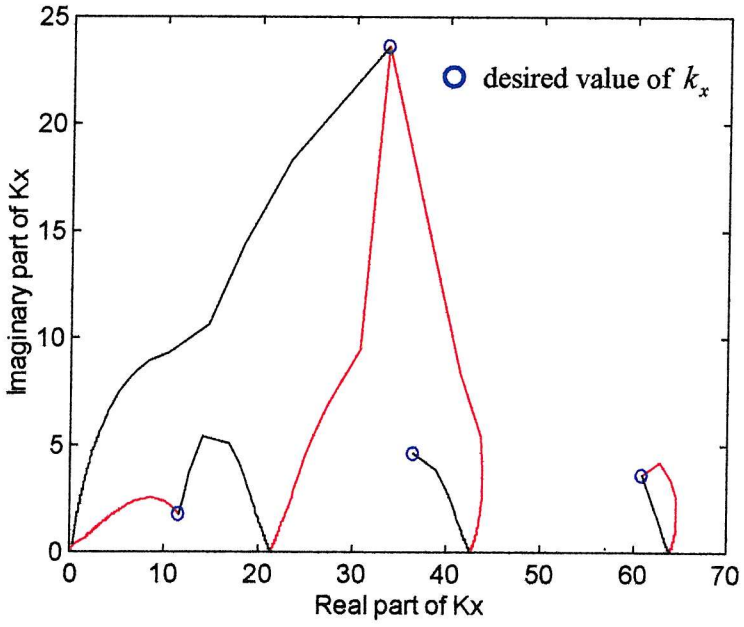

Figure 6.17 – Iterative solutions towards required wavenumber values at 470 Hz

However, for the impedances calculated by the FE model, there were a range of frequencies for which the values for k_x were more ambiguous and even incrementing from a rigid wall impedance, the result remained inconclusive. An example of this is shown in *Figure 6.17* where the transverse wavenumbers for the first four modes at 470 Hz are calculated. In this plot, whilst the desired values of k_x are found, it is unclear which mode they are associated with. The chosen starting value of impedance (either a large negative or large positive reactance) determines the final solution and one can see how the different modes overlap. Given this uncertainty of result, one final check was used to ensure that the values of k_x used in the theoretical model did indeed relate to the primary mode. Referring back to *Section 6.2.2.2* one will recall how the transverse wavenumber can be substituted into the equation describing the transverse pressure, to give the mode shape across the duct width. This is useful as the primary mode shape has no turning points and instead takes the form of a slightly curved plane wave. This distinguishing feature will allow higher order mode transverse wavenumbers to be recognisable from the primary mode wavenumbers. An example of this check is given later in the section. Firstly, the complete set of transverse wavenumbers for both side wall impedances is discussed.

6.2.2.5 Frequency Dependent Values of k_x for the Two Wall Impedances

Now that the equation for k_x has been solved and ambiguous results clarified, the results for the transverse wavenumbers of the two ducts can be shown. The purpose of the theoretical model is to explain the experimental results and shed light on the way in which the *Bass Trap* side wall is working. To that end, the dimensions of the duct in the theoretical model are not the same as the experiment. As the foam liner and angled panels have been replaced by an equivalent surface normal impedance, the theoretical duct is a little less wide. The width (b) of the duct used in the analysis is: $2\times$(duct width – foam depth – panel depth$\times\sin 20$) = 0.295 m. *Figures 6.18 & 6.19* show the different values of primary mode k_x for **every** 5 Hz from 100 to 800 Hz, for the 6 and 12 cm absorber respectively. As the frequency increases, so the values of k_x move clockwise around the loop (indicted by the arrows), multiples of 100 Hz are highlighted in green to clarify this trend. Both plots will prove critical in explaining the way the *Bass Trap* side wall works.

In *Figure 6.18* the values of k_x start with small imaginary parts, which increase as the frequency rises. Between 475 and 480 Hz the wavenumber jumps to a value much less in both the real and imaginary part, after which it remains close to the real axis.

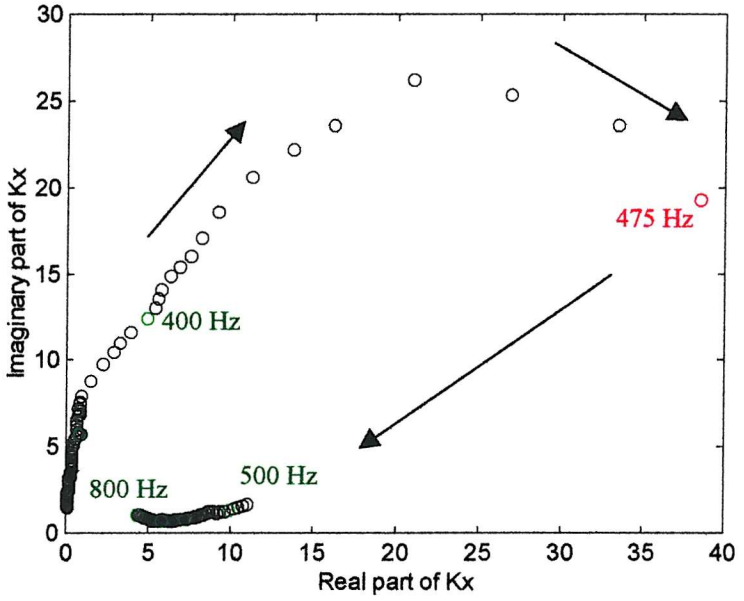

Figure 6.18 – Frequency dependent k_x for panels at 20^o and 6 cm apart

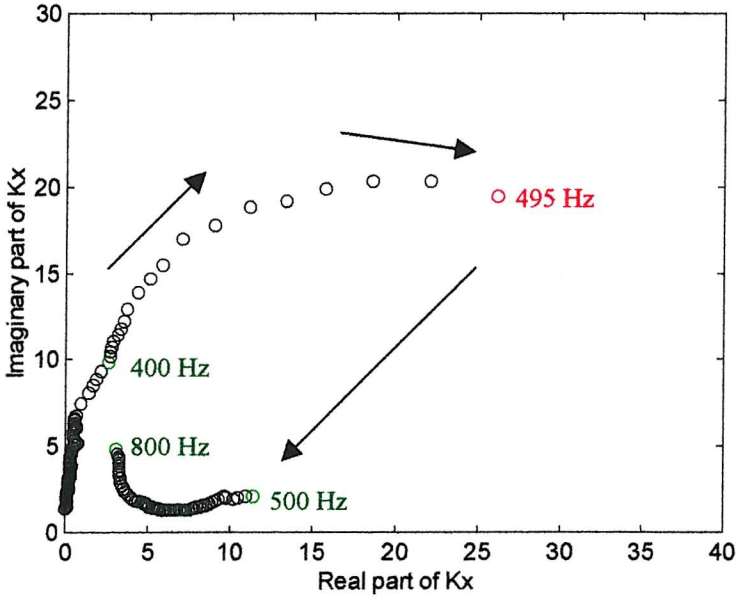

Figure 6.19 – Frequency dependent k_x for panels at 20^o and 12 cm apart

In much the same way, the plot of k_x for panels 12 cm apart (*Figure 6.19*), exhibits a large discontinuity in the loop that moves clockwise with increasing frequency. The frequency at which the value of k_x jumps is slightly higher than the previous plot. At first sight, it seemed that these results were incorrect, because of both the large magnitudes of k_x and the discontinuity in the loop. However, using the mode shape check at the ambiguous frequencies (400 – 500 Hz) proved that all wavenumbers were associated with the primary mode. An example of this is given in *Figure 6.20* where the mode shapes at a number of frequencies are given for the duct lined on one wall with the panels spaced 6 cm apart. Each correspond to different values of k_x and map the mode shapes (normalised to the soft wall) to the frequency where the maximum value of k_x is noted (475 Hz). From *Figure 6.20* it can be seen that the values of k_x do indeed relate to the primary mode, as no turning points are evident. In addition, the plot also indicates the type of sound field within the duct. The 475 Hz mode shape in *Figure 6.20* moves from a high sound pressure at the soft wall, to a far lower value at the rigid wall. The shape results in a fairly constant and low, pressure near the rigid wall, which given the symmetry of the model, translates to the middle region of the room. The pressure at the soft wall however (i.e. the opening of the *Bass Trap*) is very high and thus the difference between the two will produce a large

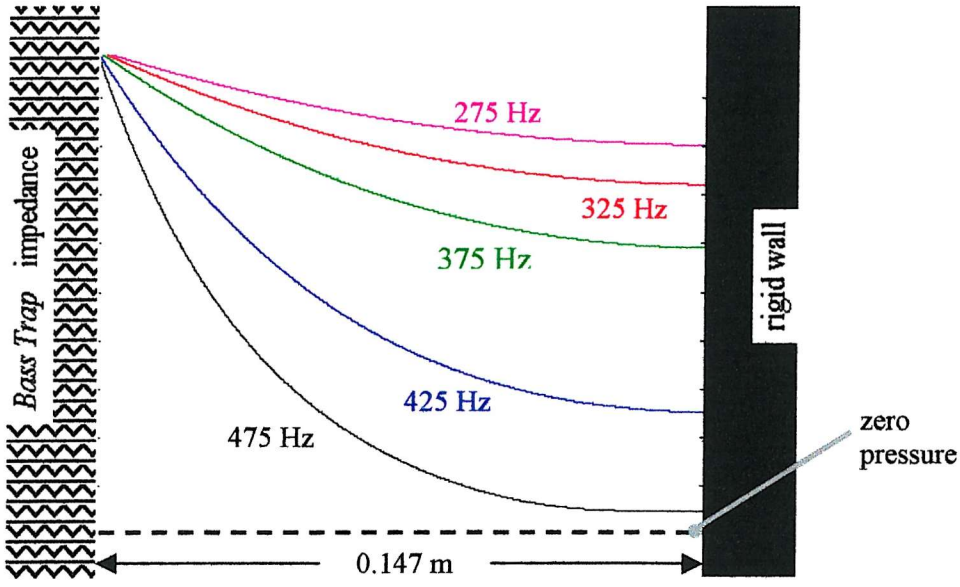

Figure 6.20 – Theoretical mode shapes across the duct width at five different frequencies

pressure gradient across the duct, for a mode which is typically the least attenuated. This particular type of mode shape is evidence of an *acoustic surface wave*. By contrast, *Figure 6.20* shows how at frequencies below 475 Hz, the pressure distribution across the duct is more plane, making the surface wave easily identifiable on account of its exponential decay in pressure amplitude from the soft side wall. At frequencies above 475 Hz, the mode shape 'flips' such that the pressure minimum is at the soft wall, not the rigid wall and the pressure distribution returns to being pseudo-plane.

More discussion on the subject of surface waves will be given later in the chapter.

6.2.2.6 Theoretical Transmission Results for Two Side Wall *Bass Traps*

Finally, the mathematical analysis has reached its conclusion, yielding a theoretical calculation of the plane wave transmission along a duct with one of two arrangements of side wall *Bass Trap*. The results are presented for 14 panels, 6cm apart and 7 panels, 12 cm apart; i.e. absorber lengths of 78 and 72 cm respectively. Given this slight difference in length, one can expect the 6 cm absorber to yield slightly more attenuation than if it were the same length as the 12 cm absorber. *Figure 6.21* shows the result. The y-axis has been truncated to –100 dB, as such attenuation effectively prevents any propagation of the sound down the duct. Considering the noise floor of a typical control rooms, a dynamic range of 100 dB is extremely optimistic.

It is immediately obvious from the plot, that both arrangements of side wall *Bass Trap* yield enormous attenuation of the primary mode over a relatively narrow range of frequencies. Both exhibit the same kind of shape, a shape noted in the experimental results. Similarilty with experiment is also seen as a lower frequency and larger magnitude of TL is evident when more panels are placed closer together (see *Figure 6.12* for comparison). The frequencies at which the maximum TL occurs is 475 Hz for the 6 cm spacing and 495 Hz when the panels are 12 cm apart. Referring back to the previous section one will recall that these are the same frequencies for which the magnitude of the transverse wavenumber reached a maximum. It is also the region where the presence of surface waves were noted, as illustrated by the theoretical mode shape presented earlier (black trace of *Figure 6.20*). From the brief discussion about the physical consequences of the surface wave, one can see how the pressure gradient causes particle velocity motion in the direction of the absorbent wall lining. Another

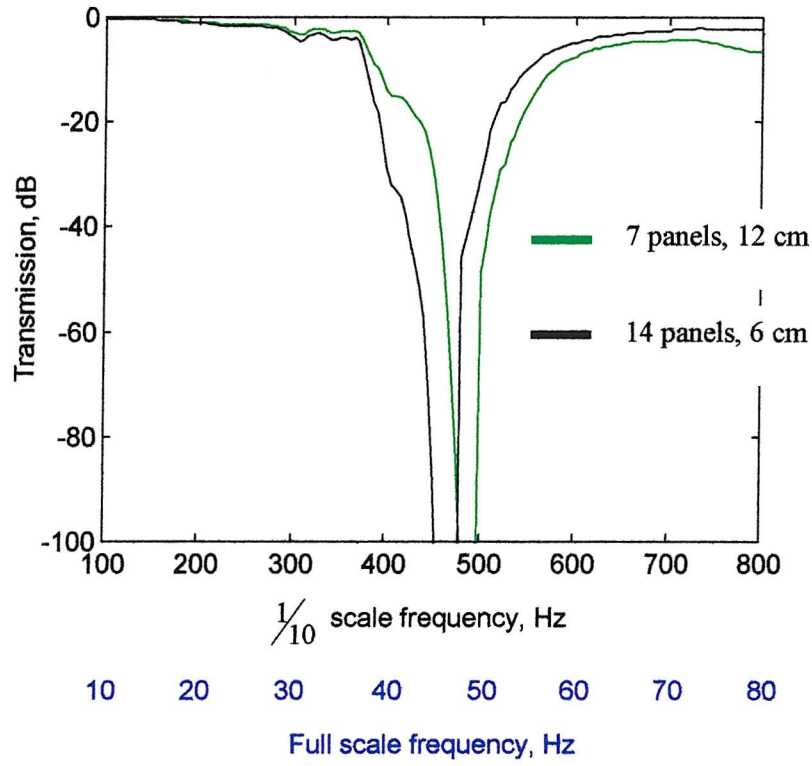

Figure 6.21 - Transmission calculated from theory

way of explaining the physical mechanism is to consider the extreme pressures at the soft wall as displacing the majority of the sound energy in the plane wave to one side of the duct/room – the sound is effectively 'sucked out' at these frequencies. If the extreme attenuation is linked with the presence of a surface wave, then the cause of this must be found if the attenuation is to be associated with a physical aspect of the *Bass Trap* design. Whilst the absorption coefficient of the *Bass Trap* channels seems to have little connection with the frequency of maximum TL, the plots of surface normal acoustic impedance, do. Within the context of this investigation, the reactive part of the channel impedance was presented and it was noted that the two traces, for the two absorbers, were slightly different. Referring to *Figure 6.14* one will see that the frequency of zero reactance (¼ wavelength resonant frequency) is almost identical to the theoretically predicted frequency of maximum attenuation. This suggests therefore, that the 'effective depth' of the *Bass Trap* channels gives rise to a ¼ wavelength resonance, which in turn allows the existence of a surface wave. Before this is investigated further, *Figure 6.22* shows the direct comparison between the

experimental result and the theory, for a side wall *Bass Trap* of 14 panels, 6cm apart and at an angle of 20° to the foam duct liner.

From the comparison it is clear that the agreement is poor in terms of the frequency and magnitude of maximum TL and Q of the trough. Whilst the shape and amount of attenuation could be explained in terms of imperfections in the duct and measurement system, the lack of agreement in frequency cannot be accounted for using such a simple argument. It undoubtedly points to the inability of the theory to adequately describe the system, the most obvious shortfall being its 2-dimensionality. Before further comment is made on this matter, a third model is introduced in the following section, which again uses Finite Element modelling, but this time to calculate the transmission along the duct.

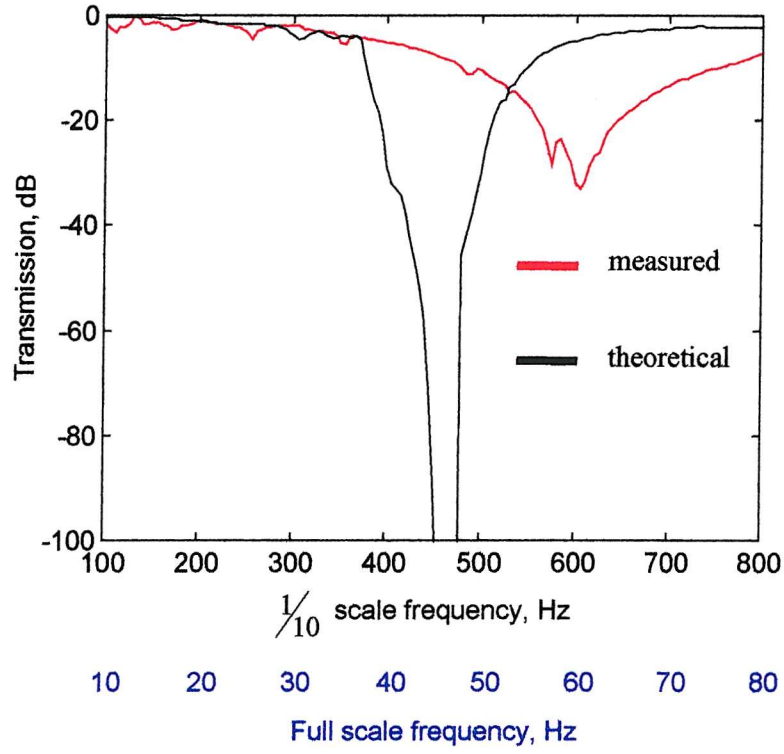

Figure 6.22 – Comparison between theoretical and experimental transmission

6.3 Numerical Investigation into *Bass Trap* Transmission

So far, in this investigation into the side wall *Bass Trap*, experimental and theoretical means have been used to model how and why it works. Both have established that significant attenuation of the primary mode occurs in a narrow bandwidth and in the last section it was hypothesised that this may be due to the presence of a surface wave. The purpose of this section, therefore, is two fold. Firstly, it is an extension of the previous investigations and another means of identifying the mechanism(s) by which the *Bass Trap* works. Secondly, it will provide a comparison with the results already obtained, thus ratifying one or the other. To this end, two FE models are presented, from which numerical results for the transmission can be obtained. The first of these models will be referred to as the **full** FE model as it includes the angled panels and foam lining. The second uses the same method as the theory of characterising the side wall *Bass Trap* as simply a surface normal acoustic impedance, itself the result of a FE model (*Section 6.2.2.1*) – as such it will be referred to as the **wall impedance** FE model. Comparison of the two, one with another and with experiment and theory will provide a solid body of evidence as to the performance of the absorber. In addition, the flexibility afforded by the FE models will enable other investigations, impossible to do any other way. Direct comparison with experiment and theory will be given once the FE results have been presented by themselves.

6.3.1 Description of the Full FE Model of the Side Wall *Bass Trap* Duct

Up until this point, all the Finite Element models have in one way or another simplified the aspect of the *Bass Trap* design under investigation. In this model, shown in *Figure 6.23*, every effort has be made to accurately describe the construction of the experimental set-up. As with the theoretical model however, it is two dimensional (as the height is ignored). Comparison between the experimental results and those obtained from the FE model will indicate whether or not the dimensionality has a significant effect on the transmission in the frequency range considered. The length of the duct is the same as described in *Figure 6.2*, with an anechoic termination specified at one end and a plane wave unit amplitude pressure source at the other. As the 26 mm thick foam is described in the model by the measured value of surface normal acoustic impedance, the width of the FE duct is

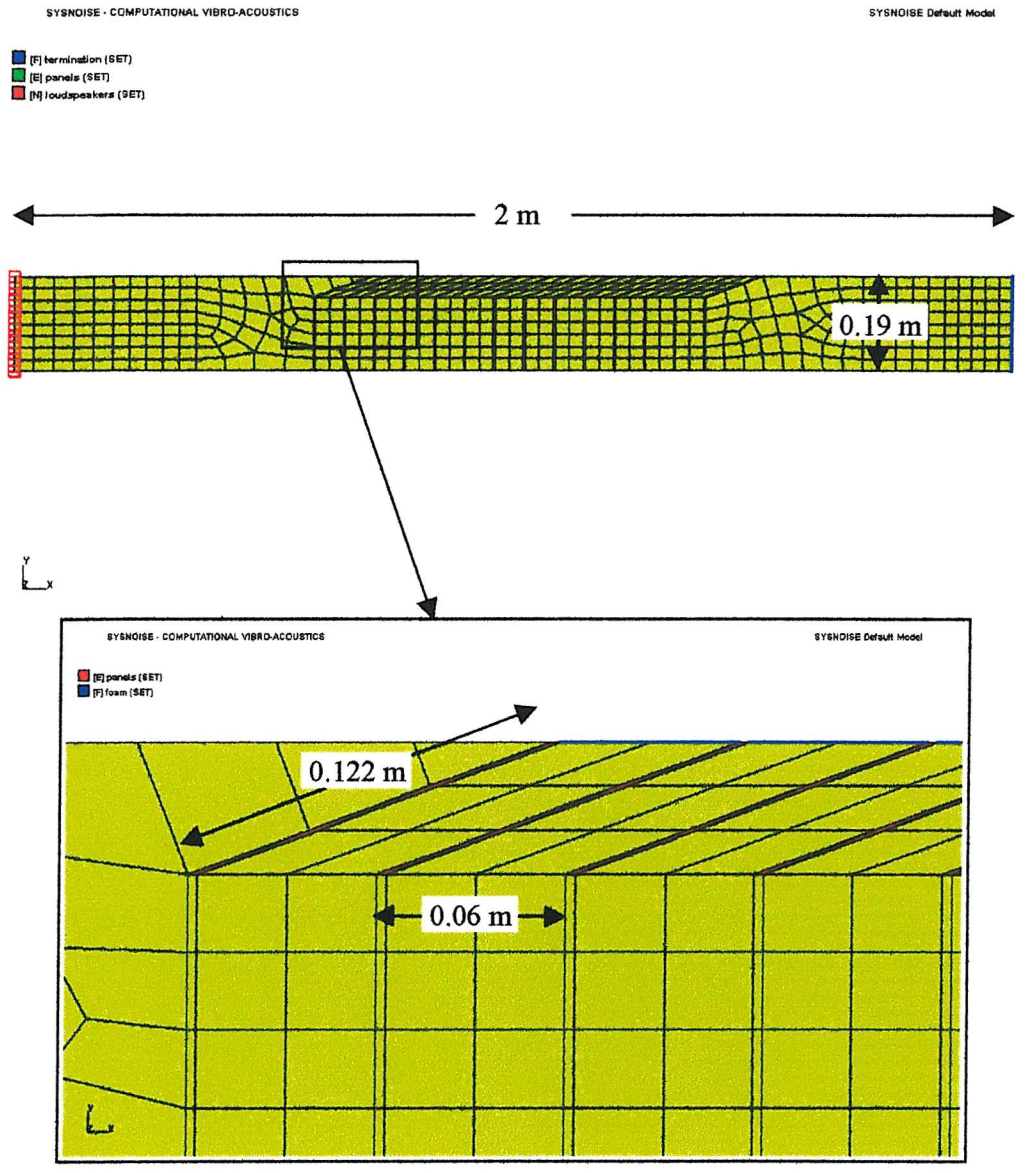

Figure 6.23 - Full Finite Element model of experimental duct

reduced accordingly, i.e. duct width – foam depth = 0.189 metres. As mentioned in *Section 5.2.1* any element in the model can be assigned a density and sound speed, to describe it as a particular material. It is important to note however that the FE model used **fluid** elements not **structural** elements. As such, the aluminium panels that protrude into the duct were modelled as dense, limp masses characterised by $\rho = 2700\ \text{kg m}^{-3}$ and $c = 5500\ \text{m s}^{-1}$. This is only valid because the chipboard panels used in the full scale design exhibit negligible vibration velocity, as described in *Chapter 1*. Elements describing 14 panels 6 cm apart were included in the mesh, however, to investigate the transmission of 7 panels 12 cm apart, every other panel

was assigned the density and sound speed of air. To decompose the sound field into the forward and backward going components necessary for the calculation of the TL, four measurement planes were described across the width of the duct, two near the pressure source and two at the opposite end. The position of the planes were $x = 0.2, 0.365, 1.7, \& 1.865$ metres, thus replicating the 0.165 m microphone separation used in the experiment. The pressure at the 15 nodes of each measurement plane were exported from *Sysnoise* into *MatLab* and the mean average calculated. This average pressure was taken as the pressure amplitude of the plane wave. From the expanded view of the panels in *Figure 6.23* one can see how the 122 mm panels at an angle of 20° were modelled.

6.3.2 Results from the Full FE Model of the Side Wall *Bass Trap* Duct

The transmission was calculated for the two *Bass Trap* side walls modelled in the theory: 14 panels, 6 cm apart and 7 panels separated by 12 cm – an approximation to the normalised distance dependency of *Section 6.1.3.4.* The result is shown in *Figure 6.24.* Both transmission traces exhibit similarities with the results

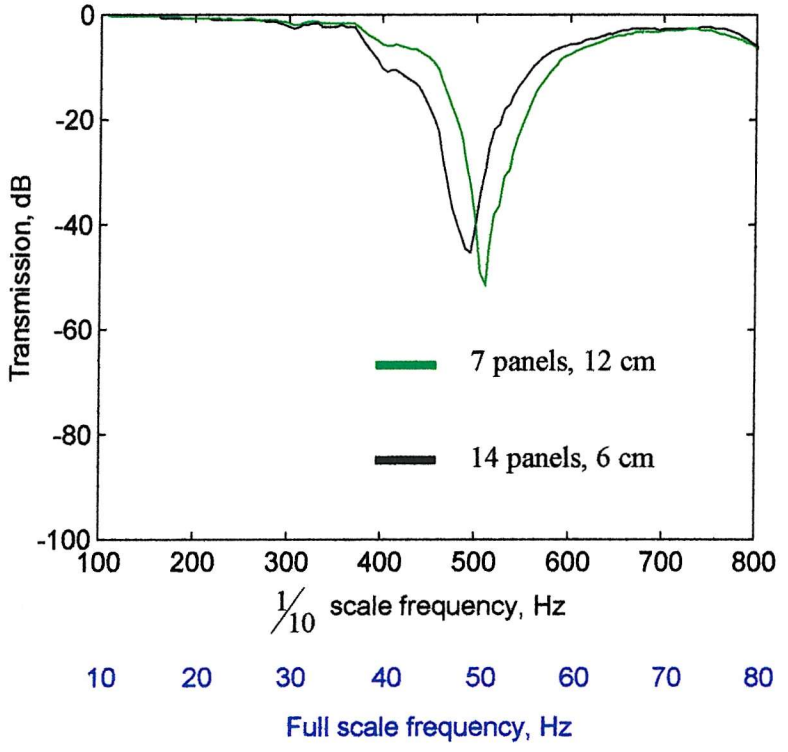

Figure 6.24 – FE calculated transmission for full panel model

obtained from the previous models. As before, the closer panel spacing yields a lower frequency of maximum TL, though half as many panels achieve a higher attenuation. The difference between the two is negligible at the extreme high and low frequencies and only in the region of the transmission trough is any difference noted. This observation would imply that the primary cause of the attenuation is particular to a narrow band of frequencies, rather than a wide band phenomenon. Such behaviour is typical of a resonance.

The full FE model result will provide an important benchmark in future discussions, as it accurately models the system of interest, including scattering from the panels and the associated diffraction and higher order mode activity. To provide a FE model slightly closer in geometry to the theory, another mesh was constructed. This and the results obtained is the subject of the next section.

6.3.3 Description of the Wall Impedance FE Model

The difference between the wall impedance FE model and the full FE model is the way in which the side wall *Bass Trap* is described. Whereas the latter includes the panels as part of the mesh, the wall impedance model uses the same lumped element approximation of the foam and panels, as the theory. The FE mesh is illustrated in *Figure 6.25*. As the same *Bass Trap* impedance descriptor is used, the duct is the same width as the theoretical model. As before, a plane pressure source is specified at the left end of the duct and a $\rho_0 c_0$ terminating impedance at the other.

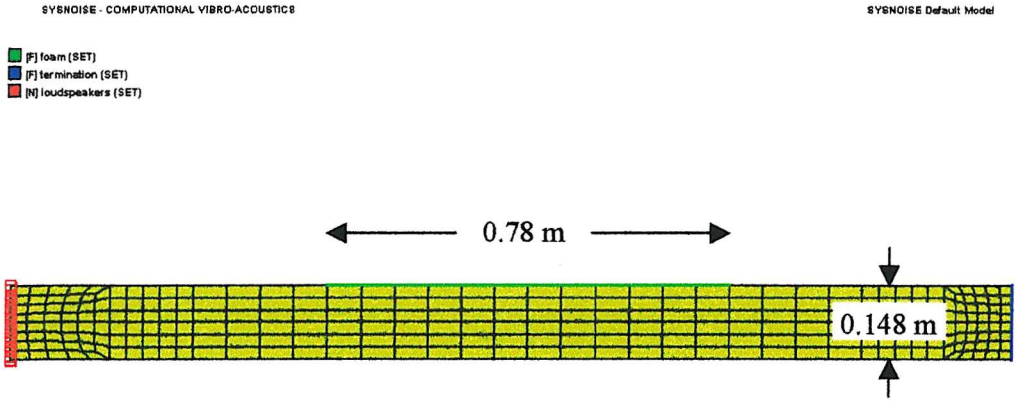

Figure 6.25 - FE model with a surface normal impedance on one wall

Unlike the theory, this FE model does include two impedance discontinuities at the positions where the side wall boundary condition changes from the impedance calculated by the model in *Section 6.2.2.1* to the infinite impedance of the rigid duct walls. At these points therefore, plane wave scattering and higher order mode activity will result, though to a lesser extent than the full FE model.

6.3.4 Results from the Wall Impedance FE Model

The transmission calculated from the aforementioned model is shown in *Figure 6.26.* The features evident in the other plots are seen here also, with a pronounced peak in attenuation at around 500 Hz. The other observation that can be made is the difference between traces at the high frequencies. No more about this result will be discussed here, as the next section will concentrate solely on directly comparing the transmissions obtained by experiment, theory and Finite Element Analysis.

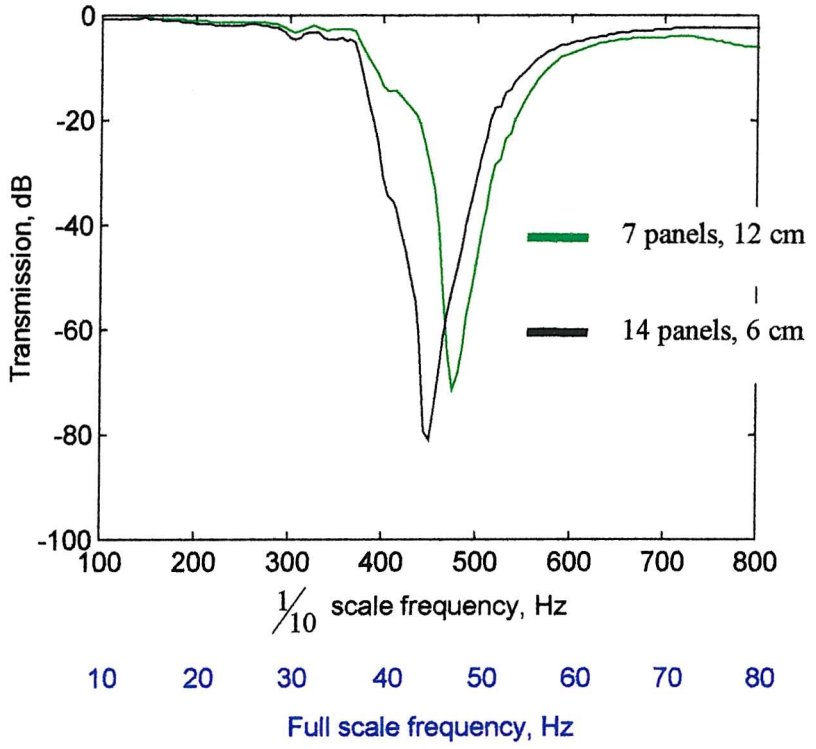

Figure 6.26 – FE calculated transmission comparison for wall impedance model

6.4 Comparison of Results Obtained Using Experimental, Theoretical and Numerical Models

The danger with such a large number of results, obtained by different means, is that one loses sight of the objective of the investigation. In order to shed any light on the way the side wall *Bass Traps* are working, the results have to be carefully analysed one with another so that useful conclusions can be made. In this section, hypotheses introduced throughout the chapter will be tested and subsequent explanation for the *Bass Trap* given. The conclusions will themselves lead to an additional section, where further evidence of the primary mechanism will be presented. The two comparisons will be grouped according to the *Bass Trap* arrangement, i.e. 14 panels at 20^{o}, 6 cm apart (experiment, theory and FEA) and 7 panels at 20^{o}, 12 cm apart (theory and FEA).

6.4.1 Comparison of Results for 14 Panels at 20^{o}, 6 cm Apart

In *Figure 6.27* the transmission results from the four investigations are shown on the same plot. As the full FE model describes the side wall *Bass Trap* exactly, it will be used as the reference against which the other three are compared. The main difference between the two FE models is in the region of the transmission loss. The simpler model predicts a higher value of attenuation between 400 and 480 Hz, attaining 30 dB more at its maximum value. The diffraction caused by the panels (resulting in a complicated sound field in the near field of the side wall *Bass Trap*) is the only mechanism by which this discrepancy in transmission can occur. In this case, it reduces the effectiveness of the absorber in the frequency range shown. Apart from this difference, the agreement is very good. The comparison between the two suggests that the surface normal impedance is a suitable way of characterising the *Bass Trap*, as it is able to account for much of the transmission loss.

The theoretical transmission is almost identical to the wall impedance FE result, with the only difference occurring near the maximum TL. This discrepancy is due to the errors introduced when solving the many equations in the FE model. Every solution has a finite accuracy and the additive effect of this 'rounding' is to reduce the dynamic range of the final result. As the theoretical analysis requires the solution to only one equation, the result is exact and no numerical errors occur. It is reassuring to

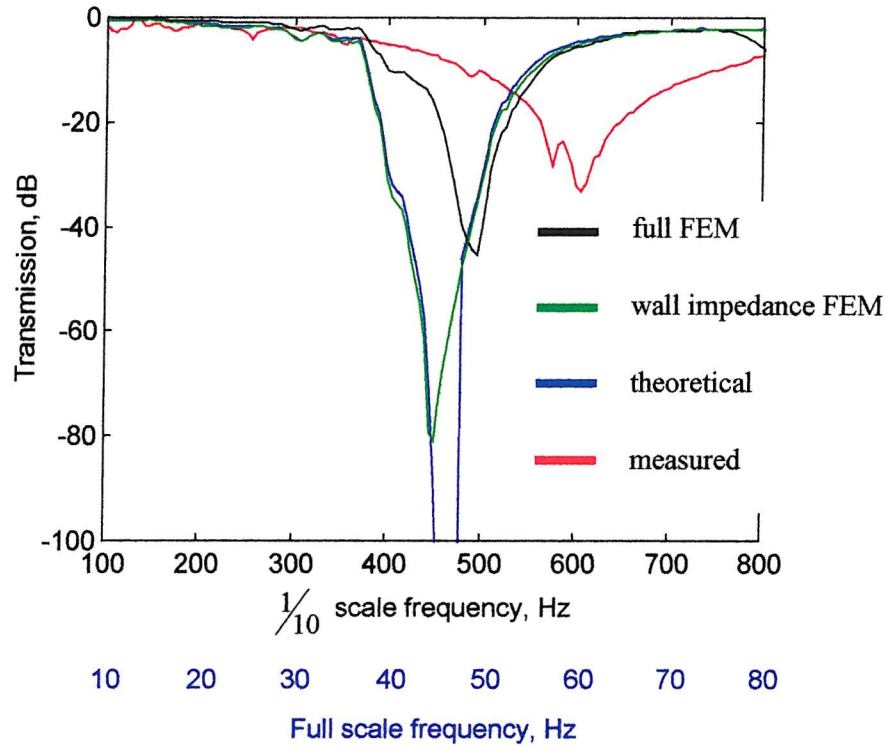

Figure 6.27 – Transmission comparison for 14 panels, 6 cm apart

note such agreement, as the two models are founded on the same side wall boundary condition. Two conclusions can be drawn from the comparisons made thus far.

The similarity between numerical models implies that the primary means of attenuation is connected to the surface normal impedance of the side wall. Whilst diffraction from the panels has an effect, it appears to be secondary. Apart from numerical errors in the simpler FE model, it is seen to be identical to the theory, from which we can conclude the theoretical model is an accurate descriptor of the primary means by which the side wall *Bass Trap* works. That being the case, the physical behaviour by which the attenuation is achieved can be found.

By contrast, the experimental results show little agreement, particularly in terms of the frequency of maximum TL. The two main reasons for this are imperfections in the experimental set-up and simplifications in the FE and theoretical models.

As previously mentioned, additional resistance to that characterised in the FE models is undoubtedly present in the experimental duct. Although every effort was taken in the positioning of the panels, it is unlikely their angle and spacing was exactly that described in the models. The investigation in *Chapter 5* showed how small changes

to these variables changes the impedance at the open end of the *Bass Trap* channel, which will in turn effect the transmission.

Regarding the two models, the use of a surface normal impedance to describe the foam liner ignores some important acoustic properties. In particular, no account can be given for particle velocity motion **through** the foam, as it is assumed to be locally reacting and does not consider **axial** velocity. The model used in the following chapter, to investigate another aspect of the *Bass Trap*, uses absorbent elements which are able to model a porous material more accurately.

A more key simplification used in the models is their two-dimensionality, which results in the vertical modes being ignored. This is not the case in the experiment, where the duct has a finite height. As the first vertical cut on mode occurs at 567 Hz, it is likely that this will have a significant effect on the transmission results. To check this, the additional vertical wavenumber corresponding to this mode was added to the compatibility equation (*equation 6.13*) such that the axial wavenumber is given by $k_z = \sqrt{k_0^{\,2} - k_x^{\,2} - k_y^{\,2}}$, where $k_y = \frac{\pi}{0.3}$. When the attenuation rate was calculated from the new axial wavenumber, considerable transmission loss was noted around 600 Hz, in addition to the attenuation due to the side wall. It would appear, therefore, that the main reason for the lack of agreement between experiment and the two models is their respective dimensionality. If the experiments were to be repeated, it would be better to reduce the height of the duct, thus forcing the vertical cut-on mode to a higher frequency.

In the next section the results for the less dense *Bass Trap* side wall are presented.

6.4.2 Comparison of Results for 7 Panels at 20°, 12 cm Apart

No experimental trace is included in *Figure 6.28* as no measurement was made which can be directly compared with the theoretical and numerical results. Even with the panels at this spacing (allowing normal line of sight to the foam), the use of surface normal impedance to describe the side wall is seen to account for the majority of the attenuation characteristic. As before, the absence of diffraction and scattering results in an improved TL at the lower frequencies. Again, excellent agreement is noted between the simple FE model and the theory.

It is this similarity between theory and Finite Element Analysis that prompts further investigation into the presence of a surface wave and its part in the attenuation evident

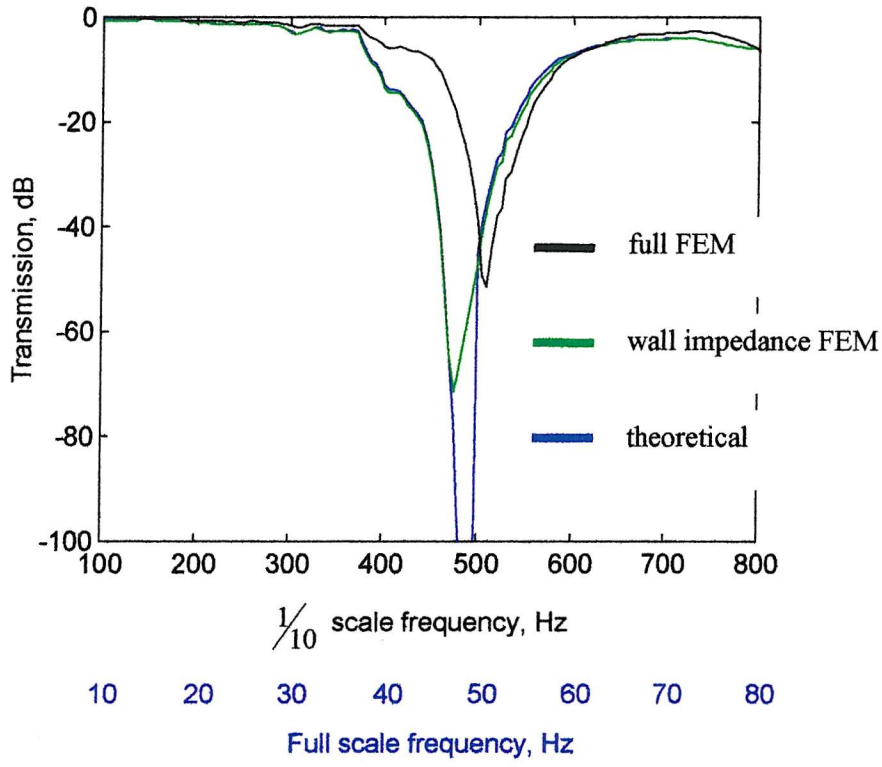

Figure 6.28 – Transmission comparison for 7 panels, 12 cm apart

in all the results. Whilst it was the theory that identified the acoustic phenomenon, it will be FEA that is used to provide more evidence of its role in attenuation of sound propagating past the side wall *Bass Trap.*

6.5 Further Finite Element Investigations

Before the revised FE model is introduced and the investigation into the surface waves described, some theory and background on this strange phenomenon will be briefly given.

6.5.1 Explanation and Discussion of Surface Waves

The existence of acoustic surface waves has long been established and are generally described by the fact that their pressure amplitude decreases exponentially away from the surface with which they are associated. In his paper, Brekhovskikh [6.8] describes how a surface with an elastic impedance is necessary for the surface waves to 'cling to'. A comb-like surface is cited as the simplest way to

achieve such an impedance and the periodic panels in the *Bass Trap* also fall into this generic category.

Tester [6.9] was the first to measure surface waves experimentally as part of his research into attenuation in jet engines; an accidental discovery, which led him to call them 'strange modes'. Tester found that surface waves were present when the duct liner had a small negative reactance, with the acoustic resistance being less influential. As part of their investigation into seat dip, Schultz & Watters [6.2] hypothesised that the presence of a surface wave may be responsible for some of the attenuation measured using a scale model, as the necessary stiffness reactance was provided by the height of the seats (another comb-like structure).

The results presented in *Section 6.2.2.5* are evidence of a surface wave over a narrow band of frequencies and have since been shown to correspond to the maximum attenuation down the duct. As mentioned, the large difference in pressure across the width of the duct will give rise to particle velocity motion into the soft wall lining, resulting in absorption.

6.5.2 Investigation into Surface Waves Using the Full FE Model

In this section, one of the post-processing features of *Sysnoise* is used to investigate the existence of surface waves in the full FE model. Although good agreement between theory and the full FE model was seen in *Section 6.4.1*, it could be argued that the association with surface waves is purely circumstantial – using the numerical model in a different way will provide the necessary clarification. Once the numerical analysis has been calculated by *Sysnoise*, the results can be presented graphically in a variety of ways. For the purposes of this investigation, the pressure distribution in the duct at 475 Hz is shown in the form of an iso-line plot. Each of the contours plotted describe positions of equal amplitude and as before, the red end of the visible spectrum corresponds to high amplitudes. From the plot therefore, two quantities will be seen – the decay in axial pressure amplitude along the duct and the mode shapes across the duct width. It is the plots of mode shape that will show whether or not surface waves are present at the frequency of maximum TL.

Figure 6.29 shows the Finite Element iso-line plot, in which both of the aforementioned quantities are evident. Firstly, the colour of the contours indicate that at this frequency, the pressure amplitude is decreasing as the sound propagates past the side wall *Bass Trap*. At the left hand side of the figure, the pressure amplitude is

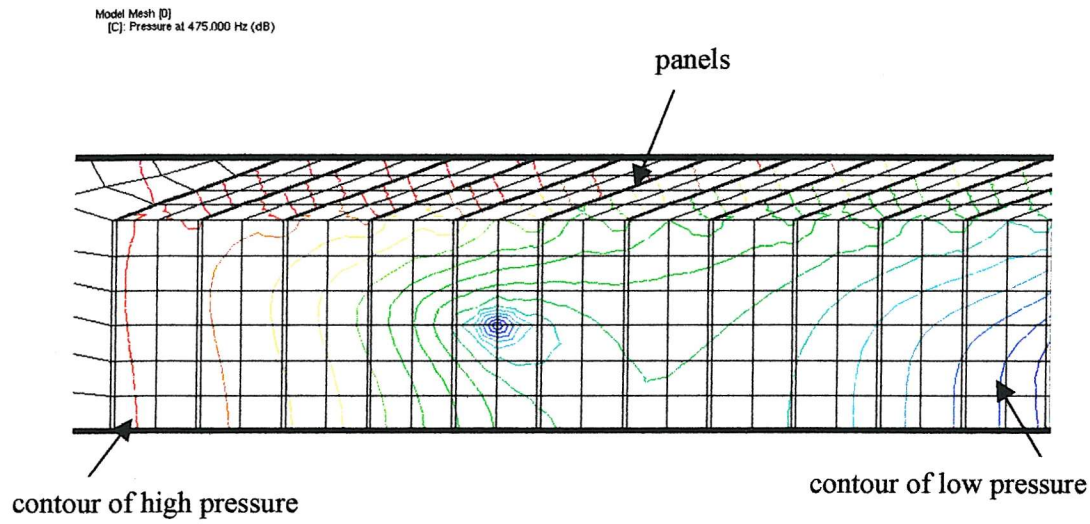

Figure 6.29 – Plan view iso-line FE plot at 475 Hz for the full model (compare with Figure 6.23)

around 95 dB SPL, while at the other end of the *Bass Trap* the blue line corresponds to 50 dB SPL. A similar trend can be seen between the angled panels, though to a lesser extent. The second quantity, more important to this investigation, is the transverse mode shape. The pressure distribution across the duct is near-plane at the beginning of the *Bass Trap*, but rapidly changes shape the further the sound propagates. As the contours are generally closer together near the *Bass Trap*, the pressure distribution across the duct at a given x-position will exhibit the exponential type decay away from a soft surface, associated with a surface wave. *Figure 6.29* clearly shows that the majority of the transverse decay in pressure amplitude occurs in the immediate vicinity of the *Bass Trap*.

6.5.3 Influence of Panel Orientation on Transmission

One of the most striking features of the *Bass Trap* is the fact that the panels are angled towards the loudspeaker in the control room. In this section, the transmission is calculated for panels orientated so they face the opposite direction, i.e. the back wall of the room (or anechoic termination in the duct).

The full FE model (*Figure 6.23*) was used to find the transmission for the panels in the reverse orientation by swapping the terminating boundary conditions, i.e. the pressure source was assigned to the $y = 2$ m boundary and the anechoic impedance at

$y = 0$. The same four measurement planes were used, but in the opposite order. The principle of reciprocity states that the transfer function of a given system between a point source and a point receiver is the same if the source is placed in the position of the receiver and vice versa. Strictly speaking reciprocity cannot be applied to this investigation as neither the source or the receiver are specified at a point, however a similar transmission result is anticipated regardless of the orientation of the panels. This does not necessarily mean that the mechanism of attenuation is the same for the two orientations, as the input impedance of the system will be different.

The direct comparison between the transmission for the two absorber arrangements is shown in *Figure 6.30*. It is clear from the plot that almost identical transmission is achieved regardless of panel orientation, with the only difference evident at the high frequencies. The principle of reciprocity, though only tentatively mentioned, appears to be vindicated in this result. Before further comment is made about the result, the backward going component of the pressure field at the loudspeaker end of the absorber is calculated. This quantity will inform us of whether or not there is a

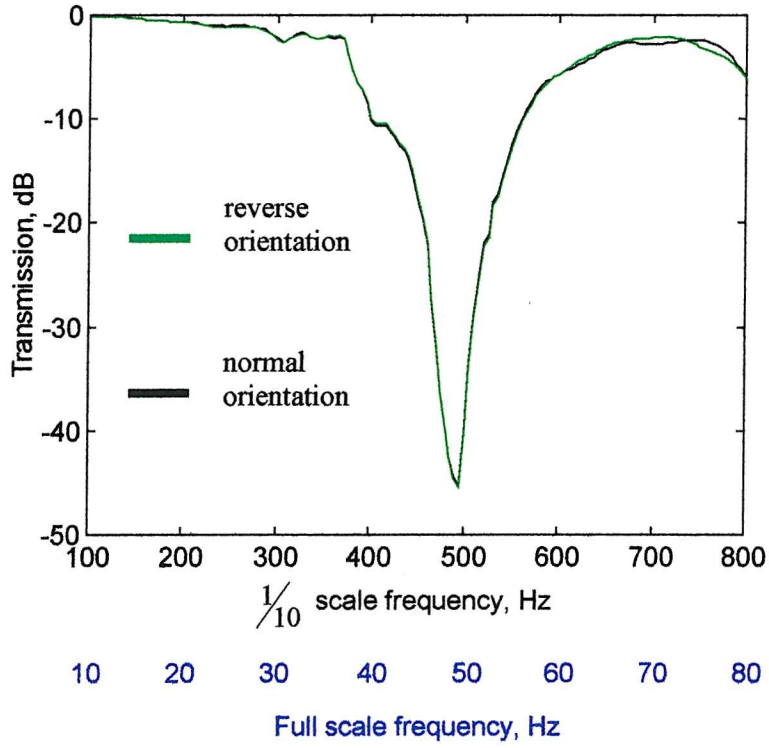

Figure 6.30 - FE calculated transmission with panels in opposite orientations

different mechanism of absorption between the two absorbers – *Figure 6.31* shows this result.

The traces shown correspond to the FE model presented in *Section 6.3.1*. The y-axis gives the pressure in dB by which the reflected wave differs in magnitude to the forward going wave, until now the only direction of propagation considered. The aspect of the result that is of particular interest is the magnitude of the reflected wave at the frequency where the maximum TL occurs. *Figure 6.31* shows that at this frequency (around 500 Hz) the reflected wave is 11 dB lower in level than the incident wave, regardless of the panel orientation. Indeed, the magnitude of the reflected wave is largely similar in both traces, apart from certain frequencies where deep troughs are apparent. The general trend is for sound to be more strongly reflected by the *Bass Trap* side wall absorber as the frequency increases.

Given that the characteristics of the reflected waves are similar and the transmission results of *Figure 6.30* are almost identical, two conclusions can be drawn. Firstly, the

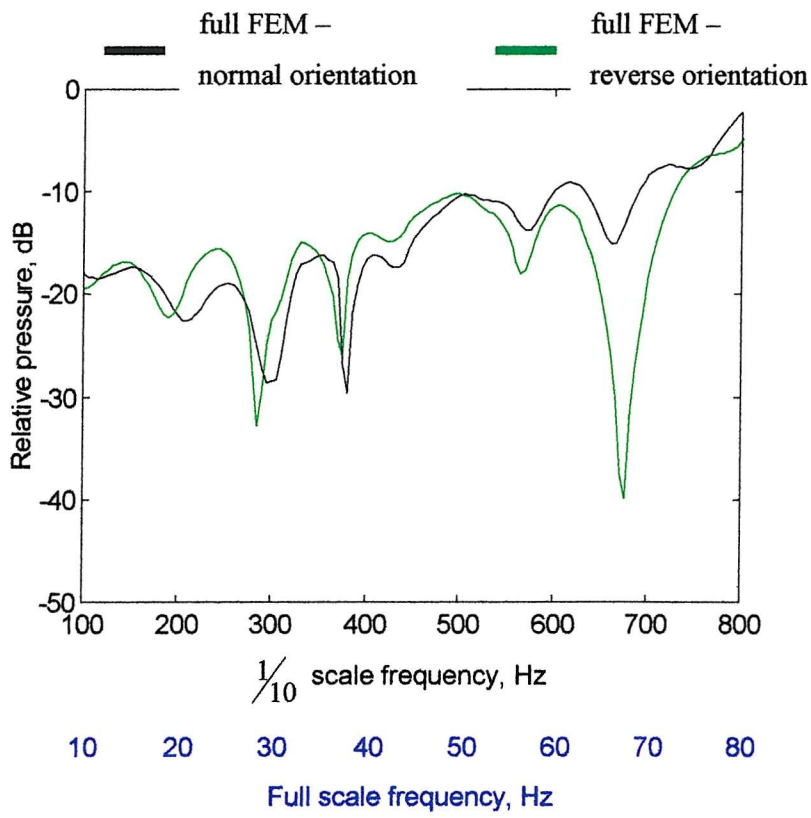

Figure 6.31 – Comparison of reflected wave amplitude for two different absorber arrangements

result in *Figure 6.31* proves that reflection is not the primary mechanism by which the large TL, noted in the experimental and FE model, is achieved. If it were, the amplitude of the reflected wave at the frequencies of maximum TL would be close to 0 dB. Secondly, the mechanisms involved are largely independent of panel orientation, in the frequency range shown.

This latter conclusion supports the hypothesis that, at low frequencies, the main means by which sound is attenuated is due to the presence of a surface wave and higher order mode activity caused by diffraction at the edges of the panels. The former has been shown to be a function of the surface normal acoustic impedance of the wall boundary, while the latter will not be sensitive to whether or not the panels face the source or not. It is likely, however, that at higher frequencies, the orientation of the panels will have a more significant effect on the transmission. Any absorption due to the *Bass Trap* channels acting like lined ducts, will be greatly reduced if the panels face the rear of the room.

The relevance of the result in *Figure 6.31* to the real life control room, is that the reflections from the *Bass Trap* side wall are significantly less than the incident sound from the loudspeakers. If this were not the case, the presence of the reflective monitor wall could result in flutter echoes in the region of the room between the loudspeakers and the position where the side wall *Bass Trap* starts.

The following section will add to this line of investigation, through experimental means.

6.6 Further Experimental Investigations

In this section the experimental rig is used to investigate the influence of panel orientation on the attenuation of sound along a duct. The measurements were made in exactly the same way as those in *Section 6.1*, except that the 26 mm of foam was not covered with sticky tape.

6.6.1 Influence of Panel Orientation on Transmission

The effect of panel orientation on the transmission along the duct was investigated by measuring the transmission twice, once with the panels facing the loudspeakers (as in *Section 6.1.3*) and once with them facing the absorbent termination. Both measurements were made with 14 panels at an angle of 40^{o} to the

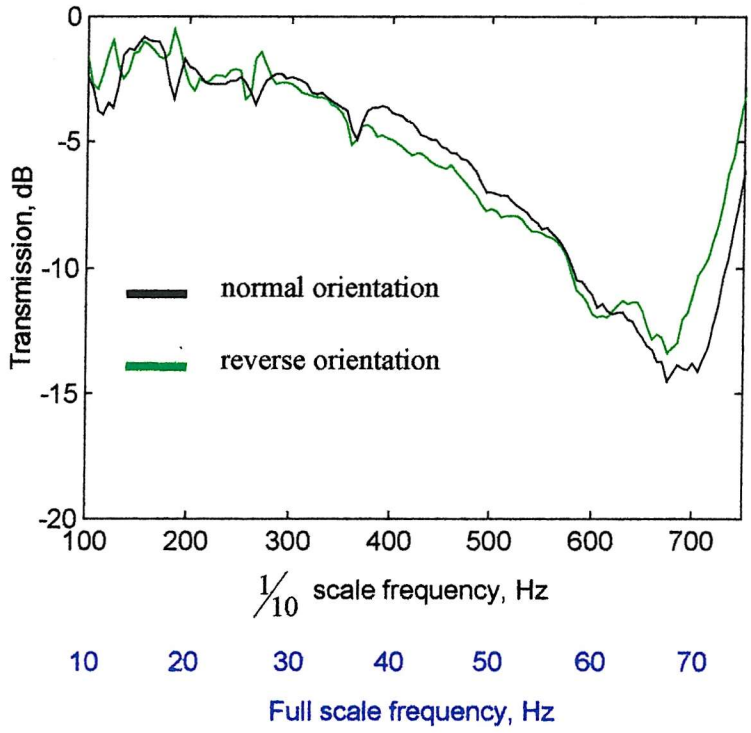

Figure 6.32 – Comparison of measured transmission for different orientations of panel

foam liner. A similar result for TL would indicate the integrity of the experiment. The transmission for the two panel orientations are shown in *Figure 6.32*. By comparing the black trace of *Figure 6.32* with the result for transmission with tape covering the foam (green trace in *Figure 6.8*), it can be seen that the absence of the tape leads to less TL at a lower frequency. Thus, one can conclude that the absorbent properties of the multi-layer wall in the real life design will have a significant effect of the resultant transmission of the *Bass Trap* as a whole.

Regarding the effect of panel orientation, the measured result shows the same similarity between the two traces, as predicted by the FE model of the previous section. Given that both numerical and experimental investigations agree in this respect, one can be confident that the orientation of the panels has little bearing on the transmission of sound from the loudspeakers to the rear wall in this frequency range. This conclusion further confirms the assertion that surface waves and diffraction are primarily responsible for the performance of the side wall *Bass Trap*. Whilst the 'trapping' of sound at **low** frequencies has been shown to be insignificant, this may not be the case as the wavelength of sound approaches the dimensions of the *Bass*

Trap channels. If this is shown to be the case, the absorber design might be more accurately named the *Mid-High Trap*.

As an extension of this investigation into panel orientation, the next section will describe how changing the angle of panels along the length of the duct affects the transmission.

6.6.2 Ceiling *Bass Trap* Transmission

Referring back to *Figure 3.1* and the discussion about the construction of the Tio Pete control room, one will recall how the ceiling panels do not make a constant angle with the ceiling. Each panel is suspended such that the leading edge faces the centre of the loudspeakers. This is impossible to do for the side and rear walls, as the loudspeakers are not in the same horizontal position. The reason given by the advocates of the *Bass Trap* absorber, for orientating the ceiling panels in this way, is to allow the propagating wavefront easy access into the *Bass Traps*, while ensuring a tortuous exit. Whilst this might be true at higher frequencies, one of the conclusions of the previous section was that 'trapping' of sound is not a significant mechanism of attenuation in the lowest three octaves of the audible frequency range.

In order to investigate whether or not gradually changing the angle of the panels has an effect on the transmission, measurements of the absorber arrangement shown in *Figure 6.33* were made and compared with a constant panel angle of 40^{o}.

The table below summarises the angle each panel (labelled from *1*, closest to the loudspeakers, to *14*, closest to the termination) makes with the side wall.

As has been shown, the angle of the *Bass Trap* channels affect the surface normal acoustic impedance and as a consequence, the frequency at which the surface wave occurs. Thus, by varying the channel angle, one would expect the maximum TL to occur over a wider range of frequencies. The comparison between the transmission for the two absorber arrangements is given in *Figure 6.34*.

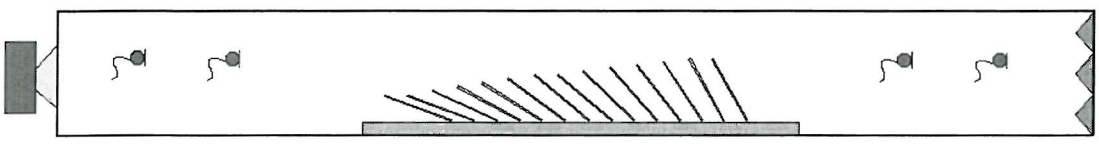

Figure 6.33 – Scale diagram of gradual angle change experimental set-up

Panel number	Angle made with wall
1 & 2	20°
3	24°
4	28°
5	32°
6	36°
7 & 8	40°
9	44°
10	48°
11	52°
12	56°
13 & 14	60°

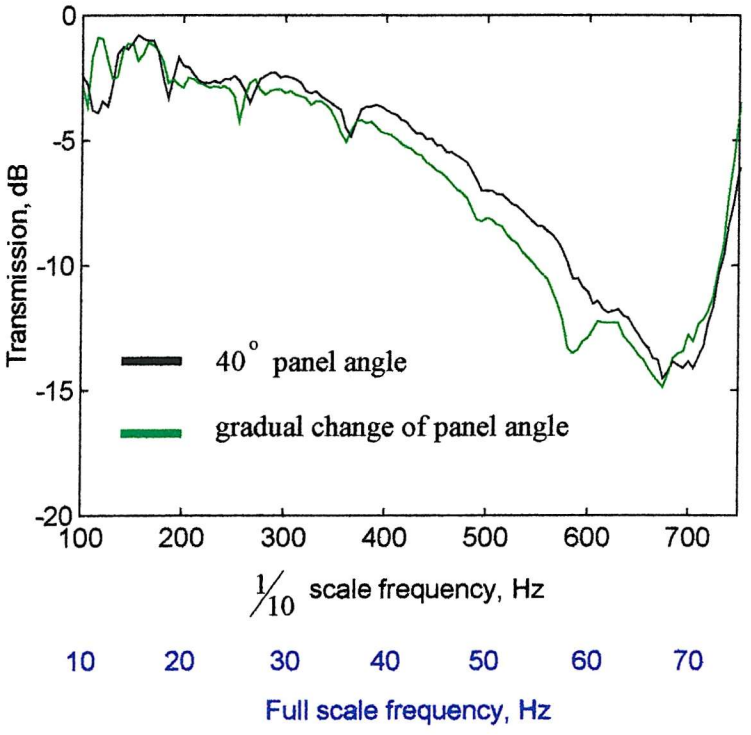

Figure 6.34 – Comparison of measured transmission for different angles of panel

While the two traces are largely similar, a small increase in attenuation is noted between 400 and 600 Hz, where there is a gradual change in panel angle. Further investigation would be necessary to prove the benefit of this particular orientation of panel.

6.7 Further Theoretical Investigation

6.7.1 Full Scale Side Wall *Bass Trap* Transmission

The final investigation into the amount of attenuation yielded by the side wall *Bass Trap* is presented in this section. In the same way as the two previous theoretical transmissions were calculated, so in this section a surface normal impedance is assigned to a side wall of a semi-infinite duct. The difference here, however, is that the impedance is that of the open end of the full scale, multi-layer wall, covered panel channel of *Section 5.5.2*. The purpose of this section is to estimate the attenuation from 10 panels placed at 20^{o} along the side walls of the Tio Pete control room of *Chapter 3* and to that end, the width of the 'duct' is 4.96 metres. The results will also shed light on the importance the terminating impedance of the *Bass Trap* channels (the multi-layer wall in this case) has on the presence of the surface wave. The analysis used in this section is identical to that of *Section 6.2*, where the imaginary part of the axial wavenumber is used to calculate the transmission loss.

Figure 6.35 shows the theoretical transmission together with the side wall surface impedance of the *Bass Trap* channels. As before, large peaks in attenuation are noted in narrow frequency bands, all of which correspond to slightly negative values of side wall reactance (shown by the dotted line in the lower part of the figure). As noted by Tester [6.9], the values of side wall resistance are also similar in the regions where the attenuation is greatest, suggesting there is an optimum value of impedance. The fact that the side wall impedance tends to this value, explains the complete stop band above 300 Hz.

6.8 Conclusions

The transmission achieved by the side wall *Bass Trap* has been thoroughly investigated in this chapter, using experimental, theoretical and numerical

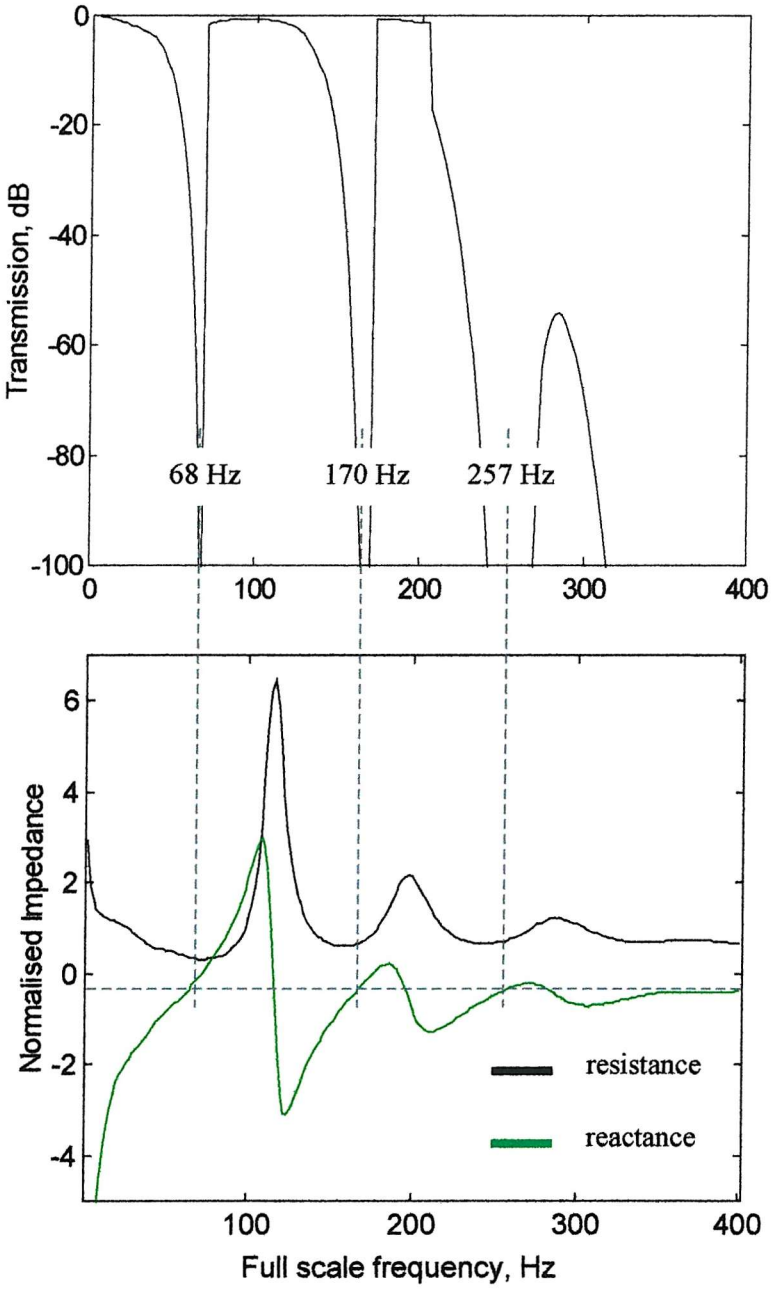

Figure 6.35 – Theoretical transmission for 5 m length of Tio Pete side wall Bass Trap

means. Between the three, the main mechanisms by which sound is attenuated as it propagates down the room/duct, have been found.

The effect of the foam in the experimental duct showed that, at wider spacings and obtuse panel angles, the onset of higher order modes caused by diffraction from the panels made a significant contribution to the high frequency attenuation.

At lower frequencies, the panels and foam liner were shown to act as a lumped element, allowing the side wall to be characterised by a surface normal acoustic impedance. Agreement between theoretical and numerical models suggested that this wall impedance supports a surface wave, which is primarily responsible for the large values of TL. Further evidence was provided by the FE iso-line plot, in which the amplitude of the transverse pressure amplitude decayed most rapidly near to the face of the *Bass Trap*. The frequency at which the surface wave occurs was shown to be primarily governed by the reactive part of the wall impedance, which itself is a function of panel depth, angle and separation.

The lack of TL dependence on the orientation of the panels provided further evidence that 'trapping' is not significant at low frequencies, though it may prove important as the wavelength of sound becomes shorter.

It was hypothesised that gradually changing the angle of the panels might broaden the surface wave attenuation and although an experiment into this did not disprove the hypothesis, it was not sufficiently conclusive to prove it either.

CHAPTER 7

Further Investigations into the Rear Wall *Bass Trap*

Introduction

In *Chapter 5* the acoustic properties of a rhomboidal channel were investigated, as the first step in considering the rear wall *Bass Trap*. Some of the results obtained also proved useful in modelling the transmission of the side wall *Bass Trap*, as described in the previous chapter. In this chapter, the absorption coefficient of the rear wall *Bass Trap* is again considered using both experiment and Finite Element Analysis. The numerical modelling will extend that already presented in this work, in order to investigate a subtle mechanism that may contribute significantly to the absorption observed. Due to limitations in the FE model, direct comparison with other results will not be possible, though this will not prove important in the investigation described. Before the revised FE model is presented, the hypothesis that is of primary interest in this chapter will be explained. The results from the FE model will then be shown, after which the associated experimental investigation is described.

7.1 Explanation of 'Horn' Hypothesis

The possible mechanism of absorption explained in this section is the brainchild of Professor F J Fahy, who suggested the idea to the author after a number of conversations on the subject. The hypothesis is based on the acoustic properties of conical horns and the principle of reciprocity. To start with, some basic theory about horns is given, using the two dimensional model illustrated in *Figure 7.1*. Horns have long been used to increase the radiation efficiency of direct radiating loudspeakers, by matching the acoustic impedance of the loudspeaker with the throat of the horn[1]. It is particularly at low frequencies that the addition of a horn is most noticeable [7.1]. Interestingly, even small changes to the flare rate have been shown to have a marked effect on the radiation efficiency when the wavelength of sound is many times greater than the dimensions of the horn [7.2].

---

[1] The narrow end of a horn is known as the throat and the wider end, the mouth.

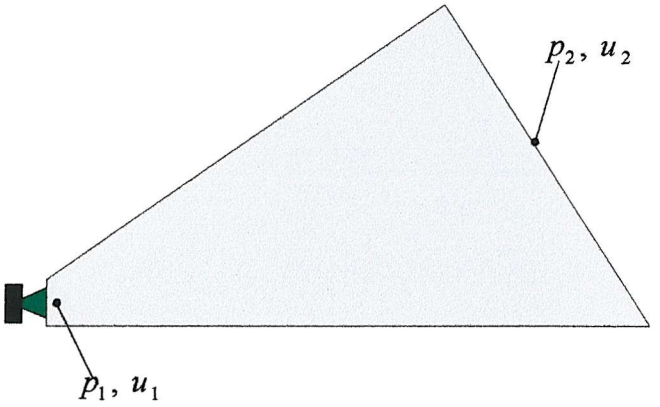

Figure 7.1 – Conical horn with pressure and velocity shown at the throat and mouth

In *Figure 7.1* a conical horn is illustrated, with a small direct radiating loudspeaker placed at the throat. The loudspeaker is assumed to act as a piston, enabling its behaviour to be characterised as a periodic velocity source, u_1. Due to the horn, the velocity source gives rise to a large pressure p_2 at the mouth. Applying the principle of reciprocity to the system, a velocity source u_2 at the mouth will cause a large pressure p_1 at the horn's throat. The significance of this elementary argument will become clear from the geometry of the rear wall *Bass Trap*, illustrated in *Figure 7.2*. In this diagram, the conical horn of the previous figure can be seen as a shaded area, together with the aforementioned pressures and velocities. Applying the same

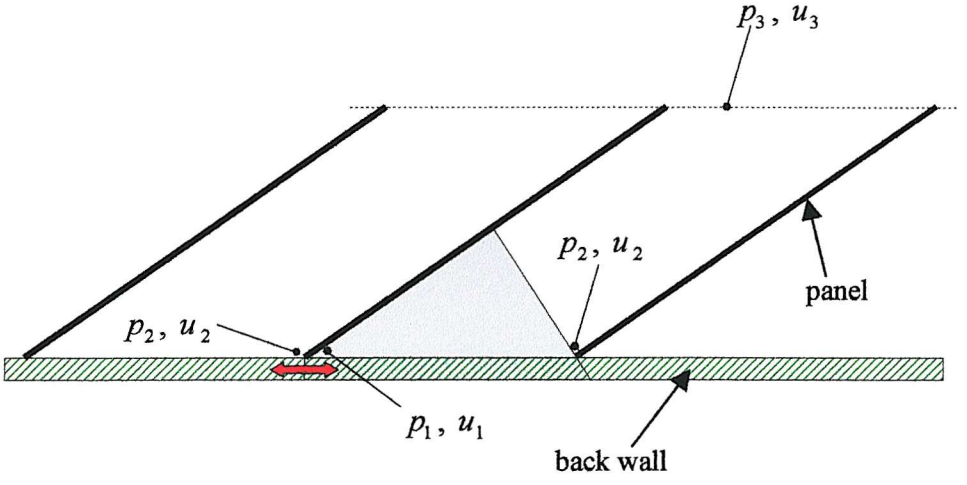

Figure 7.2 – Back wall 'horn effect' model (red arrow indicates anticipated velocity)

argument as before, a velocity source u_1 will cause a large pressure p_2 at the throat and a similarly large pressure p_3 at the open end of the *Bass Trap* channel. One would expect little difference in magnitude between p_2 and p_3 as there is no horn flare in this section of the channel. Using reciprocity again, it can be seen that a velocity source at the open end of the channel u_3 will give rise to a large pressure p_1 but a far smaller pressure p_2. It is the periodicity of the rear wall *Bass Trap* that makes this observation significant, as an equivalent set of pressures and velocities exist in the adjacent channels. Thus at the junction of the panel and absorbent wall, a large pressure difference will be evident either side of the panel, as the magnitude of p_1 will be larger than p_2. A pressure difference such as this, concentrated in a small area will result in high particle velocity **through** the porous outer layer of the absorbent wall (shown as the red arrow), it is reasonable therefore to expect significant absorption. Generally, low frequency absorption in rooms is not easily achieved through porous absorption, as the high particle velocity necessary occurs ¼ wavelength from a rigid boundary – this may represent a number of metres. The hypothesis presented here however could prove to be far more space efficient.

From the explanation given it is clear that any investigation must be able to account for particle velocity motion through an absorbent layer, therefore the channel termination cannot simply be characterised by a surface normal acoustic impedance. The FEA software used in *Chapters 5 & 6* has the capability to create absorbent elements, which allow porous materials to be modelled in 2 or 3 dimensions.

7.2 Absorbent Element Numerical Investigation

The model described in this section is full scale, thus all materials and dimensions are those of a *Bass Trap* typical of *non-environment* recording studio control room. *Figure 7.3* illustrates the Finite Element mesh.

7.2.1 Description of the Absorbent Element FE Model

Unlike the FEA investigations of previous chapters, the *Bass Trap* channels described here cannot be considered in isolation, as the hypothesis relies on their interaction with each another. For this reason, the FE model uses four channels, although only the acoustic behaviour of the middle two is analysed. By having the

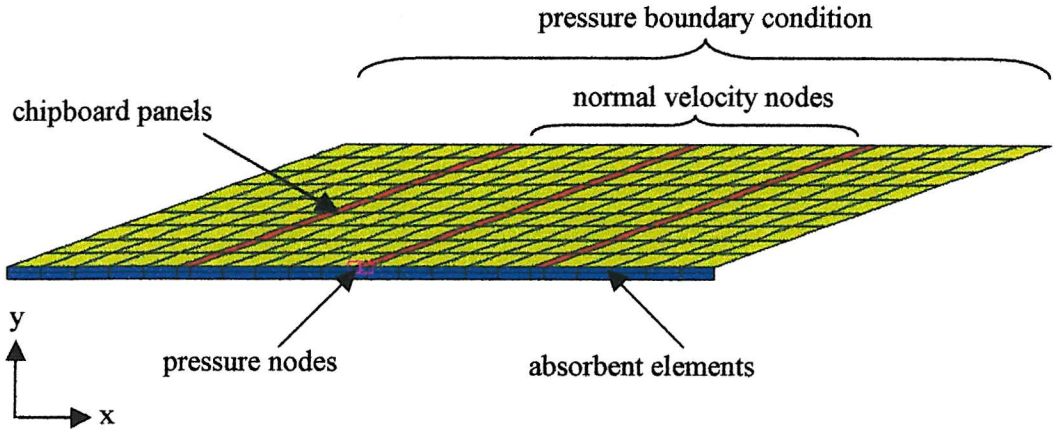

Figure 7.3 – Finite Element model of the back wall absorber

two outer 'dummy' channels, the two in the middle should be approximately characteristic of the large array employed in a typical rear wall *Bass Trap.*

As in *Chapter 5* a pressure boundary condition is specified across the open end of the channels, with the normal velocity of only the middle nodes used in the calculation of the rear wall absorption coefficient. In the same way as the aluminium panels were described in the full FE model of *Chapter 6* (*Figure 6.23*), so the chipboard panels are characterised by assigning the appropriate density and sound speed (650 kg m^{-3} and 3700 m s^{-1}) to the relevant elements. Given that a large pressure difference is anticipated at the wall between one side of the panel and the other, the pressures at two nodes in this region were calculated – these are highlighted in the figure.

The blue shading in *Figure 7.3* shows the elements used to describe the porous outer layer of the absorbent wall. As mentioned in *Chapter 5*, in addition to the aforementioned material properties, any element in a FE mesh can be assigned a porosity, structure factor and resistivity. Between these five variables, it is possible to model many porous materials, thus allowing the propagation of sound through them to be analysed. The material properties assigned to the absorbent elements in the FE model were chosen to characterise a typical medium density porous material, not the tape covered foam used in the experiment, or the cotton waste felt used in the full scale design. By choosing a medium value for resistivity and typical values of structure factor [7.3] and porosity [7.4], the colour maps of pressure and particle

velocity within the absorbent elements could be more clearly seen. Clarity in the results allowing ratification of the hypothesis, was deemed more important than making the model specific to a particular design. The sound speed and density was that of air. The table below summarises the quantities specified.

Sound speed	Density	Porosity	Structure factor	Resistivity
340 m s^{-1}	1.205 kg m^{-3}	0.95	2	2×10^{4} Pa s m^{-2}

7.2.2 Pressure, Velocity and Absorption Coefficient FEA Results

One of the advantages of Finite Element Analysis is the ability to present the results in many different ways. Until now, the results have been exported into *MatLab* for analysis and manipulation, though in this section the post-processing capabilities of *Sysnoise* are used. The results are presented according to the order in which the hypothesis was explained. Firstly, a colour map of pressure is shown at a particular frequency of interest. By this we mean a graphical illustration of the pressure magnitude (red end of the spectrum describing large values) within the rear wall *Bass Trap* FE mesh. This result will show whether or not the expected difference in pressure at the junction of wall and panel is present. The corresponding particle velocity colour map will follow, which it is hoped will illustrate an increased particle velocity within the absorbent elements. Once the colour maps have been presented, the absorption coefficient of the channel and the magnitude of the pressure difference between the aforementioned nodes will be plotted against frequency. The pressure difference is shown normalised to the pressure boundary condition p_0 at the open end of the channel and calculated according to $p_{diff} = \left| \frac{p_1 - p_2}{p_0} \right|$, where p_1 and p_2 are the complex pressures either side of the panel.

Finally, a plot of the normalised reactance and resistance at the open end of the channel will be shown. It is anticipated that between the four figures, there will be sufficient evidence to prove or disprove the hypothesis described in *Section 7.1*. The results are grouped according to the angle of the channel and will start with the most acute.

7.2.2.1 20^{o} Channel Rear Wall *Bass Trap*

In *Figure 7.4* the magnitude of the pressure is illustrated by the different colours. The absolute values, barely visible on the scale to the right of the figure, will be presented later – it is the contrast that is the important feature of this colour map. As mentioned earlier, discussion will be restricted to the centre two channels. The reason for displaying the colour map at 230 Hz, is because a peak in the absorption coefficient is evident at this frequency – this result will be shown in *Figure 7.6.*

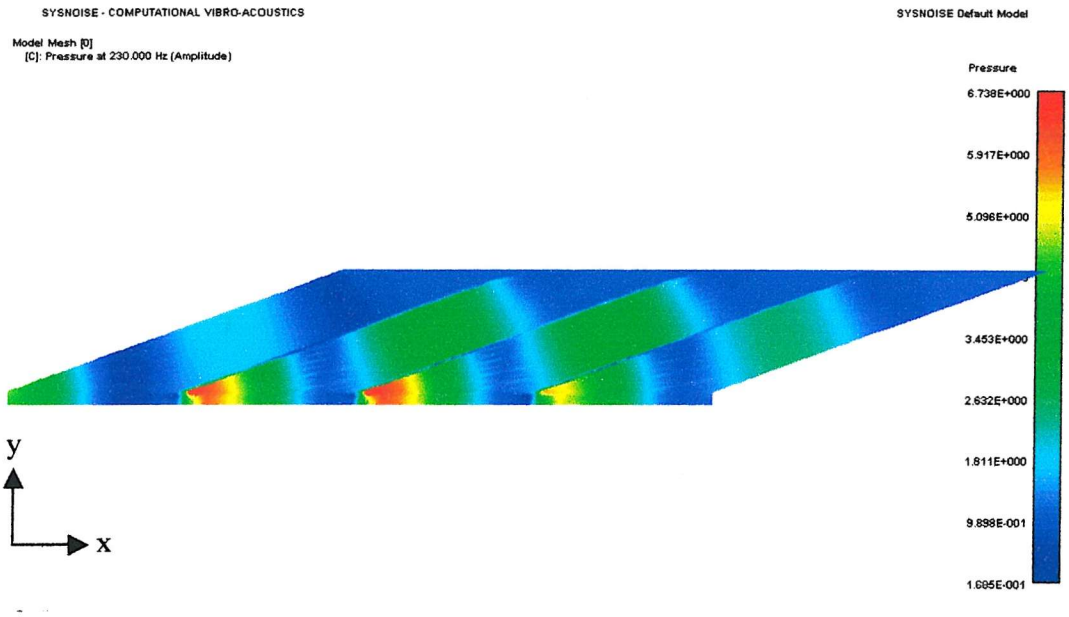

Figure 7.4 – FE calculated pressure magnitude colour map at 230 Hz for 20^{o} back wall

The figure clearly shows that a large pressure (shown in red) occurs at the throat of the horn in the third channel from the left and contrasts with the lower pressure magnitude everywhere else. In addition, the pressure on the opposite side of the panel is the lowest (extreme blue end of the spectrum) in the colour map. These two observations therefore prove the first part of the hypothesis. The following result (*Figure 7.5*) will show whether or not this pressure difference gives rise to a high particle velocity in the absorbent.

The colour map for the particle velocity is on a dB scale as the large dynamic range would make a linear representation of the result unclear. Velocity is a vector quantity, thus only one direction at a time can be illustrated using a colour map. As the hypothesis hinges on the oscillatory motion of velocity through the absorbent, it is the

x-component of the vector that is presented. As before, it is the contrast between colours that is of primary importance. Concentrating the discussion on the particle velocity within the absorbent layer, it can be seen that there is a significant increase in the region near the panel. The premise that the pressure difference identified in *Figure 7.4* would give rise to this is thus proved correct. It is important to note that velocity normal to the absorbent will also yield significant absorption and the colour map in *Figure 7.5* is not wholly representative. However, whilst it is unlikely that the

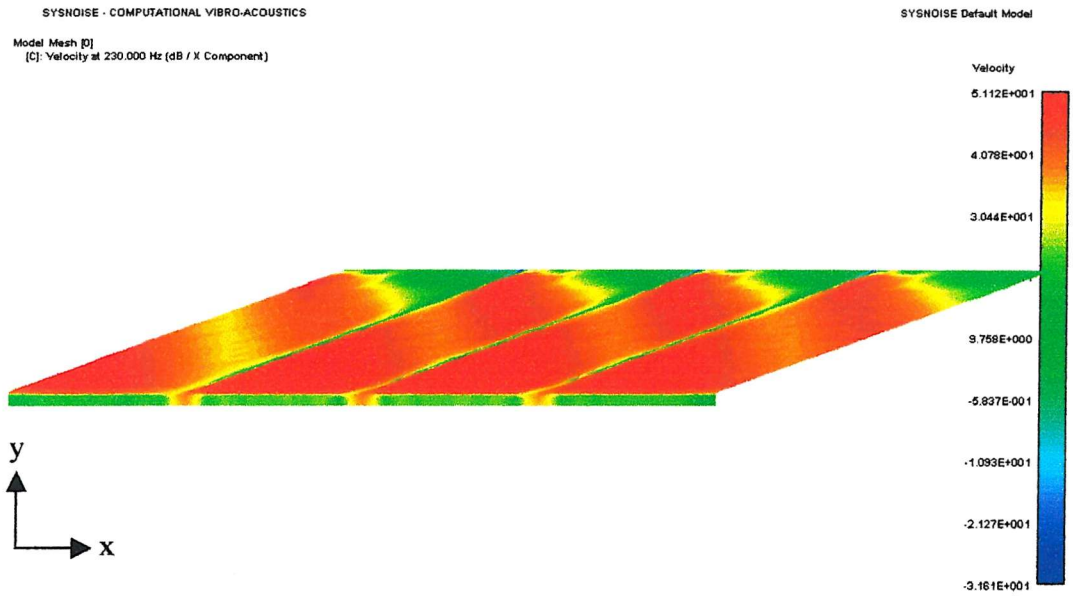

Figure 7.5 – FE calculated x-vector velocity colour map at 230 Hz for 20° back wall

x-direction velocity motion in this region of the absorbent accounts for the total absorption of the rear wall *Bass Trap*, it is a feature that will undoubtedly prove beneficial. In order to test this hypothesis, the plots of absorption coefficient and surface normal impedance to follow, will show two traces. One will be for the *Bass Trap* shown in the previous two figures, where there is an 'absorbent gap', that is, a route through the absorbent in the region of the panel and the position where the high particle velocity was noted. As a comparison, the FE mesh is altered by extending the panel to the wall through the absorbent layer, thus impeding any velocity motion in the x-direction. This change to the model will remove any absorption due to the 'horn' effect. Alongside this dual trace plot will be the pressure difference either side of the panel, as it is hoped the comparison between the two will indicate any

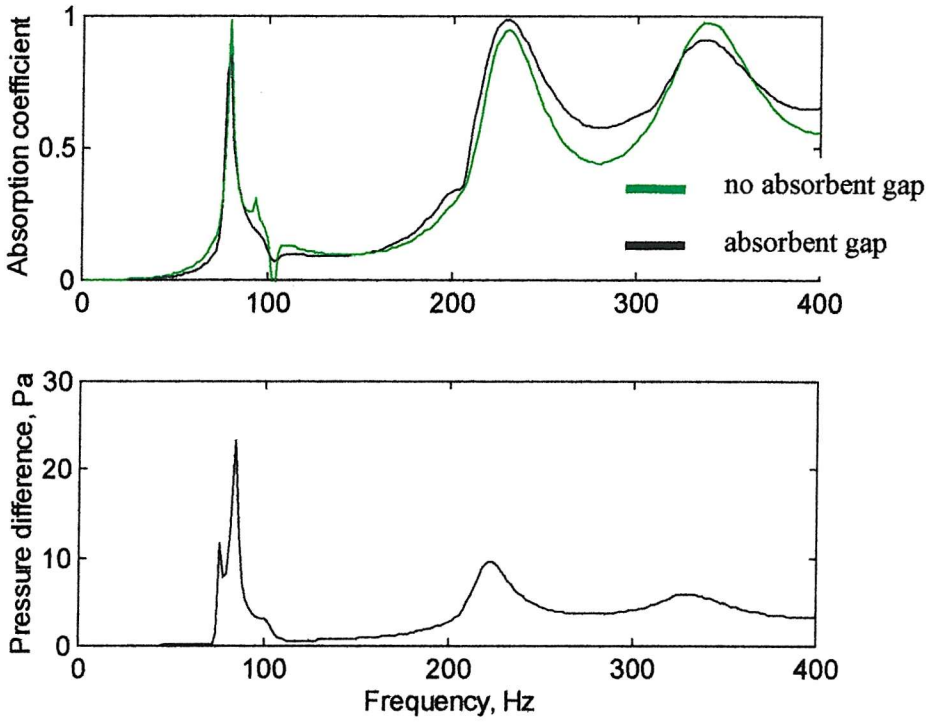

Figure 7.6 – FE calculated absorption and normalised pressure difference for back wall panels at 20°

connection between the 'horn' effect and the total absorption of the *Bass Trap.* These results are shown in *Figure 7.6.*

With no absorbent gap, the absorption coefficient exhibits three clear peaks, the second occurring at the frequency to which the colour maps related. The exact frequencies of these peaks approximate to odd integer multiples of ¼ wavelength, though as mentioned before, the rhomboidal channel means that the frequencies do not tie in precisely. Whereas the investigation in *Chapter 5* only identified the first of these resonances, the extended frequency range here allows the three to be seen. The drop in absorption coefficient between peaks is less severe as the frequency increases on account of absorption characteristics of the absorbent layer alone. From the green trace we can conclude that a ¼ wavelength resonance is primarily responsible for the absorption, though the normal incidence absorption coefficient of the absorbent layer also contributes. The absorption coefficient of the absorbent gap *Bass Trap* is largely similar, particularly at low frequencies. The differences between the peaks and the troughs are smaller, primarily because the absorption between the resonances is

greater, though the resonant frequencies remain almost the same as without the absorbent gap. Between 330 and 360 Hz, the absence of a gap yields a greater peak because the resonant behaviour is more pronounced in a fully sealed closed end pipe. The pressure difference plot shows that it too exhibits peaks associated with the 'effective depth' of the *Bass Trap*. It was hypothesised that any difference in the absorption coefficient would be accounted for by the pressure difference and while that is true to an extent, the strong resonant behaviour generally dominates. For example, at 330 Hz, any benefit from the 'horn' effect is outweighed by the weakening of the resonance and thus the absorption coefficient is greater without the gap. This is not always the case, as the high pressure difference at 230 Hz increases the absorption despite the fact it is already close to unity. In the regions between the resonances, the effect of the pressure difference (a normalised value of around 4 Pa) is even more noticeable, resulting in larger values of absorption coefficient. *Figure 7.6* has served to give great insight into the mechanism of absorption of the rear wall *Bass Trap* and the significance of the 'horn' effect. The primary effect of resonance at odd integer multiples of ¼ wavelength is slightly compromised by the 'horn' effect at some of the resonant peaks, though this is outweighed by the increase in absorption between peaks caused by the large particle velocity in the absorbent layer near the panel. The 'horn' effect thus gives a smoother absorption coefficient with frequency, an important feature if the *Bass Trap* is to be used in a recording studio control rooms. Further insight is given in the final result for this angle of *Bass Trap* – the normalised surface normal resistance and reactance at the open end of the channels, shown in *Figure 7.7.*

As with the absorption coefficient, both traces are fairly similar. Each exhibit strong ½ wavelength resonances at 140 and 260 Hz where, as explained in *Chapter 5*, the resistance maximises and the reactance transitions between a large positive to large negative value. At these frequencies, the assertion that the 'horn' effect weakens the resonance, is shown to be true, as variation in magnitude of both parts of the impedance is less. Apart from at the ½ wavelength resonances, the presence of an absorbent gap increases the acoustic resistance. The impedance of the rear wall *Bass Trap* appears to tend to a slightly negative reactance and a resistance that is close to the characteristic impedance of air, as the frequency increases.

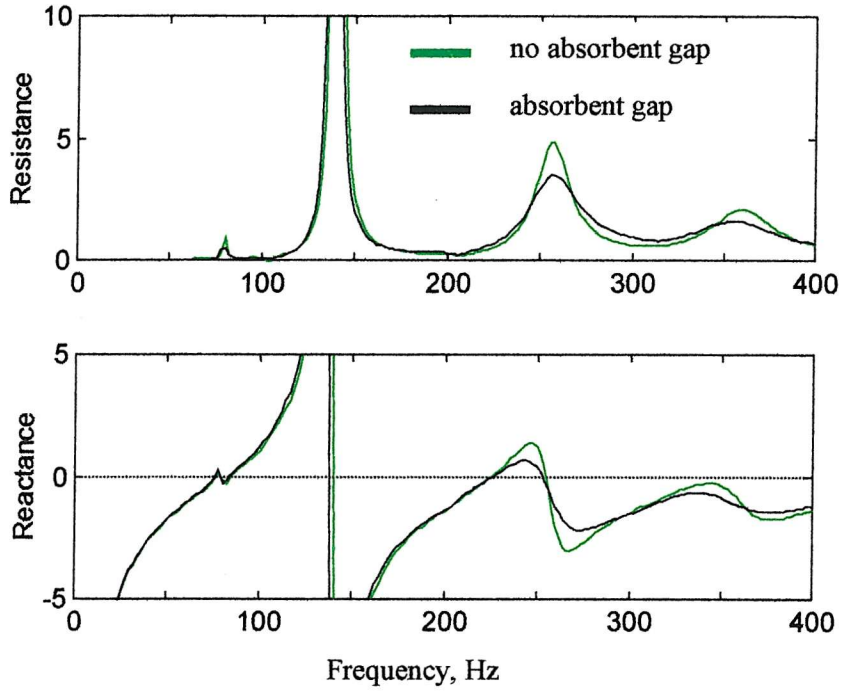

Figure 7.7 –Surface normal impedance (normalised to $\rho_0 c_0$) for back wall panels at 20°

The next section will consider the same questions, but for a 40° rear wall *Bass Trap*. The results and discussion will be particularly relevant to the real life design as this is the orientation of panel that is typically used.

7.2.2.2 40° Channel Rear Wall *Bass Trap*

As with the previous section, the frequency to which the colour maps relate corresponds to the ¾ wavelength peak in absorption that will be shown in *Figure 7.10*. *Figure 7.8* shows that with a more obtuse *Bass Trap*, the region of highest pressure still occurs at the throat of the channel 'horn'. Another point of interest is the direction of the wavefront, clearly shown as having moved from the channel normal to parallel with the axis of the panels. This observation agrees with the investigation carried out by Walter [7.5]. Detail of the pressure difference at the junction of panel and absorbent will be given later.

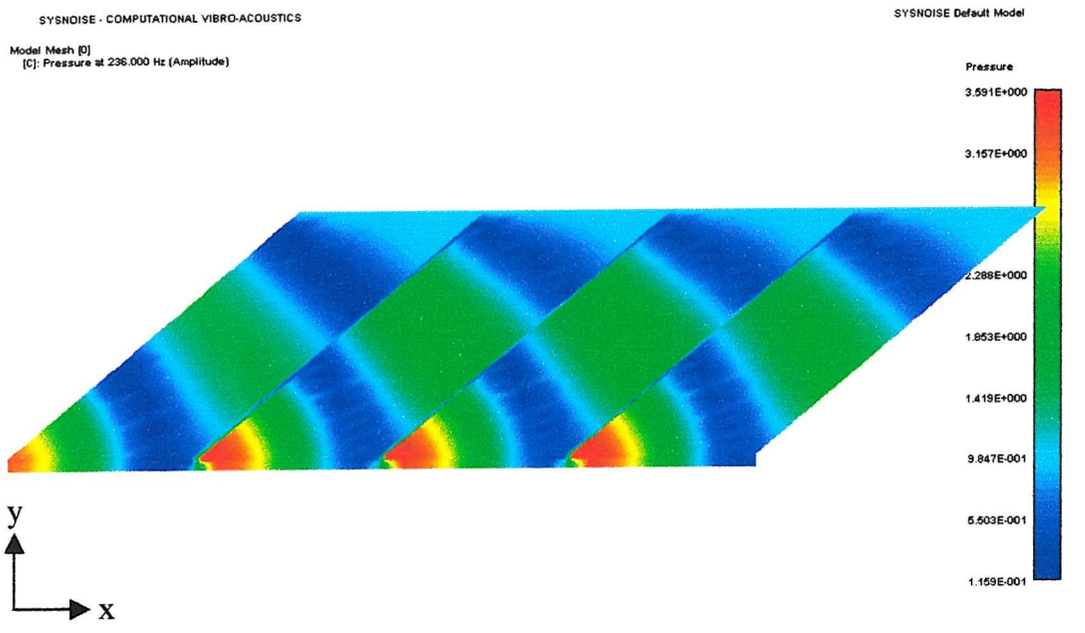

Figure 7.8 – FE calculated pressure magnitude colour map at 236 Hz for 40° back wall

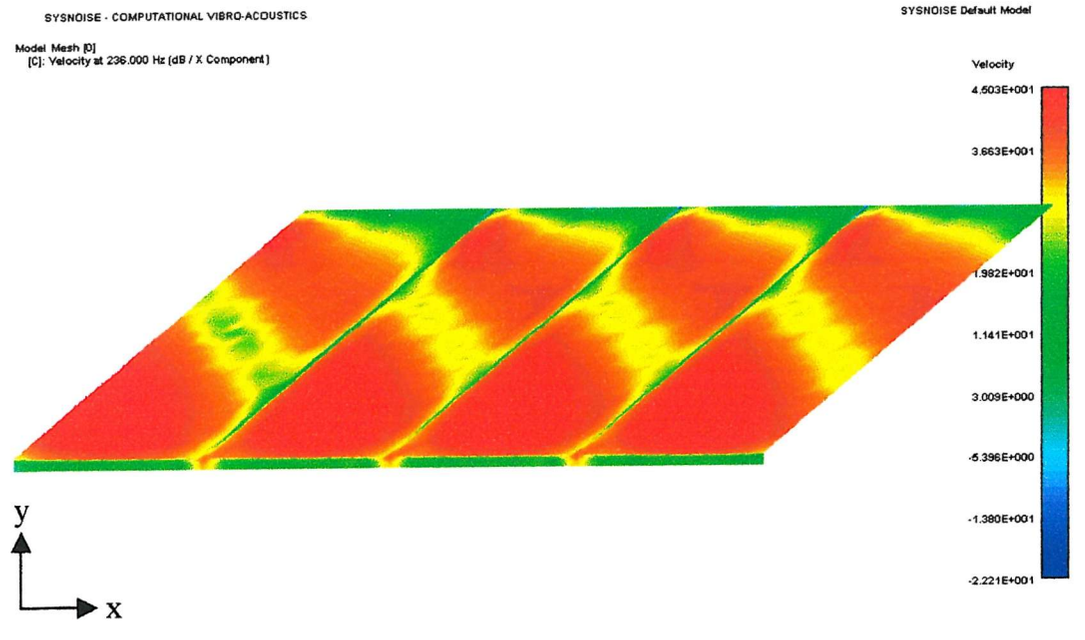

Figure 7.9 – FE calculated x-vector velocity colour map at 236 Hz for 40° back wall

In the same way as the 20° rear wall *Bass Trap*, the x-direction velocity shown in *Figure 7.9* reaches a maximum value within the absorbent layer in the region of the large pressure difference. Immediately behind the panel, the amplitude of the particle velocity is about 40 dB greater than in other parts of the absorbent. The plots of absorption coefficient will show whether or not this feature has a significant impact on the performance of the *Bass Trap* as a whole.

In contrast to the corresponding result for 20°, *Figure 7.10* shows a far less resonant absorption characteristic when the 'horn' effect is impeded. This is especially true at around 75 Hz, where the absorption coefficient is about half that in the 20° *Bass Trap.* Although peaks are evident, the general trend is a smooth rise in absorption with frequency – the peak corresponding to the ¼ wavelength is the exception to this. With an absorbent gap, the absorption is increased at all frequencies above 150 Hz. In addition to this, the 'horn' effect again reduces the difference between the resonant peaks and troughs. Whilst the 'horn' effect is more clearly seen at 40°, the absorption coefficient at 20° is greater, though it varies more with frequency. The addition of

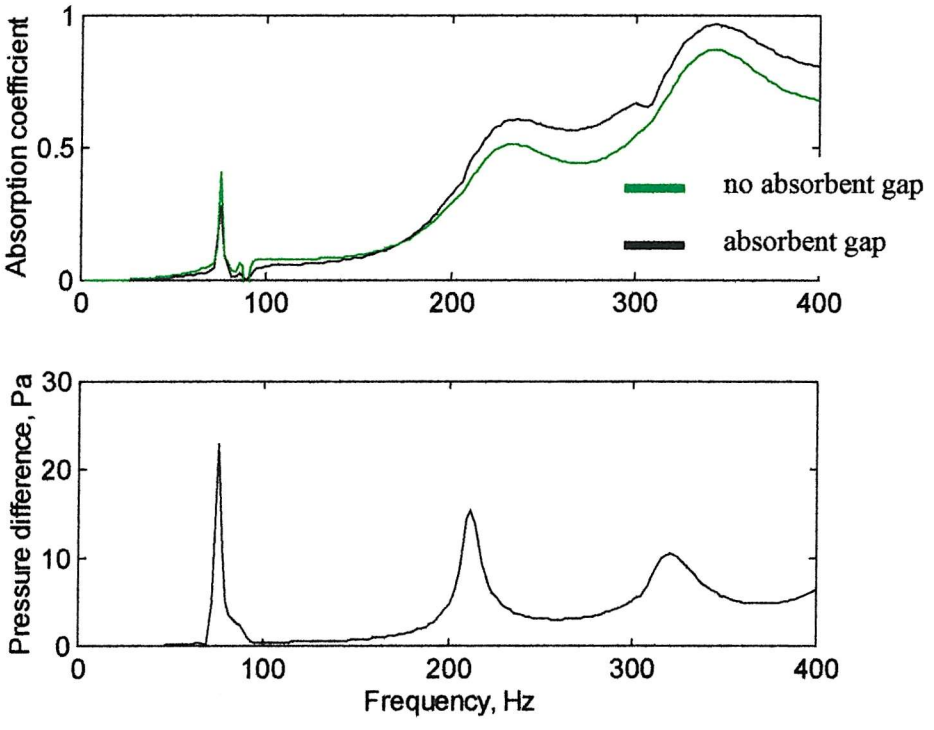

Figure 7.10 – FE calculated absorption and normalised pressure difference for back wall panels at 40°

4 cm felt on the panels would undoubtedly reduce the Q of the 20^{o} resonances, resulting in a far smoother absorption characteristic from the very lowest frequencies – more discussion along these lines will be given later.

The pressure difference either side of the panel, at the absorbent, is larger at this angle than the last, with the peaks at 210 and 320 Hz increasing the absorption of the resonance alone. It is interesting to note that the frequencies of maximum pressure difference are slightly lower than at 20^{o}. This would suggest that changing the geometry of the *Bass Trap* influences the frequency at which the 'horn' effect is most effective, in the same way that changing the flare rate of a horn influences its radiation efficiency. If therefore, the rear wall *Bass Trap* used different depths, angles and spacing of panel, the 'horn' effect could be positioned at different frequencies, enabling the *Bass Trap* as a whole, to be more effective over a wider frequency range.

The same features as *Figure 7.7* are seen in *Figure 7.11*. Again, the primary reason for the absorbent gap giving an improved absorption, is the fact that it weakens the ½ wavelength resonances of the channel, resulting in a reactance closer to zero. The resistance exhibit's the same general characteristic as the more acute panel angle.

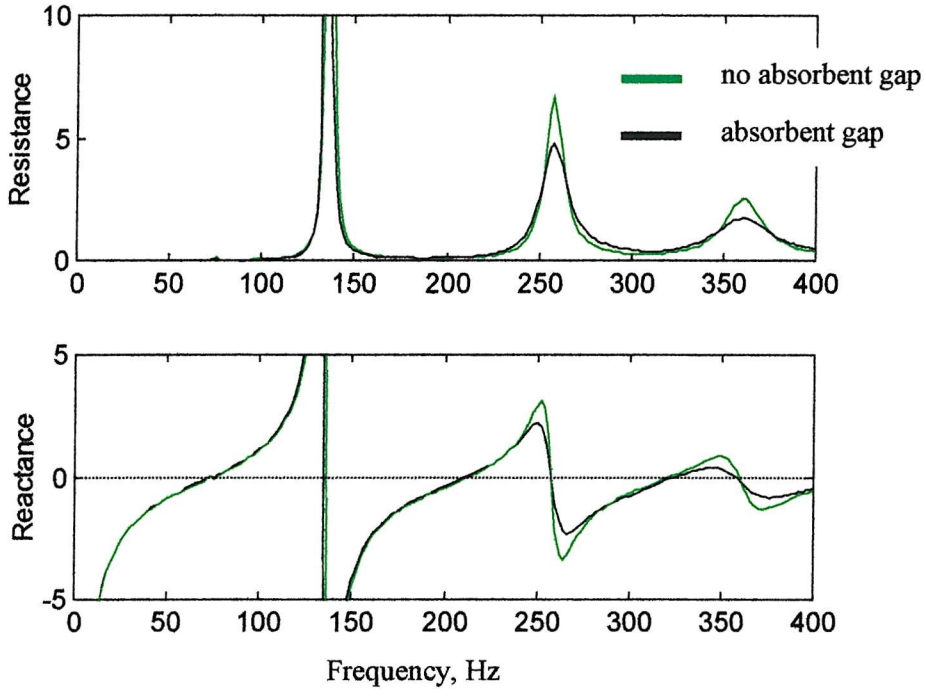

Figure 7.11 – Surface normal impedance (normalised to $\rho_0 c_0$) for back wall panels at 40^{o}

7.2.2.3 60^{o} Channel Rear Wall *Bass Trap*

The first result in this section is shown in *Figure 7.12*. The plane pressure wavefront again propagates parallel with the panels, though there is evidence of the onset of higher order modes. The concentration of pressure at the horn throat is still evident even at this obtuse angle, though this feature will disappear at 90^{o}, as will all semblance of the 'horn' effect.

In *Figure 7.13* the large x-direction velocity is very evident in the panel region of the absorbent, by virtue of all other parts exhibiting a near uniform value. This contrasts with the 20^{o} *Bass Trap* where there was variation in velocity within the absorbent away from the panel.

In the absorption coefficient plot of *Figure 7.14*, no ¼ wavelength resonance has a significant effect. The only evidence of their existence at all is small deviations in an otherwise smooth absorption-frequency trace. The peak at 340 Hz is caused by the first mode operating between the parallel panels. As the *Bass Trap* makes a more obtuse angle with the wall, so the distance between the panels increases, in this case they are 0.52 m apart.

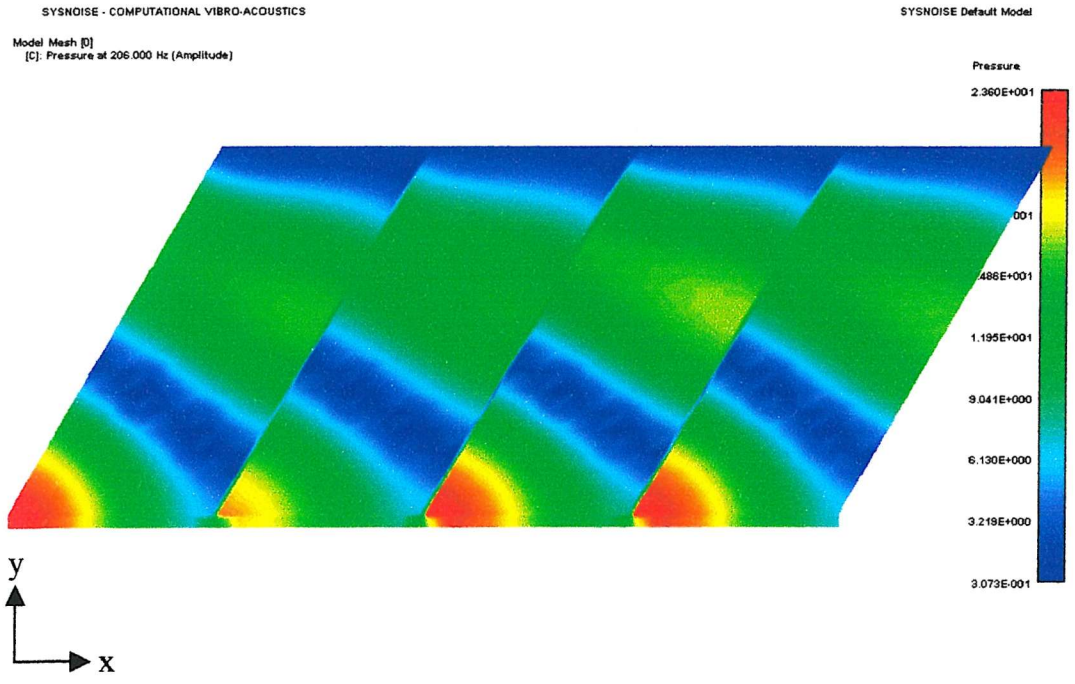

Figure 7.12 – FE calculated pressure magnitude colour map at 206 Hz for 60^{o} back wall

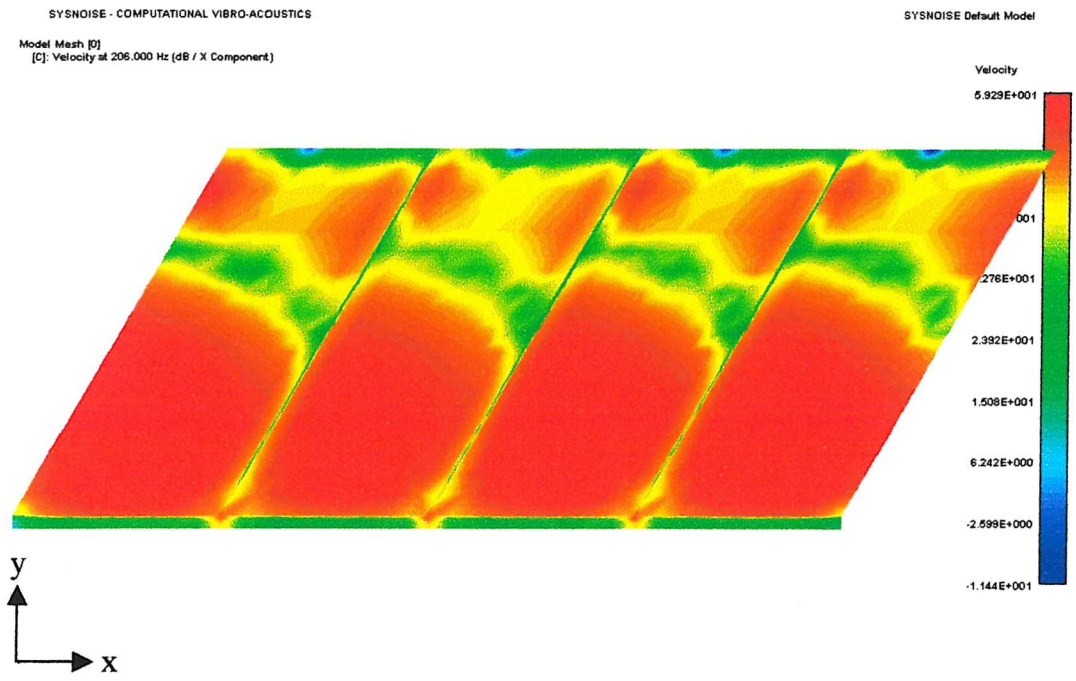

Figure 7.13 – FE calculated x-vector velocity colour map at 206 Hz for 60° back wall

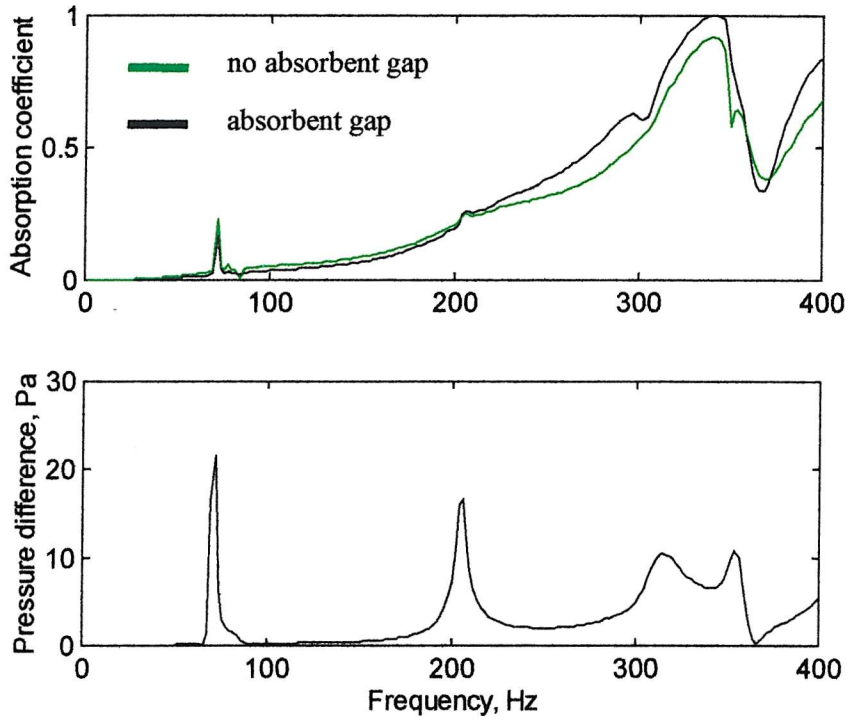

Figure 7.14 – FE calculated absorption and normalised pressure difference for back wall panels at 60°

The first cut-on mode for this distance occurs at 327 Hz and the subsequent pressure gradient across the channel width, near the absorbent layer, is responsible for the high absorption coefficient.

The large pressure difference at 206 Hz makes little impact on the absorption, suggesting that at this angle, the 'horn' effect remains a secondary effect, though this time, it is the oblique incidence absorption of the absorbent wall itself that dominates. As *Figure 7.15* shows, the peaks in absorption are more a result of a near zero reactance, than a resistance close to the characteristic impedance of air.

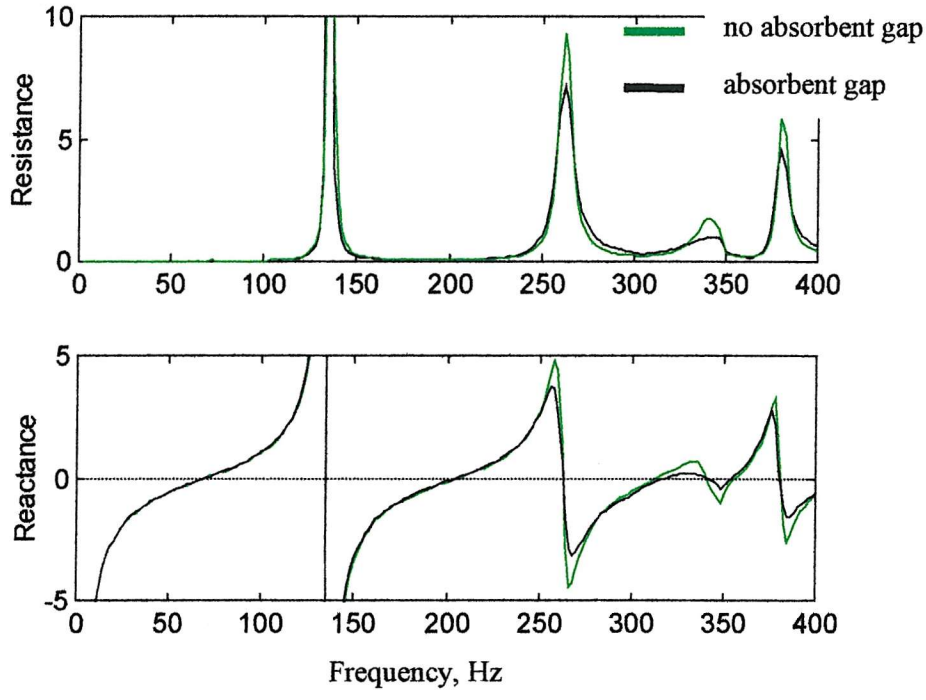

Figure 7.15 – Surface normal impedance (normalised to $\rho_0 c_0$) for back wall panels at 60°

The Finite Element Analysis will be more fully discussed at the end of the chapter, together with the results of the experimental investigation which is the subject of the following section.

7.3 Experimental Investigation

As with previous chapters, a second method of investigation was sought in order to allow comparison with the FEA results. The experimental procedure is identical to the one described in *Section 5.4.1*, so only brief mention will

be made here. Like the experiments of *Chapters 4 – 6*, the one presented in this section is a $^{1}/_{10}$ scale model, thus the results use a dual frequency axis.

7.3.1 Description of Experimental Set-up

In *Chapter 5*, the absorption coefficient of the open end of a rear wall *Bass Trap* was experimentally investigated by adapting the concrete duct used in the transmission investigations of *Chapters 4 & 6*. The purpose of the experiment described in this section was to measure the surface normal acoustic impedance at the open end of the channel, with and without the addition of a thin aluminium plate placed half way between the parallel walls of the channel. It was hoped that, with the plate, the measured results would show evidence of the 'horn' effect as an increase in the absorption coefficient. This is because, without the addition of the plate, there is no 'horn' effect with only one channel – at least two are required for velocity motion

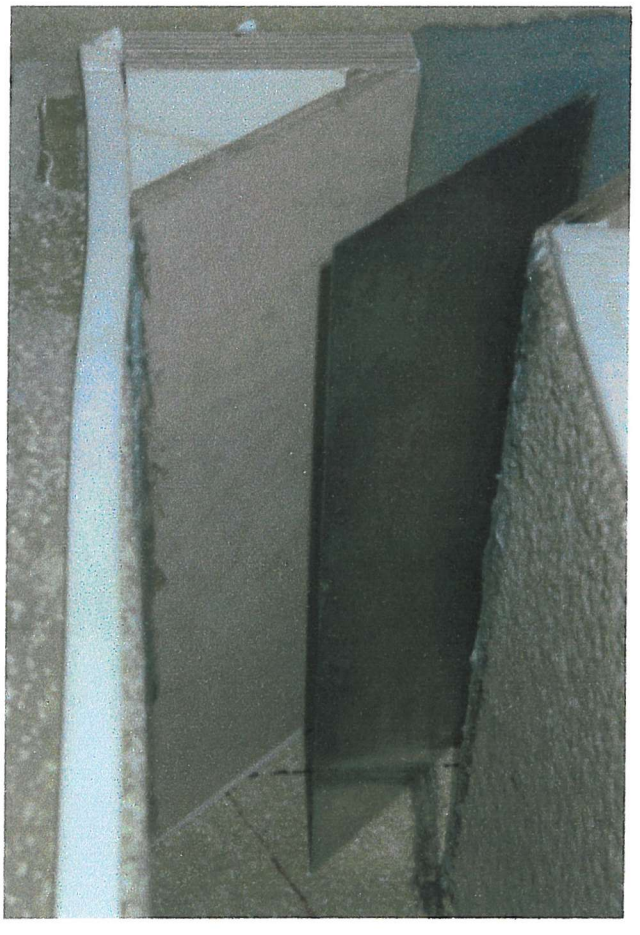

Figure 7.16 – Photograph of duct termination used to experimentally test the 'horn' hypothesis

through the absorbent. A photograph of the rear wall *Bass Trap* channel with the plate, is shown in *Figure 7.16*. Due to the problems associated with the experiment (as described in *Chapter 5*) many of the measured results were not considered reliable. For this reason only the 20^0 channel measurement is presented, as this proved to be closest to the results predicted by the FEA of *Chapter 5*.

7.3.2 Comparison of Measured Absorption Coefficient

In the light of the previous investigations it is possible to anticipate the likely outcome of the experiment. Without the plate, the absorption is expected to be dominated by the channel resonance, which for this angle, will occur at around 500 Hz (according to the FE model of *Chapter 5*). With the addition of the plate, there is likely to be a reduction in the absorption coefficient at the high frequencies, as the panels are closer together and thus present a more reflective surface to the short wavelengths. The results of *Section 7.2.2* however, suggest that if the 'horn' effect is significant, the additional plate is likely to yield an increase in absorption close to the ¼ wavelength resonance of the channel.

The solid lines in *Figure 7.17* show the comparison of absorption coefficient at the open end of the channel, with and without the aluminium plate. The red circles describe the FEA calculated channel absorption coefficient for a 20^0 channel, 12 cm apart, used as part of the investigation in *Chapter 6* (see the green trace of *Figure 6.13*). In the experiment, the channel is only 10 cm wide, so although strictly speaking, the two cannot be directly compared, it gives an idea as to the quality of the measured result.

The comparison between the FE result and the measured absorption coefficient without the plate, shows that, were it not for the inadequacies of the duct at low frequencies (outlined in *Section 5.4.3*), the agreement would be reasonably good. This comparison suggests that the experimental results are more reliable than those presented in *Chapter 5*. As expected, there is a peak in absorption at about 500 Hz, above which it drops to 0.5 at 800 Hz. When the plate is positioned half way between the channel sides and flush against the foam, a difference is noted above 300 Hz. As anticipated, the high frequency absorption is lower with the addition of the plate. Between 300 and 500 Hz, however, there is strong evidence of the 'horn' effect. Whilst the increase in absorption afforded by the plate is at most 0.1, it does point to a

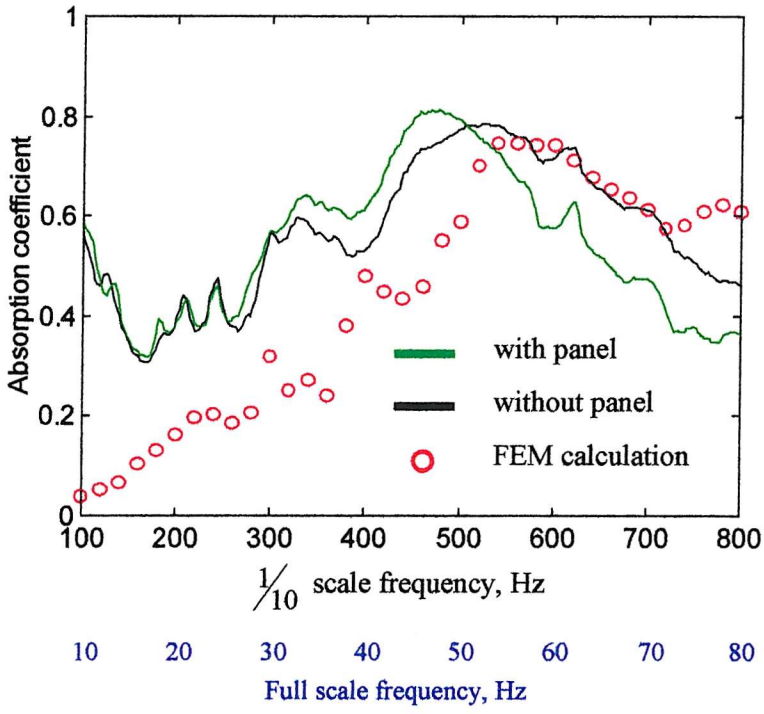

Figure 7.17 – Comparisons of absorption coefficient for the 20° rear wall channel

pressure difference at the junction of the plate and foam and subsequent porous absorption. As was noted in the FEA results, in this region the absorption is dominated by the ¼ wavelength resonance, thus any improvement due to the 'horn' effect suggests that there is significant lateral velocity through the foam.

7.4 Conclusions

In this chapter, the primary investigation has been concerned with the hypothesis that makes a connection between the radiation efficiency of conical horns and porous absorption in the rear wall *Bass Trap*.

Through the use of absorbent elements as part of a FE model, every stage in the 'horn' effect hypothesis was ratified, from the large pressure difference, to the associated particle velocity giving rise to additional absorption. The absorption afforded is (for the absorbent used) only supplemental to the primary mechanism which at the more acute angles, is a ¼ wavelength resonance noted first in the investigation of *Chapter 5*. Such an absorption characteristic is unsuitable for the control of reverberation in control rooms as it is highly frequency dependent and it

was shown that the 'horn' effect increases the absorption away from resonance. Additional aspects of the *Bass Trap* design, neglected in the FE model, will also serve to make it a highly effective means of absorption. The 4 cm thick felt covering both sides of all the angled panels will lower the Q of the resonances, particularly noted in the 20^0 *Bass Trap*, by adding significant acoustic resistance to the system. In the impedance plots presented, it was seen that the resonances were weakened by the presence of an absorbent gap. This effect will be even more accentuated in the real life design, as in practise the panels cannot be placed hard against the multi-layer wall and thus a small air gap between the two is present. The degree to which this also weakens the 'horn' effect will require further investigation, though it seems likely that the magnitude of pressure difference, particle velocity and thus absorption will all be less.

Although the 'horn' effect was investigated here in the context of the *Bass Trap*, it would undoubtedly warrant consideration in its own right. The research in this chapter has shown it to be a useful acoustic phenomenon and one that could be possibly extended into a stand-alone absorber. If a modular unit incorporating at least two horn-like geometries (though not necessarily conical) and a suitable porous material (50 kg m^{-3} mineral wool), were placed in a position of high pressure (the corner of a room would be ideal), then it might be possible to reduce low frequency reverberation without having to use the full *Bass Trap* design.

CHAPTER 8

Concluding Discussion and Future Work

Introduction

The purpose the research was to investigate how an empirically designed absorber used primarily in recording studio control rooms works. As the absorber itself has many different elements, the research investigated its overall performance by considering possible mechanisms of absorption in isolation. These individual, though not necessarily independent, investigations have sought to build up a body of scientifically based evidence to, firstly, give more than merely anecdotal documentation of the *Bass Trap's* effectiveness in absorbing sound in rooms, right down to the lowest frequency threshold of human hearing. Given this proof, the research has gone on to show that such performance can be attributed to a number of acoustic phenomenon. Some of these mechanisms of absorption are well established, though others are far more subtle, even novel. In this final chapter, the main conclusions of the work are discussed in such a way that the research is at all times related to the real world situation of designing a recording studio control room with the *Bass Trap* as its primary means of controlling reverberation time.

The concluding discussion will be presented in three main parts. Firstly, the research pertaining to the multi-layer absorbent wall will be discussed, followed by the investigations into the application of the *Bass Trap* on a rear wall. Finally, the effect the *Bass Trap* has on the sound as it propagates from the loudspeakers at the front of the room will be considered. In each section, mention will be made of the influence the research has on the future design, application and measurement of the *Bass Trap*, as well as the future academic research that remains to be done.

8.1 The *Bass Trap* Multi-Layer Wall

As with every other aspect of the *Bass Trap's* design, the multi-layer absorbent wall that separates the freely suspended covered panels from the rigid structural wall, has been empirically designed over a period spanning almost four decades. The construction as described in *Chapter 3* has its roots in a *BBC* design,

which itself was the result of considerable research on the part of the *BBC's* research and development department [8.1].

8.1.1 Present Multi-Layer Wall Absorption Coefficient

One of the main objectives of the research was to find out whether or not the effectiveness of any individual element of the *Bass Trap* was reduced by the presence of another. For example, did the hanging panels degrade the absorption of the wall? Such a question extends also to the design of the multi-layer wall and is answered in part in *Chapter 3*.

Considering the construction (*Figure 3.3*) and the resultant theoretical absorption coefficient (black trace in *Figure 3.4*), three points can be made with regard to this question.

The first is that above 200 Hz the 40 mm thick outer-most layer of cotton waste felt is the primary mechanism of absorption. The increase with increasing frequency is directly comparable to the absorption coefficient for half the thickness of felt shown in *Figure 3.2*. Previous research has shown that the chipboard panel to which the felt is attached is acoustically rigid [8.2], so one would not expect the large amounts of absorbent material further in the wall to contribute to the overall performance of the wall at frequencies where the felt alone is very effective.

At the extreme low frequencies another peak in absorption is evident, though this can not be attributed to porous absorption given that the wavelength of sound in this region is between 4 and 15 m. The performance at these low frequencies is a measure of the success of the wall as, given a thickness of only 35 cm, a normal absorption coefficient of 0.3 at 25 Hz is remarkable. As mentioned in *Chapter 3*, it is the combination of air gaps, panel masses and considerable damping from the porous materials in the wall that results in this double mass-spring-damper resonance.

Unfortunately, the final feature of *Figure 3.4* is a band of frequencies which are not very effectively absorbed. Between 80 and 200 Hz the normal absorption coefficient of the side walls is less than 0.2. In this region, the wall described has no mechanism with which to dissipate sound energy, as it falls between the high frequency porous absorption and the low frequency performance afforded by two resonances within the wall.

The results summarised above must however be discussed in the light of how the multi-layer wall is used as part of the *Bass Trap* - it is important to maintain the context.

The green trace of *Figure 3.4* showed how the inadequacies of the side wall highlighted above are compensated for by the ceiling multi-layer wall. The simpler design of the ceiling was shown to result in an absorption peak in the frequency range where the side wall is least effective. As a consequence, the two multi-layer constructions give rise to a short reverberation time that does not vary considerably with frequency. In the following section, improvements are suggested for the side wall in isolation.

8.1.2 Suggestions for Improving the Multi-Layer Wall

In smaller studios, space constraints dictate that the full *Bass Trap* design can only be applied to the rear wall. Depending on the height available, hanging panels may not even be placed on the ceiling. In such cases the performance of the multi-layer wall alone becomes that much more important to the reverberation time of the room. Ignoring, for the time being, the effect the rear panels might have, it would be wise in such a small room to modify the design of the absorbent wall. Most importantly it would be necessary to increase the absorption coefficient between 80 and 200 Hz in order to avoid a spectrally coloured reverberation time. The easiest way in which to reach this objective would be to move the higher of the two low frequency resonances to 100 – 150 Hz. The resonant frequency f_0 of a single degree of freedom system is primarily controlled by the mass and spring element, m and k respectively (damping does effect the resonance slightly) according to: $f_0 = \frac{1}{2\pi}\sqrt{\frac{k}{m}}$.

A doubling in the resonant frequency from 55 to 110 Hz would require the ratio of stiffness to mass to increase by a factor of four, i.e. doubling the stiffness and halving the mass. Practically, an air space should be reduced (increasing stiffness) and a thinner panel used (reducing mass). In order to ensure a smooth transition between the two resonances and the onset of porous absorption it would necessary to increase the damping by including thicker absorbent layers within the wall.

The situation is changed, however, when the hanging panels are placed in front of the multi-layer wall. As shown in *Chapter 7* the closed end tube formed by adjacent

panels and the wall exhibits its own resonances that occur near to odd integer multiples of ¼ wavelength equalling the depth of the panel. For the 1.22 m deep panels placed between 30^0 and 45^0, as in the real design, the first of these ¼ wavelength resonances is at about 90 Hz (see *Figure 5.11*). As before, this feature could be harnessed to increase the absorption coefficient of the multi-layer wall in the region where it is lacking. The way in which this is achieved will be discussed in greater depth in the following section and at this point it is sufficient to state that decreasing the depth of panel and increasing the separation between panels are the primary means of increasing the resonant frequency. These changes have the additional benefit of using less material and occupying less of the room.

Further discussion about how the design of the multi-layer wall might differ depending on the exact form the *Bass Trap* takes within a room, will be given in the context of the investigations into the side wall and rear wall panels. As has been briefly mentioned, these additional elements do impact the specific design of the wall.

8.2 The *Bass Trap* Rear Wall

Having considered the multi-layer wall in isolation, the discussion now turns to the performance of the *Bass Trap* rear wall. As mentioned in *Chapter 5* the positioning of the loudspeakers within a typical control room means the wavefront of the propagating sound is close to normally incident on the rear wall. For this reason, the quantity used to describe the effectiveness of the *Bass Trap* on the rear wall is that of normal absorption coefficient.

8.2.1 Investigative Procedure

The obvious starting point in researching this aspect of the *Bass Trap* was to consider only two adjacent panels, open at one end and terminated by a soft boundary at the other – herein referred to as a *channel.* From here any model used could build in complexity. *Chapter 5* dealt with the first part of the investigation, ascertaining that the channel exhibits behaviour typical of a closed end pipe containing acoustically resistive elements. The investigation was then extended in *Chapter 7* to include more than one channel and also to make allowance for particle velocity through the soft termination against which the panels are placed.

8.2.2 Present *Bass Trap* Rear Wall Absorption Coefficient

The key findings of *Chapter 5* centred on the acoustical similarity between the *Bass Trap* channels and closed end pipes. The angled channels were found to exhibit clear ¼ wavelength resonances, that is, frequencies at which the acoustic reactance at the opening of the channel equals zero. At these frequencies, the acoustic performance is dominated by the amount of acoustic resistance present and as a result the absorption coefficient reaches a maximum. A more subtle result of this finding is the associated 'depth' of the channel, i.e. the equivalent length of pipe (not angled channel) for which the zero reactance occurs at the same frequency. The results showed that when the panels are placed at 20^0 to the soft termination the effective depth of the channel is 42% more than if the panels are normal (90^0) to the termination. In addition, at such an acute angle the panels only protrude 42 cm into the room, which together with the lower resonant frequency results in a 76% saving in panel space for the same low frequency peak in absorption coefficient. The other key finding of *Chapter 5* is the effect the panels have on the termination (or wall) against which they are placed. At angles near to 90^0 the normal absorption coefficient is dominated by the characteristic of the wall (see *Figure 5.3*), where as at acute angles the aforementioned channel resonance dominates (*Figure 5.7*). The comparison of four different angles in *Figure 5.11* shows how the presence of the panels in front of the multi-layer wall yields a normal absorption coefficient always greater than the wall itself.

It was hypothesised that a more subtle mechanism may be at work in the rear wall *Bass Trap* and this 'horn effect' was investigated in *Chapter 7.* The hypothesis was formed using the principle of reciprocity together with a knowledge of the radiation efficiency of conical horns and was investigated using Finite Element Analysis. The colour map results from the numerical modelling showed that in the region where the panels meet the wall the particle velocity parallel with the wall is significantly higher (see *Figures 7.4 & 7.5* for example) . More detailed consideration of the numerical results show that while the horn effect does serve to increase the absorption coefficient of the rear wall, it is secondary to the peaks in absorption caused by the ¼ wavelength resonances that were first identified in *Chapter 5* (see *Figure 7.10*). The results summarised in this section provide a wealth of information that can be used in

increasing the absorption coefficient of the *Bass Trap* rear wall. And it is this that is the subject of the next section.

8.2.3 Suggestions for Improving the *Bass Trap* Rear Wall

As before, suggestions for the improvement of this aspect of the *Bass Trap* will be made firstly without consideration given to the effect of either the multi-layer wall or the *Bass Trap* side wall.

From the discussion of the previous section it is clear that the main absorptive mechanism at work in the *Bass Trap* rear wall is the ¼ wavelength resonance caused by the geometrical relationship between the panels and wall. Even a result as straight forward as this can have a significant influence on the future design of the *Bass Trap*. The research of *Chapters 5 & 7* have shown that the resonances are affected by the depth, angle and separation of the panels.

Considering the Finite Element model of *Chapter 5*, the angular dependency is evident from *Figures 5.4, 5.6 & 5.8* where the frequency of zero reactance (i.e. ¼ wavelength resonance) drops as the angle becomes more acute. The exact frequencies are given in the table of *Section 6.4*. When particle velocity flow through the soft wall next to the panels is included in the analysis, as in *Chapter 7*, the lowest resonance remains almost constant as the angle of panel is changed (*Figures 7.7, 7.11 & 7.15*). It would appear from this observation that this finite pressure gradient between one channel and the next, present in the real life design, weakens the resonance predicted when only a surface normal impedance is used to characterise the wall. This will undoubtedly be further emphasised in the full scale *Bass Trap* as the panels are normally positioned about 2 cm from the multi-layer wall.

The effect of differing the spacing between channels gives rise to an even more subtle change in the acoustic reactance at the mouth of the channel than when altering the panel angle. It is fair to assume therefore, that as long as adjacent panels overlap (thus forming a channel) the distance they are apart will have little influence on the ¼ wavelength resonance.

The easiest means of controlling the ¼ wavelength resonance (and thus the absorption) is by changing the depth of the panels. The further they protrude from the wall, the lower the frequency at which effective absorption is evident.

Positioning the panels at a more acute angle to the wall should therefore provide the best solution to the orientation of the panels, as they protrude less far into the room

and fewer will be needed for a given depth of panel, in order to satisfy the requirement for *Bass Trap* channels to be formed.

In the light of the 'horn effect' it is likely that the closer the panels are positioned to the wall, the better. It is paramount for any pressure gradient to have its only means of equalisation through a porous medium, otherwise no absorption will occur. Given the limited results presented in *Chapter 7* one could make a good case for using different porous material to cotton waste felt, on the wall, in the vicinity of where the panel meets. The porous absorbent in the middle of the channel termination could be chosen to maximise the absorption coefficient at resonance, while a different absorbent might be better suited to the far higher particle velocities present at the junction of the panel and wall. Such a change to the design of the multi-layer wall is suggested only because of the interaction between it and the panels placed in front.

The 'horn effect' also has an influence on the aforementioned positioning of panels. The flare rate (which is analogous to the angle of panel) has been identified in previous research on horns as having a large effect on the radiation efficiency. Given the reciprocal argument used in the horn hypothesis, this means the panel angle could be critical in maximising this subtle mechanism. More research into this is needed before more definite recommendations on the design of the *Bass Trap* are made.

8.3 The *Bass Trap* Side Wall and Ceiling

In this penultimate section, the investigations into applying the *Bass Trap* on the side wall and ceiling of a room is discussed. As mentioned in *Chapters 4 & 6*, the ceiling and walls are grouped together on account of the sound propagating past at grazing incidence, unlike the rear wall where the wavefront is close to normal.

8.3.1 Present *Bass Trap* Side Wall Transmission Loss

The first stage in investigating the effect of placing an angled periodic array of panels on the side wall of a room was to consider it purely as a reactive filter. The research described in *Chapter 4* showed that while a filtering effect is evident, it is not significant in the frequency range to which the experiment was limited. The experimental work served only to identify the depth and spacing of the panels as the variables which influence the transmission loss from one side of the reactive side wall *Bass Trap* to the other. The theoretical results confirmed this and were able to

provide plane wave transmission losses to a far higher frequency (200 Hz full scale frequency). The angle of the panel, as a variable, could not be separated from the distance the panels protrude into the duct/room in the theory and nothing in the experimental results suggested that the panel angle was important in its own right.

By contrast, the addition of a layer of foam between the panels and duct wall (an approximation to the multi-layer wall) yielded drastically different results – this was the investigation described in *Chapter 6.* The experimental results proved that a complicated relationship exists between the separation and angle of the panels and the resultant transmission of sound down the length of the duct. A measure of the TL for the foam lined duct alone proved that the results obtained from the panels and foam was not simply an addition of the filtering effect of *Chapter 4* and attenuation caused by sound grazing past a porous material.

A short investigation into the possibility of cut-on modes being responsible for the transmission showed this not to be the case.

The use of the FE calculated channel mouth impedance of *Chapter 5* provided the breakthrough, by allowing a mathematical analysis of the propagation of the primary mode along the duct. The subsequent research described in *Section 6.5 & 6.6* shows how the existence of a surface wave near the ¼ wavelength resonance of the *Bass Trap* channels causes huge TL over a narrow band of frequencies. Given the assumptions made in the theory and the inevitable inaccuracies of the experiments, the agreement in terms of shape and frequency are very good. The main reason for the differences between the experimental and theoretical results was their respective dimensionalities.

The extensive FE investigation in *Section 6.7* not only validates the theory, but gives even more insight into the way the *Bass Trap* side wall works. The similarity between the full FE model and the model in which one wall is lined with the channel mouth impedance (ref. *Chapter 4*) is evidence that the primary effect of the side wall panels is caused by the surface wave. In order to make this finding relevant to the real life design, the variables which control its operation must be identified. From the analysis of *Section 6.6* it was seen that the surface wave is at its most effective when the acoustic reactance of a side wall is slightly less than zero (see *Figures 6.14, 6.15 & 6.18*). This acoustic reactance, in the theory and FE analysis, is the imaginary part of the channel mouth impedance investigated in *Chapters 5 & 7.* Given the

discussion of *Section 8.2.3* the variables of interest are already known, as they are the same responsible for the peak in absorption coefficient of the rear wall *Bass Trap*.

In short then, in the same way as the intricacies of the *Bass Trap* cannot be visibly seen because of a protective cloth covering, so it is in the acoustic sense. As the sound propagates down the room (or duct of *Chapter 6*), it considers the panels and multi-layer wall as a lumped element, with the key acoustic quantity responsible for the vast majority of the TL, being the surface normal acoustic impedance where the cloth covering hangs.

8.3.2 Suggestions for Improving the *Bass Trap* Side Wall

Whilst the dramatic attenuation of sound as it propagates along the duct is proof of the effectiveness of the *Bass Trap*, such a characteristic is not entirely desirable in the context of a recording studio control room. The ideal side wall attenuation would be far less frequency dependent, i.e. constant over a large frequency range. Given the relationship established between *Bass Trap* geometry and maximum TL, it should be possible for the desired attenuation to be obtained through changing the separation, angle and depth of the panels. Each of these variables has been shown to influence the surface impedance at the open end of the *Bass Trap* channel and thus the frequency at which the TL is noted.

A broad band attenuation would result from varying any of the aforementioned design parameters along the length of the side wall – indeed this is the case with the ceiling *Bass Trap* where it is the angle that changes.

In addition, the placement of the panels next to the absorbent wall will have an effect, as this influences the resonant behaviour of the *Bass Trap* channel (see *Chapter 7*).

The absorbent wall itself will also have an effect on the TL, particularly the type and quantity of the outer most porous layer. A thick layer of low resistivity absorbent will yield a less frequency dependent surface impedance at the open end of the channel.

In the low frequency range considered in this research it appears that adjacent panels need only overlap slightly to yield the surface impedance required to support a surface wave. Based on this observation, one should note comparable attenuation at low frequencies with far fewer panels than are presently employed. However, the impact this might have on the higher frequencies is unknown.

8.4 Future Work

As with most research, many questions about the *Bass Trap* still remain and a number of additional lines of investigation have become apparent. The two most obvious areas of future work are :

a) a more accurate model of the attenuation of sound along a duct with a resistive liner and periodic splitters

b) a dedicated investigation into a *horn effect* bass absorber

The following sections will consider the above in more detail.

8.4.1 Modal Decomposition Analysis of Sound Propagating Along a Duct with a Resistive Liner and Periodic Splitters

The results of *Chapter 6* showed that whilst the theory approximated to the measured values of transmission, it did not fully model the behaviour of the sound in the duct. In order to improve the accuracy of the theoretical model it would need to include all three dimensions and consider both diffraction from the panels and the activity of higher order modes. One way in which this could be achieved is to decompose the sound field into an infinite sum (though for computational reasons the series would need to be truncated) of modes within the duct. Conditions of pressure and velocity continuity and the orthogonality of modes would yield $m \times n$ equations for $m \times n$ modes (where m and n are the number of modes in the two transverse dimensions) at the points where the panels protrude into the duct. Solving these equations for the complex amplitude coefficients would allow transmission to be found analytically. Such a technique has been successfully used in optimising the absorbent linings in jet engines.

A similar mode-matching method could be employed to find the surface impedance of the open end of the *Bass Trap* channels, by discretising the angled panels into a number of steps.

8.4.2 Further Investigations into *Horn Effect* Absorption

The investigation in *Chapter 7* showed that the *horn effect* does indeed influence the absorption of the rear wall *Bass Trap*, though it is a secondary mechanism. Given that such an effect has been identified, it could be taken as the starting point for research into designs which maximise the effectiveness of,

effectively, using a horn in reverse. In particular, the influence of flare rate, horn shape (exponential, hyperbolic etc.) and choice of absorbent materials could be considered. In the same way that horns are used primarily for increasing the radiation efficiency at low frequencies, it is interesting to hypothesise that the *horn effect* might enable efficient absorption at low frequencies. In addition, the mechanism involved would lend itself to a modular design – a stand-alone absorber that could be retrospectively placed in the corner of a room in which low frequency reverberation is a problem.

APPENDIX 1

Methods for the Passive Dissipation of Sound Energy in Rooms with Particular Application to Low Frequencies

Introduction

In this first appendix, some of the pertinent literature relating to research on passive sound absorption is reviewed. The different methods cited will provide a wider context to the investigations described in the preceding chapters. As with the rest of this work, much of the literature reviewed relates to the design criteria of recording studio control rooms, though application is not restricted to this niche of architectural acoustics.

Before the mechanisms of absorption are discussed, the requirement for absorption in rooms is justified from a subjective viewpoint.

A1.1 Background and Psycho-acoustic Considerations

In the past control rooms have been hardly considered from an acoustical point of view and have either suffered a hand-me-down specification from performance spaces like concert halls, or expected to approximate to an average living room of a house. In Gilford's [A.1] discussion on the matter, he identifies the two ideal characteristics of a recording studio control room. Firstly it should enable critical judgements of reproduced programme material to be made and secondly, be an environment which is acoustically similar to an average room. Whilst he himself admits that these aforementioned specifications *". . . could well be mutually conflicting."*, he maintains that both should remain. The specification of representative reverberation is further justified on account of the loudspeakers, as a room which approaches an anechoic environment will place greater emphasis on their directional characteristics (though Toole [A.2] points out that the same can be said of reverberant rooms).

Only recently has attention been given to the interaction between loudspeaker and room [A.3], the findings of which suggest that the biggest subjective difference

between monitoring environments is the acoustic characteristic of the room and the positioning of the loudspeakers. The performance of the loudspeakers themselves are shown to be far less important. Despite this, there are some qualities of a loudspeaker that do influence subjective evaluation. As the wavelength of sound approaches the diameter of the loudspeaker diaphragm, sound is not propagated spherically (this 'beaming' is particularly noticeable at high frequencies). The result of this is for the on-axis response to sound too 'treble-y', whilst the off-axis appears dull. If however, the loudspeakers exhibit a flat frequency response on and off-axis, the acoustic properties of the room can be considered as a separate issue, otherwise its characteristic is inevitably dictated to by the inadequacies of the loudspeaker.

Often, opinion on the design of a control room is based on a particular type of music and the specification of the studio to which it is attached, if this continues no truly independent specification will ever be reached [A.4]. Indeed there is much evidence to suggest that certain music is preferred in certain rooms [A.1 & A.5], which in turn leads to the conclusion that no one control room can be used for all types of music. However, this deduction is based on listeners' *preferences*, an irrelevant qualification, as it is not the purpose of the control room to compliment the programme material. As part of their on-going research into such matters the BBC Research Department investigated the preferences of a panel of recording engineers to programme material recorded in six studios and replayed in four control rooms [A.6]. In general, the reciprocal response from the studio was favoured for the control room; for example, a 'dead' control room was preferred for programme with long low frequency reverberation. If the reverberant sound field of the control room was increased, it was found that a threshold existed above which preferences among the engineers became inconsistent – the value of this threshold was 0.4 seconds. Based on these results all BBC listening rooms were (at the time of [A.6]) designed so that the reverberation did not exceed 0.4 s up to 1 kHz, decreasing to 0.3 s at 8 kHz. However, this paper does not consider the affect of reflections on critical listening.

The effects of reflections on the perception of the direct sound is well documented in psycho-acoustic literature, both in terms of the spatial and frequency domains. Blauert [A.7] deals extensively with the effects that arise from different sound sources in an enclosed environment. Of particular interest here are the effects of low frequency components, a subject addressed by Morimoto *et al* [A.8] from a spatial viewpoint. Spaciousness here is described as the psychological effect where the

spatial characteristic changes, though in such a small way that no 'discrete' change is discernible. It is typically associated with very low level reflection. This paper concludes that the degree of horizontal spaciousness is not dependent on the interaural cross-correlation function only. Listening tests suggest that with all other variables held constant, the horizontal spaciousness increases when the reflections contain increasing amounts of low frequency energy. This has significant implications for early reflections in control rooms, which by virtue of typical acoustic treatment, have most energy at low frequencies.

Reflections can also cause changes to the direct sound in the frequency domain. Somerville *et al* [A.9] investigated reports that certain concert halls exhibited unwanted tonal features consistent with early reflections. With a constant and slightly attenuated delay of 10 ms the subjects commented on *". . . a marked deterioration in the quality of orchestral music. . . Speech became coloured with both low frequency and high frequency distortions . . . random noise from the loudspeakers became very coloured".* Kuttruff [A.10] considers the change in timbre due to early reflections in signal processing terms, by performing a Fourier transform on a direct sound plus a reflection delayed by a time t and attenuated by a factor x. If multiple periodic reflections are considered, then the Q of the resulting transfer function changes.

The importance of this is that the audibility of frequency domain resonances (either peaks or troughs) depends heavily on its Q. Much research has been done on this subject, with Bücklein [A.11] responsible for much of the initial work. His major finding was that resonant troughs were far less audible than peaks of the same magnitude centred on the same frequency. Olive *et al* [A.12] however found that for low Q resonances at low frequencies (< 200 Hz) this wasn't the case and that both were equally audible. Thus low Q phenomenon will be far more noticeable at low frequencies, due to the fact that troughs are not discriminated against. On this point Gilford [A.1], referring to earlier work on room modes by Mayo [A.13] in which it is established that axial modes are the most subjectively noticeable, states that two conditions must be satisfied for an axial mode to cause colouration. Firstly it has to be driven efficiently by the loudspeaker output and secondly must be separated by at least 20 Hz from the next nearest mode. Bücklein's work is confirmed by Toole and Olive [A.2] where they summarise that the detectability of a broad resonance decreases by approximately 3 dB per doubling of Q. A listening environment dependency is also highlighted as timbre changes in transient sounds with medium

and low Q resonances are more noticeable when reverberation is present, while no advantage is evident for high Q resonances. However the authors state that the point at which the reverberation is added (on the recording, or due to the listening room) is not critical and that reverb is also responsible for poorer timbre changes in sustained programme (vowels etc.).

The significance of the test signal used is a common theme in much of this psycho-acoustic research, with most authors mentioning it as a variable. Indeed, it has been shown to have a major affect on perception thresholds [A.9]. With pink noise, a resonance was judged to cause a just discernible change in timbre at a level 12 dB quieter than orchestral music for the same delay, while speech, chamber music and piano repertoire were found to fall between these two extremes. Fryer [A.14] went on to find that popular music was even worse than orchestral music for the detection of timbre changes. *Figure 6* in [A.4] compares the thresholds of lateral reflections for a wide range of stimuli, from a number of studies. It should be noted however that real-life reflections are in general not simply pure delays of the direct sound and are normally spectrally altered.

Reflection detection is also dependent on angle of incidence and in [A.4] there is confirmation of previous research that reflections from near the principle source are masked by up to 10 dB more than those from either elevated or lateral angles. Interestingly, while these latter two variables exhibited similar magnitude of audibility, once above this threshold the effects were quite different. Lateral reflections created a feeling of spaciousness, with those in the median plane showing themselves as changes in timbre.

A1.2 Room Acoustics at Low Frequencies

Many assumptions made when considering general room acoustics do not apply at the lowest audible frequencies. Statistical niceties like the diffuse field fall far short of real life behaviour, to such an extent that the foundational quantity of reverberation time is no longer valid, as it applies only to a truly random sound field. Of course, the issue of a diffuse field arises as a direct result of the modal density increasing to such an extent that it cannot be considered in terms of discrete modes. In our frequency range of interest, the wavelengths are similar in magnitude to the dimensions of the room and through well established mathematical equations it can be

shown that at certain frequencies these lengths will coincide [A.15]. This occurrence results a standing wave resonance, or room mode. However, when all the room dimensions are less than half the acoustic wavelength, standing waves cannot be supported, this is often called the 'pressure zone'. In the pressure zone, as there is an absence of standing waves and the room acts as one – a lumped element. As such, the pressure everywhere in the room is uniform and fluctuates according to the driving source. The situation described is analogous to the behaviour of the ear canal when wearing circumaural headphones.

The significance of standing wave resonances is that they do not decay in the same way as other frequencies and thus they affect the temporal behaviour of the sound in the room. The main reasons for their different decay characteristics is the proportionally fewer boundaries that are encountered and their large wavelength – both of which result in low damping. A room mode is categorised according to how many boundaries it is cyclic between: axial – two, tangential – four and oblique – six. Given the earlier explanation on modal decay it can be seen that the axial mode will be the most energetic and in addition, will be among the modes with the lowest frequencies[1].

Room modes, therefore, present a problem if an environment is to be designed that does not accentuate any part of the audible spectrum and different authors suggest different solutions. The most basic step towards minimising audible colouration is where the dimensions of the room are dictated by a certain criteria, this is advocated by Bonello [A.16]. His criterion ensures the following:

- Modal density increases monotonically with increasing frequency
- Each $^1/_3$ octave band has at least the same number of modes as the last
- There are no double modes, though at worst they are only present in $^1/_3$ octaves with more than five modes

It should be stressed that these measures do not reduce the amplitude of the room resonances, rather they minimise any subjective objections that often arise when rooms are not designed with such things in mind.

---

[1] The exact rank order of the lowest room modes is a function of the room's dimensions, though the lowest will *always* be axial, see [A.15] for more details.

A more pro-active step is to encourage the modal frequencies to follow more oblique paths, by using diffusers. As the name suggests, these structures prevent specular reflection when sound is incident on them, thus creating a diffuse field at a lower frequency than would otherwise occur. Volkmann points out, in his discussion on poly-cylindrical diffusers [A.17], that this effect gives the subjective impression of a larger room. This observation makes sense, given that the average modal density is proportional to the volume of the room [A.16]. Whilst the use of diffusers do reduce modal energy, it is achieved by indirect means, as oblique modes are more effectively damped by the boundaries. A more detailed discussion is given by Angus [A.18]. Gilford [A.19] argues, however, that the use of diffusers to combat modes in small rooms is impracticable, as effective diffusion requires a diffuser depth of no less than a seventh of the wavelength of sound. In this context Gilford is referring to the poly-cylindrical type, whereas the previous reference considers diffusers that are more angular and based on number theory. It will be seen later that irregular distribution of absorptive material has much the same effect at low frequencies, due to diffraction.

A1.3 Novel Means of Low Frequency Absorption

The previous two sections have outlined both the need for and the difficulty in, dissipating low frequency sound energy in rooms of modest size. Given the apparent conflict between long wavelengths and small structures by which to absorb them, methods have been developed which move away from traditional means of absorption.

As a continuation of the previous discussion, we will start by considering diffusers. As mentioned, these structures are designed to reflect incident sound energy in a non-specular manner, though recent research has noted that other properties exist. Fujiwara & Miyajima [A.20], in their investigation into the *absorption* characteristics of diffusers, found that a two dimensional pseudostochastic diffuser yielded significant absorption extended to a frequency one octave below the design frequency. A couple of years later Kuttruff [A.21] published a paper that explained this surprising result. His explanation hinges on phase differences that are associated with the different channel depths and the diffuser is assumed to be small in comparison to wavelength. Though some authors claim such phase changes would give rise to a secondary pressure field in the plane of the diffuser surface, Kuttruff argues that they

result in high equalising flow of particle velocity (restricted to the near-field) such that the pressure in this plane is almost constant. The mechanism of dissipation is therefore due to viscous losses caused by high particle velocity passing over the edges of the channels. Kuttruff goes on to show that the addition of a very low resistivity porous layer in this plane serves to greatly increase the losses, yielding absorption coefficients close to 0.9 at an octave below the design frequency (see *Figure 6b* in [A.21]).

The use of phase cancellation to control undesirable low frequencies is not particularly novel and is the primary means through which active noise control is implemented. The basic idea has provided the foundation for a new design of acoustic barriers for use primarily in transport environments. Amram *et al* describe the theory behind such a barrier and field measurements to support claims of its performance [A.22]. The incident sound is effectively split into two parts; the first which diffracts around the barrier and the second which enters the low-pass filter waveguide. This latter component attenuates frequencies above the pass band and (by refraction) *slows* the low frequencies such that when it combines with the diffracted part (also low-pass filtered) the two are in anti-phase at the design frequency, resulting in cancellation. The results presented in this paper show an improvement of up to 5 dB at the design frequency over solid barriers (10 dB corresponds to a subjective halving of loudness).

A1.4 Membrane Absorption

In this section the dissipation of sound energy by membranes is considered, generally the most widely used means of reducing excessive low frequency reverberation in rooms. The mechanism is often confused with panel absorption (considered in the following section), though the two are in fact quite different.

During the Second World War, no large orchestral studios were built and as many had suffered damaged, there was a need for much modernising and rebuilding. In response to this, the BBC research department began to investigate, in the late 1940's, ways in which to improve the acoustics of these venues [A.23]. Low frequency absorption was one of the major areas of research and it was Gilford [A.24] who continued the earlier work of Goyder into membrane absorbers. Gilford favoured this

approach to the use of stiff panels, as inconsistency of material properties, large dependence on edge condition and re-radiation at resonance were seen as considerable disadvantages. The membrane absorber is modular in construction and generally smaller than the panel equivalent; its mechanism of absorption also differs. The absorber approximates to a single degree of freedom (SDoF) model of a mass-spring-damper, but unlike a panel the stiffness is primarily provided by the restoring force of the enclosed air, though the membrane stiffness becomes more important as the depth of the unit increases. A membrane made of bitumen roofing felt (high damping in the SDoF model) was generally used in the BBC design, as it exhibits a large loss factor. In addition to this basic design, rockwool was often added in the air space behind the membrane and a perforated hardboard covering in front [A.25]. The addition of the rockwool increases high frequency absorption and also serves to lower the stiffness of the air, by causing it to behave isothermally – thus resulting in a lower resonant frequency. The perforation ratio of the hardboard covering is varied depending on the high frequency cut off: 0.5% for < 300 Hz, 5% for < 700-1000 Hz and 20% slots for < 4 kHz. On the subject of efficiency Gilford [A.24] points out via Thévenin's theorem that maximum absorption will occur when the radiation resistance R equals the internal resistance of the absorber R_A. The shape of the response will depend upon the absolute value, the equation for quality factor is given as $Q = \frac{2\pi fM}{R + R_A}$, where M is the mass per unit area of the membrane.

Where general reduction in reverberation time over a large range of frequencies is required, the absorber resistance may be increased, thus lowering both the peak absorption and value for Q. [A.24] gives this matter a little more attention, when stating that the absorber should not be too tuned lest **its** reverberation time exceed that of the room. This is an issue when one considers the main application of these absorbers was extreme modal correction and as such *"The bandwidth . . . should not greatly exceed one half-octave . . ."*. Failure, in other highly resonant designs, to ensure the bandwidth of the response is not too small is, in his opinion, the reason for audible colouration in many studios. However, as mentioned in *Section A1.1*, the ear's sensitivity to high Q resonances (especially at low frequencies) is much less than for low Q's. Unfortunately, due to the reverberation procedure used to confirm performance and the small size of room, little reliable data is presented in this paper

below 100 Hz. Takahashi *et al* [A.26] considered the performance of a membrane with its permeability as the major variable, though our discussion will concentrate on a later paper [A.27] in which more attention is given to the individual mechanisms involved. A model of a porous membrane a distance from a rigid boundary is presented, with certain variables changed (surface density, admittance of membrane's back surface) while others are kept constant. As expected, the frequency at which peak absorption occurs decreases as the mass per unit area increases ($f_r \propto \frac{1}{m}$) though interestingly, it reaches an optimum value of 2 kg/m^2. Below 2 kHz absorption increases with increasing admittance of the membrane's back surface, though above this frequency little variation is seen. It is suggested that the absorption of high frequencies is more dependant on the admittance of the source side. With no absorption in the cavity there is a small dip at resonance, it appears therefore that the membrane alone cannot absorb significant amounts of energy.

A1.5 Panel Absorption

This method of dissipating sound energy is among the oldest, though for aesthetic reasons rather than acoustic ones [A.28]. The music room walls of aristocratic homes were normally lined with thin decorative hardwood panelling. Unbeknown to the interior designers of the time, the combination of shallow air cushion and thin panelling form a resonant acoustic system tuned in the region of the lowest audible octaves. It is reasonable to hypothesise, that with the mid and high frequency absorption provided by plush furniture, many Baroque and early Classical premiers would have been performed in a room with a fairly constant reverberation-frequency characteristic. In general, panel absorbers have been used in the past for subtle absorption over a large range of frequencies, with measurements in music studios in Hanover and Munich, identifying this gentle characteristic [A.29].

The theory of operation of a panel absorber is considerably more involved than for a membrane absorber, in the main because of the plate's material properties and the complex coupling that occurs between it and the sound field. Much of this theory is dealt with by Cremer & Müller [A.30] and only the salient points will be mentioned here. As mentioned in the previous section, the losses in panel absorption are due to the flexure of plate and the edge conditions. The latter quantity is a difficult one to

analytically describe and quantify, as real life examples tend to fall somewhere between clamped and simply supported. The difference between rigid fastening of the edge of the plate by screws and support in sponge rubber was experimentally determined by Sabine [A.28]. It appears that when more rigidly clamped, the absorption peak occurs at a higher frequency (~ 220 Hz) than with the sponge support (~ 170 Hz). In addition, the former seems to exhibit greater damping given the marginally lower Q and absorption peak [A.29]. No significant difference when the panel was glued rather than screwed was noted.

The general method of absorption is where oscillatory pressure fluctuations in the fluid medium are translated to sympathetic vibration in the thin, stiff, flexible plate. Thus such absorbers should be placed near room boundaries as it is the magnitude of pressure not particle velocity that causes vibration of the plate. From here, vibration velocity dissipates energy through internal losses of the plate, viscous losses of the cavity behind (enhanced if porous material is added) and frictional losses at the edges. The material properties of the plate play a larger part than membrane absorbers in determining the frequency range at which it is most effective and some interesting features can be noted. An important phenomenon occurs when the wavelength of the acoustic wave equals the free trace wavelength of the wave in the plate.

It is important to mention that coincidence[2] is not particularly relevant to this discussion as the frequency range of interest is considerably lower than this critical frequency (~1.4 kHz for the 15 mm plywood).

Meyer [A.30] discovered as long ago as 1936 that similar absorption is achieved when porous material is placed only near the edges of the panels, to when the whole cavity is filled. As Kuhl [A.31] pointed out as part of his study into artificial reverberation, the damping of a vibrating plate is heavily influenced when a porous material is placed in close proximity, but not in contact, as the magnitude of the hydrodynamic near-field is highest. Whilst selective placement of porous material yields similar absorption characteristics, only when the whole air cavity is filled with material of sufficiently high flow resistivity can the peak frequency, Q and absorption maximum be reliably predicted by analytical means.

---

[2] A phenomenon where the wavelength of an acoustic wave equals the free trace wavelength of the wave in the plate.

Ford & M^{c}Cormick [A.32] investigated some properties of panel absorbers in their paper by using aluminium plates for the panel and polyurethane foam as the porous cavity in-fill. By way of introduction, they claim that panel absorbers have advantages over membrane types, though their assertions are based on practical points like aesthetics and the range of materials that may be used in construction. Absorption characteristics results without polyurethane foam in-fill exhibit high Q peaks at only two regions in their range of interest (0.4 – 4 kHz). Unfortunately the authors only present the results for foam in the cavity in terms of an impedance diagram, as such it is difficult to gauge the likely absorption. Kenworthy & Burnam [A.33] present many experimental results in their paper of 1951, though they are limited to octave bands from 128 to 4096 Hz. 6 mm thick three-ply fir plywood is used as facings for three different geometric shapes: flat, splayed and cylindrical. In addition to these variables, the effect of placing felt to either the rigid back, or the underside of the panel was investigated. Whilst the authors go into some detail as to the subtle differences between each arrangement, it is sufficient here to state that even in the relatively high frequency range they considered, none of the absorbers achieved absorption coefficients above 0.2. No particularly useful conclusions can be drawn from this. It is interesting though, that similar work on splayed panel absorbers had been done three years earlier [A.28]. Sakagami *et al* [A.34] investigated the performance of an infinite elastic plate with back cavity as a precursor to the work on membranes already mentioned (*Section A1.4*) and using an identical theoretical approach. Once again the individual contributions of admittance on the source side and back side of the panel and back wall, are considered with respect to the overall absorption. Four cases were initially examined for a 2 mm thick plate placed 45 mm from a back wall. The arrangement for which both sides of the panel are covered in absorbent was found to be the most effective, joint second was for absorbent on only the back wall, or back surface of panel. The most ineffective arrangement was when absorbent was placed on only the source side of the panel.

A1.6 Excess Absorption due to Impedance Discontinuities

Brief mention was made in *Section A1.2* that a greater degree of diffusion is apparent when the absorptive materials are arranged in a non-uniform manner. In addition to this, however it has been widely reported that higher values of

absorption are noted when discontinuities of surface impedance exist. The implications of this are very important for the control of reverberation in rooms, from both an absorption efficiency and financial point of view. Takahashi [A.35] discusses the performance of a periodic array of absorbing strips in terms of both vertical and horizontal field incidence. The inclusion of the horizontal plane is particular to this problem of non-uniform boundaries. The theoretical analysis uses the two dimensional Green's theorem and Rayleigh's wave scattering model, from which the absorption coefficient (which is dependent on vertical and horizontal incidence, as well as the periodicity) can be found. This is compared with the average value for the absorption coefficient of the two admittances, α_{eq} in the literature. The most notable difference is the dramatic increase in the 'true' field absorption coefficient, α_{tr}, centred on frequencies whose wavelength is equal to twice the period of the discontinuity. The discrepancy evident between theory and experiment, in this figure, is associated with the 'edge effect' which ***is not*** accounted for in the analysis. It is interesting that this difference increases at low frequencies. The authors go on to investigate the affect of variations in the vertical and horizontal angles of incidence. When sound is incident perpendicular to the plane of periodicity (vertical angle = 90°) the absorption increases with decreasing values of normalised wavenumber $\bar{k} = kL$, where L is the period of the surface. This reaches a singularity below $\bar{k} = \pi$, which means maximum absorption is achieved when the period of the surface discontinuity is less than or equal to half the wavelength of the incident sound, $L \leq \frac{\lambda}{2}$. In addition to this, the absorption also increases as the sound approaches grazing incidence – reaching a maximum at around 75° and sharply decreasing to zero absorption at 90°.

A related investigation, into the performance of periodically spaced baffles for industrial noise control, is considered by Cops [A.36]. In this work, the effect of changing all the major variables are experimentally determined. It should be noted that unlike most of the other papers considered in this review, Cops makes no attempt to form any kind of theoretical model, with all conclusions based on experimental results. The baffles in question are rectangular, with the exact measurements changing with each experiment. Cops found that vertically suspended panels gave better performance than horizontal ones, apart from the lowest octave of measurement (250-500 Hz), though the difference there is far smaller than at the higher frequencies.

His next experiment determined that a 1.2 by 0.6 metre baffle exhibited better absorption when hung from its shorter side, i.e. the depth of the trap was deeper, though a similar reversal at frequencies below 250 Hz was again apparent. A difference was noted when the baffles were arranged either in a mutually parallel or perpendicular fashion, though the latter was better by only a small margin above 1 kHz. As would be expected, the degree of absorption increased with a greater density of baffles, regardless of their thickness (5 or 13 cm). When thickness was the only variable, the 13 cm type proved superior, though only below 1 kHz. The previous two experiments were combined, next, by maintaining constant material volume while varying the density and thickness, i.e. 24 baffles 4 cm thick, 12 at 8 cm, 8 at 12 cm and 6 with a thickness of 16 cm. The clear trend above 500 Hz was that a larger density of thin elements performed better.

Orlowski [A.37] performed a similar set of experiments around the same time as Cops, by using a scale model reverberation chamber. Once he had established that suspended baffles performed better, the default arrangement was the perpendicular one, as these were found to be superior to parallel ones. The most interesting result was the effect of increasing baffle density, where it was noted that the absorption *per baffle* decreases with increasing density, such that for the decade above 500 Hz the average absorption increase is 50% for every doubling. This is consistent with Cops who quotes a 60% increase in absorption at 1 kHz, when the baffle density is increased from six to twelve, or twelve to twenty-four. Their explanations are identical *" . . . there is a reduction in efficiency due to the mutual influence of the elements."*. In addition, Orlowski states that there is no difference in absorption performance between baffles with a central divider and those made only from rockwool. The effect of subdividing an area of absorbing material into many smaller ones, observed by Kuhl in 1960, is also noted in [A.37]. When the absorption of a sample of 40 m^2 is compared to that of forty 1 m^2 samples, the latter exhibits an improved performance above 250 Hz for both freely suspended and rigidly backed arrangements. Orlowski states that this effect *". . . is attributed to the diffraction of sound at the edges of that material."*.

Ten Wolde [A.38] continued the earlier work of others on the effect that varying the ratio of perimeter to area of a sample has on the absorption, building on the previously proven linear equation $\alpha_E = \alpha_\infty + \beta E$. ($\alpha_E$ is the 'true' absorption, α_∞ is the

absorption of an infinite sample, E (in m^{-1}) is the ratio of perimeter to area and β is a constant). Experiments were designed to establish this relationship for four porous samples, with the hope that graphs of β versus frequency could be produced and that extrapolation of α_E for $E=0$ may give the same results as that of an infinite sample and act as a check. Consideration was given to the effect one area of absorptive material may have on another and reference made to the work of Daniel [A.39] in 1963 on the extent of diffraction in the vicinity of a change in impedance.

For each sample and at a number of frequencies between 63 Hz and 8 kHz, Ten Wolde plots α_E vs. E and proves the linear relationship with a line of best fit - the gradient of the slope giving the value of β (dimension of metres). A note was made of the true absorption when $E=0$ and found to be in close agreement with a value for α_∞ as determined in an impedance tube. The relationship between β and frequency for each sample is most insightful, though the results below 600 Hz should be viewed with some caution, on account of the separation of samples (2 metres from each other and 1 m from the walls of the reverberation chamber). The author points out that in this frequency range, there will be a deviation from the assumed linearity which directly impacts the reliability of values for α_E, α_∞ and β. Nevertheless, these plots are able to give an idea of the potential benefits that may be had from the 'edge effect'. For example, the result for one of the materials indicates that while at around 1 kHz (where it is at a maximum) the edge effect would prove significant, this clearly is not the case at 4 kHz where $E=0$ and thus $\alpha_E=\alpha_\infty$.

A few years later, De Bruijn [A.40] set out to ascertain theoretically some of the finer points of the edge effect, raised by the investigations of Ten Wolde and others. It is interesting that the author points out that while β should have a unique value, it is actually frequency dependant. The main thrust of this paper is to investigate why the linear relationship between additional absorption and edge length becomes unreliable for sample sizes smaller than a threshold given as approximately $\frac{\lambda}{2}$ by Daniel [A.39].

Above this De Briujn states that the theoretical value of β may be found by considering each edge of a large rectangular sample as being independent, such that the analysis is based on the plane wave scattering of semi-infinite half planes on an infinite floor of zero admittance. The accuracy of this assumption is borne out by the

comparison presented in *Figure 1* of [A.40]. However for small samples he hypothesises that the diffracted field due to an edge is scattered by the opposite one resulting in more absorption. This may only be allowed for, theoretically, by including an additional factor that accounts for its *geometry.* The main point of discussion is that while, for normal incidence, the edge interaction only becomes significant for strip widths less than $\frac{\lambda}{2}$, this is certainly not the case for more grazing angles of incidence. The author claims this complicated diffraction phenomenon is a result of the disturbing field of one edge being of a similar magnitude to the incident wave at the other, as there is a greater degree of *forward* scattering. Thus even for large widths there can be strong interaction, which calls into question the reliability of the analysis for these cases, as weak interaction was assumed. In conclusion, De Bruijn points out that the results of Daniel, regarding minimum distances, are rather optimistic.

De Bruijn also investigated the associated problem of a corrugated structure, a few years earlier [A.41], in response to the increasing number of periodic structures in halls designed for speech or music. In addressing some of the apparent anomalous results from this investigation [A.42], he concluded that the main mechanisms of absorption in a corrugated surface are Wood anomalies, acoustic surface waves and waveguide resonances.

Maekawa [A.43] used some of the theory present by De Bruijn in [A.40 – A.42] and applied it to the problem of sound reflections in rooms, which he was considering from a pyschoacoustic point of view. Two structures are cited which share some of the characteristics of those of De Bruijn – periodically spaced reflective surfaces placed on a porous material. For rectangular strips of hardwood placed on a similar depth of glass fibre the absorption coefficient was found to be significantly higher between 30° and 50° than for glass fibre alone; unfortunately this result was only presented for a frequency of 5 kHz. Interestingly he also investigated the effect of replacing the strips of wood with glass plates or 'louvres' angled at 20° (a very similar scenario to the *Bass Trap*). His results show that at near grazing incidence, the corresponding reflection coefficient is less than the glass fibre alone and approaching zero – i.e. near unity absorption.

A1.7 Perforated Panel Absorbers

When considering the subject of panel absorbers in *Section A1.5* it was tacitly assumed that they were impervious, solid plates, however that is not the case for the type discussed in this section. The similarity in appearance to the untrained eye, disguises the fact that the two absorb sound by completely different mechanisms, though resonant behaviour is present in both. Perforated panels have been in use for many years, indeed their role in early BBC patents has already been mentioned (*Section A1.4*, [A.25]), however their use has always been in conjunction with other elements, normally porous materials. The reason being that acoustic resistance is necessary for absorption. Recently, however, the application of resonator theory to short tubes has shown that the resistance required can be provided by perforations that are very much smaller than those previously used. The advantages of such an absorber are obvious, as they allow, for the same acoustic performance, greater flexibility in materials, aesthetic finishes and can be made to withstand more severe conditions (though storm-proof absorbers are not a priority in recording studios). Maa [A.44] appears to be one of the first to investigate the use of so called *micro*-perforated panel absorbers in his paper of 1987, in which he outlines the pertinent theory and applies the results. The analysis starts with the equation for aerial motion inside a tube short in comparison to the wavelength of sound. Rayleigh was the first to consider this problem in his *Theory of Sound Vol. II*, though Maa uses an approximation of this, derived by Crandall. The approximation for specific acoustic impedance is only valid under certain conditions and Maa derives an equation that holds for the intermediate values, those which are of the greatest practical importance – he states that it doesn't differ from the exact solution by more than 5%. Other assumptions made are that the holes are spaced more than a diameter apart and that the orifice impedance remains linear. This latter point is important at high sound pressure levels, though the author shows that the onset of non-linearity only occurs at sound pressure levels of around 114 dB. Placing the panel in the vicinity of a rigid wall results in a resonant system and based on an electrical analogue, Maa determines expressions for the maximum absorption, resonant frequency and half absorption bandwidth. Oblique incidence will raise the frequency of peak absorption by a factor of $\frac{1}{\cos\theta}$, where θ is the angle from the normal. The discussion extends to that of a double panel design, which finds greater application at absorbing the lowest audible

frequencies. An additional tuned circuit in parallel with the first yields expressions for the impedance and thus the absorption. However, Maa shows that the while the low frequency limit is significantly changed, the high frequency limit remains almost the same, by virtue of the mass reactance dominating. Whilst the graphical examples are concerned with the mid-band audio frequencies, the author points out that micro-perforated designs are perhaps better suited to the very low frequencies. He concludes by citing an example whereby careful choice of parameters can lead to a design whose depth is only 8% of the wavelength of sound at which it has its absorption peak.

The rugged nature of this absorber attracted the interest of researchers in the U.S. Army Environmental Acoustics Team. Explosion noise is responsible for large levels of low frequency noise, however any successful method of sound energy dissipation should be able to withstand hostile conditions – porous absorbers are not suitable for such an application. In their paper [A.45], they build on the aforementioned work of Maa and relate it specifically to the absorption of low frequency sound. The theory presented in [A.44] is compared with experimental results obtained by testing single and double layer designs in a giant size impedance tube (the subject of a paper [A.46] by one of the authors of [A.45]). In [A.45] six sets of experimental results are presented, each corresponding to different depth(s) of air cavity and perforation ratio; the diameter of perforation and thickness of panel was kept constant at 2 and 20 mm respectively. The agreement between theory and experiment is very good, though subtle differences remain. As the real and imaginary part of the specific acoustic impedance accompanies each plot of absorption, one can identify the real part as being responsible for these inconsistencies. The experimentally determined value for resistance is lower than the theory predicts for all plots, while the reactive part of the impedance is extremely accurate. The difference in perforation ratio is primarily seen from the amount of maximum absorption, as while a ratio of 1% yield unity absorption, 2% perforation only peaks at around 0.9. However, for double layer structures, with a 1% perforate on the outside, unity absorption is still achieved with a 2% perforate as the second layer. The effect of increasing the cavity depth is shown, both by experiment and theory, to lower the resonant frequency. An interesting point is noted for a double layer absorber, with the depths of the two cavities interchanged, so that the overall depth is conserved. The difference between an outer and inner cavity depth of 0.3 and 0.6 metres respectively and vice versa, is more significant than

one might expect. The absorption characteristic of the two are identical at and below the peak, but start to differ above 50 Hz (~ ½ octave above the resonance). The impedance plots are dramatically different. From the results presented it is apparent that this design lends itself very well to the absorption of low frequency sound, with simple changes yielding control of peak frequency, amount of absorption and Q. Single leaf absorbers exhibit unity absorption at around 50 Hz for a depth of only 50 cm and double leaf 90 cm types can shift the same magnitude of absorption as far down as 30 Hz.

Maa [A.47] recently published a follow up paper to [A.44] in which he develops more accurate equations for the specific acoustic impedance of the perforated panel. The discrepancies between the theory and experiment of resistance in [A.46] is explained in this latest paper, as being due to an incorrect end-correction, the result of which leads to a lower value of acoustic resistance. In concluding this section it is worth mentioning the paper by Ingard [A.48] in which all the most important theory on the design of acoustic resonators is included and provides a thorough foundation to the other papers cited here and in other sections.

A1.8 Hybrid Porous Absorbers

The most common absorbers are those which dissipate sound energy through viscous losses incurred by the oscillatory movement of the air through a porous material. However, for such absorbers to be at their most effective they must be placed in positions of high particle velocity and this requires a distance of around ¼ of a wavelength from a rigid room boundary – an impracticability at the lowest of audible frequencies. Typical values for the absorption by porous materials in different positions is given in the paper by Burd *et al* [A.49], where the increase in low frequency absorption as a blanket is moved further from the wall, is clearly seen. Due to the shortfall of this mechanism in our frequency range of interest, research has considered the improvement in performance that may be had by combining porous absorption with other mechanisms. Investigations into this were carried out by Moore & Lyon [A.50], where a composite design of two different porous materials separated by a resistive screen and covered by an impervious septa is considered. Analytical equations are formed to characterise the individual components, with equations of continuity providing an expression for the behaviour of the whole unit. The

theoretical analysis allowed the authors to create an optimisation routine, where each parameter for each layer of the composite absorber was varied to give the maximum average absorption over the frequency band of 0.2 to 1 kHz. Unlike most investigations into the behaviour of porous materials, this paper considers the properties of the skeletal frame, namely its stiffness and this is shown to be a factor in some of the absorption peaks. Limits had to be stipulated, else the design would become too big, this is particularly true of the outer layer, which was restricted to less than 3 inches deep. Each peak is associated with different aspects of the design, either individual elements or their interaction. The authors explain in some detail the origin of the two lowest resonances that occur at approximately 350 and 600 Hz. The former is due to out-of-phase motion between the masses of the front face septum and internal resistive screen. The reason for the unexpectedly low frequency at which it occurs is because of the slowly propagating mode in the outer layer of porous material, which in turn is heavily dependant on the axial stiffness its frame. It is the quadrature phase of fluid and frame motion in the vicinity of the internal resistive screen that is responsible for the level of dissipation at this frequency. The absorption peak at 650 Hz is due to the same mechanism, though an additional minimum occurs in the outer layer. This paper shows that by partitioning different porous materials between thin screens (which contribute very little), phase differences between frame and fluid motion can yield absorption in a frequency range lower than if used in isolation.

Porous materials used to back perforated facings have been employed as absorbers for many years, as their performance is very easily controlled and generally have a wider band of absorption. Whilst references like [A.49] give an idea as to the influence of certain variables, it is by no means a definitive study. Davern [A.51] set out to provide exactly that in his paper of 1977. His study is split into different sections, in which the following variables are considered: percentage perforation of facing, thickness of facing, density of backing material and the effect of an air space, impervious layer, or both between the facing and backing. The results are presented both as absorption coefficients and impedance plots, the latter is particularly helpful in ascertaining whether it is the reactance or resistance that changes with different arrangements.

As the perforation increases, the resonant frequency rises and the Q becomes less. As we have seen earlier in *Section A1.7,* making the perforations smaller increases the

specific acoustic resistance and this is clearly seen in the impedance representation. The difference between the different perforations ratios at low frequencies is chiefly associated with the resistance – the reactance remains fairly constant. By contrast, changing the thickness of the facing (while keeping the total depth constant) makes the greatest difference to the reactance. It is generally the case, however, that the thickness is chosen for practical reasons, with the perforation ratio compensating where necessary. The clearest example of a variable affecting one part of the impedance and not the other, is seen in the result for varying the density of the glass fibre backing from 16, through 74 and 95 to 205 kg m^{-3}. The resonant frequency is not changed, however the degree of resistance does show a dependency, with values that are too high or too low identifying themselves by having a resistance far from the ideal that the author gives as $1.6\rho_0 c_0$. The next experiments were designed to investigate the effect of an air space or impervious layer between the facing and backing. The former resulted in a lower value for resistance, similar to that obtained by increasing the perforation ratio, the reactance changed only slightly, due to the small increase in depth of the whole absorber. Considering the influence of an impervious layer is important as they are often employed to prevent any fibre fall out from the porous backing. With standard (74 kg m^{-3}) glass fibre, inserting tissue paper modified the absorption characteristics considerably, with an increase in resistance and a frequency dependent reactance. As with the additional air space, this change was independent of both perforation ratio and facing thickness. These findings were not evident when the porous material was of a lower density (16 kg m^{-3}), indeed the tissue paper significantly improved absorption, by increasing the resistance and leaving the reactance the same. It should be noted, though, that such an improvement could have been more easily achieved using a higher density backing. When an air space and impervious layer are introduced, the effect is similar to that of the air space alone, i.e. a reduction in both the resistance and reactance. Davern concludes by stating that the influence of a perforated facing is negligible, with the performance being identical to the porous material alone, if an air space of at least 3 mm is maintained between the facing and backing.

Davern's investigation was only concerned with the normal specific acoustic impedance of perforated facing backed with porous material, whereas Guinouard *et al* [A.52] considered oblique incidence, for which theoretical predictions were compared

to measured values. The model used consists of a 0.75 mm thick metal facing (considered rigid), with a perforation ratio of 17.5%, circular holes 5 mm in diameter; 3 cm thick high density fibreglass (resistivity of 7×10^4 Pa s m^{-2}); and a 10 cm air gap between the fibreglass and rigid floor. The comparison between theory and measurement is shown to be good, with the small discrepancies blamed on the empirical laws by Delany and Bazley [A.53], which are not perfectly suited to the fibreglass used, as their study considered porous materials with lower resistivity. Further evidence of the benefit of perforated facings and deeper structures (by the addition of air gaps) is given in the plot of absorption coefficient for fibreglass only, facing and fibreglass and fibreglass backed perforated facing with an air gap. A similar investigation was carried out a little later, but this time the facing had slits instead of circular holes [A.54]. Similar theory is used where the impedance is found for frequencies where the acoustic wavelength equals an integer multiple of the slit period via Fourier series and extrapolated to include others. The absorber was constructed from a wooden facing 1.2 cm thick, with slits 2 cm long and either 1.2, 2.2 or 3.3 mm wide; it was backed with 15 mm thick fibreglass. Agreement between theory and experiment is good, particularly for the resistance. The startling effect of a periodically slit facing backed with fibreglass is clearly illustrated in the paper, with the absorption dwarfing that of the backing alone. The general trend is for lower frequency and higher Q resonance as the slit becomes more narrow.

Takahashi [A.55] took the subject of a perforated absorber system to a new level of complexity recently, by considering the effects of panel vibration and more importantly, diffraction effects due to the holes, as well as the other aforementioned contributions. He claims that inaccuracies in earlier studies are in part to do with diffraction being disregarded. The effects of scattering by the impedance discontinuities are dealt with, in much the same way as an earlier paper by the author (*Section A1.6*, [A.35]) and the specific acoustic impedance of the perforated panel is arrived in a similar manner to previously cited papers on the subject. His investigation into the importance of panel absorption, was significant to the theory, as it would determine the admittance of the non-perforated part of the panel, a key variable in predicting the impedance of the whole absorber. The theoretical results were compared to experimental diffuse field measurements made by a different set of authors, thus the results presented by Takahashi were field averaged. It is difficult to

say whether or not his analysis is more accurate than [A.52] and [A.54], as no experimental-theoretical comparisons were made in those papers for absorption coefficient, only impedance. However from the 23 individual traces (on 7 graphs) in [A.55] there appears to be good agreement for absorbers with the cavity filled with air and porous material, but less so when only air is present.

In concluding this section it is worth noting the use of conical paper shapes placed on glasswool as absorbers [A.56]. The authors first investigated the effect that shape of cone had on its absorption characteristics. They found that for the same base radius the resonant frequency dropped with increasing height and that for the same height the bandwidth of absorption increased with larger base radii. With the volume held constant, tall thin cones exhibited high Q low frequency absorption, while short fat ones gave less absorption but over a wider frequency range. This serves to support the first two results. Placing cones of different size on a layer of glasswool yielded an absorption characteristic that maintained the same peak as the cone alone, but with a far larger bandwidth.

APPENDIX 2

Analysis of Experimental Determination of Sample Absorption Coefficient

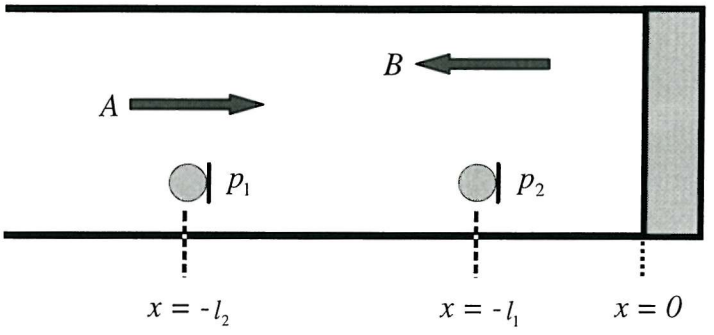

Figure A2.1 – Model for experimental determination of sample absorption coefficient

Assuming a plane wave pressure field in a duct, we can write :

$$p(x) = Ae^{-jkx} + Be^{jkx} \tag{A2.1}$$

and subsequently define the complex pressure reflection coefficient as :

$$\frac{B}{A} = R \tag{A2.2}$$

and associated absorption coefficient as : $\alpha = 1 - |R|^2$ (A2.3)

The measured complex transfer function $\frac{p_1}{p_2} = T$ may be written as :

$$T = \frac{p(-l_2)}{p(-l_1)} = \frac{Ae^{jkl_2} + Be^{-jkl_2}}{Ae^{jkl_1} + Be^{-jkl_1}} \tag{A2.4}$$

rearranging gives : $T\left(Ae^{jkl_1} + Be^{-jkl_1}\right) = Ae^{jkl_2} + Be^{-jkl_2}$, which allows the separation of A and B :

$$A\left(Te^{jkl_1} - e^{jkl_2}\right) = B\left(e^{-jkl_2} - Te^{-jkl_1}\right) \tag{A2.5}$$

From which the reflection coefficient can be expressed as :

$$R = \frac{B}{A} = -\frac{e^{jkl_2} - Te^{jkl_1}}{e^{-jkl_2} - Te^{-jkl_1}} \qquad \text{(A2.6)}$$

Thus the absorption coefficient of an unknown sample a known distance (l_1 and l_2) from two pressure microphones can be found according to :

$$\alpha = 1 - \left| \frac{e^{jkl_2} - Te^{jkl_1}}{e^{-jkl_2} - Te^{-jkl_1}} \right|^2 \qquad \text{(A2.7)}$$

APPENDIX 3

Analysis of Decomposition of Plane Wave Pressure Field

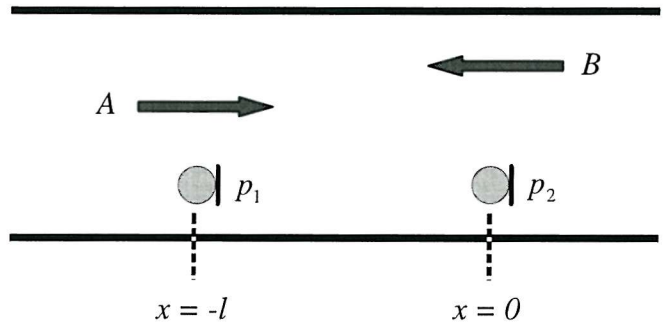

Figure A3.1 – Model for decomposition of plane wave pressure field

Given a plane wave pressure field in a duct, *Figure A3.1*, the pressure at a point $x = -l$ can be expressed as $p_1 = Ae^{-jk(-l)} + Be^{jk(-l)}$ (A3.1)

Similarly at $x = 0$ we can write $p_2 = A + B$ (A3.2)

Rearranging (A3.2) yields $B = p_2 - A$ (A3.3)

Which when substituted into (A3.1) gives $p_1 = A\left(e^{jkl} - e^{-jkl}\right) + p_2 e^{-jkl}$ (A3.4)

Rearranging (A3.4) yields $A = \dfrac{p_1 - p_2 e^{-jkl}}{e^{jkl} - e^{-jkl}}$ (A3.5)

and by substituting into (A3.5) the standard equation $\sin kl = \dfrac{e^{jkl} - e^{-jkl}}{2j}$ allows the forward going wave to be written in terms of the complex pressures at two known points : $A = \dfrac{p_1 - p_2 e^{-jkl}}{2j \sin kl}$ (A3.6)

REFERENCES

[1.1] Hidley, T., 2000: Private communication with author.

[1.2] Newell, P., & Holland, K., 2000: 'The Measurement and Analysis of a Control Room Acoustic Treatment During Construction', *Proceedings of the Institute of Acoustics*, Vol. 22, Part 6, pp. 179 - 191.

[1.3] Soares, L., 1991: 'An Experimental Study of the Responses of a Recording Studio Control Room at Low Frequencies Using a 1:10 Scale Model', MSc dissertation, ISVR, University of Southampton.

[1.4] Walter, A., 1998: BEng project, ISVR, University of Southampton.

[1.5] Colam, S., & Holland, K., 1999: 'An Investigation into the Performance of a Chipboard Panel as a Low Frequency Sound Absorber', *Proceedings of the Institute of Acoustics*, Vol. 21, Part 8, pp. 105 - 112.

[1.6] Colam, S., 1998: 'An Investigation into the Mechanisms Involved in an Empirically Designed Low Frequency Absorber for Rooms', MSc dissertation, ISVR, University of Southampton, pp. 54 - 56.

[1.7] Cremer, L., & Müller, H., 1982: *Principles and Applications of Room Acoustics Vol. 2*, (London: Applied Science), pp. 128 - 180.

[1.8] Sabine, W., 1922: *Collected Papers on Acoustics*, (Harvard University Press).

[1.9] Kinsler, L., Frey, A., Coppens, A., & Sanders, J., 1982: *Fundamentals of Acoustics (third edition)*, (New York: John Wiley & Sons), pp. 313 - 319.

[1.10] Beranek, L., & Ver, I., 1992: *Noise and Vibration Control Engineering*, (New York: John Wiley & Sons), pp. 397.

[1.11] Munjal, M., 1987: *The Acoustics of Ducts and Mufflers*, (Wiley-Interscience).

[1.12] Lapin, A., 1967: 'Application of Resonators for the Enhancement of Sound Attenuation in a Waveguide Lined with a Soundproofing Material', *Soviet Physics – Acoustics,* Vol. 12 , No. 3 (January - March), pp. 286 - 290.

[1.13] Schultz, T., & Watters, B., 1964: 'Propagation of Sound Across Audience Seating', *Journal of the Acoustical Society of America*, Vol. 36, No. 5 (May), pp. 885 - 896.

[1.14] Sessler, G., & West, J., 1964: 'Sound Transmission Over Theatre Seats', *Journal of the Acoustical Society of America*, Vol. 36, No. 9 (September), pp. 1725 - 1732.

[1.15] Bradley, J., 1991: 'Some Further Investigations of the Seat Dip Effect', *Journal of the Acoustical Society of America*, Vol. 90, No. 1 (July), pp. 324 - 333.

[1.16] Ingard, U., 1994: *Notes on Sound Absorption Technology*, (New York: Noise Control Foundation), pp. 6.1 - 6.26.

[1.17] Guy, R., 1989: 'A Preliminary Study Model for the Absorption of Transmission of Sound in Multi-Layer Systems', *Noise Control Engineering Journal*, Vol. 33, No. 3, pp. 117 - 123.

[1.18] Qunli, W., 1988: 'Empirical Relations between Acoustical Properties and Flow Resistivity of Porous Plastic Open-Cell Foam', *Applied Acoustics*, Vol. 25, pp. 141 - 148.

[1.19] Morfey, C., 2001: *Dictionary of Acoustics*, (London: Academic Press), p. 2.

[2.1] Cremer, L., & Müller, H., 1982: *Principles and Applications of Room Acoustics Vol. 1*, (London: Applied Science), pp. 315 - 318.

[2.2] Morfey, C., 2001: *Dictionary of Acoustics*, (London: Academic Press), pp. 201 - 202 .

[2.3] Newell, P., & Holland, K., 2000: 'The Measurement and Analysis of a Control Room Acoustic Treatment During Construction', *Proceedings of the Institute of Acoustics*, Vol. 22, Part 6, pp. 179 - 191.

[2.4] Cremer, L., & Müller, H., 1982: *Principles and Applications of Room Acoustics Vol. 1*, (London: Applied Science), pp. 244, 258 & 308 - 309.

[2.5] Soares, L., 1991: 'An Experimental Study of the Responses of a Recording Studio Control Room at Low Frequencies Using a 1:10 Scale Model', MSc dissertation, ISVR, University of Southampton.

[3.1] Newell, P., & Holland, K., 2000: 'The Measurement and Analysis of a Control Room Acoustic Treatment During Construction', *Proceedings of the Institute of Acoustics*, Vol. 22, Part 6, pp. 179 – 191.

[3.2] Morfey, C., 2001: *Dictionary of Acoustics*, (London: Academic Press), p. 321.

[3.3] Cremer, L., & Müller, H., 1982: *Principles and Applications of Room Acoustics Vol. 2*, (London: Applied Science), pp. 177 - 180.

[3.4] Cremer, L., & Müller, H., 1982: *Principles and Applications of Room Acoustics Vol. 1*, (London: Applied Science), pp. 201 - 207.

[3.5] Cremer, L., & Müller, H., 1982: *Principles and Applications of Room Acoustics Vol. 2*, (London: Applied Science), pp. 108 - 113.

[3.6] Fahy, F., 1984: 'Rapid Method for the Measurement of Sample Acoustic Impedance in a Standing Wave Tube', *Journal of Sound and Vibration*, Vol. 97, No. 2, pp. 168 - 170.

[3.7] Delany, M., & Bazely, E., 1970: 'Acoustic Properties of Fibrous Absorbent Materials', *Applied Acoustics*, Vol. 3, pp. 105 - 116.

[3.8] Qunli, W., 1988: 'Empirical Relations between Acoustical Properties and Flow Resistivity of Porous Plastic Open-Cell Foam', *Applied Acoustics*, Vol. 25, pp. 141 - 148.

[3.9] Burd, A., Gilford, C., & Spring, N., 1966: 'Data for the Acoustic Design of Studios', *BBC Engineering Monograph*, No. 64 (November), pp. 10 - 11.

[3.10] Gilford, C., 1952: 'Membrane Sound Absorbers and Their Application to Broadcasting Studios', *BBC Quarterly*, Vol. 7, pp. 246 - 256.

[3.11] Hidley, T., 2001: Private communication with author.

[3.12] Guy, R., 1989: 'A Preliminary Study Model for the Absorption or Transmission of Sound in Multi-Layer Systems', *Noise Control Engineering Journal*, Vol. 33, No. 3, pp. 117 - 123.

[3.13] Kinsler, L., Frey, A., Coppens, A., & Sanders, J., 1982: *Fundamentals of Acoustics (third edition)*, (New York: John Wiley & Sons), pp. 317 - 318.

[3.14] Gilford, C., 1979: 'The Acoustic Design of Talks Studios and Listening Rooms', *Journal of the Audio Engineering Society,* Vol. 27, No. 1/2 (January/February), pp. 17 - 31.

[3.15] Smith, P., 1964: 'Coupling of Sound and Panel Vibration Below the Critical Frequency', *Journal of the Acoustical Society of America,* Vol. 36, No. 8, pp. 1516 - 1520.

[3.16] Colam, S., & Holland, K., 1999: 'An Investigation into the Performance of a Chipboard Panel as a Low Frequency Sound Absorber', *Proceedings of the Institute of Acoustics*, Vol. 21, Part 8, pp. 105 - 112.

[3.17] Kuttruff, H., 2000: *Room Acoustics (fourth edition)*, (London: Spon Press), p. 76.

[4.1] Newell, P., & Holland, K., 1998: 'Acoustic Consideration for a Mobile Recording Vehicle', *Proceedings of the Institute of Acoustics*, Vol. 20, Part 5, pp. 37 - 45.

[4.2] Beranek, L., & Ver, I., 1992: *Noise and Vibration Control Engineering*, (New York: John Wiley & Sons), p. 397.

[4.3] Soares, L., 1991: 'An Experimental Study of the Responses of a Recording Studio Control Room at Low Frequencies Using a 1:10 Scale Model', MSc dissertation, ISVR, University of Southampton.

[4.4] Colam, S., & Holland, K., 1999: 'An Investigation into the Performance of a Chipboard Panel as a Low Frequency Sound Absorber', *Proceedings of the Institute of Acoustics*, Vol. 21, Part 8, pp. 105 - 112.

[4.5] Davies, P., 1988: 'Practical Flow Duct Acoustics', *Journal of Sound and Vibration*, Vol. 124, pp. 91 - 115.

[5.1] Walter, A., 1998: BEng project, ISVR, University of Southampton.

[5.2] Petyt, M., 1990: *Introduction to Finite Element Vibration Analysis*, (Cambridge: Cambridge University Press).

[5.3] Morse, P., & Ingard, U., 1968: *Theoretical Acoustics*, (New York: McGraw Hill), pp. 449 - 458.

[5.4] Kinsler, L., Frey, A., Coppens, A., & Sanders, J., 1982: *Fundamentals of Acoustics (third edition)*, (New York: John Wiley & Sons), p. 206 - 207.

[6.1] Ingard, U., 1994: *Notes on Sound Absorption Technology*, (New York: Noise Control Foundation), p. 6.7.

[6.2] Schultz, T., & Watters, B., 1964: 'Propagation of Sound Across Audience Seating', *Journal of the Acoustical Society of America*, Vol. 36, No. 5 (May), pp. 885 - 896.

[6.3] Sessler, G., & West, J., 1964: 'Sound Transmission Over Theatre Seats', *Journal of the Acoustical Society of America*, Vol. 36, No. 9 (September), pp. 1725 - 1732.

[6.4] Lapin, A., 1967: 'Application of Resonators for the Enhancement of Sound Attenuation in a Waveguide Lined with a Soundproofing Material', *Soviet Physics – Acoustics,* Vol. 12 , No. 3 (January - March), pp. 286 - 290.

[6.5] Kinsler, L., Frey, A., Coppens, A., & Sanders, J., 1982: *Fundamentals of Acoustics (third edition)*, (New York: John Wiley & Sons), pp. 214 - 222.

[6.6] Munjal, M., 1987: *The Acoustics of Ducts and Mufflers*, (Wiley-Interscience).

[6.7] Stroud, K., 1990: *Further Engineering Mathematics (second edition)*, (London: Macmillan), p. 73.

[6.8] Brekhovskikh, L., 1959: 'Surface Waves in Acoustics', *Soviet Physics – Acoustics,* Vol. 5, No. 3, pp. 3 - 12.

[6.9] Tester, B., 1976: 'The Propagation and Attenuation of Sound in Lined Ducts Containing Uniform or "Plug" Flow', *Journal of Sound and Vibration*, Vol. 28, No. 2, pp. 151 - 203.

[7.1] Kinsler, L., Frey, A., Coppens, A., & Sanders, J., 1982: *Fundamentals of Acoustics (third edition)*, (New York: John Wiley & Sons), pp. 373 - 375.

[7.2] Holland, K., 1992: 'A Study of the Physical Properties of Mid Range Loudspeaker Horns and Their Relationship to Perceived Sound Quality', PhD thesis, ISVR, University of Southampton.

[7.3] Cremer, L., & Müller, H., 1982: *Principles and Applications of Room Acoustics Vol. 1*, (London: Applied Science), p. 349.

[7.4] Cremer, L., & Müller, H., 1982: *Principles and Applications of Room Acoustics Vol. 2*, (London: Applied Science), p. 132.

[7.5] Walter, A., 1998: BEng project, ISVR, University of Southampton.

[8.1] Burd, A., Gilford, C., & Spring, N., 1966: 'Data for the Acoustic Design of Studios', *BBC Engineering Monograph*, No. 64 (November).

[8.2] Colam, S., 1998: 'An Investigation into the Mechanisms Involved in an Empirically Designed Low Frequency Absorber for Rooms', MSc dissertation, ISVR, University of Southampton.

[A.1] Gilford, C., 1972: *Acoustics for Radio and Television Studios*, (London: Peregrinus).

[A.2] Toole, F., & Olive, S., 1988: 'The Modification of Timbre by Resonances: Perception and Measurement', *Journal of the Audio Engineering Society,* Vol. 36, No. 3 (March), pp. 122 - 142.

[A.3] Olive, S., Schuck, P., Ryan., J., Sally, S., & Bonneville, M., 1994: 'The Effects of Loudspeaker Placement on Listener Preference Ratings', *Journal of the Audio Engineering Society,* Vol. 42, No. 9 (September), pp. 651 - 668.

[A.4] Olive, S., & Toole, F., 1989: 'The Detection of Reflections in Typical Rooms', *Journal of the Audio Engineering Society,* Vol. 37, No. 7/8 (July/August), pp. 539 - 553.

[A.5] Voelker, E-J., 1985: 'Control Rooms for Music Monitoring', *Journal of the Audio Engineering Society,* Vol. 33, No. 6 (June), pp.452 - 462.

[A.6] Gilford, C., 1979: 'The Acoustic Design of Talks Studios and Listening Rooms', *Journal of the Audio Engineering Society,* Vol. 27, No. 1/2 (January/February), pp. 17 - 31.

[A.7] Blauert, J., 1982: *Spatial Hearing*, (London: MIT Press), pp. 201 - 287.

[A.8] Morimoto, M., & Maekawa, Z., 1988: 'Effects of Low Frequency Components on Auditory Spaciousness', *Acustica,* Vol. 66, pp. 190 - 196.

[A.9] Somerville, T., Gilford, C., Spring, N., & Negus, R., 1966: 'Recent Work on the Effects of Reflections in Concert Halls and Music Studios', *Journal of Sound and Vibration,* Vol. 3, No. 2, pp. 127 - 134.

[A.10] Kuttruff, H., 1991: *Room Acoustics (third edition)*, (London: Elsevier Applied Science), pp. 184 - 186.

[A.11] Bücklein, R., 1962: 'The Audibility of Frequency Response Irregularities', reprinted in English in *Journal of the Audio Engineering Society*, Vol. 29, No. 3 (March), pp. 126 - 131.

[A.12] Olive, S., Schuck, P., Ryan., J., Sally, S., & Bonneville, M., 1997: 'The Detection Thresholds of Resonances at Low Frequencies', *Journal of the Audio Engineering Society,* Vol. 45, No. 3 (March), pp. 116 - 128

[A.13] Mayo, C., 1952: 'Standing Wave Patterns in Studio Acoustics', *Acustica,* Vol. 2, No. 2, pp. 49 - 64.

[A.14] Fryer, P., 1977: 'Loudspeaker Distortions, Can We Hear Them?', *Hi-Fi News and Record Review,* Vol. 22 (June), pp. 51 - 56.

[A.15] Kinsler, L., Frey, A., Coppens, A., & Sanders, J., 1982: *Fundamentals of Acoustics (third edition),* (New York: John Wiley & Sons).

[A.16] Bonello, O., 1981: 'A New Criterion for the Distribution of Normal Room Modes', *Journal of the Audio Engineering Society,* Vol. 29, No.9 (September), pp. 597 - 606.

[A.17] Volkmann, J., 1942: 'Polycylindrical Diffusers in Room Acoustic Design', *Journal of the Acoustical Society of America,* Vol. 13, No. 1 (January), pp. 234 - 243.

[A.18] Angus, J., 1997: 'The Behaviour of Rooms at Low Frequencies', presented at the 102nd Convention of the Audio Engineering Society (Munich, 22– 25 March), Preprint No. 4421.

[A.19] Gilford, C., 1979: 'The Acoustic Design of Talks Studios and Listening Rooms', *Journal of the Audio Engineering Society,* Vol. 27, No. 1/2 (January/February), pp. 17 - 31.

[A.20] Fujiwara, K., & Miyajima, T., 1992: 'Absorption Characteristics of a Practically Constructed Schroeder Diffuser of Quadratic Residue Type', *Applied Acoustics,* Vol. 35, pp. 149 - 158.

[A.21] Kuttruff, H., 1994: 'Sound Absorption by Pseudostochastic Diffusers', *Applied Acoustics,* Vol. 42, pp. 215 - 231.

[A.22] Amram, M., Chvojka, V., & Droin, L., 1987: 'Phase Reversal Barriers for Better Noise Control at Low Frequencies: Laboratory vs. Field Measurements', *Noise Control Engineering Journal,* Vol. 28, No. 1 (January/February), pp. 16 - 24.

[A.23] Somerville, T., Gilford, C., Spring, N., & Negus, R., 1966: 'Recent Work on the Effects of Reflections in Concert Halls and Music Studios', *Journal of Sound and Vibration,* Vol. 3, No. 2, pp. 127.

[A.24] Gilford, C., 1952: 'Membrane Absorbers and Their Application to Broadcasting Studios', *BBC Quarterly,* Vol. 7, pp. 246 - 256

[A.25] Burd, A. & Gilford, C., 1961: 'Improvements in and Relating to Sound Absorbers', *Patent Specification,* No. 860682, February 8th.

[A.26] Takahashi, D., Sakagami, K., & Morimoto, M., 1996: 'Acoustic Properties of Permeable Membranes', *Journal of the Acoustical Society of America*, Vol. 99, No. 5, (May), pp. 3004 - 3009.

[A.27] Sakagami, K., Kiyami, M., Morimoto, M., & Takahashi, D, 1996: 'Sound Absorption of a Cavity Backed Membrane', *Applied Acoustics*, Vol. 49, No. 3, pp. 237 - 247.

[A.28] Sabine, P., & Ramer, L., 1948: 'Absorption-Frequency Characteristics of Plywood Panels', *Journal of the Acoustical Society of America,* Vol. 20, No. 3 (May), pp. 267 - 270.

[A.29] Gilford, C., 1972: *Acoustics for Radio and Television Studios*, (London: Peregrinus), p. 160.

[A.30] Cremer, L., & Müller, H., 1982: *Principles and Applications of Room Acoustics Vol. 2*, (London: Applied Science), pp. 224 - 275

[A.31] Cremer, L., & Muller, H., 1982: *Principles and Applications of Room Acoustics Vol. 1*, (London: Applied Science), p. 288.

[A.32] Ford, R., & M^{c}Cormick, M., 1969: 'Panel Sound Absorbers', *Journal of Sound and Vibration,* Vol. 10, No. 3 (March), pp. 411 - 423.

[A.33] Kenworthy, R., & Burnam, T., 1951: 'The Absorption Coefficients of Fir Plywood Panels', *Journal of the Acoustical Society of America,* Vol. 23, No. 5 (September), pp. 531 - 532

[A.34] Sakagami, K., Takahashi, D., Gen, H., & Morimoto, M., 1993: 'Acoustic Properties of an Infinite Elastic Plate with a Back Cavity', *Acustica,* Vol. 78, pp. 288 - 295.

[A.35] Takahashi, D., 1989: 'Excess Sound Absorption due to Periodically Arranged Absorptive Materials', *Journal of the Acoustical Society of America*, Vol. 86, No. 6 (June), pp. 2215 - 2222.

[A.36] Cops, A., 1985: 'Absorption Properties of Baffles for Noise Control in Industrial Halls', *Applied Acoustics*, Vol. 18, pp. 435 - 448.

[A.37] Orlowski, R., 1984: 'The Arrangement of Sound Absorbers for Noise Reduction – Results of Model Experiments at 1:16 Scale', *Noise Control Engineering Journal*, Vol. 22, No. 2, pp. 54 - 60.

[A.38] Ten Wolde, T., 1967: 'Measurements on the Edge-Effect in Reverberation Rooms', *Acustica,* Vol. 18, pp. 207 - 212.

[A.39] Daniel, E., 1963: 'On the Dependance of Absorption Coefficients upon the Area of the Absorbent Material', *Journal of the Acoustical Society of America*, Vol. 35, No. 4 (April), pp. 571 - 573.

[A.40] De Bruijn, A., 1973: 'A Mathematical Analysis Concerning the Edge Effect of Sound Absorbing Materials', *Acustica,* Vol. 28, pp. 33 - 44.

[A.41] De Bruijn, A., 1967: 'The Sound Absorption of an Absorbing Periodically Uneven Surface of Rectangular Profile', *Acustica,* Vol. 18, No. 3, pp. 123 - 131.

[A.42] De Bruijn, A., 1971: Anomalous Effects in the Sound Absorption of Periodically Uneven Surfaces', *Acustica,* Vol. 24, pp. 75 - 84.

[A.43] Maekawa, Z-I, 1975: 'Problems of Sound Reflection in Rooms', *Applied Acoustics,* Vol. 8, pp. 157 - 172.

[A.44] Maa, D-Y., 1987: 'Microperforated-Panel Wideband Absorbers, *Noise Control Engineering Journal*, Vol. 29, No. 3 (November/December), pp. 77 - 84.

[A.45] Lee, J., & Swenson, G., 1992: 'Compact Sound Absorbers for Low Frequencies', *Noise Control Engineering Journal*, Vol. 38, No. 3, pp. 109 - 117.

[A.46] Swenson, G., 1993: 'A Standing-Wave Facility for Low Frequency Impedance/Absorption Measurement', *Applied Acoustics,* Vol. 40, pp. 355 - 362.

[A.47] Maa, D-Y., 1998: 'Potential of Microperforated Panel Absorber', *Journal of the Acoustical Society of America,* Vol. 104, No. 5 (November), pp. 2861 - 2866.

[A.48] Ingard, U., 1953: 'On the Theory and Design of Acoustic Resonators', *Journal of the Acoustical Society of America*, Vol. 25, No. 6 (November), pp. 1037 - 1061.

[A.49] Burd, A., Gilford, C., & Spring, N., 1966: 'Data for the Acoustic Design of Studios', *BBC Engineering Monograph*, No. 64 (November), p. 10.

[A.50] Moore, J. & Lyon, R., 1982: 'Porous Absorbers', *Journal of the Acoustical Society of America,* Vol. 72, No. 6 (December), pp. 1994 - 1999.

[A.51] Davern, W., 1977: 'Perforated Facings Backed with Porous Materials as Sound Absorbers – an Experimental Study', *Applied Acoustics*, Vol. 10, pp. 85 - 112.

[A.52] Guignouard, P., Meisser, M., Allard, J., Rebillard, P., & Depollier, C., 1991: 'Prediction and Measurement of the Acoustic Impedance and Absorption Coefficient at Oblique Incidence of Porous Layers with Perforated Facings', *Noise Control Engineering Journal,* Vol.36, No. 3, pp. 129 - 135.

[A.53] Delany, M., & Bazely, E., 1970: 'Acoustic Properties of Fibrous Absorbent Materials', *Applied Acoustics*, Vol. 3, pp. 105 - 116.

[A.54] Brouard, B., Allard, J., Bruneau, H., Lauriks, W., & Verhaegen, C., 1993: 'Acoustic Impedance and Absorption Coefficients of Porous Layers Covered by a Facing Perforated by Parallel Slits', *Noise Control Engineering Journal,* Vol. 41, No. 1, pp. 289 - 296.

[A.55] Takahashi, D., 1997: 'A New Method for Predicting the Sound Absorption of Perforated Absorber Systems', *Applied Acoustics,* Vol. 51, No. 1, pp. 71 - 84.

[A.56] Mohanan, V., Sharma, O., & Chhapgar, A., 1987: 'Sound Absorption by Conical Absorbers and Glasswool Layer Combination', *Applied Acoustics*, Vol. 22, pp. 91 - 101.